

Synthetic and Computational Investigations into the Development of Antivirals and Viral Protein
Dynamics

by

Ahmed Khottary Oraby

A thesis submitted in partial fulfillment of the requirements for the degree of

Doctor of Philosophy

Department of Chemistry
University of Alberta

Abstract

Respiratory viruses are the most common cause of disease in humans, causing high death rates worldwide. Among these, respiratory syncytial virus (RSV) infection is the most significant cause of severe lower respiratory infections in children in North America and one of the leading causes of infant death worldwide. There is no vaccine, and limited drug treatment options, so there is a great need for effective drugs. The emergence of SARS-CoV-2, the pathogen responsible for the COVID-19 pandemic, has created an even more urgent need to develop new antiviral drugs. The creation of antiviral drugs begins with understanding how the virus infects humans and then designing a potent compound that can target any step of the virus life cycle, including viral attachment to the cell, replication process, and release. The viral polymerase represents an attractive therapeutic target for inhibition of virus infection because it makes the virus genetic material (RNA). If this process is halted or slowed, then virus infection is stopped. This has been a highly successful approach in the antiviral drugs developed for HIV and hepatitis C virus (HCV) infections. Therefore, broad-spectrum antiviral agents are desirable because they could protect against the emergence of new viruses, like pandemic SARS-CoV-2.

In Chapter 2, we computationally evaluated the RSV polymerase complex for potential allosteric sites that can accommodate a new class of non-nucleoside polymerase inhibitors reported previously by our group. The lead bis(indole) compound, compound **1**, was used as a reference for the molecular docking and molecular dynamics simulations to develop a reliable computational model. The *in-silico* studies shed light on the putative allosteric site and potential protein-ligand interactions allowing for the design of a new series of compounds with potentially better activity. The synthesis of the compound **1** analogues is discussed. Evaluation of several analogues against RSV is also reported and showed that a new compound, compound **6**, displayed the most promising

antiviral activity using RSV viral progeny assay and viral RNA production quantification using qPCR.

In light of the recent pandemic caused by SARS-CoV-2, Chapter 3 discusses efforts to develop effective antivirals to combat the virus. This chapter describes a detailed computational strategy to identify allosteric binding pockets within the SARS-CoV-2 polymerase and their druggability and accessibility for small molecules. A library of new analogues was rationally designed where the indole fragment of the bis(indole) was substituted with a phenolic hydroxyl to establish a hydrogen bond interaction to the side chain of Thr 394. Several analogues were evaluated using cell-based and biochemical assays and yielded two compounds, **5** and **6**, with substantial low micromolar activity. The activity of the new compounds was also assessed in combination with the FDA-approved drug remdesivir, and a synergistic effect was observed when infected cells were treated with this blend.

In Chapter 4, we describe the discovery of a new way of how viruses can evade immune pressure and sterilizing conditions through a single amino acid mutation at residue 305 in the RSV fusion protein (F) that switches the profile from RSV type A to RSV type B. Molecular dynamics demonstrated that the switch from leucine at position 305 (RSV type A) to isoleucine (RSV type B) causes a shape-shift in the protein conformation, altering the conformation of the antigenic epitopes and hence changing the susceptibility profile for antibodies and patient serum neutralization. A detailed computational, viral evolution, and mutants response to antibodies is described.

Preface

Chapter 1 of this thesis is a review article and has been published as Elawar, F.; Oraby, A.K.; Kieser,Q.; Jensen, L.D.; West, F.G.; Marchant, D.J., Pharmacological Targets and Emerging Treatments for Respiratory Syncytial Virus Bronchiolitis. *Pharmacology & Therapeutics*, **2021**, 220, 107712.

Chapter 2 will be published as Oraby, A.K.; Bilawchuk, L.; Elawar, F.; Besavilla, F.D.; Marchant, D.J.; West, F.G., “Structure-Based Discovery of Allosteric Inhibitors Targeting Respiratory Syncytial Virus L protein”. I was responsible for the designing and performing all computational studies along with the design, synthesis, characterization of compounds and preparing the manuscript. D.F.B. carried out the RSV progeny assay and L.B. repeated the progeny assay and performed the qPCR analysis. F.E. carried out the viral mutant escape assay. D.J.M. and F.G.W. are supervisory authors and were involved in concept formation and manuscript composition.

Chapter 3 of this thesis will be published as Oraby, A.K.; Bilawchuk, L.; Tchesnokov, E.P.; Götte, M.; Marchant, D.J.; West, F.G., “Development of RespVirex: an Allosteric Inhibitor of SARS-CoV-2 Polymerase”. I was responsible for designing the workflow, performing, and analyzing all computational studies. I was also responsible for the design, synthesis, characterization of the new compounds. L.B. carried out the *in vitro* evaluation for the compounds. E.P.T carried out the biochemical assays under the guidance of M.G. D.J.M. and F.G.W. are supervisory authors and were involved in concept formation, funding acquisition and manuscript composition.

Chapter 4 has been submitted as Elawar, F., Oraby, A.K., Stojic, A., McClelland, R.D.; Erwin, K.; Bilawchuk, L.M.; Hazes, B.; Griffiths, C.D.; Culp, T.N.; West, F.G.; Ramilo, O.; McLellan, J.S.; Mejias, A.; Marchant, D.J., “Respiratory Syncytial Virus Evolution by Adaptation” and the manuscript is under review in *Nature Communications*. F.E., A.S., and I contributed equally to this work. F.E. and I were responsible for selecting the mutations to be carried out virtually and drafting the manuscript. I was responsible for carrying out and interpreting the computational results. S.J., L.M.B., R.D.M., B.H., T.N.C. were responsible for performing the virological validation. K.E. carried out the DS-CAV1 experiments under the guidance of J.S.M. F.G.W. supervised A.K.O. D.J.M. is supervisory author and was involved in concept formation, funding acquisition and manuscript composition.

Dedication

To my great parents, Khottary Oraby and Ahlam Shabaan: this is the fruit of your patience throughout the years. I will always be so grateful for your love, compassion, and endless support.

To my dear wife Alyaa Abdelnaser and my beloved daughter Nour Oraby... Thank you for your love and support.

Acknowledgements

This work would not have been possible without my supervisor's immense support and guidance, Dr. Frederick West. I would like to express my deepest gratitude for allowing me to work in your lab and providing me with the appropriate atmosphere to manage my Ph.D. projects successfully. I will always be so grateful for your help and flexibility to try out new techniques and pursue a multidisciplinary approach to reach this point in my project. Thank you for such a fantastic journey. I would also like to express my deepest gratitude to Dr. David Marchant for his unlimited support and guidance. Our discussions and collaborations broadened my knowledge and inspired me to explore new techniques and build my scientific career. I am also thankful to my committee member Dr. Ralf Schirmacher for his outstanding support throughout my graduate studies. Words can not express how grateful I am to Dr. Khaled Barakat for his guidance, support and discussions that enriched my computational background. I would like to sincerely thank Dr. John Pezacki and Dr. John Vederas for agreeing on examining my PhD thesis.

I must thank Leanne Bilawchuk for her help and incredible expertise throughout this work. I can not forget to sincerely thank my late colleague and friend Farah Elawar. I think you would be very proud of what we have achieved through our collaboration.

I would like to enormously thank the current and past members of the West group for creating a scientifically rich environment. I am also thankful to my dear friend and brother, Ahmed Elmenoufy. We have shared a lot throughout our undergraduate and graduate journey. I am also grateful to my friends, Ahmed Adel and Yaseen Almeahmadi, for their undoubtful love and support during my studies. I would like to extend my sincere thanks to the support staff members at the

department of chemistry who have helped me a lot throughout this journey, and this work would not have been possible without their support.

I am also grateful to Dr. Khadiga Attia, Dr. Abdallah Eletrawy, and all the faculty members at the Department of Pharmaceutical Organic Chemistry, Misr University for Science & Technology, Egypt, for allowing me to take this opportunity to pursue my doctoral research at the University of Alberta.

Finally, I can not find words to express how thankful I am for my family, especially my mother, Ahlam Shabaan and father, Khottary Oraby, my brothers Islam and Anas, and my sisters Abeer and Nany. Your prayers have always been with me, and I can not express how much I love you.

Table of Contents

Chapter 1: Pharmacological Targets and Emerging Treatments for Respiratory Syncytial Virus.....	1
1. Introduction.....	1
1.1 New therapeutics are needed to stem the burden of RSV disease	4
1.2 The RSV viral-load infection profile compared to influenza	5
1.3 RSV spread and adaptation in the community	6
1.3.1 RSV seasonality	6
1.3.2 RSV transmission.....	7
1.3.3 Adaptation of RSV and the potential for drug resistance	8
1.3.4 Evolution of RSV in the community toward decreased virulence.....	9
1.4 RSV proteins, their functions and potential as therapeutic targets	10
1.4.1 Non-structural protein 1 and non-structural protein 2	10
1.4.2 The RSV Genome and Nucleoprotein.....	10
1.4.3 Antagonism of the immune response by nucleoprotein.....	11
1.4.4 RSV-P phosphoprotein.....	12
1.4.5 RSV-M Matrix protein	12
1.4.6 Envelope proteins: RSV-F fusion protein, RSV-G glycoprotein, and RSV-SH small hydrophobic protein.....	13
1.4.7 RSV-F fusion protein	13
1.4.8 RSV-G glycoprotein.....	14
1.4.9 RSV-SH small hydrophobic protein.....	14
1.4.10 RSV-M2	14
1.4.11 RNA-dependent RNA polymerase	15
1.4.12 The structure of the RSV polymerase and implication for therapeutic development.....	15
1.4.13 Drugs targeting the RNA-dependent RNA polymerase	16
1.5 An overview of RSV therapeutic development.....	17
1.5.1 Development of RSV antivirals.....	17
1.5.2 Fusion inhibitors.....	18
1.5.2.1 GS-5806.....	18
1.5.2.2 MDT-637.....	21
1.5.2.3 JNJ-2408068.....	21
1.5.2.4 JNJ-53718678.....	22
1.5.2.5 TMC-353121	24
1.5.2.6 RV521	24
1.5.3 Replication inhibitors	25

1.5.3.1	RSV604	25
1.5.3.2	ALN-RSV01.....	25
1.5.4	Nucleoside and non-nucleoside inhibitors of RSV-L.....	26
1.5.4.1	Nucleoside analogues as RSV antivirals	27
1.5.4.1.1	Ribavirin.....	27
1.5.4.1.2	PC786 28	
1.5.4.1.3	ALS-8112	29
1.5.4.1.4	Lumicitabine (ALS-8176).....	29
1.6	Biologicals; therapeutic antibodies.....	31
1.6.1	Nirsevimab MEDI 8897	32
1.7	Vaccines	32
1.7.1	The first failed RSV vaccine	32
1.7.2	Enhanced respiratory disease.....	33
1.7.3	Lessons learned about enhanced respiratory disease.....	34
1.7.4	Live attenuated RSV vaccines in clinical trials	34
1.7.4.1	cpts248/404	34
1.7.4.2	MEDI-559	35
1.7.5	Subunit vaccines in clinical trials	36
1.8	Prophylaxis.....	36
1.8.1	Efficacy and cost-effectiveness of palivizumab	36
1.8.2	RSV drug resistance	38
1.9	Preclinical therapeutic models of RSV infection.....	39
1.10	Conclusions	40
1.11	References	43
Chapter 2: Structure-Based Discovery of Allosteric Inhibitors Targeting Respiratory Syncytial Virus L protein.....		62
2.1	Introduction	62
2.2	Results and Discussion:.....	65
2.2.1	Assessment of The Replication Complex for Putative Druggable Pockets.....	65
2.2.2	Molecular Dynamics Simulations of The Apo RSV L Protein	68
2.2.3	Putative Binding Poses of The New Bis(Indole) Compounds.....	69
2.2.4	Design of The New Analogues.....	70
2.2.5	Assessment of Ligands Stability and Poses During MD simulation	72
2.2.6	Relative Binding Free Energy Analyses of Ligand-Protein Complexes	75
2.2.7	Chemical Synthesis	82
2.2.8	Evaluation of the Antiviral Activity of the Designed Bis(Indole) Compounds Against RSV.....	84

2.2.9	Mutant Escape Assay	86
2.3	Conclusion.....	87
2.4	Experimental Section.....	89
2.4.1	Chemical Synthesis.	89
2.4.1.1	Representative Procedure for the Synthesis of Bis(Indole) Compounds 5a-e.....	89
2.4.1.2	Representative Procedure for the Synthesis of the Bis(Indole) Compounds (6a-e and 10a-e).....	93
2.4.2	Computational Details	101
2.4.2.1	Preparation of the Target Protein for MD Simulations	101
2.4.2.2	Binding site identification	101
2.4.2.3	Molecular docking.....	102
2.4.2.4	MD Simulations and MM-GBSA Rescoring.....	102
2.4.3	Virological Assays.....	103
2.4.3.1	Cells and Virus	103
2.4.3.2	Compounds Evaluation and Infectious RSV Quantification	104
2.4.3.3	Viral RNA Quantification by qRT-PCR	104
2.5	References	105
Chapter 3: Development of RespVirex: an Allosteric Inhibitor of SARS-CoV-2 Polymerase.....		109
3.1	Introduction	109
3.2	Results and Discussion:.....	111
3.2.1	RespVirex Inhibits SARS-CoV-2 RNA Synthesis	111
3.2.2	Computational Investigation of Druggable Binding Pockets in the SARS-CoV-2 Polymerase Identifies a Possible Allosteric Site.....	112
3.2.3	Investigation of Compound 1 Putative Binding Pose.....	116
3.2.4	Design of New Analogues Based on the Lead Compound.....	117
3.2.5	Computational Evaluation of the Newly Designed Ligands using MD Simulations	120
3.2.6	Chemical Synthesis	123
3.2.7	RespVirex Inhibits SARS-CoV-2 Replication in Cell Culture.....	130
3.2.8	RespVirex Targets the RdRp Enzyme of SARS-CoV-2	132
3.2.9	RespVirex Can be Used in Combination with Nucleotide Inhibitors.....	134
3.2.10	Inhibition of RNA Synthesis by Compound 5 Enantiomers.....	137
3.3	Conclusions	137
3.4	Experimental	140
3.4.1	Computational Details.....	140
3.4.1.1	Preparation of the SARS-CoV-2 Polymerase for MD simulation.....	140
3.4.1.2	Allosteric Binding Site Identification.....	141
3.4.1.3	Molecular Docking.....	141

3.4.1.4	MD Simulations and MM-GBSA Rescoring.....	142
3.4.1.5	Binding Pose Metadynamics	143
3.4.1.6	Theoretical ECD Spectra Calculations	144
3.4.2	Chemical Synthesis	144
3.4.2.1	Synthesis of RespVirex Analogues	144
3.4.3	Virological Assays.....	154
3.4.3.1	SARS-CoV2 Replication Assay	154
3.4.4	RdRp Assay.....	155
3.4.4.1	Protein Expression and Purification	155
3.4.4.2	RNA Synthesis Inhibition Assay.....	156
3.5	References	157
Chapter 4: Conformational Shift by A Single Amino Acid Switch in the Respiratory Syncytial Virus Fusion Glycoprotein Causes Global Neutralizing Antibody Evasion		
		162
4.1	Introduction	162
4.2	Results	163
4.2.1	RSV Types A and B have Different Susceptibilities to Antibodies	163
4.2.2	RSV-F Site II of RSVA and B Differ at Flanking Amino Acid 305	166
4.2.3	Recombinant I305 RSV type-A is More Susceptible to Palivizumab	168
4.2.4	Amino Acid Substitution at Position 305 Causes a Significant Change in RSV-F Protomer Conformation.....	172
4.2.5	MD Simulations Predicted RSV F Breathing upon Nirsevimab (MEDI8897) Binding.....	176
4.2.6	RSV-F with Leucine and Isoleucine 305 have Different Binding Affinities to Neutralizing Sera and Monoclonal Antibodies	178
4.2.7	Mutation at RSVA-F Amino Acid Position 305 and RSVB-F Amino Acid Position 127 Occurs at Evolutionary Bottlenecks Caused by Anti-RSV Sera	182
4.2.8	Identification of New Mutations in RSV B	183
4.2.9	WT and L305I rgRSV Viruses have Different Susceptibilities to RSVA and B Patient Sera.....	183
4.3	Discussion	185
4.4	Conclusion.....	186
4.5	Experimental Details	186
4.5.1	Cell Culture	186
4.5.2	Antibodies, Antisera, and DNA Aptamers (Reagents).....	187
4.5.3	Virus Isolation, Propagation, and Purification	187
4.5.4	Construction of the RSV L305I Mutant	188
4.5.5	RSV Reverse Genetics	189
4.5.6	Infectious RSV Quantification	190
4.5.7	RSV Evolution Experiment.....	190

4.5.8	Neutralization Assays with Antibodies and Anti-Nucleolin Aptamer using RSV Clinical Isolates.	191
4.5.9	Whole Genome Sequencing	191
4.5.10	Surface Plasmon Resonance	192
4.5.11	Determining the Percentage Identity and Similarity of RSV Isolates	192
4.5.12	Aligning Multiple Clinical Isolates of RSV and Determine Amino Acid Differences in F Protein	192
4.5.13	Computational Details	193
4.5.13.1	Preparation of Protein for MD simulation	193
4.5.13.2	Molecular Dynamics Simulations of the RSV F Protomer.....	193
4.5.13.3	Protein-Protein Docking.....	194
4.5.13.4	Structural Analysis of Molecular Dynamics Simulations.....	194
4.5.13.5	Statistical Analysis	194
4.6	References	196
Chapter 5: Summary and Future Directions		199
Compiled References		203
Appendix I Selected NMR Spectra (Chapter 2).....		233
Appendix II Selected NMR Spectra (Chapter 3)		266
Appendix III HPLC chromatogram of Compounds 5 & 6 (Chapter 3).....		293

List of Figures

Chapter 1

Figure 1.1: Experimental therapeutic strategies target different points in the RSV replication cycle.....	16
Figure 1.2: The structure and configuration of the RSV polymerase consisting of RSV-L and P proteins	17
Figure 1.3: Structures of RSV fusion and entry inhibitors.	20
Figure 1.4: Mechanisms of inhibition of two RSV-F entry inhibitors.....	23
Figure 1.5 : Nucleoside analogues inhibitors of RSV polymerase.	31

Chapter 2

Figure 2.1: RSV L protein domains.....	64
Figure 2.3: Surface representation of the RSV L bound to the P protein showing compound 1 bound near the NTP entry pore.....	67
Figure 2.4: Water shell analysis of the MD trajectory.....	68
Figure 2.5: Trajectory analysis of the RSV L apo protein.	69
Figure 2.6: Design of compound 1 based derivatives for SAR analysis as RSV RdRp inhibitors.	70
Figure 2.7: Mapping of pocket 1.....	72
Figure 2.9: MD analysis of compound 1	73
Figure 2.10: Trajectory analysis of compound 6a.....	77
Figure 2.11: Lowest energy MD snapshot of compound 10e.....	78
Figure 2.12: Per-residue energy decomposition of ligand-receptor binding energy of compound 6a.....	78
Figure 2.13: Effect of Bis-indoles on RSV progeny production.....	85

Chapter 3

Figure 3.1: Core structure of RespVirex and its derivative compound 1.....	111
Figure 3.2: Activity of Bis(indole) derivatives on SARS-CoV-2.....	112
Figure 3.3: Structure of the SARS-CoV-2 replication complex.	114
Figure 3.5: MD snapshot of 1 and 2 binding to the allosteric pocket of SARS-CoV-2.....	118
Figure 3.6: Allosteric site analysis.....	119
Figure 3.7: The design of new bis-indole derivatives based on compound 1.....	120
Figure 3.8: MD snapshot of 5 and 6 complexes	121
Figure 3.9: Structures of the designed SARS-CoV-2 polymerase inhibitors.....	125

Figure 3.10: Calculated vs Experimental ECD.....	129
Figure 3.11: Activity of RespVirex analogues on SARS-CoV-2	130
Figure 3.12: Inhibition of RNA synthesis by RespVirex analogues.....	133
Figure 3.13: Effect of RespVirex analogues on SARS-CoV-2 replication.....	135
Figure 3.14: Cytotoxicity and IC50 values for compounds 5 and 6.	136
Figure 3.15: SARS-CoV-2 RdRp-catalyzed RNA synthesis in presence of compounds 5a and 5b.....	138

Chapter 4

Figure 4.1: Clinical isolates of RSV type-A and B.....	165
Figure 4.2: Mutation in RSV-F at amino acid position 305 occurs at evolutionary bottlenecks and changes the shape and antibody neutralization sensitivity of RSV.....	167
Figure 4.3: L305I is less susceptible to polyclonal antisera and D25 monoclonal antibody but produces less infectious particles.	171
Figure 4.4: Conformational changes in the RSV F protein.....	174
Figure 4.5: MD analysis of N228D mutant.	175
Figure 4.6: Conformational analysis of RSV F bound to MEDI8897.	177
Figure 4.7: Example surface plasmon resonance traces of antibody binding to L305 and I305 rgRSV virions.	179
Figure 4.8: Example surface plasmon resonance traces of antibody binding to L305 and I305 DS-CAV1 RSV-F recombinant proteins.....	180
Figure 4.9: Leucine 305-RSVs are more susceptible to RSV antisera from infants infected with RSV A and B.	184

List of Tables

Chapter 1

Table 1.1: Recent RSV antivirals in development or in clinical trials.....	3
---	---

Chapter 2

Table 2.1: Summary of MM/GBSA results for series I and II compounds.....	80
---	----

Table 2.2: Pair-residue energy decomposition values for compounds 1 and 6a.	81
---	----

Chapter 3

Table 3.1: summary of MM/GBSA results showing the relative binding free energy of the proposed new compounds	123
---	-----

Chapter 4

Table 4.1: RSV F sequence alignment and identity. a. RSV F protein sequence alignment of clinical isolates. b. Sequence identity between RSV subtypes A and B.....	170
---	-----

Table 4.2: Inhibitory concentration 50 and Molar dissociation constants (K_D) of antibodies to sites Ø and II.....	181
---	-----

List of Schemes

Chapter 2

Scheme 2.1: Synthesis of series I Compounds.....	83
Scheme 2.2: Synthesis of compound 9.	83
Scheme 2.3: Synthesis of series II bis-indole derivatives 10a-e.	84

Chapter 3

Scheme 3.1: Synthesis of Targeted Compounds.....	126
Scheme 3.2: Synthesis of Compounds 13 to 16.....	127
Scheme 3.3: Synthesis of compound 19.	128

Chapter 5

Scheme 5.1: Potential modifications on the lead compound 5 for SAR analysis.	202
---	-----

Abbreviations

°C	Celsius
μs	microsecond
1HAEo-	human airway epithelial cell line
ACE2	angiotensin-converting enzyme 2
ATCC	American Type Culture Collection
BPMD	Binding Pose MetaDynamics
CC ₅₀	half-maximal cytotoxic concentration
CDCl ₃	deuterated chloroform
CLD	chronic lung disease
CPE	cytopathic effect
Cryo-EM	cryogenic electron microscopy
Cu(OTf) ₂	Copper(II) triflate
CV	collective variable
DCM	dichloromethane
DMEM	Dulbecco's modified Eagle's medium
DMSO	dimethyl sulfoxide
ECD	electronic circular dichroism
ERD	enhanced respiratory disease
ESI	electrospray ionization

Et ₃ N	triethylamine
EtOAc	ethyl acetate
EtOH	ethanol
FBS	fetal bovine serum
FFU	focus forming unit
Fsp ³	fraction of sp ³ carbon atoms
GE	gene end
GFP	green fluorescent protein
GS	gene start
GTP	Guanosine-5'-triphosphate
HOAc	acetic acid
HPLC	high performance liquid chromatography
HPRT1	Hypoxanthine Phosphoribosyl transferase 1
HRB	heptad repeat B
HRMS	high resolution mass spectrometry
Hz	hertz
IAV	influenza A virus
IBV	influenza B virus
IC ₅₀	half maximal inhibitory concentration
ICU	intensive care unit
IFN	interferon

<i>in silico</i>	refers to computer simulations
<i>in vitro</i>	refers to the studies performed in living organisms
IPA	isopropyl alcohol
<i>J</i>	coupling constant (in NMR)
KD	dissociation constant
kDa	kilodalton
LRTI	lower respiratory tract infection
mAb	monoclonal antibody
MAVS	mitochondria antiviral signaling molecule
MD	molecular dynamics
MM/GBSA	Molecular Mechanics/Generalized Born Surface area
MOI	multiplicity of infection
NiRAN	Nidovirus associated nucleotidyl transferase domain
ns	nanosecond
NTP	nucleoside triphosphate
OPLS	Optimized Potentials for Liquid Simulations
PEG	polyethylene glycol
PFU	plaque forming unit
PKR	protein kinase R
PPA	polyphosphoric acid

PRNTase	polyribonucleotidyl transferase
PZMB	Palivizumab
qPCR	quantitative polymerase chain reaction
RdRp	RNA-dependent RNA polymerase
RDV	remdesivir
RMSD	root mean square deviation
RMSF	root mean square fluctuation
RSV	respiratory syncytial virus
RV	rhinovirus
SAR	structure-activity relationships
SARS-CoV-2	severe acute respiratory syndrome coronavirus 2
TIP3P	transferable intermolecular potential with 3 points
WT	wild type
δ	chemical shift in parts per million
μM	micromolar

Chapter 1:

Pharmacological Targets and Emerging Treatments for Respiratory Syncytial Virus*

1. Introduction

Respiratory Syncytial Virus (RSV) is a member of the *Orthopneumovirus* genus, *Pneumoviridae* family, and *Mononegavirales* order.¹ RSV has two major sub-types, type A and type B, that share 95% sequence identity and have similar disease manifestations. Originally referred to as Chimpanzee Coryza Agent, RSV was first identified in 1955 in a chimpanzee colony at the Walter Reed Army Institute of Research.² RSV was immediately suspected as a human pathogen, as the authors noted that RSV neutralizing antibodies were present in a laboratory worker who contracted an upper respiratory tract infection after working closely with infected chimpanzees. Soon after, pre-existing neutralizing antibodies were detected in the serum of patients who had no contact with the chimpanzee colony. RSV was successfully isolated from a human patient in 1957³, and in subsequent years the importance of RSV as a major contributor of disease in pediatric⁴ and elderly⁵ populations became apparent.

Despite the discovery of RSV dating back over six decades, no vaccine to prevent infection or efficacious antiviral for treating infection are available. Lack of licensed medication is not due to a lack of drug development activity as there have been several high-profile failures of RSV vaccines and therapeutics in the last four years (**Table 1.1**). Recently in the Fall of 2018 and winter

The contents of this chapter have been copied and/or adapted from the following publication: Elawar, F.; Oraby, A.K.*; Kieser, Q.*; Jensen, L.D.; West, F.G.; Marchant, D.J., Pharmacological Targets and Emerging Treatments for Respiratory Syncytial Virus Bronchiolitis. *Pharmacology & Therapeutics*, **2021**, 220, 107712.

*Authors equally contributed

of 2020, three promising compounds, all of which targeted different stages of RSV replication, were withdrawn from clinical trials.⁶ Furthermore, there were two high-profile failed vaccine trials of different strategies.⁷ While these vaccines saw little success in a primary setting, there was limited achievement in reducing both hospitalization due to lower respiratory tract infection and severe hypoxemia. As a result, these vaccines may see restricted use exclusively for high-risk populations.⁸ Therefore, RSV continues to impose a significant global burden of disease with few experimental therapeutic options. In this review, we discuss the classes of compounds in clinical trials, their targets, and some of the recent and historical failures of RSV therapeutics. It is only after learning from the mistakes of the past and incorporating understanding of RSV replication that we will develop efficacious therapies and vaccines.

Compound Name	Development Stage	Mechanism of action	Citation
JNJ-53718678 (JNJ-678)	Phase 2 CT completed	Small molecule RSV-F inhibitor	NCT02387606 NCT03379675 {Perron, 2015
GS-5806 (Presatovir)	Phase 2b CT completed	Small molecule RSV-F inhibitor	#453;DeVincenzo, 2014 #841} NCT02135614
BTA-C585	Phase 2 CT completed	Small molecule RSV-F inhibitor	{Heylen, 2017 #663} NCT02718937
ALX-0171	Phase 1 and 2 CT ongoing	Antibody-like RSV-F inhibitor	{Detalle, 2016 #459} NCT02979431 NCT03418571
AK-0529	Phase 1b and 2 CT ongoing	Small molecule RSV-F inhibitor	NCT02654171 NCT02460016

MDT 637 (VP-14637)	Phase 1 CT completed; results not released	Small molecule RSV-F inhibitor	{Douglas, 2005 #461} NCT01355016
BMS-433771	No investigation in CT	Small molecule RSV-F inhibitor	{Cianci, 2005 #462}
TMC-353121	No investigation in CT	Small molecule RSV-F inhibitor	{Bonfanti, 2008 #464}
ALN-RSV01	Phase 2b CT; partial success	siRNA targeting RSV mRNA encoding RSV-N	{Gottlieb, 2016 #456} NCT01065935
RSV604	Phase 1 CT completed; results not released	Binds RSV-N protein; blocks RNA synthesis	{Challa, 2015 #420} NCT00416442
ALS-008176 (lumicitabine)	Phase 2 CT completed; development on hold, results not released	Targets RSV-L; causes chain termination	{Deval, 2015 #418;DeVincenzo, 2015 #457} NCT02673476
PC786	Phase 2 CT ongoing	Targets RSV-L	{Coates, 2017 #662} NCT03382431
AZ-27	No investigation in CT	Inhibits de novo RNA synthesis initiation by RSV	{Noton, 2015 #466}
BI-D	No investigation in CT	Inhibits RSV mRNA elongation and capping producing IFN response	{Fearn, 2016 #463}
YM-53403	No investigation in CT	Targets RSV L	{Sudo, 2005 #419}
GS-5734	Phase 2 CT ongoing*	Inhibits polymerization by RSV-L in vitro	{Warren, 2016 #478} NCT02818582
BCX-4430	Phase 1 CT*	Inhibits polymerization by RSV-L in vitro	{Warren, 2014 #465} NCT02319772

Table 1.1: Recent RSV antivirals in development or in clinical trials.

Currently, there are two therapeutics licensed for managing disease due to severe RSV infection. Ribavirin, the first licensed therapeutic, is an antiviral nucleoside analogue that was recommended for the treatment of severe RSV infection in 1993. However, clinical trials leading

to this recommendation were methodologically flawed, and the efficacy of ribavirin was exaggerated.^{10, 11} Subsequent studies found that the benefits of ribavirin were limited or non-existent^{12, 13}, and ribavirin is no longer included as a standard of care for RSV infection. Currently, the only licensed prophylaxis, Palivizumab, a humanized monoclonal antibody against RSV, was licensed in 1998 for the prophylactic prevention of RSV infections. Due to its high cost, limited efficacy, and the necessity of monthly prophylactic injections, Palivizumab is only administered to high-risk infants. A majority of hospitalized infants are not eligible for Palivizumab, so there is no decrease in hospitalization rates in full term infants that contract RSV from older siblings¹⁴. Palivizumab is not efficacious in the treatment of ongoing RSV infection and has a less significant effect on overall RSV transmission rates than previously thought.^{15, 16} In summary, the limited efficacy of therapeutics for the treatment and prevention of RSV means that development of therapeutics in this arena is ongoing and rapidly gaining more attention.

1.1 New therapeutics are needed to stem the burden of RSV disease

RSV is a leading cause of both infant mortality and hospitalization worldwide¹⁷, so there is a great need for direct-acting antivirals. In fact, RSV has been recognized by the World Health Organization (WHO) as the number one vaccine priority.¹⁸ Anti-infectives are likely to be utilized most during neonatal intensive care unit (NICU) stays and shortly after discharge.^{19, 20} While individuals will be re-infected with the same strain of RSV throughout life, the primary infection during infancy is typically the most severe and so is of the highest priority. In the community, approximately 40% of all primary infections in infancy result in lower respiratory tract infections (LRTI), which manifest as bronchiolitis or pneumonia. However, not all of these cases will be reported to the hospital and 0.5-2% of all otherwise healthy infants will require hospitalization due

to RSV LRTI²¹. In Canada and the United States, RSV LRTI in infants results in approximately 12 000 and 77 000 annual hospitalizations, respectively.²²

In 2010, Nair *et al.* estimated that LRTI caused by RSV in children under five years old resulted in 3.4 million hospitalizations and 66 000 to 199 000 deaths annually (examining data from 2005).²³ A decade later, the RSV Global Epidemiology Network observed a comparable worldwide burden of disease in children under five years of age, with RSV LRTI responsible for 3.2 million hospital admissions and 94 600 to 149 400 deaths annually.²⁴ RSV-related mortality disproportionately affects developing countries more than western nations. Unfortunately, in these settings, newly licensed therapeutics will likely not be available initially due to the tremendous financial cost of new drugs. Nevertheless, it is developing countries where RSV drugs are needed most. However, if treatment of the human immunodeficiency virus (HIV) pandemic is to be a model, then generic production of any licensed RSV drugs would be beneficial. Generic drugs that were produced in the Indian, Brazilian and South African biotechnology complex were of tremendous benefit in resource poor settings.⁷ They contributed greatly to reducing the burden of HIV in sub-Saharan Africa. Efforts such as these typically don't come without legal challenges to possible patent infringement.⁷ Nevertheless, generically manufactured drugs at a fraction of the cost of the name brand product may help to fulfil the need to stem the burden of RSV in these settings.

1.2 The RSV viral-load infection profile compared to influenza

Acute viral infections can be difficult to treat with antivirals because, typically, the patient must be treated shortly after the onset of symptoms for the intervention to be effective. In other words, intervention must be effective before the viral load reaches its peak, preventing viral spread and damage to the host's cells from direct virally induced cytopathic effect and the immune

response to infected cells. Of course, antivirals only offer therapeutic potential if viral replication drives disease; if viral load has already been controlled by the immune response at the time of symptom onset, then an antiviral will be of little benefit. This important consideration is exemplified by influenza A virus (IAV), where peak viral shedding precedes peak symptom severity.²⁵ Neuraminidase inhibitors such as zanamivir (Relenza) and oseltamivir (Tamiflu) effectively inhibit IAV replication *in vitro* and have been stockpiled to address the threat posed by pandemic influenza outbreaks. However, the clinical benefits of these antivirals are limited. Zanamivir and oseltamivir have no effect on hospitalization rates or serious complications, and only a minor decrease in the time to symptom alleviation.²⁶

Human challenge studies that compared the viral load progression of RSV to influenza showed that there was a significantly longer therapeutic window to treat RSV infection²⁷, suggesting that RSV infections will be more responsive to antivirals than influenza. Furthermore, in experimentally inoculated adult volunteers, RSV replication and titers mirrored symptom severity.²⁸ Likewise, in hospitalized children, RSV load paralleled disease severity²⁹, unlike influenza where peak symptoms followed after the peak of viral load.²⁵ Therefore, when an RSV antiviral becomes available, the drug is expected to have a reasonable window of opportunity to treat the infected individual.

1.3 RSV spread and adaptation in the community

1.3.1 RSV seasonality

In temperate climates, such as North America, the RSV season lasts 3-5 months; typically, beginning in autumn, peaking in winter, and tapering off in the spring. RSV transmission is significantly reduced, or not detected during the summer months.³⁰⁻³³ In contrast, very cold or tropical climates do not obey this pattern, and RSV transmission occurs year-round.^{32, 33} A variety

of hypotheses have been proposed to explain the transmission patterns observed across these different regions, including changes to viral stability in the environment that are dependent on temperature, humidity, and ultraviolet light intensity. Alternatively, changes in human behavior throughout the seasons have been proposed to play a role.³⁰⁻³³ No animal reservoir is known or suspected for RSV, and the reintroduction of RSV in regions with seasonal transmission cycles is not understood.^{30 34, 35}

When novel clades emerge, they have been observed to displace ancestral clades and spread globally. The RSV type B BA clade emerged in 1999 and became the dominant global RSV type B clade in the ensuing decade.³⁶ RSV BA strain continued to evolve with four genotypes emerging in the ten years following its emergence. We have proposed that this behaviour supports the emergence of RSV into a community by high-titer clades.³⁷ The high-titer clade hypothesis will be described in further detail below. These aspects of RSV adaptation/mutation suggest that it will be important to modify or even replace drugs as new RSV strains emerge.

1.3.2 RSV transmission

RSV is primarily transmitted via large nasopharyngeal droplets from infected individuals.²² Large droplets (>100 µm in size) remain in the air for only a matter of seconds, quickly falling onto surfaces due to gravity.³⁸ Therefore, direct contact with an infected individual, or contact with contaminated surfaces, is required for transmission via large droplets. Infectious RSV can be isolated from solid surfaces 6 hours after transfer and can survive on hands for 25 minutes.³⁹ Rubbing one's eyes and face with hands contaminated by these surfaces can lead to infection. RSV gathers a foothold on the host here by first replicating in the conjunctiva of the eyes or in the nose.⁴⁰ It then goes on to infect the upper and lower respiratory tracts.

Recently, it was observed that viable RSV is present in aerosols produced by infants with bronchiolitis.⁴¹ The air was sampled at distances of 1 metre, 5 metres and 10 metres from infected infants. Air was also sampled in the presence of infants and 2 hours after discharge. RSV titers from airborne particles were highest at a distance of 1 metre; however, RSV was detected up to a distance of 5 metres from patients. RSV titers were highest when sampling was conducted in the presence of the patient, yet aerosols containing viable RSV remained detectable at 2 hours post-discharge. Furthermore, RSV was found in particles less than 4.7 μm in diameter. While large diameter particles are typically caught in the upper respiratory tract, particles less than 5 μm in size may be directly inhaled into the lower airways.^{41, 42} The possibility of airborne transmission of RSV has implications for public health measures used to prevent nosocomial RSV transmission.

Surfaces contaminated with RSV represent another major source of transmission.⁴⁰ RSV conjugated with air pollution can last for weeks on a dry surface,⁴³ and serves as a significant source of nosocomial transmission. Thus, the best prophylaxis measures to protect from RSV infection are likely handwashing, stifled coughs-sneezes, and social distancing.

1.3.3 Adaptation of RSV and the potential for drug resistance

Owing to the low fidelity of its RNA-dependent RNA polymerase (RdRp), RSV evolves rapidly. The constant population-level evolution of RSV results in the replacement of antigenic epitopes and contributes to the explanation of how RSV successfully reinfects individuals throughout life.⁴⁴ This viral evolution occurs within the individual host due to selective pressures imposed by the immune response.⁴⁵ In an infant lacking an adaptive immune response, RSV genetic diversity was relatively stagnant but increased rapidly upon reconstitution of the adaptive response with a bone marrow transplant.⁴⁵ Thus, the rapid generation of genetic diversity following the introduction of a selective pressure, such as the host immune response, will likely translate to

the emergence of drug resistance following the introduction of a new therapeutic. In summary, similar to other RNA viral infections, drug resistance will represent a significant hurdle in the efficacy of treatment over time.

1.3.4 Evolution of RSV in the community toward decreased virulence

While novel clades spread rapidly, they are not necessarily more virulent. The association of pathogenesis with RSV subtype has remained a pressing question since RSV was first divided into RSV type A and RSV type B in the 1980s. Conflicting evidence suggests that RSV subtype does,⁴⁶⁻⁴⁸ or does not,^{49, 50} predict disease severity. The ability to further organize subtypes into genetic clades may help address this question. Recently, a pilot study observed that RSV strains that replicate to high titers in patients and have high replication kinetics in cell culture are genetically similar. These were termed High Titre clades.³⁷ This study did not directly examine the severity of illness; however, an association of RSV viral load and disease severity has been observed previously.⁵¹ Thus, identification of high-titer clades may enable forecasting of dominant strains causing severe infections in the subsequent RSV season.

Our group also showed that newly emerging RSV strains into communities were driven by strains that produced the highest titers in patients and tissue culture. These may be quasispecies that are imported, and so they have emerged with an ability to replicate to a higher titer in a naïve population. However, we also noted the presence of ‘resident clade’ RSV strains that circulate at a lower titer relative to high-titer clades. While resident clade viruses produced lower titers in patients and tissue culture, we found that they were more infectious in culture. Thus, we propose that there is a natural evolution of RSV toward strains that linger in the community, replicate slower, and have less of a propensity to cause disease. This evolution is driven by the fact that the resident strains are more infectious but cannot replicate to high titres. Any virus that undergoes

fitness adaptation through mutation will likely evolve drug resistance. This is especially true for direct-acting antivirals where evolutionary pressure is placed upon the population of quasispecies; a member of the population that is resistant to drug pressure will outgrow the susceptible species.

1.4 RSV proteins, their functions and potential as therapeutic targets

1.4.1 Non-structural protein 1 and non-structural protein 2

The RSV non-structural 1 (RSV-NS1) and non-structural 2 (RSV-NS2) proteins demonstrate a remarkable number of immunomodulatory functions centered around antagonism of the host IFN response (reviewed in ⁵²), delaying apoptosis ⁵³, and arresting the cell cycle in the G₀/G₁ phase ⁵⁴. They are the first proteins to be expressed during infection, underlining the importance of shutting down the IFN response to the virus. Therefore, therapeutic potential may exist in blocking NS protein-mediated immune-suppression to augment the innate immune response against RSV. Targeting NS1 and NS2 may decrease viral titres in a preventative setting or a therapeutic setting in infants as this has already been shown in preclinical studies ⁵⁵. Recently, studies suggested NS2 could be targeted and inhibited by small molecule drugs ⁵⁶. It may be worthwhile to pursue non-structural proteins in antiviral discovery and perhaps in combination with drugs targeting other RSV proteins.

1.4.2 The RSV Genome and Nucleoprotein

RSV has a single-stranded negative-sense RNA genome of approximately 15.2kb that encodes 10 genes and 11 proteins.⁵⁷ The RNA genome is tightly bound to RSV nucleoprotein (RSV-N) in a helical ribonucleoprotein (RNP) complex. RSV-N arranges into a homodecameric ring with each individual subunit interacting with 7 bases of the RSV genome.⁵⁸ The RNA itself is bound to the

decameric ring in a basic groove near the external surface in a way that the RNA can be readily accessed by the viral RdRp, which is critical given that RSV-N has been implicated in viral RNA replication (Grosfeld et al., 1995). Interestingly, the function of RSV-N during infection by RSV extends beyond genomic packaging to antagonism of the host innate immune response.

1.4.3 Antagonism of the immune response by nucleoprotein

There are two mechanisms by which RSV-N modulates the host immune response. The first mechanism relies on the interaction of RSV-N with a multitude of host proteins including: retinoic-acid-inducible gene-I (RIG-I), melanoma differentiation-associated gene 5 (MDA5), and mitochondrial antiviral signaling protein⁵⁹ (MAVS; also known as IPS-1, CARDIF, or VISA⁶⁰). RIG-I and MDA5 are cytosolic pattern recognition receptors (PRRs).^{61, 62} RIG-I detects 5'-triphosphorylated RNA and double-stranded RNA (dsRNA), while MDA5 detects only the latter.⁶³ Following activation by their cognate ligands, both RIG-I and MDA5 signal through the MAVS adaptor protein to stimulate an interferon (IFN)- β response. Transfection of RSV-N into cells infected with Newcastle Virus (which elicits a strong IFN- β response) attenuates the IFN- β response via inhibition of RIG-I and MDA5 signaling through sequestration of MAVS to inclusion bodies.⁵⁹ This represents one strategy by which the RSV-N protein antagonizes the innate immune response, supporting the argument that it is a bona fide therapeutic target.

The second known mechanism hinges upon the interaction between RSV-N and a protein kinase termed PKR.⁶⁴ PKR is produced in response to type I IFNs as a means of inducing an antiviral state in cells.⁶⁵ PKR is activated by cytosolic dsRNA (reviewed in⁶⁶). Briefly, binding to dsRNA results in activation of PKR via phosphorylation of multiple serine and threonine residues. Phosphorylated PKR inactivates eukaryotic initiation factor 2 α (eIF-2 α) via phosphorylation. In the absence of eIF-2 α , cellular translation of mRNA into protein ceases.

During RSV infection, there is an accumulation of phosphorylated PKR; however, eIF-2 α is not inactivated. Instead, phosphorylated PKR is bound by RSV-N.⁶⁷ Given the localization of RSV-N to inclusion bodies during RSV infection, binding of PKR by RSV-N likely sequesters PKR into inclusion bodies.⁵⁹

A viral protein such as RSV-N that is indispensable for viral replication is a good therapeutic target such that suppressing RSV-N activity may release innate immune mechanisms from inhibition while decreasing RSV replication.

1.4.4 RSV-P phosphoprotein

The phosphoprotein in RSV (RSV-P) helps make up the RNA-dependant RNA polymerase complex RSV needs to transcribe and replicate its genome. Since the polymerase complex is made up of 3 different proteins, targeting the polymerase complex is an option that has not been comprehensively explored. The polymerase complex structure has recently been resolved, thereby opening opportunities for designing antivirals to target novel RSV sites.⁶⁸ Furthermore, RSV-P has been implicated as a strong target for antiviral compound design.⁶⁹ The position RSV-P fits in the polymerase complex demonstrates that antivirals can inhibit the RSV-P function because it would have access to a binding pocket. RSV-P is essential for viral replication and transcription, therefore, halting the P protein function will halt RSV-L activity as well.

1.4.5 RSV-M Matrix protein

The matrix protein (RSV-M) is a structural protein which lines the inside of the viral envelope and associates with the RNP via RSV-M2-1.⁷⁰ RSV-M does not have characterized antigenic regions that are assessible to the host immune system for neutralization; therefore, it is not currently a suitable RSV protein target in a vaccine or antiviral.

1.4.6 Envelope proteins: RSV-F fusion protein, RSV-G glycoprotein, and RSV-SH small hydrophobic protein

The RSV viral envelope proteins include fusion protein (RSV-F), glycoprotein (RSV-G), and small hydrophobic protein (RSV-SH). RSV entry is mediated by a complex interaction between RSV-F and RSV-G envelope proteins and host cell proteins (reviewed by ³⁰). Briefly, proposed candidate receptors include CX3 chemokine receptor 1 (CX3CR1) ⁷¹, epidermal growth factor receptor (EGFR) ^{72, 73}, annexin II ⁷⁴, calcium-dependent lectins, Toll-like receptor 4 (TLR4) ⁷⁵, intercellular adhesion molecule 1 (ICAM-1) ⁷⁶, nucleolin ⁷⁷, and heparan sulfate proteoglycans (HSPGs) PMID: 10864656. The functions of these proteins include tethering RSV to the surface and triggering fusion.³⁰

1.4.7 RSV-F fusion protein

RSV-F is essential for entry because it triggers the fusion of virion and host cell membranes that allow delivery of the virus capsid contents into the host cell. Before interaction with the host cell, it exists as a trimer in a pre-fusion conformation. ⁷⁸ It is hypothesized that fusion of the viral membrane to the host cell is driven by a conformational shift in multiple spring-loaded, metastable, RSV-F proteins ³⁰. Host-cell nucleolin was first identified as a candidate receptor for RSV-F via a virus overlay protein binding assay and is necessary for optimal RSV entry. ⁷⁷ RSV-F has been the focus point for many pharmaceutical companies as a vaccine candidate. Until recently, the more stable RSV-F in its post-fusion state was predominantly used in vaccine development. However, after multiple years of clinical trial failure, we know the RSV-F post-fusion conformation does not confer protective antibodies against infectious RSV particles.

1.4.8 RSV-G glycoprotein

Depending on the type of immortalized cell line, RSV-G is dispensable for infectivity in cell culture.⁷⁹ However, interaction between RSV-G and the cellular membrane protein CX3CR1 is necessary for optimal infection of *in vivo* models.⁷¹ Soluble RSV-G is secreted by virions to serve as an immune and antibody decoy.⁸⁰ RSV-G is also the most variable protein expressed in the RSV genome and, as such, has been used to characterize RSV strains. The variability of this protein makes it unattractive as a vaccine target because the vaccine would have to be adapted frequently.

1.4.9 RSV-SH small hydrophobic protein

Like RSV-G, RSV-SH is not essential for RSV replication in cell culture^{79, 81}, and recombinant RSV strains lacking RSV-SH were only slightly attenuated in mice.⁸¹ In chimpanzees, RSV lacking RSV-SH were attenuated in the lower, but not upper, respiratory tract.⁸² While the role of RSV-SH in RSV replication is not well characterized, these observations have precipitated investigations of RSV-SH deletion vaccine candidates.⁸³ Furthermore, RSV-SH does not physically protrude as far as RSV-F and RSV-G, therefore it is not an ideal neutralization target.

1.4.10 RSV-M2

The RSV polymerase consists of a complex formed by RSV-L, RSV-P, and RSV-M2-1 to transcribe and replicate its RNA genome (Reviewed in (PMID:16760383)). RSV-M2-1 is primarily involved in the complex as transcription terminator. There are reports of RSV-M2-1 interacting substantially with RSV-P in the complex.⁸⁴ Therefore RSV-M2-1 is an essential part of the RSV lifecycle and can be targeted with an antiviral either by directly targeting the protein or the complex the protein folds into. Furthermore, recent studies have suggested that M2-1 has a

role in downstream transcription to translation.⁸⁵ The importance of M2-1 in transcription and translation of RSV makes M2-1 a more attractive therapeutic target.

1.4.11 RNA-dependent RNA polymerase

The RSV RdRp is encoded by the RSV-L gene and is packaged within the virion in conjunction with the genome. This protein, in complex with RSV-P, catalyses transcription and replication of the RSV genome (**Figures 1.1 and 1.2**). The polymerase complex of a virus is critical because it produces the mRNA from which viral proteins are made and it replicates the genome to be packaged into progeny viruses. These activities are crucial for an infection to happen and so the polymerase makes for a strong therapeutic target.

1.4.12 The structure of the RSV polymerase and implication for therapeutic development

Even though the RSV-L protein is the core polymerase enzyme, the RSV-L and -P proteins are the minimal constituents of the RSV polymerase that are required for activity.^{86, 87} Recently, the structure of the RSV-L and P polymerase complex has been elucidated to 3.2-Å resolution by cryoelectron microscopy.⁶⁸ This provides a high-resolution picture of the RSV-L and P core RdRp complex that on its own has in vitro RNA-polymerase activity. The RSV-P protein encompasses the RSV-L core catalytic protein in a “tentacular” formation in a 4:1 stoichiometry, meaning that the four RSV-P proteins emanate from the core protein structure like tentacles and each RSV-P takes on a distinct conformation. There are two primary functions of RSV-L, transcription of individual mRNA transcripts and genome replication, the regulation of which was only elucidated recently.⁸⁸ The structure of the polymerase provides a model from which new compounds can be made and explains the generation of resistance to antiviral drugs.

The RSV-L/-P complex can initiate transcription or replication and produce short transcripts up to 200 nucleotides in length.^{87, 88} Expression of RSV-L, -P and -N is sufficient for minigenome replication, indicating that concurrent encapsidation of the growing genome by RSV-N is required for optimal RdRp replicase processivity.⁸⁹ Conversely, transcriptase activity by RSV RdRp requires the RSV-M2-1 anti-termination factor.⁹⁰ As a result, a full complement of RSV-L, -P, -M2-1, and -N is required to produce full infectious RSV from a cDNA antigenome.⁹¹

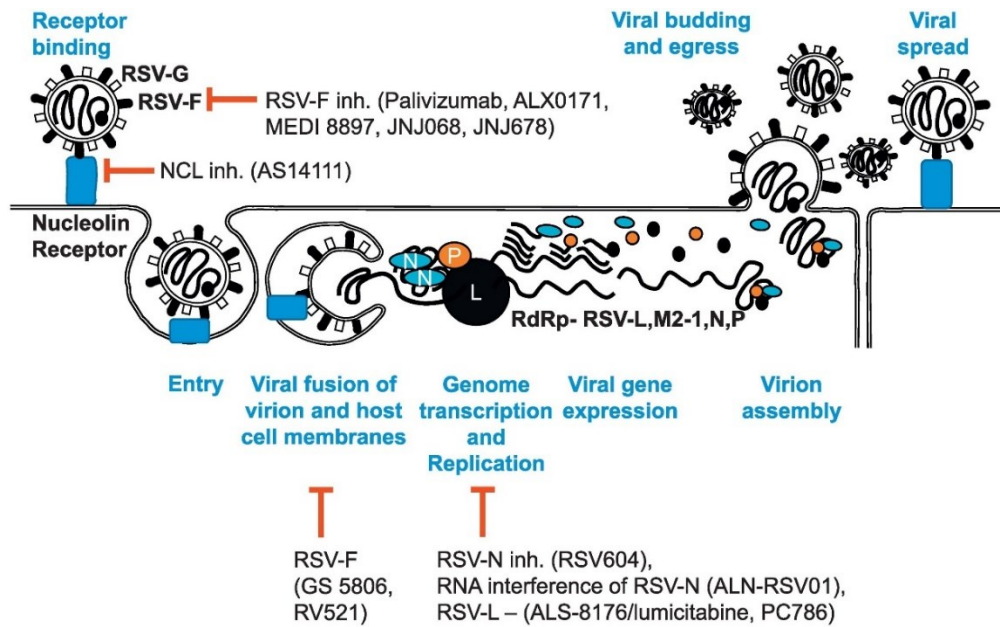


Figure 1.1: Experimental therapeutic strategies target different points in the RSV replication cycle. The RSV replication cycle from receptor binding, entry, to genome replication, viral budding and spread to adjacent cells are shown. Drugs targeting each of the steps or RSV proteins are shown in parentheses.

1.4.13 Drugs targeting the RNA-dependent RNA polymerase

RSV-L is the catalytic subunit of RSV RdRp, responsible for polymerizing genome and transcript chain elongation⁹², polyadenylation (reviewed by⁹³), and 5' capping⁹⁴. The RSV RdRp, as with all RNA viruses, is central to viral replication and is thus a logical therapeutic target.

The RSV-P protein is also a necessary subunit of RdRp along with RSV-L. Phosphorylation of RSV-P at serine-232 is required for chain elongation⁹⁵, and phosphorylation of RSV-P at threonine-108 enables interaction of the RdRp with RSV-M2-1.⁹⁶ Thus, blocking these interactions or phosphorylation of RSV-P could lead to new classes of therapeutics.

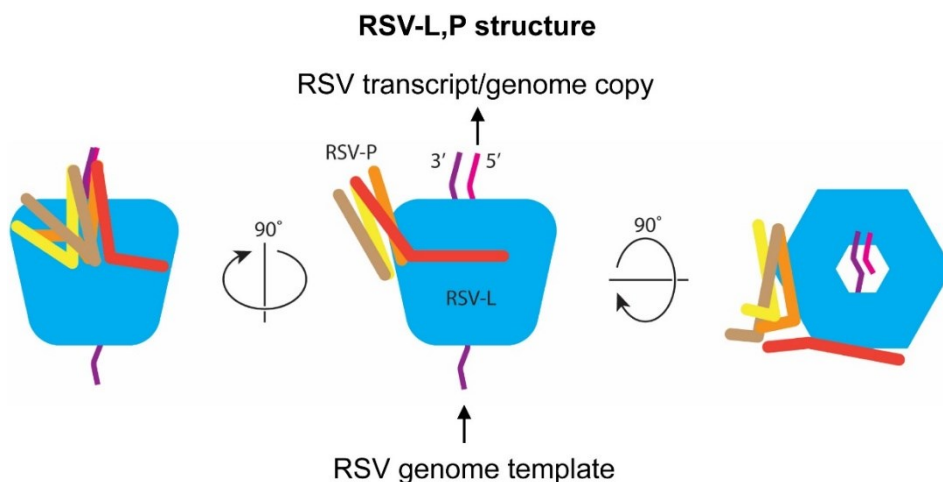


Figure 1.2: The structure and configuration of the RSV polymerase consisting of RSV-L and P proteins.

1.5 An overview of RSV therapeutic development

1.5.1 Development of RSV antivirals

Millions of compounds have been screened for antiviral activity against RSV in high throughput platforms and a small handful of these compounds have entered clinical trials (**Table 1.1 and Figure 1.3**). Despite RSV antiviral drug discovery spanning decades, no efficacious antivirals have entered the market. The absence of efficacious RSV antivirals in the clinic

highlights the need for creative efforts to identify novel chemical entities with antiviral activity against RSV.

A wide range of strategies have been employed in the search for RSV antivirals, and numerous compounds have undergone clinical trials. These include nucleoside analogues and non-nucleoside analogues which target the RSV polymerase complex, an siRNA which targets RSV-N, and small molecules which interfere with viral fusion (**Table 1.1**).⁹⁷ Alternatively, therapeutics such as Danirixin, an oral small molecule drug that inhibits the CXCR2 receptor, seek to mitigate the damage due to inflammation which occurs during RSV infection, seek to mitigate the damage due to inflammation which occurs during RSV infection.⁹⁷ Rather than describe the myriad of compounds that have *in vitro* antiviral activity we will discuss those compounds with the most promise or that have failed clinical trials.

1.5.2 Fusion inhibitors

1.5.2.1 GS-5806

GS-5806, also referred to as presatovir, is an RSV-F inhibitor.⁹⁸ Gilead Sciences employed a high-throughput antiviral screening campaign in their efforts to discover and optimize hits against RSV.⁹⁹ A result was the discovery of a structurally distinct class of RSV fusion inhibitors bearing a pyrazolo[1,5-a]-pyrimidin-2-yl moiety. A phenotypic screening of ~400,000 compounds, using human epithelial type-2 (Hep-2) cells to assess CPE (cytopathic effects) by RSV A2 virus identified a racemic hit **1** with an *in vitro* EC₅₀ = 202 nM (**Figure 1.3A**).

GS-5806 functions by locking RSV-F in the pre-fusion conformation and preventing the subsequent conformational change required for fusion with the host cell membrane thereby preventing entry of the virus.¹⁰⁰ In healthy adult volunteers inoculated with RSV, GS-5806

reduced symptom scores and viral replication ^{101, 102} and in a direct comparison, GS-5806 offered a greater therapeutic index than VP-14637, TMC-353121, BMS-433771, BI-D, YM-53403, RSV604, and ribavirin. ⁹⁸ Mutations that confer resistance to GS-5806 map to the fusion peptide (L138F and F140L) or heptad repeat B (HRB) (F488L/S) regions of RSV-F. GS-5806 resistant mutants also exhibited resistance to other inhibitors of RSV-F such as VP-14637. Similarly, mutations within RSV-F fusion peptide and HRB domains that confer resistance to other fusion inhibitors reduced the efficacy of GS-5806. ¹⁰³ Interestingly, GS-5806 resistant mutants are still susceptible to palivizumab, and ribavirin and the converse is true as well. This means that should resistance to one treatment option arise, an efficacious therapeutic in the form of either palivizumab or GS-5806 will remain. In April of 2017, GS-5806 completed phase 2b clinical trials in adults hospitalized with RSV, however, results have not been released (NCT02135614).

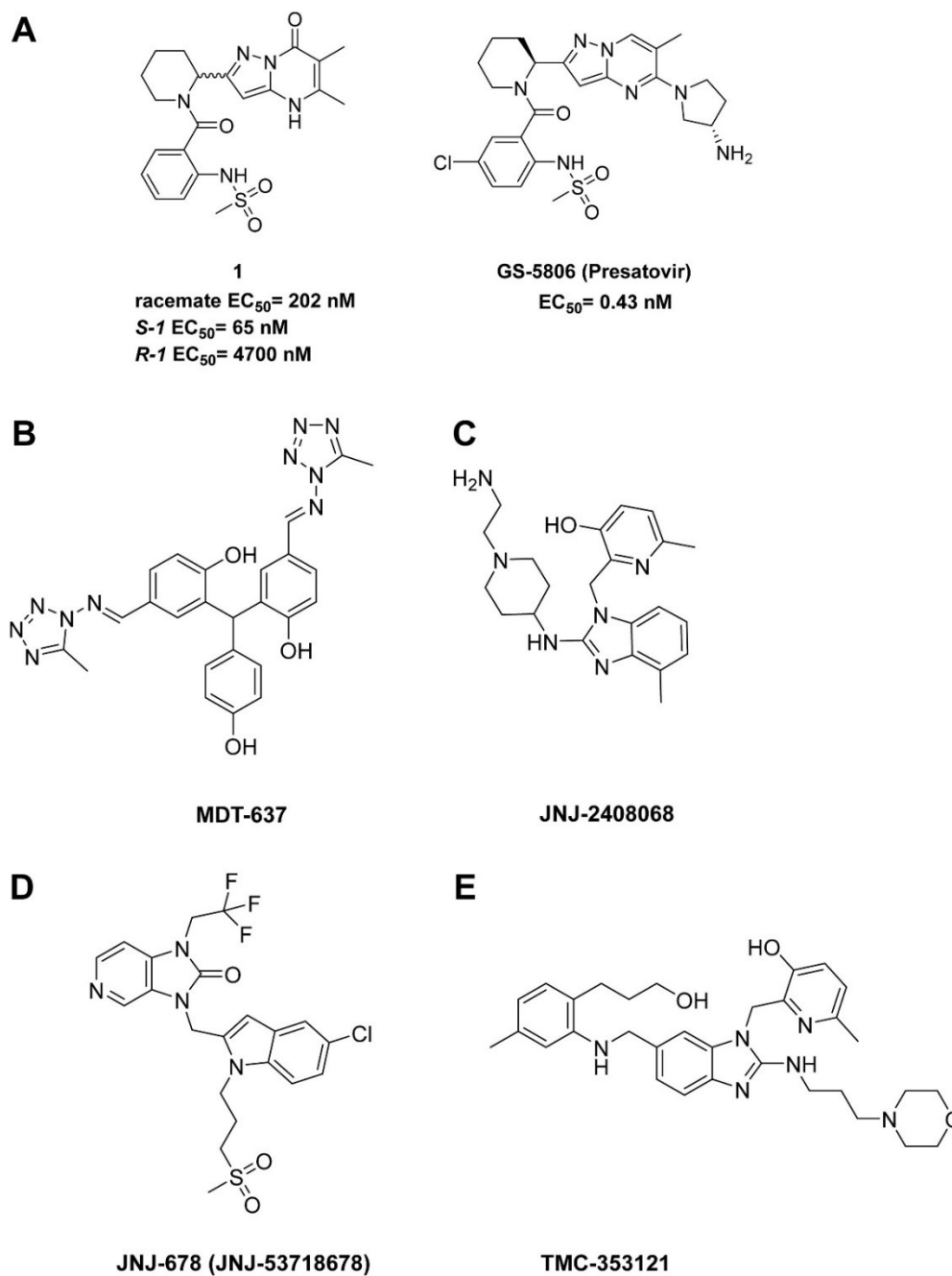


Figure 1.3: Structures of RSV fusion and entry inhibitors.

Recently, in a phase 2 clinical trial, presatovir was unsuccessful at improving virological and clinical outcomes ⁶, in that there was no significant change in RSV viral load over nine days of infection. Furthermore, the need for supplemental oxygen and mechanical ventilation was no

different between the placebo and presatovir treatment groups. As with many antivirals that target virus entry, one must consider that failure of the trial may have been due to treatment delay during the course of patients' infection. We would suggest that entry inhibitor such as presatovir could be more useful as prophylactic drugs that would be administered during RSV seasons to those at risk from infection.

1.5.2.2 MDT-637

MDT-637, formerly known as VP-14637 (**Figure 1.3B**), is a substituted bis-tetrazole-benzhydryl phenol, which has been reported to inhibit RSV cell entry. Evaluation of MDT-637 against RSV clinical isolates and cotton rats showed that the compound had a hundred- to thousand-fold greater potency than ribavirin.¹⁰⁴ Moreover, MDT-637 showed broad *in vitro* antiviral activity on clinical strains of different RSV genotypes. Douglas and coworkers used an RSV-induced cell fusion assay to confirm that MDT-637 acts by inhibiting viral fusion.^{105, 106} Drug-resistant variants have been selected and genotypic analysis of the resistant viruses revealed various mutations in the F protein. Structural analysis of the F protein revealed a hydrophobic cavity formed by six amino acids. This pocket can accommodate two hydrophobic residues (F483 and F488) during the formation of the six-helix bundle (6HB).¹⁰⁷ Identifying the mechanism of action of this compound opened the door for a detailed understanding of the mechanism surrounding RSV fusion protein inhibition and hence the progress toward more potent compounds with different scaffolds.

1.5.2.3 JNJ-2408068

JNJ-2408068 is a benzimidazole derivative that has been reported to have potent RSV fusion inhibitory activity (**Figure 1.3C**). Battles and coworkers assessed the antiviral activity of JNJ-2408068 in different cellular RSV assays.¹⁰⁸ JNJ-2408068 binds to a three-fold-symmetric pocket

in the metastable pre-fusion conformation of RSV-F. This binding stabilizes the RSV-F pre-fusion conformation by tethering two regions that undergo a structural arrangement that facilitates membrane fusion. Binding of JNJ-2408068 has revealed a π - π stacking interaction with the aromatic side chains of Phe140 and Phe488 located in the RSV-F fusion peptide and HRB domains (**Figure 1.4**).¹⁰⁵ The fusion peptide and HRB domains are located in the N-terminus and C-terminus of RSV-F, respectively, that undergo conformational rearrangements during the fusion process.

Moreover, the positively charged piperidine nitrogen of JNJ-2408068 reaches down to the negatively charged Asp 486 and Glu 487 in the binding pocket (**Figure 1.4**). This observation showed that the inhibitor acted as an antagonist, with both hydrophobic and electrostatic interactions, to prevent RSV-F rearrangement and stabilize the RSV-F pre-fusion conformation. However, JNJ-2408068 was found to have a long tissue retention time (half-life in the lung is about 153 h), which raised safety concerns and led to a decision surrounding the drug's suitability for further development.

1.5.2.4 JNJ-53718678

JNJ-53718678 (JNJ-678) is another potent RSV-F protein inhibitor developed by Johnson & Johnson (**Figure 1.3D**). Isothermal titration calorimetry (ITC) has been used to assess the binding of JNJ-678 to the RSV fusion protein, involving both pre- and post-fusion F protein conformations.¹⁰⁹ Results showed that the compound bound tightly to the pre-fusion conformation of RSV-F. The compound exhibited exceptionally potent *in vitro* activity against RSV A2 strain with an EC₅₀ of 480 pM. Investigation of the binding mode and structure-activity relationship of this compound compared to other reported fusion inhibitors showed that the same pocket was being targeted. The replacement of the benzimidazole, which has been reported to be essential for

the activity of JNJ-2408068, with an indole moiety retained the antiviral activity. The chloroindole moiety of JNJ-678 was shown by X-ray crystallographic analysis to be involved in a π - π stacking interaction with Phe488 and Phe140 (**Figure 1.4**).

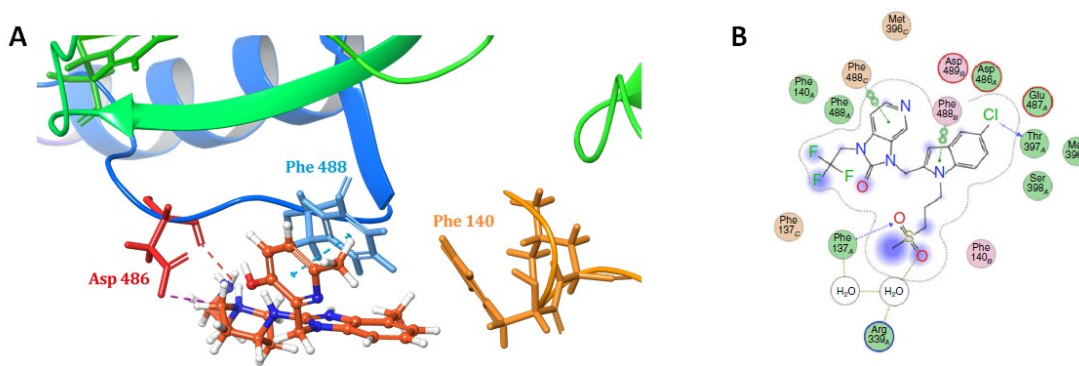


Figure 1.4: Mechanisms of inhibition of two RSV-F entry inhibitors. A, JNJ-2408068 bound to the RSV-F envelope glycoprotein of RSV with important amino acids involved in the binding with hydrogen bonds shown in dashed red lines, ion pairing shown in magenta and π -cation interaction in cyan (PDB accession=5EA3). B, Ligand interaction diagram of JNJ-678 indicating the key binding interactions of the compound with F protein (π - π stacking represented by circled green arrows, Hydrogen, and halogen bonds by green arrows). Adapted with permission from (Dirk Roymans et al.). Copyright 2017 Springer Nature.

In addition, once the compound is bound to the F protein, the chlorine atoms established a halogen bond with the backbone of Thr397 in a sub-pocket formed by amino acids Asp489, Asp486, Thr397 and Phe137. These results confirm that members of this class of compounds share similar mechanisms of binding. Several studies have reported the use of an oral treatment against RSV infections involving the use of JNJ-53718678 and these studies supported the efficacy and safety of this compound in inhibiting viral replication and reducing disease severity in infected adults.^{9,110}

Like GS-5806, JNJ-678 stabilizes the pre-fusion conformation of RSV-F to inhibit viral fusion.¹¹¹ Due to the similar mechanisms of action, it is unsurprising that mutations that confer resistance to JNJ-678 map to regions in the fusion peptide (L141W) or HRB (D489Y) domains of RSV-F. In HeLa cells, the average concentration at which viral infection was reduced by 50% was

0.46 nM. Additionally, JNJ-678 was observed to reduce viral titer and RSV-induced lung inflammation, two major contributors to RSV disease severity, in mouse, cotton rat, and lamb models. As was observed for GS-5806, treatment with JNJ-678 also reduced viral load and symptom scores in healthy adult volunteers experimentally infected with RSV.⁹

1.5.2.5 TMC-353121

Molecular modeling and pharmacokinetics studies were carried out by Johnson & Johnson to identify critical substructures responsible for the long tissue retention time of JNJ-2408068. As a result, TMC-353121, a morpholinopropylaminobenzimidazole RSV fusion inhibitor (**Figure 1.3E**), has been developed as an improved derivative of JNJ-2408068.¹¹² TMC-353121 retained the antiviral activity against RSV F that was seen in the earlier compounds, with a pEC₅₀= 9.9 nM and a half-life around 14h in lung tissues. Preclinical studies in cotton rats and African monkeys revealed a dose-dependent antiviral activity of TMC-353121 varying from one log₁₀ reduction of viral load to complete inhibition of RSV replication.¹¹³ TMC-353121 has been cocrystallized with a construct of the RSV F protein.¹⁰⁷ Analysis of the binding mode of TMC-353121 within the prefusion F protein conformation has shown that this binding did not eliminate all the interactions between the heptad repeats, HR1 and HR2, of the F protein which can be envisioned as a zipper that can close completely in the absence of the inhibitor. However, the binding of TMC-353121 and other benzimidazole RSV-F protein inhibitors, such as JNJ-2408068, induced a distorted form of the RSV fusion protein trimer which rendered the zipper only partially closed. This distortion has been proved to be sufficient to potently inhibit RSV viral replication.^{105, 107}

1.5.2.6 RV521

A fusion inhibitor called RV521 has a favourable 50 % inhibitory concentration in vitro of about 1 nM. The drug candidate, developed by ReViral in the United Kingdom has undergone a

phase 2a, double blind, placebo controlled human challenge study of antiviral efficacy.¹¹⁴ Participants were medicated with the experimental medication five days after challenge with RSV or when infection was detected. Both viral load and disease severity were reduced significantly, and recovery of viral load back to detection threshold was faster in those treated with both 350 mg and 200 mg doses of the inhibitor. The reported treatment emergent adverse events were mild and transient. In summary, the RSV research and drug development community will be watching the development of this compound in further clinical trials in the years to come.

1.5.3 Replication inhibitors

1.5.3.1 RSV604

RSV-N plays indispensable roles in RNA transcription and replication given that it is an essential component of the RSV polymerase complex. A compelling antiviral compound that targets RSV-N is RSV604. One mechanism of action proposed for RSV604 involves direct binding of RSV-N by RSV604 to prevent interaction of accessory proteins required for optimal viral transcription.¹¹⁵ It is not unexpected that interference with a variety of target proteins inhibits RSV RdRp, given the essential nature of multiple viral and cellular proteins. Specifically, cellular proteins, including heat shock protein 90 (HSP90), are necessary for optimal RdRp processivity.¹¹⁶ Antagonism of any RdRp enzymatic process or antagonism of interactions between RdRp constituents are mechanisms by which antivirals may inhibit RSV replication (**Table 1.1**).

1.5.3.2 ALN-RSV01

Alternatively, siRNAs are being explored as a potential RSV antiviral. The RNA interference response in host cells is triggered by siRNA loaded onto argonaute proteins in mammals to form

the RNA-induced Silencing Complex (RISC), an endoribonuclease that degrades sequence specific mRNA transcripts and is responsible for translation repression.¹¹⁷

ALN-RSV01 is the first antiviral siRNA approved for testing in clinical trials that targets RSV-N transcripts. In a phase 2 clinical trial using healthy adult volunteers inoculated with RSV, ALN-RSV01 given prophylactically reduced the number of volunteers infected.²⁸ In a separate phase 2 clinical trial, ALN-RSV01 was administered to adult lung transplant recipients with RSV infections. While ALN-RSV01 reduced progression of bronchiolitis obliterans syndrome, no reduction was observed in symptom severity, viral shedding, or viral load.¹¹⁸ ALN-RSV01 completed phase 2b clinical trials in May 2012 but the results have not yet been posted (NCT01065935).

1.5.4 Nucleoside and non-nucleoside inhibitors of RSV-L

Nucleoside analogues have long been a cornerstone of antiviral research. In 1963, the deoxyuridine analogue idoxuridine, used to treat HSV eye infections, became the first licensed antiviral. In 1985, azidothymidine (AZT) became the first nucleoside reverse transcriptase inhibitor and drug licensed to treat HIV infection. Most recently, the hepatitis C virus (HCV) antiviral nucleotide analogue, Sofosbuvir, was licensed. HCV is a blood borne pathogen in which chronic infection can lead to a lifelong disease. Sofosbuvir offers the first curative treatment for HCV infection.¹¹⁹ Of the nucleoside analogues our group has tested experimentally, modest antiviral activity against RSV was noted for cytarabine⁸⁶, a chemotherapeutic cytosine analogue.¹²⁰

To date, 32 compounds derived from nucleosides have been approved for clinical use against HIV, HBV, HCV, HSV, VZV, HCMV, and IAV.^{119, 121} Nucleoside analogues typically take

advantage of the reliance of viruses on viral polymerase complexes for replication. Interfering with these polymerase complexes can result in chain termination or catastrophic mutagenesis through non-complementary base pairing.¹¹⁹ Nucleoside analogues have previously been investigated for antiviral activity against RSV. Two nucleoside analogues which inhibit RSV replication, ribavirin and lumicitabine, have been described.¹²² Ribavirin is a potent inhibitor of RSV replication in cell culture while lumicitabine has demonstrated efficacy in adult human volunteers, but it is currently halted after phase 2 clinical trials (Table 1.1).¹²²

1.5.4.1 Nucleoside analogues as RSV antivirals

Nucleoside analogues have proven effective as a cure for chronic infections like hepatitis-C and controlling HIV infection and transmission. However, they are not without their side-effects like lipodystrophy, headaches, bone loss, and kidney, liver, and pancreas damage. Therefore, it is important to determine the side-effects in children and whether the benefits of treating an acute infection like RSV, with a nucleoside analogue outweigh the cons, especially in children. One must remember that, with respect to pharmacology, children can respond quite differently to drugs, than adults do. However, nucleoside analogues like zidovudine (azidothymidine) have proven safe and effective at preventing vertical HIV transmission in newborns. Whether they will be effective and safe in the treatment of acute infectious disease in infants and children remains unclear.

1.5.4.1.1 Ribavirin

In 1972, synthesis of 1,2,4-triazole nucleosides in the pursuit of antiviral compounds led to the discovery of ribavirin (1- β -D-ribofuranosyl-1,2,4-triazole-3-carboxamide) (**Figure 1.5**). In this initial study, *in vitro* antiviral activity was described for a broad array of many different viruses: VSV, PIV-3, RV, herpes simplex virus type 1 (HSV1), herpes simplex virus type 2 (HSV2), pseudorabies virus, murine cytomegalovirus (mCMV), vaccinia virus, myxoma virus, adenovirus

(AdV), parainfluenza virus type 1 (PIV-1), influenza A virus (IAV), influenza B virus (IBV), coxsackievirus, and poliovirus.¹²³ Ribavirin was later found to also have antiviral activity against RSV, HCV, HIV, Sendai virus, MeV, and Newcastle virus.¹²⁴⁻¹³¹ In the clinic, ribavirin plus pegylated IFN was the standard of care for HCV infection for many years until this treatment was surpassed by curative direct-acting antivirals^{132, 133}, but due to its toxicity and limited efficacy it has fallen out of favour in the clinic.

Ribavirin is effective against RSV in cell culture, with reported effective concentration 50% (EC₅₀) values of 6.3 to 28.38 μ M.^{124-126, 134, 135} Given the efficacy of ribavirin in cell culture, it has been widely used to validate screening assays, provide a point of reference for compounds identified in these screens, and offers a standard through which different screening assays can be compared.

1.5.4.1.2 PC786

PC786 contrasts lumicitabine as it is a nonnucleoside small molecule inhibitor of RSV-L.¹³⁶ During serial passaging of PC786, escape mutants (RSV-L Y1631H or Y1631L) emerged at passage three. As PC786 is not a nucleoside analogue it is not surprising that the locations of mutations differed between lumicitabine and PC786. The RSV-L Y1631H mutation also conferred resistance to PC786 parent compounds AZ-27 and YM-53403.^{125, 137} While the mechanisms of inhibition differ, lumicitabine and PC786 both target RSV-L and it will be interesting to learn whether similar compounds target RSV-L or another component of the RdRp complex.^{137, 138} PC786 development has been halted after Phase 2 clinical trials (NCT03382431).

1.5.4.1.3 ALS-8112

Wang *et al.* (Alios BioPharma) developed a series of novel sugar-modified nucleosides that inhibited RSV polymerase in a cell-based assay (**Figure 1.5**).¹³⁹ The modified nucleoside analogues were also converted to their 5'-triphosphate counterparts and were tested against RSV isolates for their activity against viral polymerization. The phenotypic screening identified 4'-azido-2'-deoxy-2',2'-difluorocytidine as a potent inhibitor of RSV-induced cytopathic effect with an EC₅₀ of 1 μM. Similar analogues have previously been reported to inhibit HCV polymerase.¹⁴⁰ However, due to reports of potential safety concerns caused by 4'-azidocytidine prodrugs in phase 2 clinical trials, the search for other analogue(s) with specific RSV inhibitory activity and safety margin was a necessity.¹⁴¹ Optimization processes led to the identification of novel nucleoside analogues, including the 4'-chloromethylene compound ALS-8112 (**Figure 4B**), with improved potency and selectivity against RSV polymerase. The RSV-L protein was identified as the molecular target of ALS-8112 by the characterization of drug resistance-associated mutations in the L gene.¹⁴² The 5'-triphosphate form of ALS-8112 (ALS-8112-TP) caused chain termination of RNA synthesis and inhibition of RSV viral polymerization activity in enzymatic assays. ALS-8112-TP did not show any inhibitory activity against host or HCV polymerases proving its specificity against RSV polymerase.

1.5.4.1.4 Lumicitabine (ALS-8176)

Poor oral bioavailability of ALS-8112 necessitated the use of a prodrug strategy to overcome this problem which resulted in the development of ALS-8176, a 3',5'-di-*O*-isobutyryl-2'-fluorocytidine prodrug of ALS-8112.¹³⁹ (**Figure 1.5**) Following entry into the host cell, lumicitabine is triphosphorylated and competes with cytidine triphosphate for access to RSV RdRp. Lumicitabine binds RSV RdRp near the active site and results in chain termination. The

parent compound of lumicitabine also inhibits PIV-3 and VSV RdRp *in vitro*. Interestingly, slight structural modifications to lumicitabine conferred activity against HCV RdRp, a positive sense ssRNA virus.¹⁴³ Serial passaging of RSV in the presence of increasing concentrations of lumicitabine yielded resistant mutants. These mutants possessed 4 amino acid substitution mutations, each mapping to the third conserved region of RSV RdRp within motif B which lies near the catalytic active site. These mutations included RSV-L M628L, A789V, L795I, and I796V.

There were promising results from lumicitabine clinical trials where adult volunteers were experimentally challenged with RSV. Participants were inoculated with RSV and began treatment with lumicitabine after infection was confirmed by RT-PCR. This scenario resembled a more realistic scenario where infection would be confirmed prior to treatment. Here, it was found that lumicitabine reduced viral load and duration of infection.¹²² It should be noted that this is the furthest RSV-L inhibitors have progressed in clinical trials to date. There were promising results from lumicitabine clinical trials where adult volunteers were experimentally challenged with RSV. Participants were inoculated with RSV and began treatment with lumicitabine after infection was confirmed by RT-PCR. This scenario resembled a more realistic scenario where infection would be confirmed prior to treatment. Here, it was found that lumicitabine reduced viral load and duration of infection.¹²² It should be noted that this is the furthest RSV-L inhibitors have progressed in clinical trials to date. Unfortunately, clinical trials studying lumicitabine were recently cancelled (late 2018). An ascending dose study in infants hospitalized with RSV infection showed treatment-emergent neutrophil abnormalities. This result led to a cessation of further clinical trials with lumicitabine.¹⁴⁴

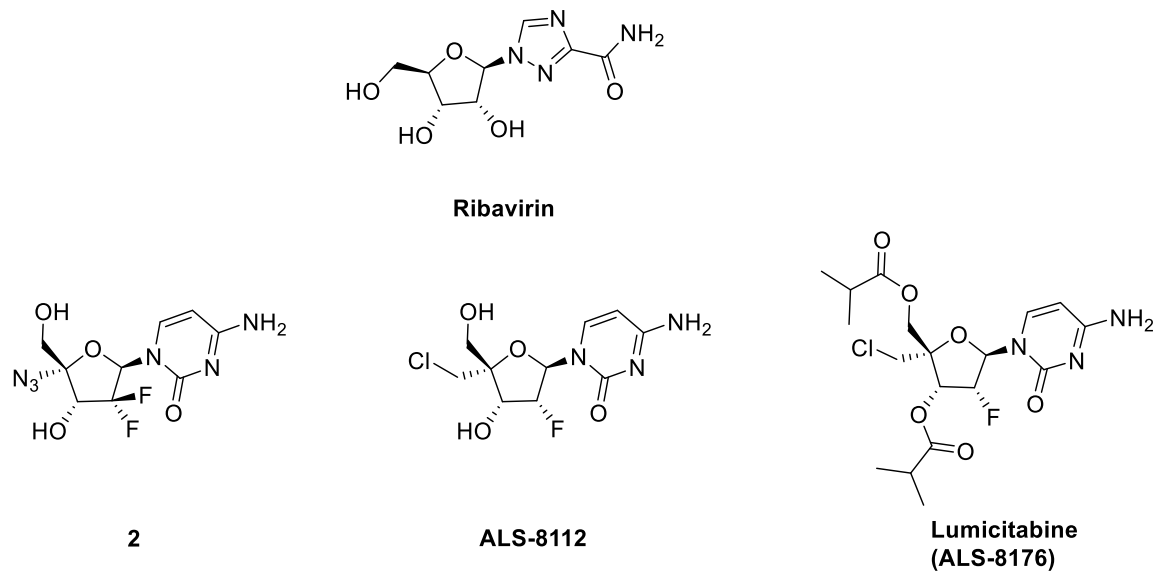


Figure 1.5 : Nucleoside analogues inhibitors of RSV polymerase.

1.6 Biologicals; therapeutic antibodies

Biologicals have been extensively investigated for potential therapeutic use against RSV infection. Palivizumab was originally licensed for prophylactic treatment against RSV in high-risk infants and failed to demonstrate efficacy as a therapeutic intervention during ongoing infection.^{145,}
¹⁴⁶ Motavizumab is a humanized monoclonal antibody which was derived from palivizumab. Motavizumab failed to gain regulatory approval for prophylactic or therapeutic treatment against RSV infection after hypersensitivity reactions were observed and no improved efficacy versus palivizumab was observed. The most recent attempt at producing a biologic intervention was ALX-0171; heavy chain antibody fragments generated in llamas were genetically linked via glycine-serine segments to form trimeric nanobodies.^{147, 148} Results in cotton rats were promising, with 2-log reductions in viral titers observed. A phase 1 clinical trial is ongoing (NCT02979431).

1.6.1 Nirsevimab MEDI 8897

A new prophylactic monoclonal called nirsevimab (MEDI 8897) is being developed by MedImmune, Astra Zeneca.^{149, 150} This new monoclonal antibody will be an improvement over palivizumab in that it has a longer half-life of about 70 days (as opposed to palivizumab's 20 days), requiring only one intramuscular injection a season. Furthermore, whereas palivizumab binds to site II on the side of pre- and post-fusion RSV-F protein, nirsevimab neutralises RSV by binding to the prefusion RSV-F glycoprotein at the more sensitive neutralisation site Ø, at the apex of the RSV-F glycoprotein. It has completed a phase 1 trial in adults¹⁵¹ and a phase 1/2a trial in infants.¹⁵⁰ The phase 2b trial was conducted on infants between 29 weeks 0 days and 34 weeks 6 days gestation, and those who were entering their first full RSV season at the time of screening.

1.7 Vaccines

A fundamental challenge to the development of RSV vaccines is that natural infection with RSV in immunocompetent adults offers very little protection.¹⁵² Any vaccine will need to elicit a stronger immune response than natural infection and do so in the absence of deleterious side effects. RSV is able to either evade or suppress memory IgA B cells. Measles virus infection is similar in this regard that was overcome with a replication competent live-attenuated vaccine. So far, all attenuated RSV vaccines strategies have failed clinical trials.

1.7.1 The first failed RSV vaccine

Shortly after the discovery of RSV, Kim *et al* in the 1960s attempted to develop a vaccine through formalin inactivation of RSV.¹⁵³ This approach had been successful for Jonas Salk, who had recently developed the world's first vaccine against poliovirus.¹⁵⁴ A clinical trial was completed with a group of 31 infants less than one year of age. These infants were primarily from

African American and families of low socioeconomic status.¹⁵³ The increase in neutralizing antibodies following immunization was limited to a 4-fold increase in 43% of immunized infants and this rise in neutralizing antibodies afforded no protection from natural infection during the subsequent RSV season. Instead, enhanced respiratory disease (ERD) was observed upon natural infection. 80% of RSV-infected vaccinated infants required hospitalization while only 5% of the control group required hospitalization. In the vaccinated group the duration of hospitalization was significantly increased, the rate of serious complications increased, and two infants died. Understandably, this tragedy stunted RSV vaccine development campaigns.

1.7.2 Enhanced respiratory disease

Over the ensuing decades, mechanisms of ERD have been proposed. One explanation for ERD is based on the pathogenic deposition of antibody-antigen immune complexes (IC) in the lungs. While IC formation can be beneficial towards virus neutralization during viremia, the deposition of ICs into tissue drives the pathogenesis of a variety of infectious and autoimmune diseases.¹⁵⁵ In mice vaccinated with formalin-inactivated RSV (FI-RSV), ERD (measured as an increase in airway hyperresponse) and IC formation in the lungs was observed. ERD was absent in complement-deficient mice and in B cell-deficient mice (which lack antibodies required for IC formation).¹⁵⁶ The authors concluded that IC deposition in the lungs and subsequent complement activation drives ERD following vaccination with FI-RSV. This study relies on airway hyperresponse acting as an appropriate measure of ERD, which is only modestly appropriate. However, the authors bolster their conclusions by noting extensive complement activation in lung biopsies obtained from the two infants who succumbed to ERD in the vaccine trial by Kim *et al*

153

Building on these results, Delgado *et al.* observed that FI-RSV elicited non-protective low-avidity antibodies.¹⁵⁷ Insufficient TLR stimulation in plasmacytoid dendritic cells (pDCs) resulted in reduced CD4⁺ T lymphocyte proliferation and activation. Resultantly, B cells failed to form germinal centers and undergo the affinity maturation process necessary for increasing antibody avidity. In this study, complementing FI-RSV vaccination with UV-inactivated RSV was sufficient to induce a protective antibody response.

1.7.3 Lessons learned about enhanced respiratory disease

In the wake of the failed vaccine attempt by Kim *et al.*, candidate vaccines are now carefully monitored for ERD in animal models (the cotton rat model is especially useful for detecting ERD) prior to clinical trials. While no vaccine has been developed to treat RSV, neither has any vaccine which elicits ERD entered clinical trials in infants. Modern RSV vaccination attempts have included the production of immunogenic nanoparticles¹⁵⁸ or generation of live-attenuated RSV virus vaccines through random mutagenesis, guided attenuation through recombinant RSV generation, or generation of recombinant bovine RSV or PIV expressing human RSV-F and RSV-G (reviewed¹⁵⁹). Owing to the difficult challenge of generating an immune response in the first months of life when protection against RSV is most important, maternal vaccination strategies are also currently being explored in a phase 3 clinical trial (NCT02624947).

1.7.4 Live attenuated RSV vaccines in clinical trials

1.7.4.1 cpts248/404

cpts248/404 was the last live attenuated vaccine candidate to enter clinical trials prior to the utilization of recombinant genetic engineering technologies to introduce specific mutations. “cp” and “ts” refer to mutations generated through cold passaging or chemical mutagenesis-induced

temperature sensitive mutations, respectively.¹⁵⁹ In phase I clinical trials, *cpts248/404* was tested in steadily younger age cohorts, culminating in administration to infants less than two months of age.¹⁶⁰ In seropositive children between 15 and 59 months of age *cpts248/404* live virus was not shed, and antibody responses were nearly non-existent. In seronegative children less than 24 months of age, *cpts248/404* live virus was shed and neutralizing antibodies against RSV were observed in serum, however, this study was not powered to determine the efficacy of protection against natural RSV infection. In the youngest cohort of 1- to 2-month-old infants, neutralizing antibody development was rare – as is the case for natural infection in this age group. As expected, maternal antibody levels antagonized the development of most infant antibody responses, including IgG antibodies against RSV-F and RSV -G, and IgA antibodies against RSV-F. Finally, congestion associated with peak *cpts248/404* shedding precluded the vaccine candidate from further study in the 1- to 2-month-old cohort.¹⁶⁰

1.7.4.2 MEDI-559

MEDI-559 is an attenuated mutant RSV molecular virus clone that was created via reverse genetics. *Cpts248/404* was further attenuated by deletion of RSV-SH and introduction of a temperature sensitive Y1321K mutation in RSV-L.¹⁶¹ In RSV-seronegative children aged 5 to 24 months of age, MEDI-559 produced neutralizing antibody responses in 59% of infants versus 9% for the placebo group. Protection from natural RSV infection was not measured. Lower respiratory tract illness was higher in the MEDI-559 arm than placebo yet was comparable to the rate observed in placebo groups in other studies making the safety of MEDI-559 difficult to interpret.¹⁶¹ To date, subsequent clinical trials on MEDI-559 have not been initiated. Results are not available for other live attenuated vaccine virus candidates including MEDI- Δ M2-2 which lacks the RSV-M2-2 gene (NCT01459198) or a genetically stabilized version of MEDI-599 (NCT01852266). Lastly, results

are not available for RSV Δ NS2 Δ I1313 I1314L which lacks RSV-NS2, has a deletion of the 1313 codon in the RSV-L protein, and a temperature sensitive mutation introduced through an I1314L mutation in the RSV-L protein (NCT01893554).

1.7.5 Subunit vaccines in clinical trials

Novavax has led the development of nanoparticle-based RSV vaccines. Nanoparticles were created through infection of Sf9 insect cells with a recombinant baculovirus containing a modified RSV-F gene. RSV-F nanoparticles consist of multiple peptide homotrimers joined via a micelle core.¹⁵⁸ A phase 3 clinical trial in adults over 60 years of age observed no protection against lower respiratory tract infection (0.47% in the vaccinated group versus 0.44% in the placebo arm) (NCT02608502). A separate phase 3 clinical trial is ongoing to investigate whether immunization of pregnant women in their third trimester with the RSV-F nanoparticle confers protection to infants via maternal antibodies (NCT02624947). It is estimated that this study will be completed in June of 2020.

1.8 Prophylaxis

1.8.1 Efficacy and cost-effectiveness of palivizumab

Palivizumab is a humanized monoclonal antibody containing murine-origin complementarity-determining regions specific for the pre-fusion conformation of RSV-F.¹⁶² Palivizumab was licensed for prophylactic treatment against RSV infection in high-risk infants following the IMpact clinical trial. This clinical trial included 1502 infants born at less than 35 weeks gestational age.¹⁶³ Monthly administration of palivizumab in premature infants without bronchopulmonary dysplasia, a type of chronic lung disease (CLD), reduced the rate of hospitalization in this cohort from 8.1 % in the placebo arm to 1.8% in the palivizumab arm ($P < 0.001$). For infants with bronchopulmonary

dysplasia the rate of hospitalization was reduced from 12.8% to 7.9% between placebo and treated groups, respectively (P = 0.038). Shortly thereafter, another large clinical trial was focused specifically on 1287 infants with hemodynamically significant chronic heart disease (CHD). This study observed a reduction in hospitalization from 9.7% to 5.3% (P = 0.003) ¹⁶⁴. Subsequent population-based studies typically confirmed that palivizumab effectively reduced the rate of hospitalization due to RSV infection.¹⁶⁵ Owing to these successes in clinical trials, palivizumab is widely prescribed to high-risk infants.

Many limitations reduce the impact of palivizumab on the annual RSV burden of disease. These include prohibitive cost, the time burden on families and physicians associated with monthly injections throughout the RSV season, the lack of efficacy against ongoing infection, and the development of resistant RSV strains. Cost-benefit analyses vary widely between studies and study populations. Hampf *et al.* found that for premature infants in Florida, 30 infants must be treated to avoid a single hospitalization; thus, the cost per hospitalization avoided in this population was approximately \$302,103. This is dramatically more expensive than the cost of hospitalization in this region, approximately \$8,910 per infant in this population.¹⁶⁶ In contrast, for inhabitants of Baffin Island in Nunavut where medical evacuation to the Children's Hospital of Eastern Ontario drastically increases the cost of hospitalization, administering palivizumab to all infants less than 6 months of age (as opposed to only high-risk infants) may be a cost-effective strategy.¹⁶⁷ The Canadian Pediatric Society notes that palivizumab treatment in Canada costs approximately \$5,600 per infant, and the number needed to treat to prevent hospitalization ranges from 16-23 for various high-risk groups.¹⁵ As such, outside of Baffin Island palivizumab is not a cost-effective treatment. Currently, the Canadian Pediatric Society recommends prophylactic palivizumab

treatment for preterm infants, infants with CHD, immunocompromised infants, and infants with CLD.¹⁵

Palivizumab has been examined as an intervention to treat serious RSV infection, and a significant reduction in tracheal RSV concentration was observed.¹⁶⁸ However, treatment with palivizumab did not produce clinically relevant benefits as there was no reduction in the duration of hospitalization, duration of mechanical ventilation, or duration of supplemental oxygen therapy.¹⁶⁸ Similarly, other studies have found no clinically relevant benefits of treatment of RSV infection with palivizumab.¹⁶⁹

1.8.2 RSV drug resistance

As an RNA virus with an error-prone RdRp, RSV exists as a quasispecies.¹⁷⁰ Therefore, RSV is expected to have the capacity to rapidly develop mutations which confer resistance to antiviral interventions. The clinical implications of these resistant mutants depend on the fitness cost associated with each mutation. Prior to the licensure of palivizumab, RSV mutations in the antigenic A site of the RSV-F protein had already been observed to confer resistance to antibody peptide fragments.¹⁷¹ Resistance to palivizumab was first noted via the K272M mutation in RSV-F which developed readily in cell culture during serial passaging in increasing palivizumab concentrations.¹⁷² This mutation was not associated with a reduction in fitness as growth kinetics in cell culture were not affected. Resistance to palivizumab via the K272M mutation was confirmed *in vivo* in the Cotton Rat model. The known list of RSV-F mutations which confer resistance to palivizumab has grown to include N262S, N268I, K272N, K272T, K272Q, S275F, and S275L.¹⁷³ An RSV strain with an RSV-F K272E mutation was the first clinic isolate with suspected resistance to palivizumab.¹⁷⁴ In untreated populations, mutations associated with resistance are less common yet remain present. Of 145 untreated infants infected with RSV,

palivizumab-resistant isolates RSV-F N262D and S275F were identified with a frequency of 0.7% each.¹⁷³ Some studies have found that wild type RSV strains outcompete palivizumab-resistant RSV strains in direct competition assays.¹⁷⁵ This has likely limited the spread of palivizumab-resistant strains in the general population. Studies specifically examining whether palivizumab efficacy has been reduced since licensure, due to the circulation of resistant strains, have not been conducted. These results on palivizumab, which was once thought to target a conserved epitope on RSV¹⁷⁶, suggest that resistance mutations to new biologics will likely emerge and surveillance will have to continue to understand the effect on prophylaxis.

1.9 Preclinical therapeutic models of RSV infection

There have been many *in vivo* models that have been developed to study the efficacy of candidate RSV therapeutics. A variety of model systems for RSV infection are available and include mice, cotton rats, lambs, nonhuman primates, and healthy adult human volunteers.¹⁷⁷ An exhaustive review has been written on these models¹⁷⁸, so we will provide only an outline of the models available for preclinical evaluation of promising anti-RSV compounds.

A variety of animal models exist, with benefits and drawbacks to each. These include the use of lab-adapted and clinical human RSV strains. There are also models of bovine RSV infection in cattle or pneumonia virus of mice (PVM) infection in mice.¹⁷⁷ Mice have been used extensively in the study of RSV, and an interesting range of susceptibility exists between different inbred strains. Stark *et al.* found AKR/J to be the most permissive mouse strain tested, followed by 129P3/J, BALB/cJ, CBA/J, C3H/HeJ, DBA/J, and A/J.¹⁷⁹ Finally, C57/BL6J was the least permissive to RSV infection.¹⁷⁹ It is important to note that in this study all mouse strains were inoculated with 10⁷ plaque forming units (PFU), a relatively high amount of virus. This inoculum reflects how resistant mice are to RSV infection in general.

Cotton rats are a popular small animal model of RSV infection. Infection in the upper and lower respiratory tracts can be established with an intranasal inoculation with 10^4 PFU and resultant peak viral titers are approximately 100-fold higher than in mice.¹⁸⁰ Therefore, cotton rats are much more susceptible to RSV infection. A limitation of the cotton rat model is that symptoms during infection are limited.¹⁷⁷ This limitation is not as critical in antiviral studies as viral titers can simply be measured in lung homogenates. However, this would limit the applicability of the cotton rat model for studying enhancement of RSV infection severity. Cotton rats have been used in preclinical studies of RSV antiviral compounds including JNJ-678¹¹¹, TMC353121¹⁸¹, MDT-637, BMS-433771, and BTA-C585.¹⁸⁰ Cotton rats would provide a good small animal model for examining the antiviral effects of certain compounds against RSV *in vivo*, before moving on to larger animals or adult human volunteer challenge studies.

Therefore, answering the aforementioned questions on clinical efficacy will require a new line of experimentation. It is essential to monitor disease severity through a variety of parameters including weight loss, viral load in the lungs, airway hyper responsiveness, and airway inflammation. Selecting the appropriate animal model will be important to studying the effect of compounds on disease severity.

1.10 Conclusions

RSV infection imposes a significant burden of disease on infants, the elderly, and immunocompromised individuals. Despite intensive efforts, no efficacious antivirals to treat RSV infection are available, nor are vaccines available to prevent infection. The discovery of compounds with antiviral activity against RSV is of paramount importance.

Despite a decades long search, an efficacious antiviral drug for the treatment of RSV infection has not been discovered. To address the substantial burden of disease imposed by RSV, more drugs need to be identified and tested in clinical trials. Therefore, there is still room to design new protocols which could rapidly identify compounds with antiviral activity against RSV.

In this thesis, we describe a computer-aided drug design campaign to design, synthesize and evaluate a new series of bis(indole) compounds as broad-spectrum antiviral agents based on the compounds previously published by our group.¹⁸²

In Chapter 2, we investigated the RSV polymerase complex with the aim of identifying the target of the bis(indole) compounds. MD simulations were carried out for: 1) minimizing the protein structure and relax residue clashes, 2) identify potential allosteric binding sites, and 3) evaluate the best hit compound from the previous virological screening for model validation. Afterwards, the newly designed compounds were ranked based on their relative binding energy to the protein and synthesized using a straightforward synthetic strategy previously developed in the West lab. *In vitro* virological evaluation of several compounds using RSV progeny assay and qPCR is described.

Chapter 3 comprise an in-depth computational approach for the identification of allosteric binding site on the SARS-CoV-2 replication complex. The molecular docking and MD simulations along with binding pose metadynamics studies that led to the design of a new library of compounds with potentially better activity is discussed. Compounds were ranked based on their interactions and binding affinity and synthesized for biological screening. The antiviral evaluation identified two compounds with substantially improved inhibitory effect on the SARS-CoV-2 viral polymerase compared to the parent compound.

Chapter 4 describes the discovery of a single amino acid mutation on the RSV fusion glycoprotein (RSV F) that can switch the virus from type A to type B. Computational modelling, reverse genetics, and viral evolution experiments are described. In this chapter, we describe the discovery on a new way of viral evasion under sterilizing conditions with by only one amino acid which affects the virus susceptibility to antibodies and patient serum neutralization.

Chapter 5 provides a general summary of the thesis findings regarding the development of a novel class of antiviral inhibitors with the potential of combating several RNA viruses. It also addresses the future work needed for the advancement of these compounds from *bench-to bedside*.

1.11 References

1. Rima, B.; Collins, P.; Easton, A.; Fouchier, R.; Kurath, G.; Lamb, R. A.; Lee, B.; Maisner, A.; Rota, P.; Wang, L.; Ictv Report, C., ICTV Virus Taxonomy Profile: Pneumoviridae. *J Gen Virol* **2017**, *98*, 2912-2913.
2. Blount, R. E., Jr.; Morris, J. A.; Savage, R. E., Recovery of cytopathogenic agent from chimpanzees with coryza. *Proc Soc Exp Biol Med* **1956**, *92*, 544-9.
3. Chanock, R.; Finberg, L., Recovery from infants with respiratory illness of a virus related to chimpanzee coryza agent (CCA). II. Epidemiologic aspects of infection in infants and young children. *Am J Hyg* **1957**, *66*, 291-300.
4. Andrew, J. D.; Gardner, P. S., Occurrence of Respiratory Syncytial Virus in Acute Respiratory Diseases in Infancy. *Br Med J* **1963**, *2*, 1447-8.
5. Morales, F.; Calder, M. A.; Inglis, J. M.; Murdoch, P. S.; Williamson, J., A study of respiratory infections in the elderly to assess the role of respiratory syncytial virus. *J Infect* **1983**, *7*, 236-47.
6. Marty, F. M.; Chemaly, R. F.; Mullane, K. M.; Lee, D. G.; Hirsch, H. H.; Small, C. B.; Bergeron, A.; Shoham, S.; Ljungman, P.; Waghmare, A.; Blanchard, E.; Kim, Y. J.; McKeivitt, M.; Porter, D. P.; Jordan, R.; Guo, Y.; German, P.; Boeckh, M.; Watkins, T. R.; Chien, J. W.; Dadwal, S. S., A Phase 2b, Randomized, Double-blind, Placebo-Controlled Multicenter Study Evaluating Antiviral Effects, Pharmacokinetics, Safety, and Tolerability of Presatovir in Hematopoietic Cell Transplant Recipients with Respiratory Syncytial Virus (RSV) Infection of the Lower Respiratory Tract. *Clin Infect Dis* **2019**.
7. Ruckwardt, T. J.; Morabito, K. M.; Graham, B. S., Immunological Lessons from Respiratory Syncytial Virus Vaccine Development. *Immunity* **2019**, *51*, 429-442.
8. Jares Baglivo, S.; Polack, F. P., The long road to protect infants against severe RSV lower respiratory tract illness. *Fl000Res* **2019**, *8*.
9. Stevens, M.; Rusch, S.; DeVincenzo, J.; Kim, Y. I.; Harrison, L.; Meals, E. A.; Boyers, A.; Fok-Seang, J.; Huntjens, D.; Lounis, N.; Mari, N. K.; Remmerie, B.; Roymans, D.; Koul, A.; Verloes, R., Antiviral Activity of Oral JNJ-53718678 in Healthy Adult Volunteers Challenged With Respiratory Syncytial Virus: A Placebo-Controlled Study. *J Infect Dis* **2018**, *218*, 748-756.
10. Smith, D. W.; Frankel, L. R.; Mathers, L. H.; Tang, A. T.; Ariagno, R. L.; Prober, C. G., A controlled trial of aerosolized ribavirin in infants receiving mechanical ventilation for severe respiratory syncytial virus infection. *N Engl J Med* **1991**, *325*, 24-9.

11. Smith, E. A., "Management of the infant with respiratory syncytial virus". *J Pediatr Nurs* **1991**, 6, 434.
12. Meert, K. L.; Sarnaik, A. P.; Gelmini, M. J.; Lieh-Lai, M. W., Aerosolized ribavirin in mechanically ventilated children with respiratory syncytial virus lower respiratory tract disease: a prospective, double-blind, randomized trial. *Crit Care Med* **1994**, 22, 566-72.
13. Law, B. J.; Wang, E. E.; MacDonald, N.; McDonald, J.; Dobson, S.; Boucher, F.; Langley, J.; Robinson, J.; Mitchell, I.; Stephens, D., Does ribavirin impact on the hospital course of children with respiratory syncytial virus (RSV) infection? An analysis using the pediatric investigators collaborative network on infections in Canada (PICNIC) RSV database. *Pediatrics* **1997**, 99, E7.
14. Hardelid, P.; Verfuenden, M.; McMenamin, J.; Smyth, R. L.; Gilbert, R., The contribution of child, family and health service factors to respiratory syncytial virus (RSV) hospital admissions in the first 3 years of life: birth cohort study in Scotland, 2009 to 2015. *Euro Surveill* **2019**, 24.
15. Robinson, J. L.; Le Saux, N.; Canadian Paediatric Society, I. D.; Immunization, C., Preventing hospitalizations for respiratory syncytial virus infection. *Paediatr Child Health* **2015**, 20, 321-33.
16. Murray, J.; Bottle, A.; Sharland, M.; Modi, N.; Aylin, P.; Majeed, A.; Saxena, S.; Medicines for Neonates Investigator, G., Risk factors for hospital admission with RSV bronchiolitis in England: a population-based birth cohort study. *PLoS One* **2014**, 9, e89186.
17. Shi, T.; Denouel, A.; Tietjen, A. K.; Campbell, I.; Moran, E.; Li, X.; Campbell, H.; Demont, C.; Nyawanda, B. O.; Chu, H. Y.; Stoszek, S. K.; Krishnan, A.; Openshaw, P.; Falsey, A. R.; Nair, H.; Investigators, R., Global Disease Burden Estimates of Respiratory Syncytial Virus-Associated Acute Respiratory Infection in Older Adults in 2015: A Systematic Review and Meta-Analysis. *J Infect Dis* **2019**.
18. Chanock, R. M.; Murphy, B. R.; Collins, P. L.; Coelingh, K. V.; Olmsted, R. A.; Snyder, M. H.; Spriggs, M. K.; Prince, G. A.; Moss, B.; Flores, J.; et al., Live viral vaccines for respiratory and enteric tract diseases. *Vaccine* **1988**, 6, 129-33.
19. Leader, S.; Jacobson, P.; Marcin, J.; Vardis, R.; Sorrentino, M.; Murray, D., A method for identifying the financial burden of hospitalized infants on families. *Value Health* **2002**, 5, 55-9.
20. Mitchell, I.; Defoy, I.; Grubb, E., Burden of Respiratory Syncytial Virus Hospitalizations in Canada. *Can Respir J* **2017**, 2017, 4521302.
21. Paes, B.; Mitchell, I.; Li, A.; Lanctot, K. L., Respiratory hospitalizations and respiratory syncytial virus prophylaxis in special populations. *Eur J Pediatr* **2012**, 171, 833-41.

22. Paes, B. A.; Mitchell, I.; Banerji, A.; Lanctot, K. L.; Langley, J. M., A decade of respiratory syncytial virus epidemiology and prophylaxis: translating evidence into everyday clinical practice. *Can Respir J* **2011**, *18*, e10-9.
23. Nair, H.; Nokes, D. J.; Gessner, B. D.; Dherani, M.; Madhi, S. A.; Singleton, R. J.; O'Brien, K. L.; Roca, A.; Wright, P. F.; Bruce, N.; Chandran, A.; Theodoratou, E.; Sutanto, A.; Sedyaningsih, E. R.; Ngama, M.; Munywoki, P. K.; Kartasasmita, C.; Simoes, E. A.; Rudan, I.; Weber, M. W.; Campbell, H., Global burden of acute lower respiratory infections due to respiratory syncytial virus in young children: a systematic review and meta-analysis. *Lancet* **2010**, *375*, 1545-55.
24. Shi, T.; McAllister, D. A.; O'Brien, K. L.; Simoes, E. A. F.; Madhi, S. A.; Gessner, B. D.; Polack, F. P.; Balsells, E.; Acacio, S.; Aguayo, C.; Alassani, I.; Ali, A.; Antonio, M.; Awasthi, S.; Awori, J. O.; Azziz-Baumgartner, E.; Baggett, H. C.; Baillie, V. L.; Balmaseda, A.; Barahona, A.; Basnet, S.; Bassat, Q.; Basualdo, W.; Bigogo, G.; Bont, L.; Breiman, R. F.; Brooks, W. A.; Broor, S.; Bruce, N.; Bruden, D.; Buchy, P.; Campbell, S.; Carosone-Link, P.; Chadha, M.; Chipeta, J.; Chou, M.; Clara, W.; Cohen, C.; de Cuellar, E.; Dang, D. A.; Dash-Yandag, B.; Deloria-Knoll, M.; Dherani, M.; Eap, T.; Ebruke, B. E.; Echavarria, M.; de Freitas Lazaro Emediato, C. C.; Fasce, R. A.; Feikin, D. R.; Feng, L.; Gentile, A.; Gordon, A.; Goswami, D.; Goyet, S.; Groome, M.; Halasa, N.; Hirve, S.; Homaira, N.; Howie, S. R. C.; Jara, J.; Jroundi, I.; Kartasasmita, C. B.; Khuri-Bulos, N.; Kotloff, K. L.; Krishnan, A.; Libster, R.; Lopez, O.; Lucero, M. G.; Lucion, F.; Lupisan, S. P.; Marcone, D. N.; McCracken, J. P.; Mejia, M.; Moisi, J. C.; Montgomery, J. M.; Moore, D. P.; Moraleda, C.; Moyes, J.; Munywoki, P.; Mutyara, K.; Nicol, M. P.; Nokes, D. J.; Nymadawa, P.; da Costa Oliveira, M. T.; Oshitani, H.; Pandey, N.; Paranhos-Baccala, G.; Phillips, L. N.; Picot, V. S.; Rahman, M.; Rakoto-Andrianarivelo, M.; Rasmussen, Z. A.; Rath, B. A.; Robinson, A.; Romero, C.; Russomando, G.; Salimi, V.; Sawatwong, P.; Scheltema, N.; Schweiger, B.; Scott, J. A. G.; Seidenberg, P.; Shen, K.; Singleton, R.; Sotomayor, V.; Strand, T. A.; Sutanto, A.; Sylla, M.; Tapia, M. D.; Thamthitawat, S.; Thomas, E. D.; Tokarz, R.; Turner, C.; Venter, M.; Waicharoen, S.; Wang, J.; Watthanaworawit, W.; Yoshida, L. M.; Yu, H.; Zar, H. J.; Campbell, H.; Nair, H.; Network, R. S. V. G. E., Global, regional, and national disease burden estimates of acute lower respiratory infections due to respiratory syncytial virus in young children in 2015: a systematic review and modelling study. *Lancet* **2017**, *390*, 946-958.
25. Carrat, F.; Vergu, E.; Ferguson, N. M.; Lemaître, M.; Cauchemez, S.; Leach, S.; Valleron, A. J., Time lines of infection and disease in human influenza: a review of volunteer challenge studies. *Am J Epidemiol* **2008**, *167*, 775-85.
26. Jefferson, T.; Jones, M. A.; Doshi, P.; Del Mar, C. B.; Hama, R.; Thompson, M. J.; Spencer, E. A.; Onakpoya, I.; Mahtani, K. R.; Nunan, D.; Howick, J.; Heneghan, C. J., Neuraminidase inhibitors for preventing and treating influenza in healthy adults and children. *Cochrane Database Syst Rev* **2014**, CD008965.

27. Bagga, B.; Woods, C. W.; Veldman, T. H.; Gilbert, A.; Mann, A.; Balaratnam, G.; Lambkin-Williams, R.; Oxford, J. S.; McClain, M. T.; Wilkinson, T.; Nicholson, B. P.; Ginsburg, G. S.; Devincenzo, J. P., Comparing influenza and RSV viral and disease dynamics in experimentally infected adults predicts clinical effectiveness of RSV antivirals. *Antivir Ther* **2013**, *18*, 785-91.
28. DeVincenzo, J. P.; Wilkinson, T.; Vaishnav, A.; Cehelsky, J.; Meyers, R.; Nochur, S.; Harrison, L.; Meeking, P.; Mann, A.; Moane, E.; Oxford, J.; Pareek, R.; Moore, R.; Walsh, E.; Studholme, R.; Dorsett, P.; Alvarez, R.; Lambkin-Williams, R., Viral load drives disease in humans experimentally infected with respiratory syncytial virus. *Am J Respir Crit Care Med* **2010**, *182*, 1305-14.
29. El Saleeby, C. M.; Bush, A. J.; Harrison, L. M.; Aitken, J. A.; Devincenzo, J. P., Respiratory syncytial virus load, viral dynamics, and disease severity in previously healthy naturally infected children. *J Infect Dis* **2011**, *204*, 996-1002.
30. Griffiths, C.; Drews, S. J.; Marchant, D. J., Respiratory Syncytial Virus: Infection, Detection, and New Options for Prevention and Treatment. *Clin Microbiol Rev* **2017**, *30*, 277-319.
31. Sloan, C.; Heaton, M.; Kang, S.; Berrett, C.; Wu, P.; Gebretsadik, T.; Sicignano, N.; Evans, A.; Lee, R.; Hartert, T., The impact of temperature and relative humidity on spatiotemporal patterns of infant bronchiolitis epidemics in the contiguous United States. *Health Place* **2017**, *45*, 46-54.
32. Welliver, R. C., Sr., Temperature, humidity, and ultraviolet B radiation predict community respiratory syncytial virus activity. *Pediatr Infect Dis J* **2007**, *26*, S29-35.
33. Janet, S.; Broad, J.; Snape, M. D., Respiratory syncytial virus seasonality and its implications on prevention strategies. *Hum Vaccin Immunother* **2018**, *14*, 234-244.
34. Bilawchuk, L. M.; Griffiths, C. D.; Jensen, L. D.; Elawar, F.; Marchant, D. J., The Susceptibilities of Respiratory Syncytial Virus to Nucleolin Receptor Blocking and Antibody Neutralization are Dependent upon the Method of Virus Purification. *Viruses* **2017**, *9*.
35. Collins, P. L.; Graham, B. S., Viral and host factors in human respiratory syncytial virus pathogenesis. *J Virol* **2008**, *82*, 2040-55.
36. Trento, A.; Casas, I.; Calderon, A.; Garcia-Garcia, M. L.; Calvo, C.; Perez-Brena, P.; Melero, J. A., Ten years of global evolution of the human respiratory syncytial virus BA genotype with a 60-nucleotide duplication in the G protein gene. *J Virol* **2010**, *84*, 7500-12.

37. Elawar, F.; Griffiths, C. D.; Zhu, D.; Bilawchuk, L. M.; Jensen, L. D.; Forss, L.; Tang, J.; Hazes, B.; Drews, S. J.; Marchant, D. J., A Virological and Phylogenetic Analysis of the Emergence of New Clades of Respiratory Syncytial Virus. *Sci Rep* **2017**, *7*, 12232.
38. Morawska, L., Droplet fate in indoor environments, or can we prevent the spread of infection? *Indoor Air* **2006**, *16*, 335-47.
39. Hall, C. B.; Douglas, R. G., Jr.; Geiman, J. M., Possible transmission by fomites of respiratory syncytial virus. *J Infect Dis* **1980**, *141*, 98-102.
40. Hall, C. B.; Douglas, R. G., Jr., Modes of transmission of respiratory syncytial virus. *J Pediatr* **1981**, *99*, 100-3.
41. Kulkarni, H.; Smith, C. M.; Lee Ddo, H.; Hirst, R. A.; Easton, A. J.; O'Callaghan, C., Evidence of Respiratory Syncytial Virus Spread by Aerosol. Time to Revisit Infection Control Strategies? *Am J Respir Crit Care Med* **2016**, *194*, 308-16.
42. Roy, C. J.; Milton, D. K., Airborne transmission of communicable infection--the elusive pathway. *N Engl J Med* **2004**, *350*, 1710-2.
43. Cruz-Sanchez, T. M.; Haddrell, A. E.; Hackett, T. L.; Singhera, G. K.; Marchant, D.; Lekivetz, R.; Meredith, A.; Horne, D.; Knight, D. A.; van Eeden, S. F.; Bai, T. R.; Hegele, R. G.; Dorscheid, D. R.; Agnes, G. R., Formation of a stable mimic of ambient particulate matter containing viable infectious respiratory syncytial virus and its dry-deposition directly onto cell cultures. *Anal Chem* **2013**, *85*, 898-906.
44. Zlateva, K. T.; Lemey, P.; Vandamme, A. M.; Van Ranst, M., Molecular evolution and circulation patterns of human respiratory syncytial virus subgroup a: positively selected sites in the attachment g glycoprotein. *J Virol* **2004**, *78*, 4675-83.
45. Grad, Y. H.; Newman, R.; Zody, M.; Yang, X.; Murphy, R.; Qu, J.; Malboeuf, C. M.; Levin, J. Z.; Lipsitch, M.; DeVincenzo, J., Within-host whole-genome deep sequencing and diversity analysis of human respiratory syncytial virus infection reveals dynamics of genomic diversity in the absence and presence of immune pressure. *J Virol* **2014**, *88*, 7286-93.
46. Martinello, R. A.; Chen, M. D.; Weibel, C.; Kahn, J. S., Correlation between respiratory syncytial virus genotype and severity of illness. *J Infect Dis* **2002**, *186*, 839-42.
47. Laham, F. R.; Mansbach, J. M.; Piedra, P. A.; Hasegawa, K.; Sullivan, A. F.; Espinola, J. A.; Camargo, C. A., Jr., Clinical Profiles of Respiratory Syncytial Virus Subtypes A AND B Among Children Hospitalized with Bronchiolitis. *Pediatr Infect Dis J* **2017**, *36*, 808-810.

48. Walsh, E. E.; McConnochie, K. M.; Long, C. E.; Hall, C. B., Severity of Respiratory Syncytial Virus Infection Is Related to Virus Strain. *JID* **1997**, *175*, 814-820.
49. Fodha, I.; Vabret, A.; Ghedira, L.; Seboui, H.; Chouchane, S.; Dewar, J.; Gueddiche, N.; Trabelsi, A.; Boujaafar, N.; Freymuth, F., Respiratory syncytial virus infections in hospitalized infants: association between viral load, virus subgroup, and disease severity. *J Med Virol* **2007**, *79*, 1951-8.
50. Devincenzo, J. P., Natural infection of infants with respiratory syncytial virus subgroups A and B: a study of frequency, disease severity, and viral load. *Pediatr Res* **2004**, *56*, 914-7.
51. Buckingham, S. C.; Bush, A. J.; Devincenzo, J. P., Nasal quantity of respiratory syncytial virus correlates with disease severity in hospitalized infants. *Pediatr Infect Dis J* **2000**, *19*, 113-7.
52. Barik, S., Respiratory syncytial virus mechanisms to interfere with type 1 interferons. *Curr Top Microbiol Immunol* **2013**, *372*, 173-91.
53. Bitko, V.; Shulyayeva, O.; Mazumder, B.; Musiyenko, A.; Ramaswamy, M.; Look, D. C.; Barik, S., Nonstructural proteins of respiratory syncytial virus suppress premature apoptosis by an NF-kappaB-dependent, interferon-independent mechanism and facilitate virus growth. *J Virol* **2007**, *81*, 1786-95.
54. Wu, W.; Tran, K. C.; Teng, M. N.; Heesom, K. J.; Matthews, D. A.; Barr, J. N.; Hiscox, J. A., The interactome of the human respiratory syncytial virus NS1 protein highlights multiple effects on host cell biology. *J Virol* **2012**, *86*, 7777-89.
55. Zhang, W.; Yang, H.; Kong, X.; Mohapatra, S.; San Juan-Vergara, H.; Hellermann, G.; Behera, S.; Singam, R.; Lockey, R. F.; Mohapatra, S. S., Inhibition of respiratory syncytial virus infection with intranasal siRNA nanoparticles targeting the viral NS1 gene. *Nat Med* **2005**, *11*, 56-62.
56. Vasou, A.; Paulus, C.; Narloch, J.; Gage, Z. O.; Rameix-Welti, M. A.; Eleouet, J. F.; Nevels, M.; Randall, R. E.; Adamson, C. S., Modular cell-based platform for high throughput identification of compounds that inhibit a viral interferon antagonist of choice. *Antiviral Res* **2018**, *150*, 79-92.
57. Collins, P. L.; Melero, J. A., Progress in understanding and controlling respiratory syncytial virus: still crazy after all these years. *Virus Res* **2011**, *162*, 80-99.
58. Tawar, R. G.; Duquerroy, S.; Vonrhein, C.; Varela, P. F.; Damier-Piolle, L.; Castagne, N.; MacLellan, K.; Bedouelle, H.; Bricogne, G.; Bhella, D.; Eleouet, J. F.; Rey, F. A., Crystal structure of a nucleocapsid-like nucleoprotein-RNA complex of respiratory syncytial virus. *Science* **2009**, *326*, 1279-83.

59. Lifland, A. W.; Jung, J.; Alonas, E.; Zurla, C.; Crowe, J. E., Jr.; Santangelo, P. J., Human respiratory syncytial virus nucleoprotein and inclusion bodies antagonize the innate immune response mediated by MDA5 and MAVS. *J Virol* **2012**, *86*, 8245-58.
60. Mogensen, T. H., Pathogen recognition and inflammatory signaling in innate immune defenses. *Clin Microbiol Rev* **2009**, *22*, 240-73, Table of Contents.
61. Yoneyama, M.; Kikuchi, M.; Natsukawa, T.; Shinobu, N.; Imaizumi, T.; Miyagishi, M.; Taira, K.; Akira, S.; Fujita, T., The RNA helicase RIG-I has an essential function in double-stranded RNA-induced innate antiviral responses. *Nat Immunol* **2004**, *5*, 730-7.
62. Yoneyama, M.; Kikuchi, M.; Matsumoto, K.; Imaizumi, T.; Miyagishi, M.; Taira, K.; Foy, E.; Loo, Y. M.; Gale, M., Jr.; Akira, S.; Yonehara, S.; Kato, A.; Fujita, T., Shared and unique functions of the DExD/H-box helicases RIG-I, MDA5, and LGP2 in antiviral innate immunity. *J Immunol* **2005**, *175*, 2851-8.
63. Hornung, V.; Ellegast, J.; Kim, S.; Brzozka, K.; Jung, A.; Kato, H.; Poeck, H.; Akira, S.; Conzelmann, K. K.; Schlee, M.; Endres, S.; Hartmann, G., 5'-Triphosphate RNA is the ligand for RIG-I. *Science* **2006**, *314*, 994-7.
64. Clemens, M. J.; Hershey, J. W.; Hovanessian, A. C.; Jacobs, B. C.; Katze, M. G.; Kaufman, R. J.; Lengyel, P.; Samuel, C. E.; Sen, G. C.; Williams, B. R., PKR: proposed nomenclature for the RNA-dependent protein kinase induced by interferon. *J Interferon Res* **1993**, *13*, 241.
65. Garcia, C. S.; Curiel, R. E.; Mwatibo, J. M.; Pestka, S.; Li, H.; Espinoza-Delgado, I., The antineoplastic agent bryostatin-1 differentially regulates IFN-gamma receptor subunits in monocytic cells: transcriptional and posttranscriptional control of IFN-gamma R2. *J Immunol* **2006**, *177*, 2707-16.
66. Clemens, M. J.; Elia, A., The double-stranded RNA-dependent protein kinase PKR: structure and function. *J Interferon Cytokine Res* **1997**, *17*, 503-24.
67. Groskreutz, D. J.; Babor, E. C.; Monick, M. M.; Varga, S. M.; Hunninghake, G. W., Respiratory syncytial virus limits alpha subunit of eukaryotic translation initiation factor 2 (eIF2alpha) phosphorylation to maintain translation and viral replication. *J Biol Chem* **2010**, *285*, 24023-31.
68. Gilman, M. S. A.; Liu, C.; Fung, A.; Behera, I.; Jordan, P.; Rigaux, P.; Ysebaert, N.; Tcherniuk, S.; Sourimant, J.; Eleouet, J. F.; Sutto-Ortiz, P.; Decroly, E.; Roymans, D.; Jin, Z.; McLellan, J. S., Structure of the Respiratory Syncytial Virus Polymerase Complex. *Cell* **2019**, *179*, 193-204 e14.

69. Hara, K.; Yaita, K.; Khamrin, P.; Kumthip, K.; Kashiwagi, T.; Eleouet, J. F.; Rameix-Welti, M. A.; Watanabe, H., A small fragmented P protein of respiratory syncytial virus inhibits virus infection by targeting P protein. *J Gen Virol* **2020**, *101*, 21-32.
70. Kiss, G.; Holl, J. M.; Williams, G. M.; Alonas, E.; Vanover, D.; Lifland, A. W.; Gudheti, M.; Guerrero-Ferreira, R. C.; Nair, V.; Yi, H.; Graham, B. S.; Santangelo, P. J.; Wright, E. R., Structural analysis of respiratory syncytial virus reveals the position of M2-1 between the matrix protein and the ribonucleoprotein complex. *J Virol* **2014**, *88*, 7602-17.
71. Johnson, S. M.; McNally, B. A.; Ioannidis, I.; Flano, E.; Teng, M. N.; Oomens, A. G.; Walsh, E. E.; Peeples, M. E., Respiratory Syncytial Virus Uses CX3CR1 as a Receptor on Primary Human Airway Epithelial Cultures. *PLoS Pathog* **2015**, *11*, e1005318.
72. Lingemann, M.; McCarty, T.; Liu, X.; Buchholz, U. J.; Surman, S.; Martin, S. E.; Collins, P. L.; Munir, S., The alpha-1 subunit of the Na⁺,K⁺-ATPase (ATP1A1) is required for macropinocytic entry of respiratory syncytial virus (RSV) in human respiratory epithelial cells. *PLoS Pathog* **2019**, *15*, e1007963.
73. Krzyzaniak, M. A.; Zumstein, M. T.; Gerez, J. A.; Picotti, P.; Helenius, A., Host cell entry of respiratory syncytial virus involves macropinocytosis followed by proteolytic activation of the F protein. *PLoS Pathog* **2013**, *9*, e1003309.
74. Malhotra, R.; Ward, M.; Bright, H.; Priest, R.; Foster, M. R.; Hurle, M.; Blair, E.; Bird, M., Isolation and characterisation of potential respiratory syncytial virus receptor(s) on epithelial cells. *Microbes Infect* **2003**, *5*, 123-33.
75. Marchant, D.; Singhera, G. K.; Utokaparch, S.; Hackett, T. L.; Boyd, J. H.; Luo, Z.; Si, X.; Dorscheid, D. R.; McManus, B. M.; Hegele, R. G., Toll-like receptor 4-mediated activation of p38 mitogen-activated protein kinase is a determinant of respiratory virus entry and tropism. *J Virol* **2010**, *84*, 11359-73.
76. Behera, A. K.; Matsuse, H.; Kumar, M.; Kong, X.; Lockey, R. F.; Mohapatra, S. S., Blocking intercellular adhesion molecule-1 on human epithelial cells decreases respiratory syncytial virus infection. *Biochem Biophys Res Commun* **2001**, *280*, 188-95.
77. Tayyari, F.; Marchant, D.; Moraes, T. J.; Duan, W.; Mastrangelo, P.; Hegele, R. G., Identification of nucleolin as a cellular receptor for human respiratory syncytial virus. *Nat Med* **2011**, *17*, 1132-5.
78. McLellan, J. S.; Chen, M.; Leung, S.; Graepel, K. W.; Du, X.; Yang, Y.; Zhou, T.; Baxa, U.; Yasuda, E.; Beaumont, T.; Kumar, A.; Modjarrad, K.; Zheng, Z.; Zhao, M.; Xia, N.; Kwong, P. D.; Graham, B. S., Structure of RSV fusion glycoprotein trimer bound to a prefusion-specific neutralizing antibody. *Science* **2013**, *340*, 1113-7.

79. Karron, R. A.; Buonagurio, D. A.; Georgiu, A. F.; Whitehead, S. S.; Adamus, J. E.; Clements-Mann, M. L.; Harris, D. O.; Randolph, V. B.; Udem, S. A.; Murphy, B. R.; Sidhu, M. S., Respiratory syncytial virus (RSV) SH and G proteins are not essential for viral replication in vitro: clinical evaluation and molecular characterization of a cold-passaged, attenuated RSV subgroup B mutant. *Proc Natl Acad Sci U S A* **1997**, *94*, 13961-6.
80. Bukreyev, A.; Yang, L.; Collins, P. L., The secreted G protein of human respiratory syncytial virus antagonizes antibody-mediated restriction of replication involving macrophages and complement. *J Virol* **2012**, *86*, 10880-4.
81. Bukreyev, A.; Whitehead, S. S.; Murphy, B. R.; Collins, P. L., Recombinant respiratory syncytial virus from which the entire SH gene has been deleted grows efficiently in cell culture and exhibits site-specific attenuation in the respiratory tract of the mouse. *J Virol* **1997**, *71*, 8973-82.
82. Whitehead, S. S.; Bukreyev, A.; Teng, M. N.; Firestone, C. Y.; St Claire, M.; Elkins, W. R.; Collins, P. L.; Murphy, B. R., Recombinant respiratory syncytial virus bearing a deletion of either the NS2 or SH gene is attenuated in chimpanzees. *J Virol* **1999**, *73*, 3438-42.
83. Karron, R. A.; Wright, P. F.; Belshe, R. B.; Thumar, B.; Casey, R.; Newman, F.; Polack, F. P.; Randolph, V. B.; Deatly, A.; Hackell, J.; Gruber, W.; Murphy, B. R.; Collins, P. L., Identification of a recombinant live attenuated respiratory syncytial virus vaccine candidate that is highly attenuated in infants. *J Infect Dis* **2005**, *191*, 1093-104.
84. Selvaraj, M.; Yegambaram, K.; Todd, E.; Richard, C. A.; Dods, R. L.; Pangratiou, G. M.; Trinh, C. H.; Moul, S. L.; Murphy, J. C.; Mankouri, J.; Eleouet, J. F.; Barr, J. N.; Edwards, T. A., The Structure of the Human Respiratory Syncytial Virus M2-1 Protein Bound to the Interaction Domain of the Phosphoprotein P Defines the Orientation of the Complex. *MBio* **2018**, *9*.
85. Bouillier, C.; Cosentino, G.; Leger, T.; Rincheval, V.; Richard, C. A.; Desquesnes, A.; Sitterlin, D.; Blouquit-Laye, S.; Eleouet, J. F.; Gault, E.; Rameix-Welti, M. A., The Interactome analysis of the Respiratory Syncytial Virus protein M2-1 suggests a new role in viral mRNA metabolism post-transcription. *Sci Rep* **2019**, *9*, 15258.
86. Tchesnokov, E. P.; Raesisimakiani, P.; Ngure, M.; Marchant, D.; Gotte, M., Recombinant RNA-Dependent RNA Polymerase Complex of Ebola Virus. *Sci Rep* **2018**, *8*, 3970.
87. Fearn, R.; Collins, P. L., Model for polymerase access to the overlapped L gene of respiratory syncytial virus. *J Virol* **1999**, *73*, 388-97.

88. Noton, S. L.; Deflube, L. R.; Tremaglio, C. Z.; Fearn, R., The respiratory syncytial virus polymerase has multiple RNA synthesis activities at the promoter. *PLoS Pathog* **2012**, *8*, e1002980.
89. Grosfeld, H.; Hill, M. G.; Collins, P. L., RNA replication by respiratory syncytial virus (RSV) is directed by the N, P, and L proteins; transcription also occurs under these conditions but requires RSV superinfection for efficient synthesis of full-length mRNA. *J Virol* **1995**, *69*, 5677-86.
90. Collins, P. L.; Hill, M. G.; Cristina, J.; Grosfeld, H., Transcription elongation factor of respiratory syncytial virus, a nonsegmented negative-strand RNA virus. *Proc Natl Acad Sci U S A* **1996**, *93*, 81-5.
91. Collins, P. L.; Hill, M. G.; Camargo, E.; Grosfeld, H.; Chanock, R. M.; Murphy, B. R., Production of infectious human respiratory syncytial virus from cloned cDNA confirms an essential role for the transcription elongation factor from the 5' proximal open reading frame of the M2 mRNA in gene expression and provides a capability for vaccine development. *Proc Natl Acad Sci U S A* **1995**, *92*, 11563-7.
92. Poch, O.; Sauvaget, I.; Delarue, M.; Tordo, N., Identification of four conserved motifs among the RNA-dependent polymerase encoding elements. *EMBO J* **1989**, *8*, 3867-74.
93. Cowton, V. M.; McGivern, D. R.; Fearn, R., Unravelling the complexities of respiratory syncytial virus RNA synthesis. *J Gen Virol* **2006**, *87*, 1805-21.
94. Barik, S., The structure of the 5' terminal cap of the respiratory syncytial virus mRNA. *J Gen Virol* **1993**, *74* (Pt 3), 485-90.
95. Dupuy, L. C.; Dobson, S.; Bitko, V.; Barik, S., Casein kinase 2-mediated phosphorylation of respiratory syncytial virus phosphoprotein P is essential for the transcription elongation activity of the viral polymerase; phosphorylation by casein kinase 1 occurs mainly at Ser(215) and is without effect. *J Virol* **1999**, *73*, 8384-92.
96. Asenjo, A.; Calvo, E.; Villanueva, N., Phosphorylation of human respiratory syncytial virus P protein at threonine 108 controls its interaction with the M2-1 protein in the viral RNA polymerase complex. *J Gen Virol* **2006**, *87*, 3637-42.
97. Broadbent, L.; Groves, H.; Shields, M. D.; Power, U. F., Respiratory syncytial virus, an ongoing medical dilemma: an expert commentary on respiratory syncytial virus prophylactic and therapeutic pharmaceuticals currently in clinical trials. *Influenza Other Respir Viruses* **2015**, *9*, 169-78.
98. Perron, M.; Stray, K.; Kinkade, A.; Theodore, D.; Lee, G.; Eisenberg, E.; Sangi, M.; Gilbert, B. E.; Jordan, R.; Piedra, P. A.; Toms, G. L.; Mackman, R.; Cihlar, T., GS-5806 Inhibits a Broad Range of

- Respiratory Syncytial Virus Clinical Isolates by Blocking the Virus-Cell Fusion Process. *Antimicrob Agents Chemother* **2015**, *60*, 1264-73.
99. Mackman, R. L.; Sangi, M.; Sperandio, D.; Parrish, J. P.; Eisenberg, E.; Perron, M.; Hui, H.; Zhang, L.; Siegel, D.; Yang, H.; Saunders, O.; Booramra, C.; Lee, G.; Samuel, D.; Babaoglu, K.; Carey, A.; Gilbert, B. E.; Piedra, P. A.; Strickley, R.; Iwata, Q.; Hayes, J.; Stray, K.; Kinkade, A.; Theodore, D.; Jordan, R.; Desai, M.; Cihlar, T., Discovery of an Oral Respiratory Syncytial Virus (RSV) Fusion Inhibitor (GS-5806) and Clinical Proof of Concept in a Human RSV Challenge Study. *J. Med. Chem.* **2015**, *58*, 1630-1643.
100. Samuel, D.; Xing, W.; Niedziela-Majka, A.; Wong, J. S.; Hung, M.; Brendza, K. M.; Perron, M.; Jordan, R.; Sperandio, D.; Liu, X.; Mackman, R.; Sakowicz, R., GS-5806 inhibits pre- to postfusion conformational changes of the respiratory syncytial virus fusion protein. *Antimicrob Agents Chemother* **2015**, *59*, 7109-12.
101. Mackman, R. L.; Sangi, M.; Sperandio, D.; Parrish, J. P.; Eisenberg, E.; Perron, M.; Hui, H.; Zhang, L.; Siegel, D.; Yang, H.; Saunders, O.; Booramra, C.; Lee, G.; Samuel, D.; Babaoglu, K.; Carey, A.; Gilbert, B. E.; Piedra, P. A.; Strickley, R.; Iwata, Q.; Hayes, J.; Stray, K.; Kinkade, A.; Theodore, D.; Jordan, R.; Desai, M.; Cihlar, T., Discovery of an oral respiratory syncytial virus (RSV) fusion inhibitor (GS-5806) and clinical proof of concept in a human RSV challenge study. *J Med Chem* **2015**, *58*, 1630-43.
102. DeVincenzo, J. P.; Whitley, R. J.; Mackman, R. L.; Scaglioni-Weinlich, C.; Harrison, L.; Farrell, E.; McBride, S.; Lambkin-Williams, R.; Jordan, R.; Xin, Y.; Ramanathan, S.; O'Riordan, T.; Lewis, S. A.; Li, X.; Toback, S. L.; Lin, S. L.; Chien, J. W., Oral GS-5806 activity in a respiratory syncytial virus challenge study. *N Engl J Med* **2014**, *371*, 711-22.
103. Stray, K.; Perron, M.; Porter, D. P.; Anderson, F.; Lewis, S. A.; Perry, J.; Miller, M.; Cihlar, T.; DeVincenzo, J.; Chien, J. W.; Jordan, R., Drug resistance assessment following administration of RSV fusion inhibitor presatovir to participants experimentally infected with respiratory syncytial virus. *J Infect Dis* **2020**.
104. Kim, Y.-I.; Pareek, R.; Murphy, R.; Harrison, L.; Farrell, E.; Cook, R.; DeVincenzo, J., The antiviral effects of RSV fusion inhibitor, MDT-637, on clinical isolates, vs its achievable concentrations in the human respiratory tract and comparison to ribavirin. *Influenza and Other Respiratory Viruses* **2017**, *11*, 525-530.
105. Douglas, J. L.; Panis, M. L.; Ho, E.; Lin, K.-Y.; Krawczyk, S. H.; Grant, D. M.; Cai, R.; Swaminathan, S.; Chen, X.; Cihlar, T., Small Molecules VP-14637 and JNJ-2408068 Inhibit Respiratory Syncytial Virus Fusion by Similar Mechanisms. *Antimicrob. Agents Chemother.* **2005**, *49*, 2460.
106. Douglas, J. L.; Panis, M. L.; Ho, E.; Lin, K.-Y.; Krawczyk, S. H.; Grant, D. M.; Cai, R.; Swaminathan, S.; Cihlar, T., Inhibition of Respiratory Syncytial Virus Fusion by the Small Molecule VP-14637 via Specific Interactions with F Protein. *J. Virol.* **2003**, *77*, 5054.

107. Roymans, D.; De Bondt, H. L.; Arnoult, E.; Geluykens, P.; Gevers, T.; Van Ginderen, M.; Verheyen, N.; Kim, H.; Willebrords, R.; Bonfanti, J.-F.; Bruinzeel, W.; Cummings, M. D.; van Vlijmen, H.; Andries, K., Binding of a potent small-molecule inhibitor of six-helix bundle formation requires interactions with both heptad-repeats of the RSV fusion protein. *Proc. Natl. Acad. Sci. USA* **2010**, *107*, 308.
108. Battles, M. B.; Langedijk, J. P.; Furmanova-Hollenstein, P.; Chaiwatpongsakorn, S.; Costello, H. M.; Kwanten, L.; Vranckx, L.; Vink, P.; Jaensch, S.; Jonckers, T. H. M.; Koul, A.; Arnoult, E.; Peeples, M. E.; Roymans, D.; McLellan, J. S., Molecular mechanism of respiratory syncytial virus fusion inhibitors. *Nat. Chem. Biol.* **2016**, *12*, 87-93.
109. Roymans, D.; Alnajjar, S. S.; Battles, M. B.; Sitthicharoenchai, P.; Furmanova-Hollenstein, P.; Rigaux, P.; Berg, J. V. d.; Kwanten, L.; Ginderen, M. V.; Verheyen, N.; Vranckx, L.; Jaensch, S.; Arnoult, E.; Voorzaat, R.; Gallup, J. M.; Larios-Mora, A.; Crabbe, M.; Huntjens, D.; Raboisson, P.; Langedijk, J. P.; Ackermann, M. R.; McLellan, J. S.; Vendeville, S.; Koul, A., Therapeutic efficacy of a respiratory syncytial virus fusion inhibitor. *Nat Commun* **2017**, *8*, 167.
110. Israel, S.; Rusch, S.; DeVincenzo, J.; Boyers, A.; Fok-Seang, J.; Huntjens, D.; Lounis, N.; Mariën, K.; Stevens, M.; Verloes, R., Effect of Oral JNJ-53718678 (JNJ-678) on Disease Severity in Healthy Adult Volunteers Experimentally Inoculated With Live Respiratory Syncytial Virus (RSV): A Placebo-Controlled Challenge Study. *Open Forum Infectious Diseases* **2016**, *3*.
111. Roymans, D.; Alnajjar, S. S.; Battles, M. B.; Sitthicharoenchai, P.; Furmanova-Hollenstein, P.; Rigaux, P.; Berg, J. V. D.; Kwanten, L.; Ginderen, M. V.; Verheyen, N.; Vranckx, L.; Jaensch, S.; Arnoult, E.; Voorzaat, R.; Gallup, J. M.; Larios-Mora, A.; Crabbe, M.; Huntjens, D.; Raboisson, P.; Langedijk, J. P.; Ackermann, M. R.; McLellan, J. S.; Vendeville, S.; Koul, A., Therapeutic efficacy of a respiratory syncytial virus fusion inhibitor. *Nat Commun* **2017**, *8*, 167.
112. Bonfanti, J.-F.; Meyer, C.; Doublet, F.; Fortin, J.; Muller, P.; Queguiner, L.; Gevers, T.; Janssens, P.; Szel, H.; Willebrords, R.; Timmerman, P.; Wuyts, K.; van Remoortere, P.; Janssens, F.; Wigerinck, P.; Andries, K., Selection of a Respiratory Syncytial Virus Fusion Inhibitor Clinical Candidate. 2. Discovery of a Morpholinopropylaminobenzimidazole Derivative (TMC353121). *J. Med. Chem.* **2008**, *51*, 875-896.
113. Ispas, G.; Koul, A.; Verbeeck, J.; Sheehan, J.; Sanders-Beer, B.; Roymans, D.; Andries, K.; Rouan, M.-C.; De Jonghe, S.; Bonfanti, J.-F.; Vanstockem, M.; Simmen, K.; Verloes, R., Antiviral Activity of TMC353121, a Respiratory Syncytial Virus (RSV) Fusion Inhibitor, in a Non-Human Primate Model. *PLoS ONE* **2015**, *10*, e0126959.
114. DeVincenzo, J.; Tait, D.; Efthimiou, J.; Mori, J.; Kim, Y. I.; Thomas, E.; Wilson, L.; Harland, R.; Mathews, N.; Cockerill, S.; Powell, K.; Littler, E., A Randomized, Placebo-Controlled, Respiratory

- Syncytial Virus Human Challenge Study of the Antiviral Efficacy, Safety, and Pharmacokinetics of RV521, an Inhibitor of the RSV-F Protein. *Antimicrob Agents Chemother* **2020**, *64*.
115. Challa, S.; Scott, A. D.; Yuzhakov, O.; Zhou, Y.; Tiong-Yip, C. L.; Gao, N.; Thresher, J.; Yu, Q., Mechanism of action for respiratory syncytial virus inhibitor RSV604. *Antimicrob Agents Chemother* **2015**, *59*, 1080-7.
116. Munday, D. C.; Wu, W.; Smith, N.; Fix, J.; Noton, S. L.; Galloux, M.; Touzelet, O.; Armstrong, S. D.; Dawson, J. M.; Aljabr, W.; Easton, A. J.; Rameix-Welti, M. A.; de Oliveira, A. P.; Simabuco, F. M.; Ventura, A. M.; Hughes, D. J.; Barr, J. N.; Fearn, R.; Digard, P.; Eleouet, J. F.; Hiscox, J. A., Interactome analysis of the human respiratory syncytial virus RNA polymerase complex identifies protein chaperones as important cofactors that promote L-protein stability and RNA synthesis. *J Virol* **2015**, *89*, 917-30.
117. Lam, J. K.; Chow, M. Y.; Zhang, Y.; Leung, S. W., siRNA Versus miRNA as Therapeutics for Gene Silencing. *Mol Ther Nucleic Acids* **2015**, *4*, e252.
118. Gottlieb, J.; Zamora, M. R.; Hodges, T.; Musk, A. W.; Sommerwerk, U.; Dilling, D.; Arcasoy, S.; DeVincenzo, J.; Karsten, V.; Shah, S.; Bettencourt, B. R.; Cehelsky, J.; Nochur, S.; Gollob, J.; Vaishnav, A.; Simon, A. R.; Glanville, A. R., ALN-RSV01 for prevention of bronchiolitis obliterans syndrome after respiratory syncytial virus infection in lung transplant recipients. *J Heart Lung Transplant* **2016**, *35*, 213-21.
119. De Clercq, E.; Li, G., Approved Antiviral Drugs over the Past 50 Years. *Clin Microbiol Rev* **2016**, *29*, 695-747.
120. Lichtman, M. A., A historical perspective on the development of the cytarabine (7days) and daunorubicin (3days) treatment regimen for acute myelogenous leukemia: 2013 the 40th anniversary of 7+3. *Blood Cells Mol Dis* **2013**, *50*, 119-30.
121. De Clercq, E.; Schinazi, R. F., Editorial overview: Antiviral strategies. *Curr Opin Virol* **2016**, *18*, v-vi.
122. DeVincenzo, J. P.; McClure, M. W.; Symons, J. A.; Fathi, H.; Westland, C.; Chanda, S.; Lambkin-Williams, R.; Smith, P.; Zhang, Q.; Beigelman, L.; Blatt, L. M.; Fry, J., Activity of Oral ALS-008176 in a Respiratory Syncytial Virus Challenge Study. *N Engl J Med* **2015**, *373*, 2048-58.
123. Witkowski, J. T.; Robins, R. K.; Sidwell, R. W.; Simon, L. N., Design, synthesis, and broad spectrum antiviral activity of 1-*D*-ribofuranosyl-1,2,4-triazole-3-carboxamide and related nucleosides. *J Med Chem* **1972**, *15*, 1150-4.

124. Kim, Y. I.; Pareek, R.; Murphy, R.; Harrison, L.; Farrell, E.; Cook, R.; DeVincenzo, J., The antiviral effects of RSV fusion inhibitor, MDT-637, on clinical isolates, vs its achievable concentrations in the human respiratory tract and comparison to ribavirin. *Influenza Other Respir Viruses* **2017**, *11*, 525-530.
125. Sudo, K.; Miyazaki, Y.; Kojima, N.; Kobayashi, M.; Suzuki, H.; Shintani, M.; Shimizu, Y., YM-53403, a unique anti-respiratory syncytial virus agent with a novel mechanism of action. *Antiviral Res* **2005**, *65*, 125-31.
126. Chapman, J.; Abbott, E.; Alber, D. G.; Baxter, R. C.; Bithell, S. K.; Henderson, E. A.; Carter, M. C.; Chambers, P.; Chubb, A.; Cockerill, G. S.; Collins, P. L.; Dowdell, V. C.; Keegan, S. J.; Kelsey, R. D.; Lockyer, M. J.; Luongo, C.; Najarro, P.; Pickles, R. J.; Simmonds, M.; Taylor, D.; Tyms, S.; Wilson, L. J.; Powell, K. L., RSV604, a novel inhibitor of respiratory syncytial virus replication. *Antimicrob Agents Chemother* **2007**, *51*, 3346-53.
127. Hong, Z.; Cameron, C. E., Pleiotropic mechanisms of ribavirin antiviral activities. *Prog Drug Res* **2002**, *59*, 41-69.
128. Sidwell, R. W.; Huffman, J. H.; Khare, G. P.; Allen, L. B.; Witkowski, J. T.; Robins, R. K., Broad-spectrum antiviral activity of Virazole: 1-beta-D-ribofuranosyl-1,2,4-triazole-3-carboxamide. *Science* **1972**, *177*, 705-6.
129. Scholtissek, C., Inhibition of influenza RNA synthesis by virazole (ribavirin). *Arch Virol* **1976**, *50*, 349-52.
130. Huffman, J. H.; Sidwell, R. W.; Khare, G. P.; Witkowski, J. T.; Allen, L. B.; Robins, R. K., In vitro effect of 1-beta-D-ribofuranosyl-1,2,4-triazole-3-carboxamide (virazole, ICN 1229) on deoxyribonucleic acid and ribonucleic acid viruses. *Antimicrob Agents Chemother* **1973**, *3*, 235-41.
131. Hruska, J. F.; Bernstein, J. M.; Douglas, R. G., Jr.; Hall, C. B., Effects of ribavirin on respiratory syncytial virus in vitro. *Antimicrob Agents Chemother* **1980**, *17*, 770-5.
132. Feld, J. J.; Liang, T. J., HCV persistence: cure is still a four letter word. *Hepatology* **2005**, *41*, 23-5.
133. Houghton, M., Hepatitis C: the next 25years. *Antiviral Res* **2014**, *110*, 77-8.
134. Tiong-Yip, C. L.; Aschenbrenner, L.; Johnson, K. D.; McLaughlin, R. E.; Fan, J.; Challa, S.; Xiong, H.; Yu, Q., Characterization of a respiratory syncytial virus L protein inhibitor. *Antimicrob Agents Chemother* **2014**, *58*, 3867-73.
135. Noah, J. W.; Severson, W.; Chung, D. H.; Moore, B.; Jia, F.; Xu, X.; Maddox, C.; Rasmussen, L.; Sosa, M. I.; Tower, N. A.; Ananthan, S.; White, E. L.; Jonsson, C.; Matharu, D. S.; Golden, J. E.; Prisinzano,

- T. E.; Aube, J., A Cell Based HTS Approach for the Discovery of New Inhibitors of RSV. In *Probe Reports from the NIH Molecular Libraries Program*, Bethesda (MD), 2010.
136. Coates, M.; Brookes, D.; Kim, Y. I.; Allen, H.; Fordyce, E. A. F.; Meals, E. A.; Colley, T.; Ciana, C. L.; Parra, G. F.; Sherbukhin, V.; Stockwell, J. A.; Thomas, J. C.; Hunt, S. F.; Anderson-Dring, L.; Onions, S. T.; Cass, L.; Murray, P. J.; Ito, K.; Strong, P.; DeVincenzo, J. P.; Rapeport, G., Preclinical Characterization of PC786, an Inhaled Small-Molecule Respiratory Syncytial Virus L Protein Polymerase Inhibitor. *Antimicrob Agents Chemother* **2017**, *61*.
137. Noton, S. L.; Nagendra, K.; Dunn, E. F.; Mawhorter, M. E.; Yu, Q.; Fearn, R., Respiratory Syncytial Virus Inhibitor AZ-27 Differentially Inhibits Different Polymerase Activities at the Promoter. *J Virol* **2015**, *89*, 7786-98.
138. Plant, H.; Stacey, C.; Tiong-Yip, C. L.; Walsh, J.; Yu, Q.; Rich, K., High-Throughput Hit Screening Cascade to Identify Respiratory Syncytial Virus (RSV) Inhibitors. *J Biomol Screen* **2015**, *20*, 597-605.
139. Wang, G.; Deval, J.; Hong, J.; Dyatkina, N.; Prhavic, M.; Taylor, J.; Fung, A.; Jin, Z.; Stevens, S. K.; Serebryany, V.; Liu, J.; Zhang, Q.; Tam, Y.; Chanda, S. M.; Smith, D. B.; Symons, J. A.; Blatt, L. M.; Beigelman, L., Discovery of 4'-chloromethyl-2'-deoxy-3',5'-di-O-isobutyryl-2'-fluorocytidine (ALS-8176), a first-in-class RSV polymerase inhibitor for treatment of human respiratory syncytial virus infection. *J Med Chem* **2015**, *58*, 1862-78.
140. Smith, D. B.; Kalayanov, G.; Sund, C.; Winqvist, A.; Maltseva, T.; Leveque, V. J. P.; Rajyaguru, S.; Pogam, S. L.; Najera, I.; Benkestock, K.; Zhou, X.-X.; Kaiser, A. C.; Maag, H.; Cammack, N.; Martin, J. A.; Swallow, S.; Johansson, N. G.; Klumpp, K.; Smith, M., The Design, Synthesis, and Antiviral Activity of Monofluoro and Difluoro Analogues of 4'-Azidocytidine against Hepatitis C Virus Replication: The Discovery of 4'-Azido-2'-deoxy-2'-fluorocytidine and 4'-Azido-2'-dideoxy-2',2'-difluorocytidine. *J. Med. Chem.* **2009**, *52*, 2971-2978.
141. Nelson, D. R.; Zeuzem, S.; Andreone, P.; Ferenci, P.; Herring, R.; Jensen, D. M.; Marcellin, P.; Pockros, P. J.; Rodriguez-Torres, M.; Rossaro, L.; Rustgi, V. K.; Sepe, T.; Sulkowski, M.; Thomason, I. R.; Yoshida, E. M.; Chan, A.; Hill, G., Balapiravir plus peginterferon alfa-2a (40KD)/ribavirin in a randomized trial of hepatitis C genotype 1 patients. *Ann Hepatol* **2012**, *11*, 15-31.
142. Deval, J.; Hong, J.; Wang, G.; Taylor, J.; Smith, L. K.; Fung, A.; Stevens, S. K.; Liu, H.; Jin, Z.; Dyatkina, N.; Prhavic, M.; Stoycheva, A. D.; Serebryany, V.; Liu, J.; Smith, D. B.; Tam, Y.; Zhang, Q.; Moore, M. L.; Fearn, R.; Chanda, S. M.; Blatt, L. M.; Symons, J. A.; Beigelman, L., Molecular Basis for the Selective Inhibition of Respiratory Syncytial Virus RNA Polymerase by 2'-Fluoro-4'-Chloromethyl-Cytidine Triphosphate. *PLoS Pathog.* **2015**, *11*, e1004995.

143. Deval, J.; Hong, J.; Wang, G.; Taylor, J.; Smith, L. K.; Fung, A.; Stevens, S. K.; Liu, H.; Jin, Z.; Dyatkina, N.; Prhac, M.; Stoycheva, A. D.; Serebryany, V.; Liu, J.; Smith, D. B.; Tam, Y.; Zhang, Q.; Moore, M. L.; Fearn, R.; Chanda, S. M.; Blatt, L. M.; Symons, J. A.; Beigelman, L., Molecular Basis for the Selective Inhibition of Respiratory Syncytial Virus RNA Polymerase by 2'-Fluoro-4'-Chloromethyl-Cytidine Triphosphate. *PLoS Pathog* **2015**, *11*, e1004995.
144. Beigel, J. H.; Nam, H. H.; Adams, P. L.; Krafft, A.; Ince, W. L.; El-Kamary, S. S.; Sims, A. C., Advances in respiratory virus therapeutics – A meeting report from the 6th isirv Antiviral Group conference. *Antiviral Research* **2019**, *167*, 45-67.
145. Palivizumab, a Humanized Respiratory Syncytial Virus Monoclonal Antibody, Reduces Hospitalization From Respiratory Syncytial Virus Infection in High-risk Infants. *Pediatrics* **1998**, *102*, 531-7.
146. Saez-Llorens, X.; Moreno, M. T.; Ramilo, O.; Sanchez, P. J.; Top, F. H., Jr.; Connor, E. M.; Group, M.-S., Safety and pharmacokinetics of palivizumab therapy in children hospitalized with respiratory syncytial virus infection. *Pediatr Infect Dis J* **2004**, *23*, 707-12.
147. Detalle, L.; Stohr, T.; Palomo, C.; Piedra, P. A.; Gilbert, B. E.; Mas, V.; Millar, A.; Power, U. F.; Stortelers, C.; Allosery, K.; Melero, J. A.; Depla, E., Generation and Characterization of ALX-0171, a Potent Novel Therapeutic Nanobody for the Treatment of Respiratory Syncytial Virus Infection. *Antimicrob Agents Chemother* **2016**, *60*, 6-13.
148. Hultberg, A.; Temperton, N. J.; Rosseels, V.; Koenders, M.; Gonzalez-Pajuelo, M.; Schepens, B.; Ibanez, L. I.; Vanlandschoot, P.; Schillemans, J.; Saunders, M.; Weiss, R. A.; Saelens, X.; Melero, J. A.; Verrips, C. T.; Van Gucht, S.; de Haard, H. J., Llama-derived single domain antibodies to build multivalent, superpotent and broadened neutralizing anti-viral molecules. *PLoS One* **2011**, *6*, e17665.
149. Zhu, Q.; McLellan, J. S.; Kallewaard, N. L.; Ulbrandt, N. D.; Palaszynski, S.; Zhang, J.; Moldt, B.; Khan, A.; Svabek, C.; McAuliffe, J. M.; Wrapp, D.; Patel, N. K.; Cook, K. E.; Richter, B. W. M.; Ryan, P. C.; Yuan, A. Q.; Suzich, J. A., A highly potent extended half-life antibody as a potential RSV vaccine surrogate for all infants. *Sci Transl Med* **2017**, *9*.
150. Domachowske, J. B.; Khan, A. A.; Esser, M. T.; Jensen, K.; Takas, T.; Villafana, T.; Dubovsky, F.; Griffin, M. P., Safety, Tolerability and Pharmacokinetics of MEDI8897, an Extended Half-life Single-dose Respiratory Syncytial Virus Prefusion F-targeting Monoclonal Antibody Administered as a Single Dose to Healthy Preterm Infants. *Pediatr Infect Dis J* **2018**, *37*, 886-892.
151. Griffin, M. P.; Khan, A. A.; Esser, M. T.; Jensen, K.; Takas, T.; Kankam, M. K.; Villafana, T.; Dubovsky, F., Safety, Tolerability, and Pharmacokinetics of MEDI8897, the Respiratory Syncytial Virus Prefusion F-

- Targeting Monoclonal Antibody with an Extended Half-Life, in Healthy Adults. *Antimicrob Agents Chemother* **2017**, *61*.
152. Hall, C. B.; Walsh, E. E.; Long, C. E.; Schnabel, K. C., Immunity to and frequency of reinfection with respiratory syncytial virus. *J Infect Dis* **1991**, *163*, 693-8.
153. Kim, H. W.; Canchola, J. G.; Brandt, C. D.; Pyles, G.; Chanock, R. M.; Jensen, K.; Parrott, R. H., Respiratory syncytial virus disease in infants despite prior administration of antigenic inactivated vaccine. *Am J Epidemiol* **1969**, *89*, 422-34.
154. Baicus, A., History of polio vaccination. *World J Virol* **2012**, *1*, 108-14.
155. Jancar, S.; Sanchez Crespo, M., Immune complex-mediated tissue injury: a multistep paradigm. *Trends Immunol* **2005**, *26*, 48-55.
156. Polack, F. P.; Teng, M. N.; Collins, P. L.; Prince, G. A.; Exner, M.; Regele, H.; Lirman, D. D.; Rabold, R.; Hoffman, S. J.; Karp, C. L.; Kleeberger, S. R.; Wills-Karp, M.; Karron, R. A., A role for immune complexes in enhanced respiratory syncytial virus disease. *J Exp Med* **2002**, *196*, 859-65.
157. Delgado, M. F.; Coviello, S.; Monsalvo, A. C.; Melendi, G. A.; Hernandez, J. Z.; Batalle, J. P.; Diaz, L.; Trento, A.; Chang, H. Y.; Mitzner, W.; Ravetch, J.; Melero, J. A.; Irusta, P. M.; Polack, F. P., Lack of antibody affinity maturation due to poor Toll-like receptor stimulation leads to enhanced respiratory syncytial virus disease. *Nat Med* **2009**, *15*, 34-41.
158. Smith, G.; Raghunandan, R.; Wu, Y.; Liu, Y.; Massare, M.; Nathan, M.; Zhou, B.; Lu, H.; Boddapati, S.; Li, J.; Flyer, D.; Glenn, G., Respiratory syncytial virus fusion glycoprotein expressed in insect cells form protein nanoparticles that induce protective immunity in cotton rats. *PLoS One* **2012**, *7*, e50852.
159. Karron, R. A.; Buchholz, U. J.; Collins, P. L., Live-attenuated respiratory syncytial virus vaccines. *Curr Top Microbiol Immunol* **2013**, *372*, 259-84.
160. Wright, P. F.; Karron, R. A.; Belshe, R. B.; Thompson, J.; Crowe, J. E., Jr.; Boyce, T. G.; Halburnt, L. L.; Reed, G. W.; Whitehead, S. S.; Anderson, E. L.; Wittek, A. E.; Casey, R.; Eichelberger, M.; Thumar, B.; Randolph, V. B.; Udem, S. A.; Chanock, R. M.; Murphy, B. R., Evaluation of a live, cold-passaged, temperature-sensitive, respiratory syncytial virus vaccine candidate in infancy. *J Infect Dis* **2000**, *182*, 1331-42.
161. Malkin, E.; Yogev, R.; Abughali, N.; Sliman, J.; Wang, C. K.; Zuo, F.; Yang, C. F.; Eickhoff, M.; Esser, M. T.; Tang, R. S.; Dubovsky, F., Safety and immunogenicity of a live attenuated RSV vaccine in healthy RSV-seronegative children 5 to 24 months of age. *PLoS One* **2013**, *8*, e77104.

162. Johnson, S.; Oliver, C.; Prince, G. A.; Hemming, V. G.; Pfarr, D. S.; Wang, S. C.; Dormitzer, M.; O'Grady, J.; Koenig, S.; Tamura, J. K.; Woods, R.; Bansal, G.; Couchenour, D.; Tsao, E.; Hall, W. C.; Young, J. F., Development of a humanized monoclonal antibody (MEDI-493) with potent in vitro and in vivo activity against respiratory syncytial virus. *J Infect Dis* **1997**, *176*, 1215-24.
163. Prevention of respiratory syncytial virus infections: indications for the use of palivizumab and update on the use of RSV-IGIV. American Academy of Pediatrics Committee on Infectious Diseases and Committee of Fetus and Newborn. *Pediatrics* **1998**, *102*, 1211-6.
164. Feltes, T. F.; Cabalka, A. K.; Meissner, H. C.; Piazza, F. M.; Carlin, D. A.; Top, F. H., Jr.; Connor, E. M.; Sondheimer, H. M.; Cardiac Synagis Study, G., Palivizumab prophylaxis reduces hospitalization due to respiratory syncytial virus in young children with hemodynamically significant congenital heart disease. *J Pediatr* **2003**, *143*, 532-40.
165. Geskey, J. M.; Thomas, N. J.; Brummel, G. L., Palivizumab: a review of its use in the protection of high risk infants against respiratory syncytial virus (RSV). *Biologics* **2007**, *1*, 33-43.
166. Hampp, C.; Kauf, T. L.; Saidi, A. S.; Winterstein, A. G., Cost-effectiveness of respiratory syncytial virus prophylaxis in various indications. *Arch Pediatr Adolesc Med* **2011**, *165*, 498-505.
167. Banerji, A.; Lanctot, K. L.; Paes, B. A.; Masoud, S. T.; Tam, D. Y.; Macdonald, W. A.; Roberts, A., Comparison of the cost of hospitalization for respiratory syncytial virus disease versus palivizumab prophylaxis in Canadian Inuit infants. *Pediatr Infect Dis J* **2009**, *28*, 702-6.
168. Malley, R.; DeVincenzo, J.; Ramilo, O.; Dennehy, P. H.; Meissner, H. C.; Gruber, W. C.; Sanchez, P. J.; Jafri, H.; Balsley, J.; Carlin, D.; Buckingham, S.; Vernacchio, L.; Ambrosino, D. M., Reduction of respiratory syncytial virus (RSV) in tracheal aspirates in intubated infants by use of humanized monoclonal antibody to RSV F protein. *J Infect Dis* **1998**, *178*, 1555-61.
169. Helmink, B. J.; Ragsdale, C. E.; Peterson, E. J.; Merkel, K. G., Comparison of Intravenous Palivizumab and Standard of Care for Treatment of Respiratory Syncytial Virus Infection in Mechanically Ventilated Pediatric Patients. *J Pediatr Pharmacol Ther* **2016**, *21*, 146-54.
170. Lauring, A. S.; Andino, R., Quasispecies theory and the behavior of RNA viruses. *PLoS Pathog* **2010**, *6*, e1001005.
171. Crowe, J. E.; Firestone, C. Y.; Crim, R.; Beeler, J. A.; Coelingh, K. L.; Barbas, C. F.; Burton, D. R.; Chanock, R. M.; Murphy, B. R., Monoclonal antibody-resistant mutants selected with a respiratory syncytial virus-neutralizing human antibody fab fragment (Fab 19) define a unique epitope on the fusion (F) glycoprotein. *Virology* **1998**, *252*, 373-5.

172. Zhao, X.; Chen, F. P.; Sullender, W. M., Respiratory syncytial virus escape mutant derived in vitro resists palivizumab prophylaxis in cotton rats. *Virology* **2004**, *318*, 608-12.
173. Zhu, Q.; Patel, N. K.; McAuliffe, J. M.; Zhu, W.; Wachter, L.; McCarthy, M. P.; Suzich, J. A., Natural polymorphisms and resistance-associated mutations in the fusion protein of respiratory syncytial virus (RSV): effects on RSV susceptibility to palivizumab. *J Infect Dis* **2012**, *205*, 635-8.
174. Boivin, G.; Caouette, G.; Frenette, L.; Carbonneau, J.; Ouakki, M.; De Serres, G., Human respiratory syncytial virus and other viral infections in infants receiving palivizumab. *J Clin Virol* **2008**, *42*, 52-7.
175. Zhu, Q.; McAuliffe, J. M.; Patel, N. K.; Palmer-Hill, F. J.; Yang, C. F.; Liang, B.; Su, L.; Zhu, W.; Wachter, L.; Wilson, S.; MacGill, R. S.; Krishnan, S.; McCarthy, M. P.; Losonsky, G. A.; Suzich, J. A., Analysis of respiratory syncytial virus preclinical and clinical variants resistant to neutralization by monoclonal antibodies palivizumab and/or motavizumab. *J Infect Dis* **2011**, *203*, 674-82.
176. DeVincenzo, J. P.; Hall, C. B.; Kimberlin, D. W.; Sanchez, P. J.; Rodriguez, W. J.; Jantusch, B. A.; Corey, L.; Kahn, J. S.; Englund, J. A.; Suzich, J. A.; Palmer-Hill, F. J.; Branco, L.; Johnson, S.; Patel, N. K.; Piazza, F. M., Surveillance of clinical isolates of respiratory syncytial virus for palivizumab (Synagis)-resistant mutants. *J Infect Dis* **2004**, *190*, 975-8.
177. Bem, R. A.; Domachowske, J. B.; Rosenberg, H. F., Animal models of human respiratory syncytial virus disease. *Am J Physiol Lung Cell Mol Physiol* **2011**, *301*, L148-56.
178. Taylor, G., Animal models of respiratory syncytial virus infection. *Vaccine* **2017**, *35*, 469-480.
179. Stark, J. M.; McDowell, S. A.; Koenigsnecht, V.; Prows, D. R.; Leikauf, J. E.; Le Vine, A. M.; Leikauf, G. D., Genetic susceptibility to respiratory syncytial virus infection in inbred mice. *J Med Virol* **2002**, *67*, 92-100.
180. Heylen, E.; Neyts, J.; Jochmans, D., Drug candidates and model systems in respiratory syncytial virus antiviral drug discovery. *Biochem Pharmacol* **2017**, *127*, 1-12.
181. Rouan, M. C.; Gevers, T.; Roymans, D.; de Zwart, L.; Nauwelaers, D.; De Meulder, M.; van Remoortere, P.; Vanstockem, M.; Koul, A.; Simmen, K.; Andries, K., Pharmacokinetics-pharmacodynamics of a respiratory syncytial virus fusion inhibitor in the cotton rat model. *Antimicrob Agents Chemother* **2010**, *54*, 4534-9.
182. Atienza, B. J. P.; Jensen, L. D.; Noton, S. L.; Ansalem, A. K. V.; Hobman, T.; Fearn, R.; Marchant, D. J.; West, F. G., Dual Catalytic Synthesis of Antiviral Compounds Based on Metallocarbene–Azide Cascade Chemistry. *The Journal of Organic Chemistry* **2018**, *83*, 6829-6842.

Chapter 2:

Structure-Based Discovery of Allosteric Inhibitors Targeting Respiratory Syncytial Virus L protein

2.1 Introduction

Human respiratory syncytial virus (RSV) is the leading cause of upper and lower respiratory tract infections in pediatric patients worldwide.¹ The severity of RSV infections is clearly manifested in infants and immunocompromised adults with approximately 60,000 children under the age of 5 and ~ 177,000 adults are being hospitalized each year.¹⁻⁴ The viral infection can be processed from the upper to the lower respiratory tract which can result in more complicated symptoms and illness including pneumonia, bronchiolitis, asthma and, in some cases, cardiopulmonary distress.⁵⁻⁷

Although the virus was first isolated in 1955 from chimpanzees, there is no vaccine available, and limited drug treatment options beyond the prophylactic drug palivizumab, a highly expensive monoclonal antibody (mAB) used only for high-risk premature infants.^{8,9} Ribavirin, a well-known antiviral drug, was approved for aerosol treatment against RSV infections; however, its use has been curtailed due to risks of carcinogenic and teratogenic effects.¹⁰ The absence of any effective small-molecule antiviral drugs represents a significant unmet need in the health care delivery system.

Human respiratory syncytial virus exists as two subtypes: A and B which are found within the genus *Orthopneumovirus*, family *Pneumoviridae*, order *Mononegavirales*. RSV is an enveloped, negative-sense, single-stranded (ss) RNA virus with spherical virion particles of 100-350 nm in diameter or as long filaments of 60-200 nm in diameter.¹¹

The RSV genome is 15.2 kb and codes for 11 proteins: nonstructural proteins (NS-1 and NS-2), matrix protein (M), nucleoprotein (N), phosphoprotein (P), polymerase (L), small hydrophobic protein (SH), glycoprotein (G), fusion protein (F) and the M2 protein.^{12, 13}

Several targets have been investigated for the development of an effective therapeutic agent against RSV infections. Viral RNA and DNA polymerases are among the most attractive targets for inhibition of viral replication and targeting these proteins is the most common approach for antiviral drug development.¹⁴ RSV contains a non-segmented negative-sense RNA genome, which requires the virus-encoded RNA-dependant RNA polymerase (RdRp) complex for genome replication and transcription of viral RNA.¹⁵ Three viral proteins are essential for replication of the RSV genome: the nucleoprotein (N), the large protein (L), and the phosphoprotein (P). The large polymerase protein (L) contains the enzymatic domains involved in the transcription and replication, and the phosphoprotein (P), acts as an essential co-factor (**Figure 2.1**).¹⁶⁻¹⁸ Recent approaches in drug development have identified several chemical moieties that can effectively inhibit RSV replication complexes.¹⁹ However, the continuous search for small molecules with high potency, selectivity, and improved pharmacokinetics is still an ongoing field. In this study, we carried out a structure-based drug discovery campaign to identify the exact target of previously discovered RSV anti-infective agents for which the replication complex had been tentatively identified as the likely target.²⁰ Molecular docking and molecular dynamics (MD) simulations were carried out to evaluate the possible binding pocket and mode of the previously reported polymerase inhibitors and correlate the activity observed with the computational results. These approaches could potentially lead to better understanding of the potential mechanism by which these molecules inhibit viral replication with an ultimate goal of designing more potent inhibitors.

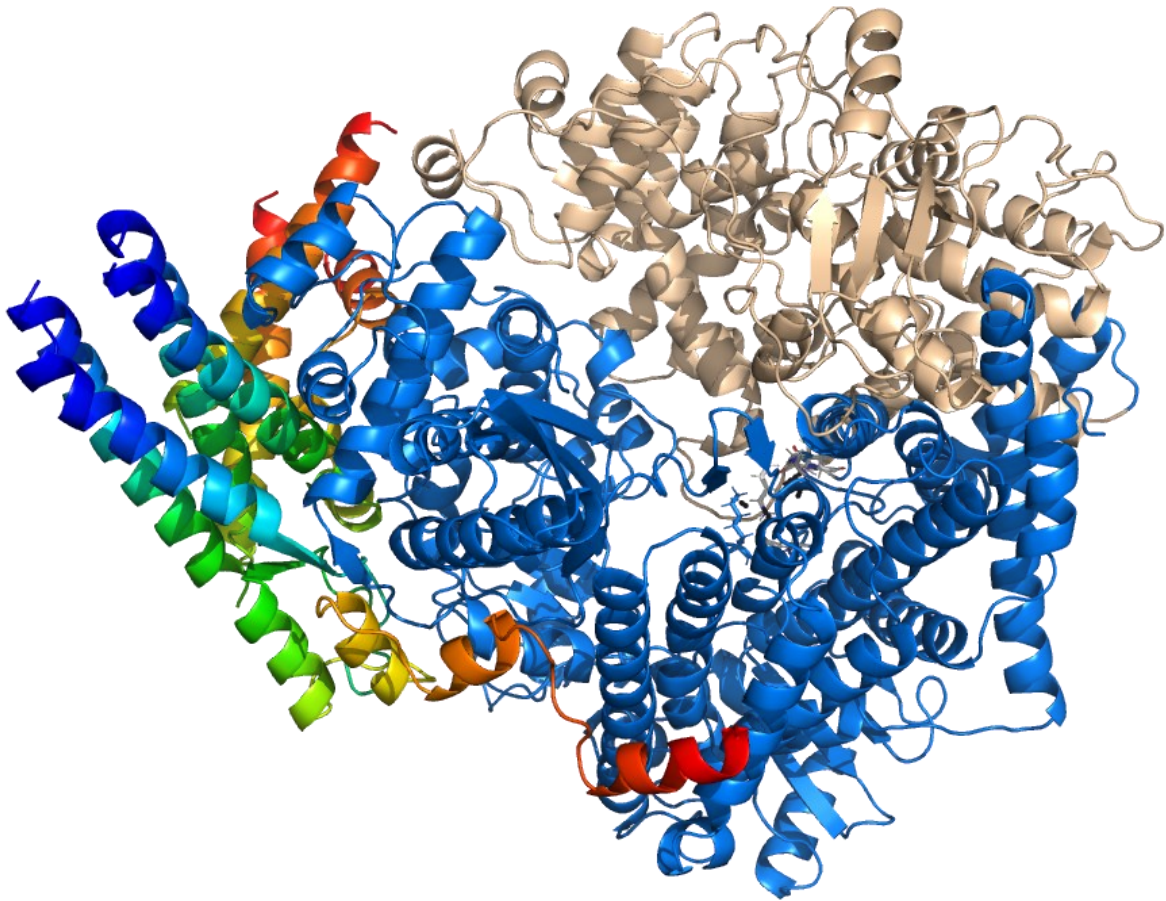


Figure 2.1: RSV L protein domains (domains are color coded). The P protein helices are shown in the left (PDB ID: 6PZK) with. Figure generated using PyMOL.²¹

2.2 Results and Discussion:

2.2.1 Assessment of The Replication Complex for Putative Druggable Pockets

The 250 kDa L protein harbors three conserved enzymatic domains: the RNA-dependent RNA polymerase (RdRp) domain, the polyribonucleotidyl-transferase (PRNTase or capping domain), and the methyltransferase (MTase) domain (**Figure 2.1**).²² The cryo-EM structure of wild-type RSV L protein was experimentally reported in 2019 and deposited in the Protein Data Bank (PDB ID: 6PZK). *In silico* modeling has been previously employed to study the binding and interactions between small molecules and RSV viral proteins, for instance, the fusion (F) protein.²³ However, to date, there are no reports of a co-crystallized ligands with the RSV L protein. Based on our previous findings, it is thought that this class of compounds are targeting the replication complex of the virus. In this work, we opt to narrow down our search approach and focus on the L protein as the primary target. In this context, computational docking and MD simulations were employed to elucidate any potential binding with RSV L protein.

Initially, the fpocket script, Site Finder implemented in MOE and SiteMap utility implemented in Schrodinger discovery suite were used to identify putative RSV L binding pockets.²⁴⁻²⁷ This approach identified 122 possible pockets within the Cryo-EM structure of the L protein with druggability score ranging from 0 to 0.99 on a scoring range between 0 and 1, where a score of 1 would indicate a perfect druggable site. The search was narrowed down by ranking pockets using druggability scores and comparing pockets identified by each program which downsized the search to 6 possible druggable pockets (**Figure 2.2**). Among the examined pockets, pocket 1 is located in close proximity to the NTP entry channel and is formed of charged amino acids which aid the incoming NTPs to be placed in the active site.^{18, 28} The pocket had a druggability score of 0.99, and a volume of $\sim 489 \text{ \AA}^3$ and the electrostatic aspects were taken into consideration in

supporting the selection of this pocket. Visual inspection of the Cryo-EM structure of L protein revealed that the pocket is surrounded by several positively charged residues including Arg 621, Arg 747, Lys 20 and Lys 540 which line the NTP entry tunnel (**Figure 2.3**). These observations could support the possibility that binding of non-nucleoside inhibitors to this pocket could interfere with the incoming NTPs or by allosterically altering the conformation of the active site which will subsequently inhibit viral replication. To evaluate the potential accessibility of this pocket to small molecules, the water hydration was studied by counting the number of water molecules within the first and second hydration shells throughout the MD simulation.

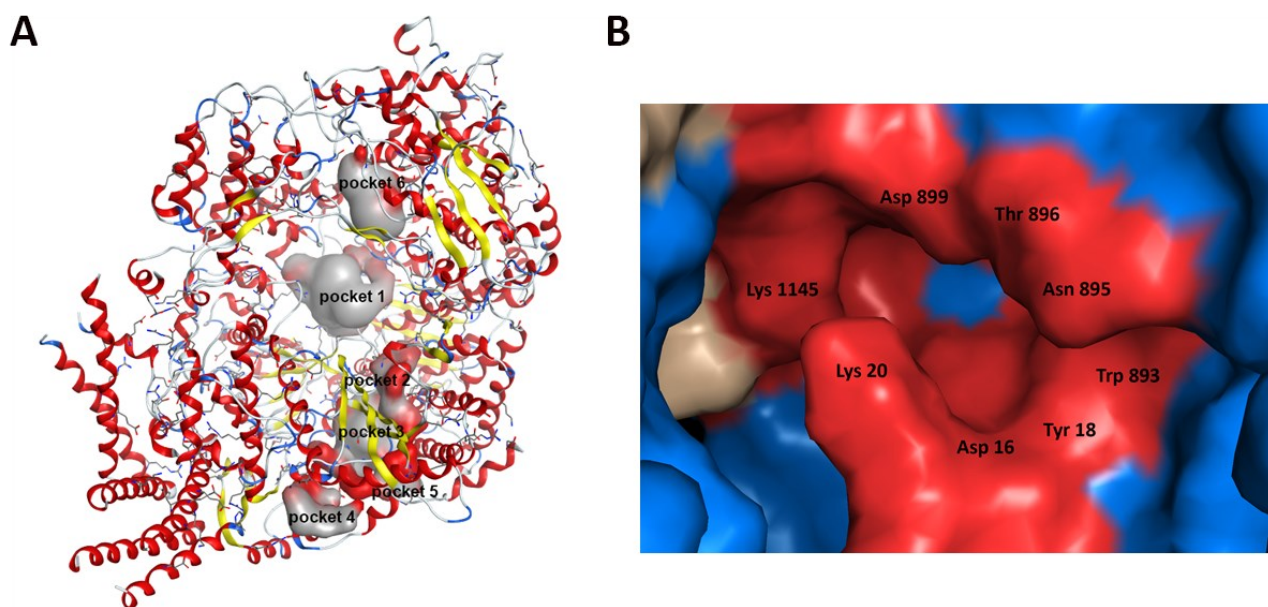


Figure 2.2: Allosteric Pocket on the RSV L protein. **A.** Druggable pockets identified in the L protein **B.** Surface representation of pocket 1 highlighting key pocket residues in red.

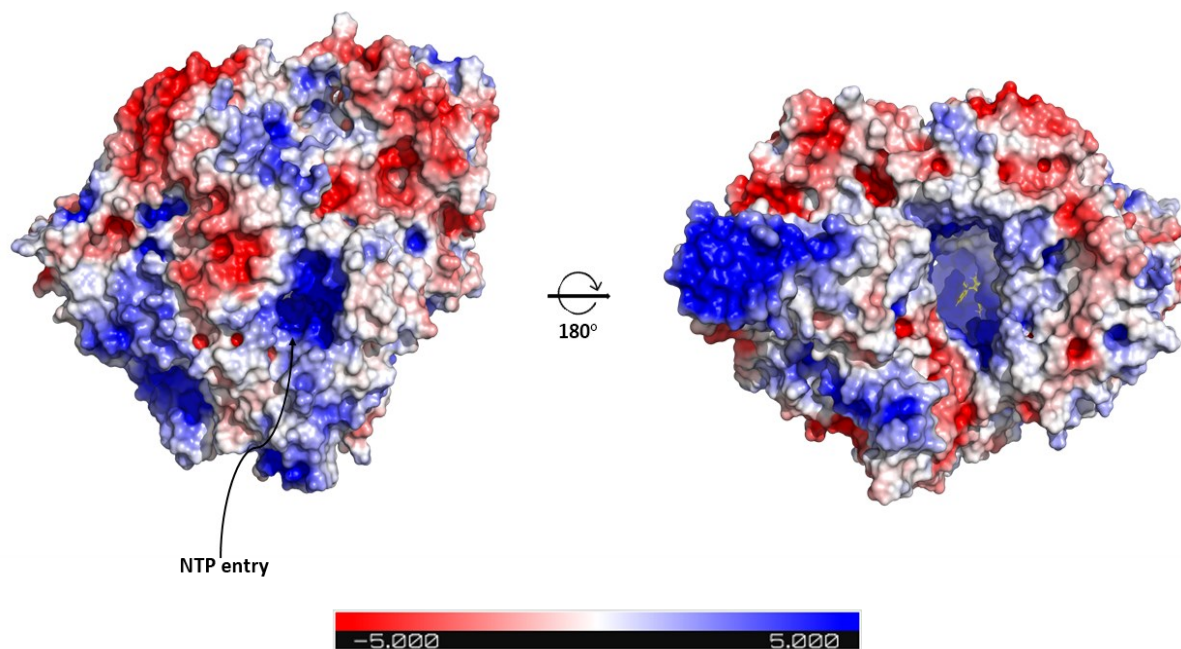


Figure 2.3: Surface representation of the RSV L bound to the P protein showing compound 1 bound near the NTP entry pore. Surface electrostatic potential was calculated using the Poisson-Boltzmann equation using the APBS server (<https://server.poissonboltzmann.org/>)

The selected pocket allowed up to 30 water molecules to enter in the first hydration shell while allowing 105 to 120 water molecules in the second hydration shell (**Figure 2.4**). These results support the possibility that this site could be targeted for potential allosteric inhibitors. Interestingly, the pocket is located away from the residues that form the QUAD mutations responsible for viral escape arising from nucleoside analog inhibitors such as ALS-8112.²⁹ We believe that if targeting this pocket is successful, it could potentially identify a new class of inhibitors with a novel mechanism of viral protein inhibition.

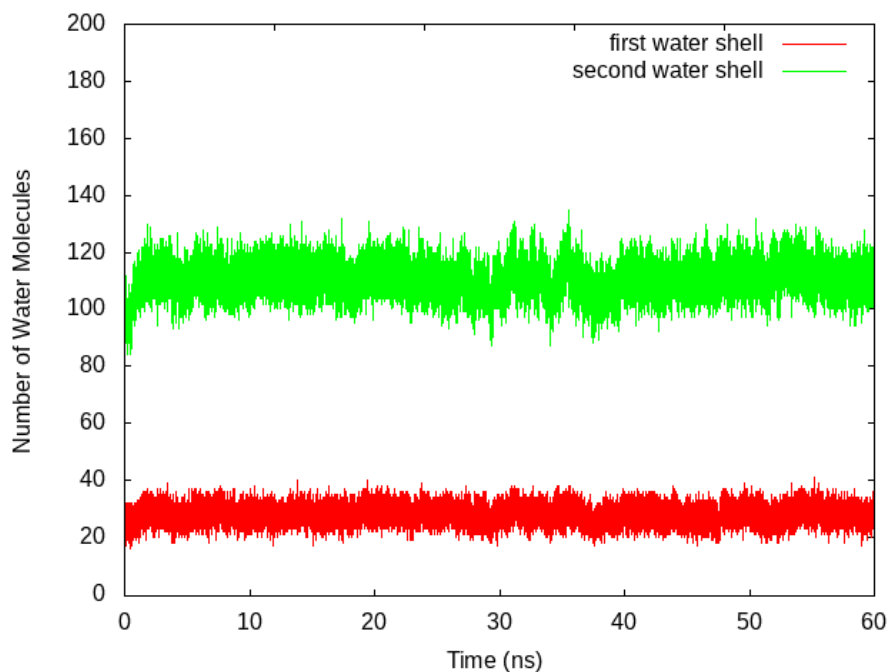


Figure 2.4: Water shell analysis of the MD trajectory showing the number of water molecules accessing the first and second water shell of pocket 1 during the 60 ns simulation.

2.2.2 Molecular Dynamics Simulations of The Apo RSV L Protein

Molecular dynamics has been used widely in validating and refining docking poses to shed a light on an accurate representation of the ligand-protein interactions.³⁰ Initially, missing residues (609-626) from the cryo-EM map were built and refined using Prime module implemented in Schrödinger Suite.³¹ To understand the dynamicity of the RSV L protein in the unbound state, a 60 ns long MD simulation of the apo structure (PDB ID: 6PZK) was performed. Root mean square deviation (RMSD) was assessed throughout the simulation which accounts for the system stability. The RMSD of the protein backbone equilibrated around 25 ns and once a stable conformation was achieved, the system remained stable with a fluctuation of 1.7 Å from its initial coordinates over the whole simulation (**Figure 2.5**). Flexibility of residues was further analyzed using the atomic fluctuation (beta factors) of the protein backbone atoms. The majority of the residues were stable

during the whole simulation with the most flexible regions occurred at the N and C termini of the protein. In addition, a region from residues 200-230 displayed elasticity during the MD trajectories. Despite the displayed flexibility within this region, the apo protein structure proved to be quite stable. Clusters from the whole simulation trajectory were generated and the lowest energy cluster was then used for docking purposes.

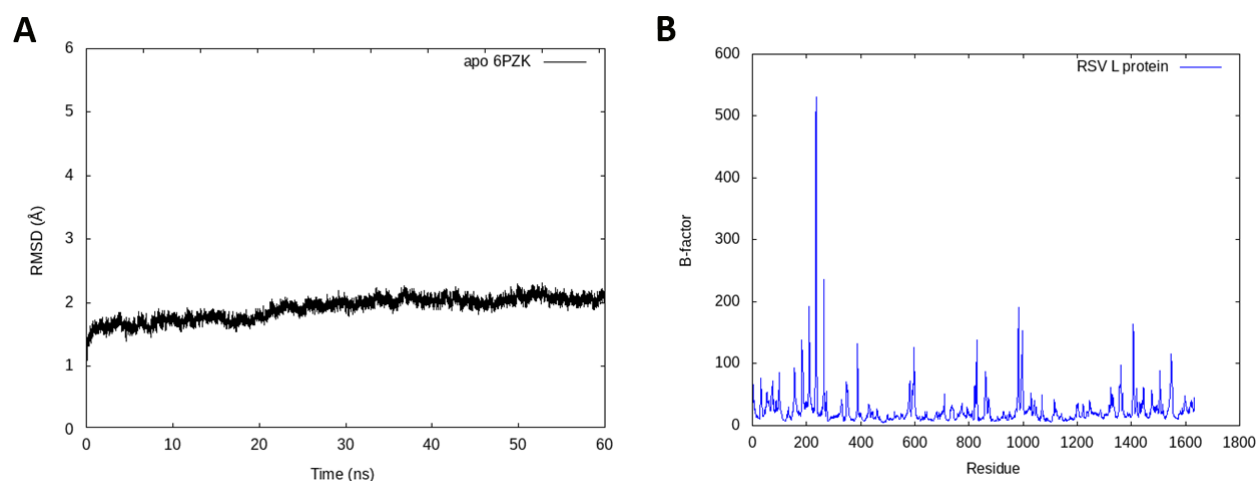


Figure 2.5: Trajectory analysis of the RSV L apo protein. **A.** RMSD trend of the RSV Polymerase complex (L in complex with the P protein). **B.** Atomic fluctuations for the L and P proteins showing regions with very little flexibility.

2.2.3 Putative Binding Poses of The New Bis(Indole) Compounds

Our previously reported lead, compound **1**, was used as a docking control since this compound showed the best activity against RSV and Zika viruses (**Figure 2.6**).²⁰ The bis-indole hit **1** was determined to inhibit a RSV-induced cytopathic effect with an $EC_{50}=9 \mu\text{M}$. To explore how the compounds could potentially bind in the identified pockets, molecular docking was employed, and the binding pose and docking score of compound **1** were evaluated. Examination of the binding poses of **1** and the correlation between docking scores and the activity revealed that the compound could possibly be binding to pocket 1 with a binding energy of -9.50 kcal/mol , as calculated using extra precision (XP) Glide scoring function implemented in Schrödinger Suite.³²

Analysis of the ligand-protein complex revealed that the compound formed several hydrogen bond interactions to residues Asp 16, Lys 20, Tyr 18, Asn 895 and Thr 896. Moreover, our model identified an important key hydrogen bond interaction within the allosteric pocket between the indole (-NH) and the backbone carbonyl oxygen of Trp 893. The importance of this interaction will be discussed further below. Although, the active site of the L protein is usually considered to be the primary target of any docking simulations, it has been excluded from our search due to structural differences between nucleotides and this class of compounds. This assumption was further confirmed by docking of compound **1** in the active site which showed a negligible docking score of -3.2 kcal/mol.

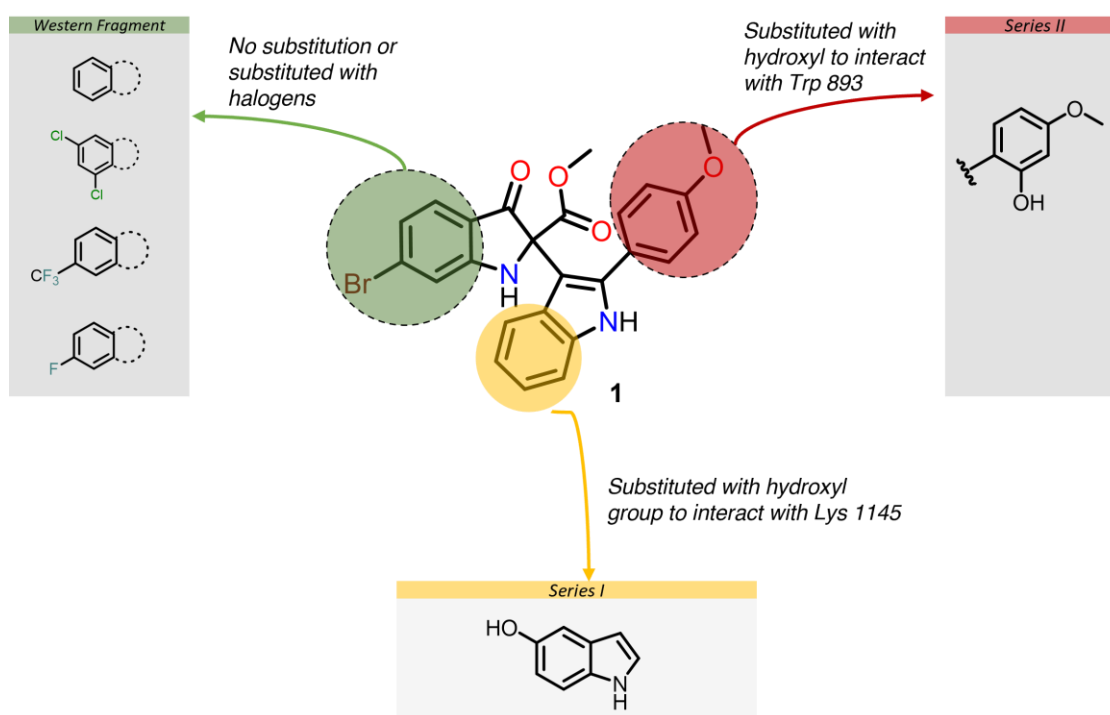


Figure 2.6: Design of compound **1** based derivatives for SAR analysis as RSV RdRp inhibitors.

2.2.4 Design of The New Analogues

Giving the stability observed for compound **1** in the putative binding pose, the question was whether modifying the indole part of the parent compound could be beneficial and could lead

to a stable ligand-protein interactions. Visual inspection of the binding pocket revealed that several residues could contribute to more binding of the lead compound with the L protein. In this regard, we wanted to capitalize on building a good hydrogen bonding network to increase the capacity of the ligand-protein binding and stability following a detailed computational analysis of the hydrophobic and hydrophilic properties and spaces in the selected pocket (**Figure 2.7**). The first thought was given to a substitution with hydroxyl group on the C5 of the indole as this may result in a new hydrogen bond contact with Lys 1145. Moreover, the removal of the aryl moiety at the indole C2 position was also considered to evaluate the minimum requirements for the activity of this class of inhibitors. These modifications were divided into two series of compounds where series I would have the aryl substitution at the C2 of the indole removed and an additional hydroxyl group would be added at the C5 of the indole and series II will have a single modifications on 2-phenylindole moiety (**Figure 2.6**).

A new designed library of compounds was used for the initial virtual screening (**Figure 2.8**). Docking simulations of (series I) showed that the absence of the 2-aryl substitution on the indole moiety could be tolerated. Compound **6a** exhibited five hydrogen bond interactions to residues (Asn 895, Asp 899, Asp16, Lys 20 and Lys 1145) with a docking score of -7.21 kcal/mol. Virtual screening of this library was performed and best scoring poses for each analog was retained for further investigation using MD simulations.

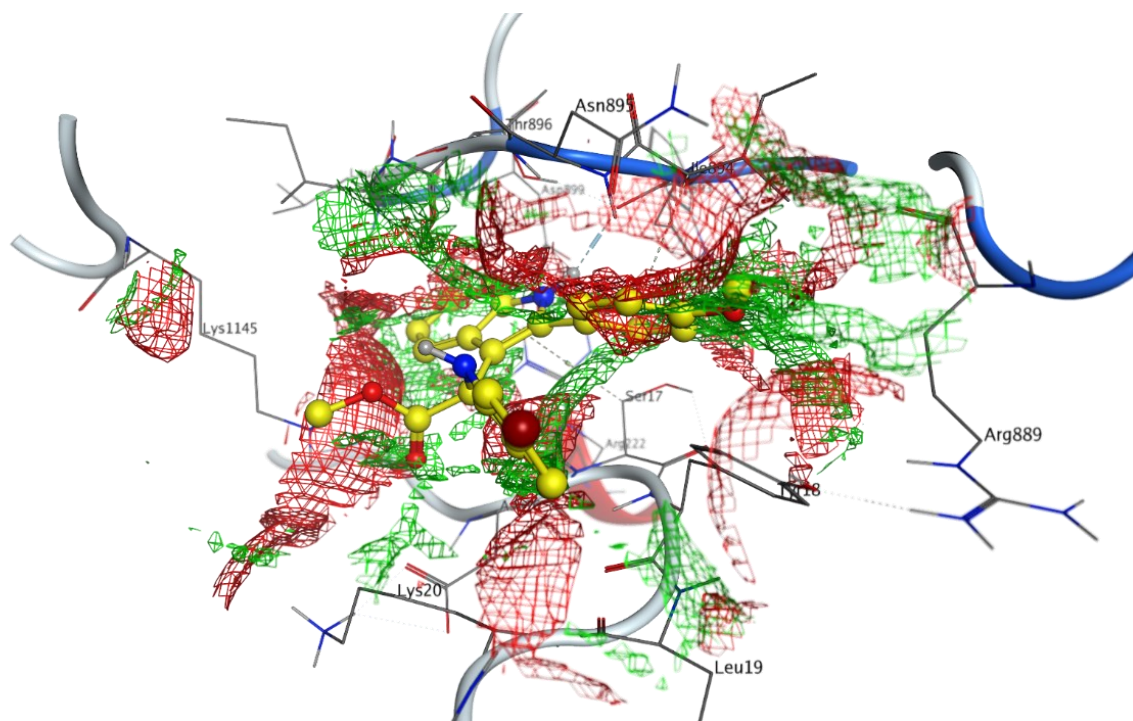


Figure 2.7: Mapping of pocket 1: Red highlights hydrophobic regions while green highlights hydrophilic regions. (Compound 1 is represented as ball and sticks in yellow)

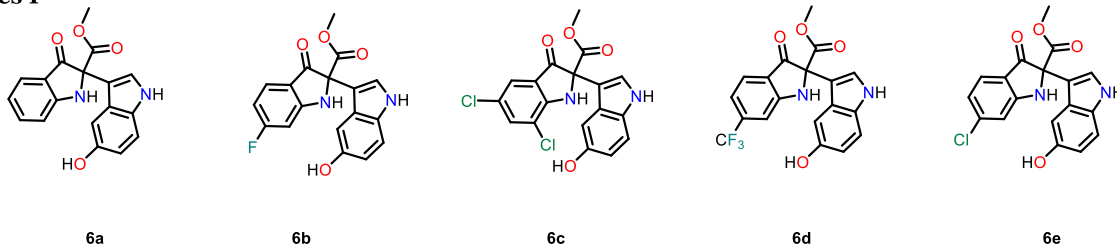
It is worth noting that for each compound, both enantiomers were docked, and the high scoring isomer was carried forward for the molecular dynamics simulation (MD).

2.2.5 Assessment of Ligands Stability and Poses During MD simulation

To validate the protein-ligand complex of the docked compound and to assess the stability of the ligand binding in the allosteric site, molecular dynamics simulation studies were conducted for the top hit molecules. To evaluate the stability of the L protein complex during MD simulations, the root mean square deviation (RMSD) value was calculated over a 25 ns long simulation time. Since compound **1** and its analogues are racemic, evaluation of each isomer was crucial to determine which isomer would be more suitable for binding and complement the pocket cavity. Analysis of the trajectories indicated that the *S* isomer of compound **1** was stable in the binding site during the simulation with an average RMSD for the complex of 2.1 Å. The compound showed

a very strong stability in the complex with a small deviation of 0.74 Å from the original coordinates throughout the whole trajectory (**Figure 2.9**).

Series I



Series II

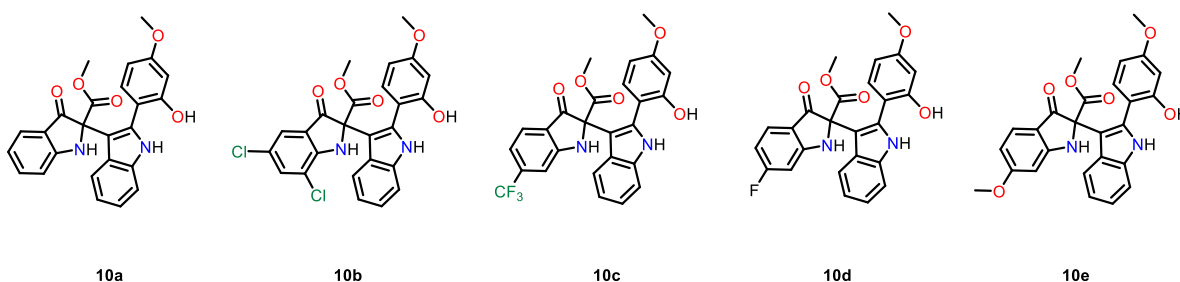


Figure 2.8: Structures of Series I and II compounds.

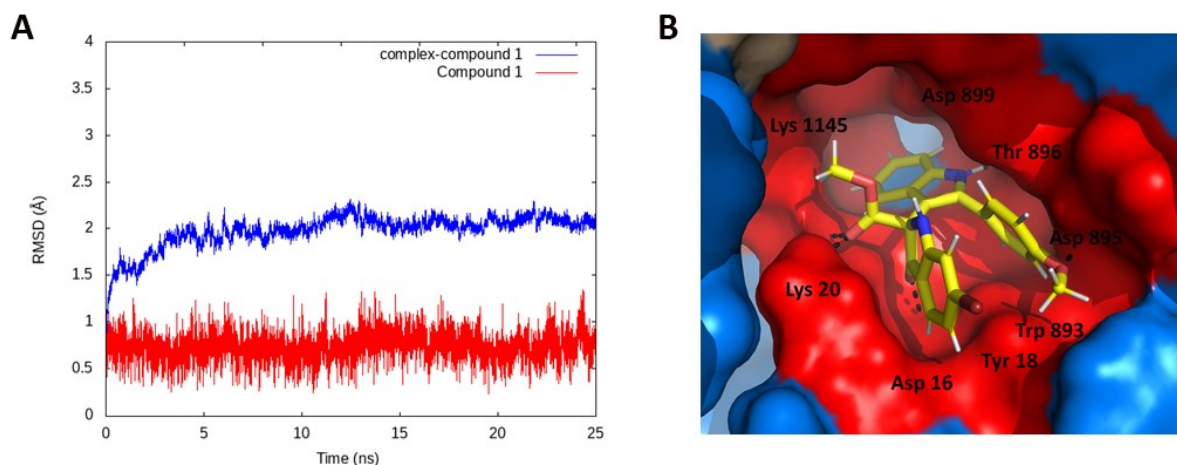


Figure 2.9: MD analysis of compound 1. **A.** RMSD trends of compound 1 in complex with the L protein. **B.** Putative binding pose of compound 1 (Pocket surface is depicted in red highlighting main pocket residues).

Clustering in AMBER tools via the average-linkage algorithm were used to obtain a representative structure of the last 15 ns of simulation for all ligands. On this basis, simulation

times were set to 25 ns to evaluate all complexes. Protein-ligand interactions were assessed throughout the simulation which includes hydrogen bonds, electrostatic and hydrophobic interactions. Analysis of the simulation trajectories revealed that the carbonyl oxygen of the ester forms a hydrogen bond with the (-NH) of Lys 20. The nitrogen of the 4-methoxyphenyl indole part of the molecule interacted extensively with side chains of Asp 899 and Thr 896 through hydrogen bonding. Moreover, the methoxy oxygen formed a hydrogen bond with the backbone of Asn 895. Insertion of the benzene part of the indole skeleton into a tunnel formed of Ile 896 and Lys 1145 contributed to the effective binding by filling the pocket (**Figure 2.9**).

The results of compound **1** stability drove our interest toward exploring the tolerability of different functionalities on this moiety. MD simulations were performed on the *S* isomer of **6a**. Interestingly, the absence of the 2-phenyl substitution on the indole did not affect the stability of the ligand binding and the complex for 50 ns long simulation. Importantly, the extended simulation time was crucial at this stage to further validate the results and to avoid any false positives. Binding of compound **6a** to the RSV L protein stabilized the replication complex with a mean RMSD of 1.8 Å and a ligand RMSD of 0.65 Å (**Figure 2.10**). The orientation of **6a** was similar to that of compound **1** in the binding pocket with small deviation in which the 5-hydroxyl group was placed near Lys 1145. This orientation led to the desired hydrogen bond interaction between the phenolic oxygen of the molecule and the hydrogen of the lysine side chain. Interestingly, the compound occupied a hydrophobic cleft inside the pocket and the substitutions complemented the electrostatic required for that pocket as shown in (**Figure 2.10**). These results suggested that the proposed modification of the parent molecule could be tolerable and might lead to a strong inhibitor.

Based on the previous results, another generation of compounds based on **6a** was investigated. In this generation, series II, the core structure of the parent compound **1** was maintained. The presence of a methoxy group at the C4 was believed to decrease the cytotoxicity of this class of compounds.²⁰ In this work, the introduction of a hydroxyl group at C2 of the 2-phenyl-4-methoxyindole is sought to potentially contribute to an enhanced hydrogen bond network within the pocket. In contrast to previously observed binding modes, the indole part of compounds **10a-e** flipped from its initial position, after 10 ns of the simulation, forcing the ligands to rotate inside the pocket to avoid being solvent exposed (**Figure 2.11**). Although this rotation did not result in any hydrogen bond contact with Lys 1145, the ligands were still able to build more hydrogen bonds within the pocket. Ligands maintained some of the previously observed hydrogen bonds to Asp 16, Thr 896 and Asn 895. A significant hydrogen bond was the one between the C2 (-OH) and the backbone oxygen of Trp 893 as demonstrated in the putative binding of compound **10e** which had an extra methoxy substitution at the C4 of the indolyl part of the molecule (**Figure 2.11**).

The results of the MD simulations led to the identification of four compounds as possible better inhibitors of the RSV L. However, a more accurate predication of the binding free energy was needed to lead our synthesis decision.

2.2.6 Relative Binding Free Energy Analyses of Ligand-Protein Complexes

The combination of MD simulations and end-point free energy calculation such as the Molecular Mechanics/Generalized Born Surface area (MM/GBSA) has proven to be very useful in the accurate assessment of protein-ligand complexes.³³⁻³⁵ Building on our previous analyses, the MM-GBSA method was employed on the snapshots of the complexes sampled from the MD trajectories to get better insights into ligands contributions to binding. The

trajectory of each complex was sampled at an interval of 10 ps from the last 10 ns of the simulation to yield 1000 frames for the MM-GBSA rescoring. MM-GBSA results showed that **10e** was the compound with the best ΔG with a value of -48.25 kcal/mol followed by compound **10b**, which showed a binding affinity of -41.41 kcal/mol. The affinity of those two compounds outperformed that of the positive control, compound **1**, which showed ΔG of -36.91 ± 3.0 kcal/mol. Interestingly, the flipped orientation exhibited by these analogues in the binding pocket contributed more to the binding free energy and the stability of the complexes.

Furthermore, compounds **6a** and **6d** had relative binding free energies of -37.60 ± 2.7 and -30.45 ± 3.8 kcal/mol, respectively. These compounds belong to series I and their weak binding affinity could be attributed to the inability of these compounds to contribute to hydrophobic interactions upon binding as will be discussed later on. Compounds **10c**, **6c** and **6e** showed the weaker binding affinities with values -22.11 ± 4.6 , -24.31 ± 3.6 , and -24.84 ± 2.6 kcal/mol, respectively as shown in Table 2.1. Further, per-residue decomposition analyses were performed to obtain the energetic contributions of each residue in the binding pocket toward inhibitor binding. The residues that consistently contributed to the binding of compound **1** were identified as Asp 16, Ser 17, Tyr 18, Thr 896 and Ile 897, where van der Waals interactions dominated the binding. Moreover, the analysis indicated that Asp 899 contributed mainly to electrostatic interactions as summarized in Table 2.2. However, energy decomposition for series I revealed that most pocket residues contributed a small portion to van der Waals interactions while electrostatic interactions by Asp 899 and Thr 896 were more dominant as shown in Table 2.2. On the basis of these results, the two computationally investigated libraries were synthesized and evaluated for their antiviral activities.

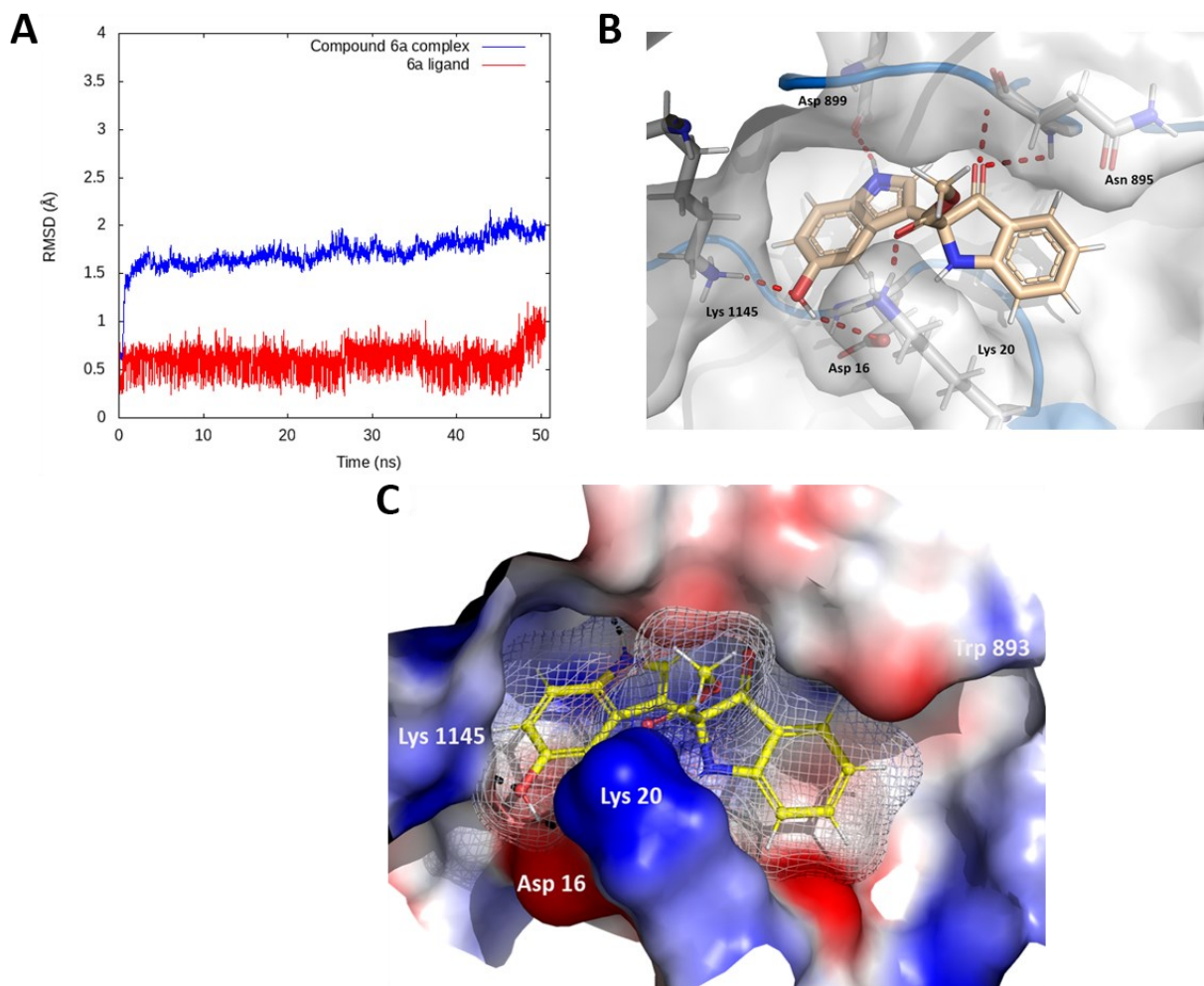


Figure 2.10: Trajectory analysis of compound **6a**. **A.** RMSD of the backbone atoms of compound **6a** in complex with L protein. **B.** MD snapshot of compound **6a** binding pose. (Hydrogen bonds are shown as red dashed lines) **C.** Electrostatic mapping of the binding pocket showing compound **1** complementing the shape and electrostatics of the pocket.

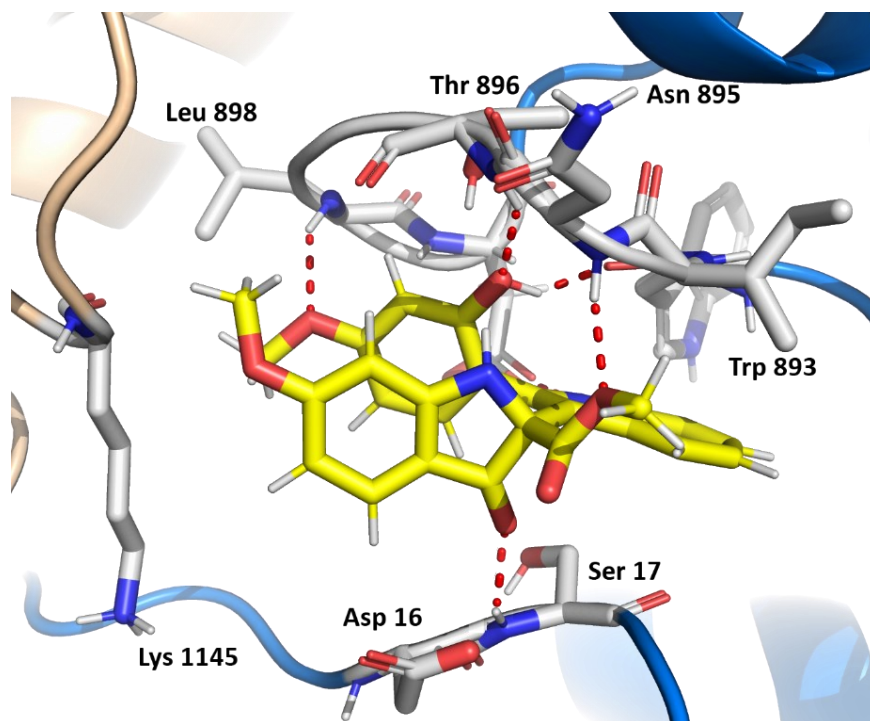


Figure 2.11: Lowest energy MD snapshot of compound **10e**. (Hydrogen bonds are depicted as red dashed lines.)

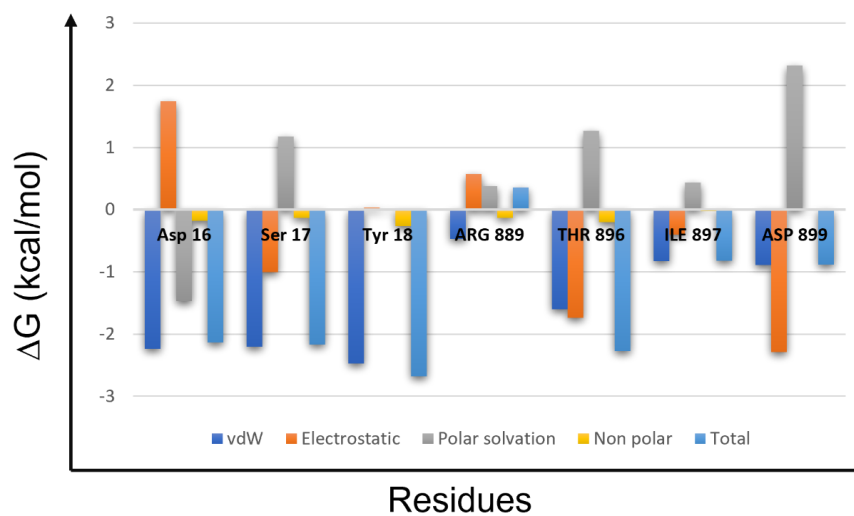
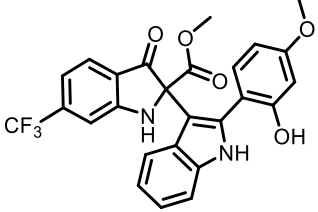
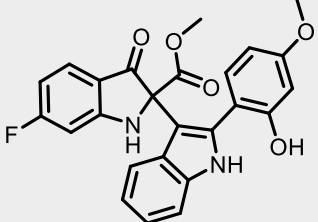
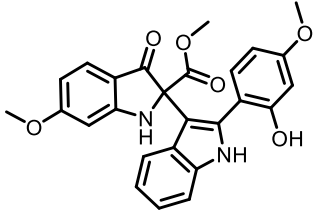


Figure 2.12: Per-residue energy decomposition of ligand-receptor binding energy of compound **6a**.

Compound	Structure	ΔG_{bind} (kcal/mol)
1		-36.91 ± 3.0
6a		-37.60 ± 2.7
6b		-34.55 ± 3.2
6c		-24.31 ± 3.6
6d		-30.45 ± 3.8
6e		-24.84 ± 2.6

10b		-41.41 ± 2.7
10c		-22.11 ± 4.6
10d		-26.60 ± 3.0
10e		-48.25 ± 4.7

^a Values represent the calculations of the *S* isomer of each ligand.

Table 2.1: Summary of MM/GBSA results for series I and II compounds.

Interacting Residue	vdW^b	Electrostatic	Polar solvation	Non-polar solvation	Total
1					
Asp 16	-2.236	1.745	-1.467	-0.175	-2.133
Ser 17	-2.205	-1.006	1.174	-0.133	-2.17
Tyr 18	-2.473	0.039	0.014	-0.26	-2.68
Arg 889	-0.469	0.572	0.383	-0.128	0.358
Thr 896	-1.599	-1.738	1.266	-0.202	-2.272
Ile 897	-0.827	-0.398	0.433	-0.028	-0.82
Asp 899	-0.892	-2.292	2.314	-0.012	-0.881
6a					
Asp 16	-2.097	3.807	-3.296	-0.129	-1.715
Ser 17	-1.736	0.119	0.19	-0.123	-1.549
Tyr 18	-1.386	0.073	0.125	-0.151	-1.339
Arg 889	-0.086	-0.231	0.688	-0.013	0.357
Thr 896	-1.027	-4.106	3.237	-0.185	-2.081
Ile 897	-1.249	-0.648	0.774	-0.129	-1.252
Asp 899	-0.548	-7.621	5.968	-0.03	-2.23

Table 2.2: Pair-residue energy decomposition values for compounds **1** and **6a**.^a

^a All values are expressed in kcal/mol.

^b Van der Waals interactions.

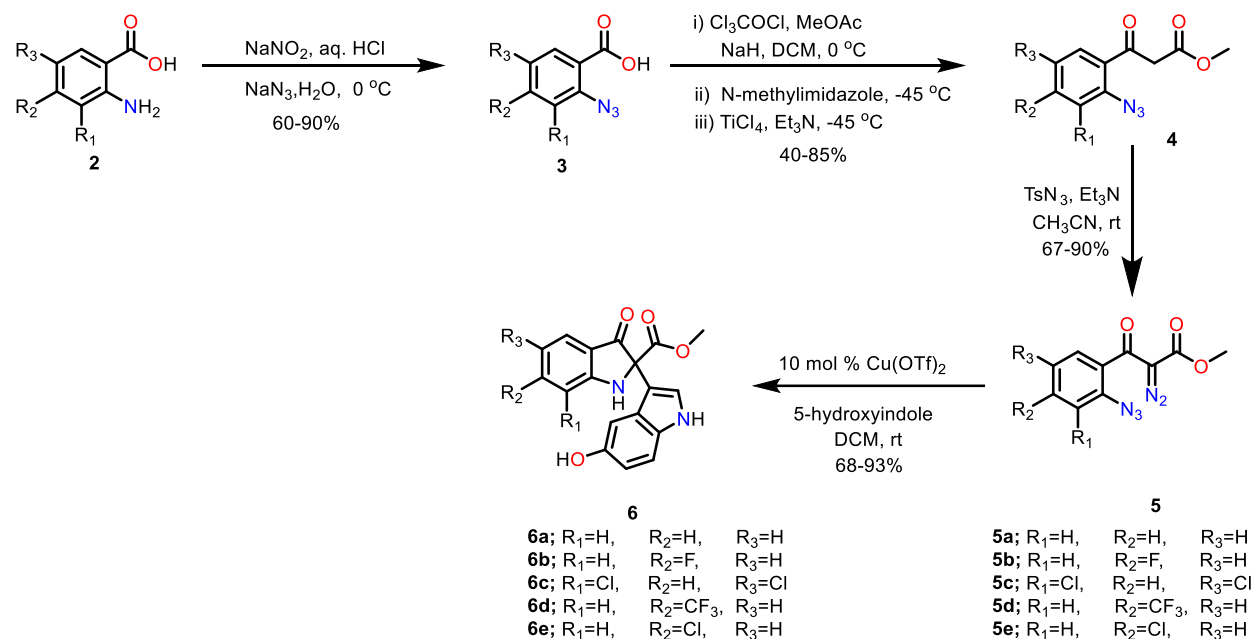
2.2.7 Chemical Synthesis

To explore the structure-activity relationships (SAR) at the western part of the bis-indole scaffold, the synthesis of several analogues of series I was achieved according to the route outlined in Scheme 2.1 and according to a previously published literature procedure.²⁰

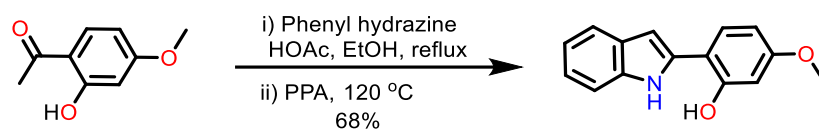
Starting from commercially available anthranilic acid derivatives, the route began with a diazotization reaction followed by the addition of sodium azide to afford compound **3**. The beta-keto ester compound **4** was formed, according to the Ti-crossed-Claisen condensation reported by Misaki *et al.*, from the reaction of the carboxylic acid **2** with trichloroacetyl chloride and methyl acetate promoted by TiCl₄ and N-methylimidazole at -45 °C to furnish this intermediate in good yields.³⁶ The Regitz-diazo transfer was the key step to produce the diazo-azide intermediate **5** by the reaction of **4** with tosyl azide in the presence of triethylamine at room temperature for 12 h.

The synthesis of targeted bis(indole) compounds processed through a dual catalytic cycle described previously by our group.²⁰ In this dual catalytic cycle, intermediate **5** was treated with catalytic amount (10 mol %) of Cu(OTf)₂ in DCM to catalytically produce copper metallocarbenes after an *in-situ* reduction of copper (II) precatalyst to copper(I) by the indole as the reducing agent. This led to the conversion of **5** into a C-acylimine intermediate followed by Brønsted acid activation of the imine for the Friedel-Crafts alkylation by the indole trap. This step produced our targeted compounds **6a-e** in good to moderate yields. In order to prepare targeted compounds **10a-e**, the intermediate 2-(1H-indol-2-yl)-5-methoxyphenol **9** was synthesized through Fischer indole synthesis by reacting 2'-hydroxy-4'-methoxyacetophenone **7** with phenyl hydrazine under acidic conditions which gave the desired product in 68 % yield as shown in Scheme 2.2.³⁷ The synthesis of compounds **10a-e** followed the synthetic route discussed above but using compound **9** instead of 5-hydroxyindole as shown in Scheme 2.3. Compound **11** was also synthesized the reaction of

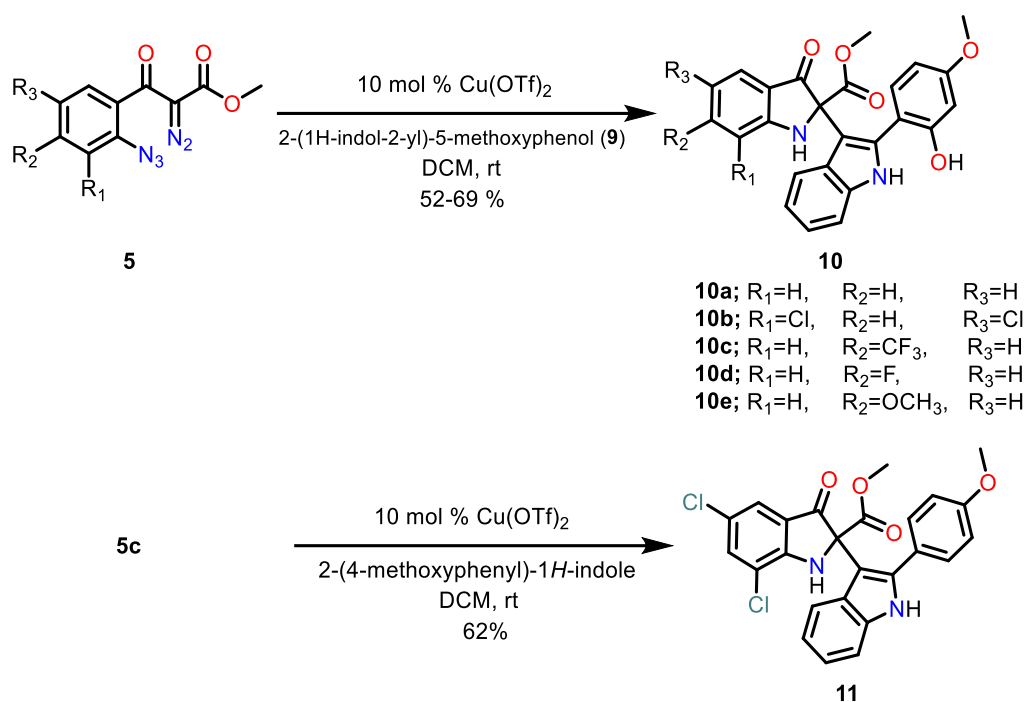
intermediate **5c** with 2-(4-methoxyphenyl)-1H-indole (Scheme 2.3). The purpose of compound **11** was to be evaluated for antiviral activity as a control representing the first generation of bis(indoles) reported previously but having two chlorines at positions 2 and 5 of the indolinone fragment.



Scheme 2.1: Synthesis of series I Compounds.



Scheme 2.2: Synthesis of compound **9**.



Scheme 2.3: Synthesis of series II bis-indole derivatives **10a-e**.

2.2.8 Evaluation of the Antiviral Activity of the Designed Bis(Indole) Compounds Against RSV

To investigate the antiviral activity of the newly designed compounds against RSV, five compounds from series I and series II were selected to explore the structure-activity relationships (SAR) of this class of compounds. The selection criteria were solely made based on having representatives from the computationally studied compounds to establish SAR and to validate our model. Three compounds from Series I, **6a**, **6b**, and **6c** along with **10d** from series II and compound **11** were selected for the initial antiviral screening using the viral progeny inhibition assay at 10 μ M. Among the tested compounds, compound **6a** showed significantly reduced RSV progeny production with no observable impact on cell viability (**Figure 2.13B**). Although compounds **6b** and **6c** share the same scaffold but with different substituents on the indolinone fragment, both compounds exhibited non-significant reduction of the RSV progeny production when compared

to **6a** which have no substitutions on the indolinone part. The activity of compound **10d** was also assessed along with compound **11** which is structurally similar to the lead compound **1** except for the substitution of 2 chlorine atoms at positions C 2 and C 5 instead of a bromine at C 3. Both compounds did not elicit a reduction in RSV progeny production at 10 μ M (**Figure 2.13B**).

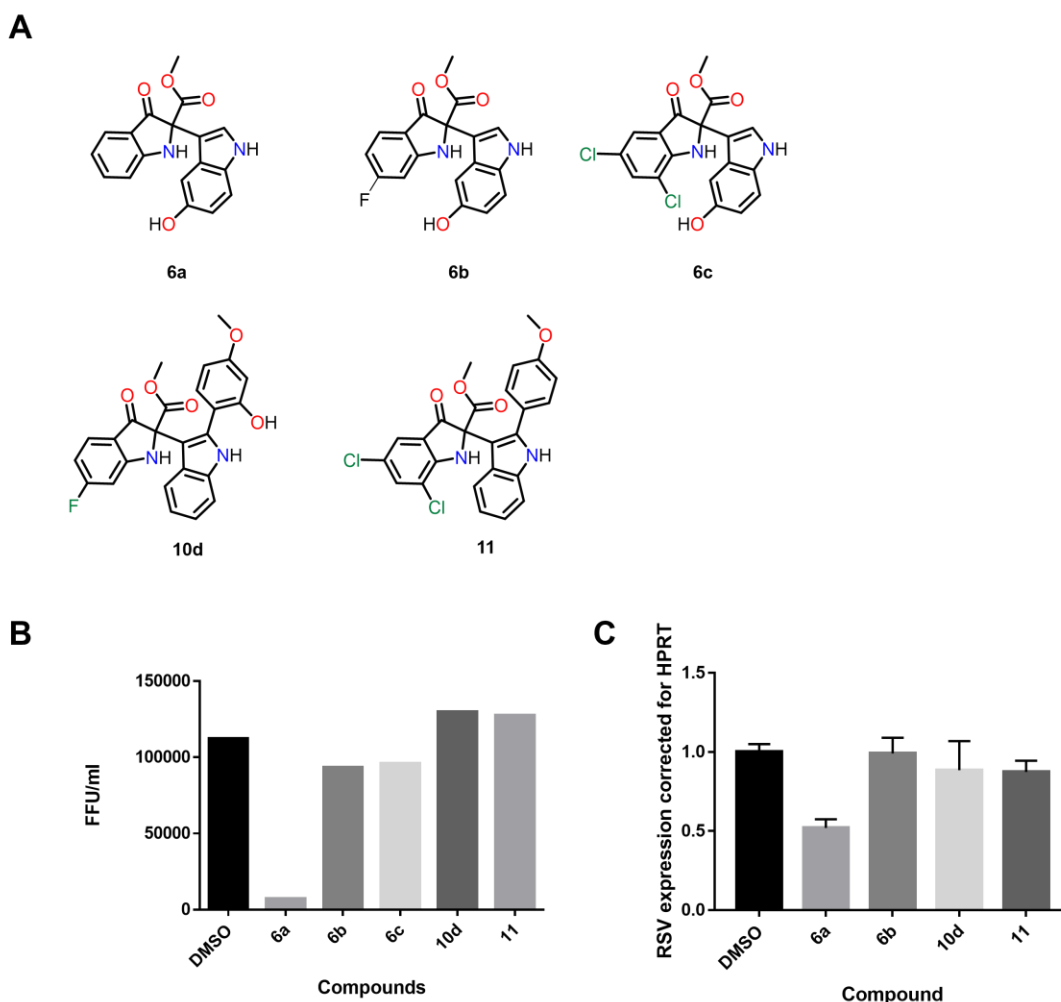


Figure 2.13: Effect of Bis-indoles on RSV progeny production. **A.** Structures of the tested compounds. **B.** RSV viral progeny inhibition assay in the presence of the test compounds showing substantial inhibition of viral progeny in the presence of compound **6a**. Viral titers were performed in triplicate and expressed as focus-forming units (FFU/ml) and compounds were tested at 10 μ M concentration. **C.** Effect of bis-indole compounds on RSV viral RNA production quantified by qRT-PCR in the presence of DMSO as a negative control. Data represent treatments performed in biological triplicate while the qPCR was performed in technical duplicate.

To further evaluate the antiviral activity of the bis-indole compounds selected for screening, the RSV viral RNA production was measured in the presence of the compounds by

qPCR. As expected, compound **6a** showed the most promising activity in inhibiting viral replication compared to other compounds in this test set (**Figure 2.13C**).

These results confirm the antiviral activity observed in the viral progeny assay and come in agreement with our computational model where compound **6a** showed a relative binding free energy -37.60 ± 2.7 kcal/mol and complemented the conformation of the allosteric binding site while the rest of the tested compounds exhibited a relatively low binding free energy ranging from -24 to -34 kcal/mol. Based on these precedents, it is notable that the substitutions on the bis-indole greatly affect their antiviral activity.

It is worth noting that at this point of the work the world was impacted by the emergence of the COVID-19 pandemic caused by severe acute respiratory syndrome coronavirus 2 (SARS-CoV-2) and our attention was shifted to developing a drug that can combat the virus as will be discussed in the Chapter 3. As the results are not conclusive at this stage, we were not able to draw a SAR for this class of compound. Further investigations will be carried out including structural optimization and virological testing for the hit compound **6a**.

2.2.9 Mutant Escape Assay

The emergence of viral resistance following the treatment with a biologically active compound confers a great challenge in the development of pharmaceutically active drugs, especially in the elucidation of the viral target and the mechanism of action for such drugs. Previous efforts to develop a resistant mutant against the lead compound **1** were unsuccessful even with 14 serial passages over 5 weeks.²⁰ This may suggest that the burden of resistant mutations to evade this class of compounds is extravagant and do not suggest a fit and highly resistant RSV strain emerged. We thought to explore this further by serially passaging RSV in the presence of high concentrations (20 and 50 μ M) compound **1** for 20-24 passages in order to force the virus to

evade the treatment and develop resistance. Preliminary data, will be discussed further in Chapter 4, revealed the emergence of a resistant mutant (W893F) following treatment with compound **1**. This result suggests that the bis-indole compounds are targeting the RSV L protein and further validates our model which predicted the compounds possibly binding in a pocket where the identified resistance occurred. Future work will comprise isolation of the resistance escape mutants and further validation by measuring the compound IC₅₀s for the wild type and the mutant.

2.3 Conclusion

Respiratory syncytial virus (RSV) is the most common cause of infant hospitalizations worldwide. Various efforts have been made to combat RSV infections by developing small molecule antivirals; however, to date, the only FDA approved treatment for severe respiratory tract infections is ribavirin and the monoclonal antibody palivizumab for prophylaxis. Moreover, the absence of X-ray structures for the RdRp enzyme before 2019 halted several drug discovery attempts to develop effective therapeutics targeting the viral replication complex.

In this work, we utilized the recently published cryo-EM structure of the RSV L protein to structurally guide the design of a novel class of non-nucleoside polymerase inhibitors based on our previously discovered bis(indole) antivirals. A computational drug design approach has been employed to analyze the RSV L protein for possible druggable binding sites based on compound **1**. Our investigation led to the identification of an allosteric binding site located near the NTP entry site, and the stability of the residues lining this pocket was extensively investigated by MD simulations. Following a 60 ns long MD simulation of the apoprotein, *in silico* screening of the lead compound identified several residues that the compound can interact with and form a stable complex. We used our model to modify and optimize the lead compound, which eventually led to some modifications on the parent molecule, including removing the 2-aryl moiety at the indole C2

position and incorporating a hydroxyl group at the C5 of the indole. This modification was envisioned to enrich the binding by building a strong network of hydrogen bond interactions. Another series of compounds were also designed carrying only a single change from the parent compound where a hydroxyl group was incorporated at the C2 position on the aryl group of the 2-aryl indole. All the designed compounds have been ranked for their relative binding free energy using the MM/GBSA method to inform our synthesis decision.

The synthesis of all compounds followed our previously published dual catalytic metallocarbene-azide cascade chemistry involving an *in-situ* formation of a C-acylimine followed by Friedel-Crafts alkylation with an indole nucleophile. The antiviral activity of selected compounds represented both designed libraries has been screened *in vitro* for their ability to inhibit RSV viral progeny production and RNA production. Among the tested compounds, compound **6a** showed the most promising hit, which reduced the viral progeny production and reduced viral loads. This result agreed with our computational model regarding the possible binding site of this class of compounds, potentially leading to identifying a novel mechanism of viral protein inhibition. Viral resistant mutants following the treatment with the lead compound for several passages (~20 passages) emerged a viral mutant with a mutation at residue Trp 893, which has been computationally identified to interact with our compounds.

In the future, plans were set to isolate resistant mutants and evaluate the antiviral activity of our compounds in order to get insights into the mechanism of action of this class of compounds. Co-crystallization of our lead compound with the RSV L protein is also in progress, and the evaluation of the untested compounds. In conclusion, we have built a computational model that identified the putative binding site of a novel class of antiviral compounds against RSV with potential broad-spectrum activity, as discussed in Chapter 3.

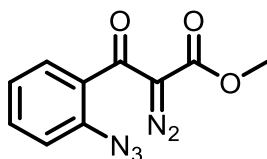
2.4 Experimental Section[†]

2.4.1 Chemical Synthesis.

Unless otherwise noted, all commercially available reagents were purchased and used without further purification unless otherwise noted. All the solvents used for reactions. Flash chromatography columns were packed with 230–400 mesh silica gel (Silicycle). Nuclear magnetic resonance (NMR) spectra were obtained using Agilent/ Varian VNMRS 400, 500, or 700 MHz spectrometers. For ¹H spectra, δ values were referenced to CDCl₃ (7.26 ppm) or DMSO-d₆ (2.49 ppm), and for ¹³C spectra, δ values were referenced to CDCl₃ (77.16 ppm) or DMSO-d₆ (39.5 ppm). Low-resolution mass was measured using Agilent Technologies 1100MSD LCMS (Single Quadruple) or Waters (Micromass) Q-TOF Premier LCMS/MS quadruple time of flight (TOF). High-resolution mass was measured using Agilent Technologies 6220 orthogonal time of flight or Kratos Analytical MS-50G double focusing sector.

2.4.1.1 Representative Procedure for the Synthesis of Bis(Indole) Compounds 5a-e

Synthesis of methyl 3-(2-azidophenyl)-2-diazo-3-oxopropanoate (**5a**).

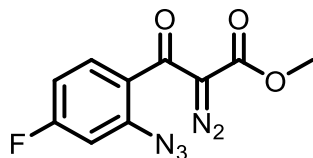


The title compounds were obtained following Scheme 2.1. For compound **5a** 2-azidobenzoic acid (0.82 g, 1.0 equiv.) was added to a round-bottomed flask charged with DCM (35 mL) under N₂ atmosphere and the suspension was cooled to 0 °C before the addition of

[†] I was responsible for the design and synthesis of all compounds in addition to designing and performing all the computational experiments. Leanne Bilawchuk and Danica Fae Besavilla were responsible for conducting *in vitro* virological assays. Farah Elawar carried out the mutant escape assay.

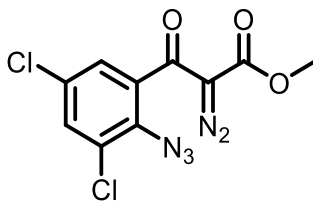
trichloroacetyl chloride (0.70 mL, 1.20 equiv.) followed by the addition of methyl acetate (0.40 mL, 1.0 equiv.). The solution was then transferred to a suspension of NaH (0.33 g, 1.50 equiv.) in DCM (10 mL) cooled at 0 °C. The solution was stirred at 0 °C for 15 min before being cooled to -45 °C followed by the addition of 1-methylimidazole (0.50 mL, 1.20 equiv.). After stirring for an additional 10 min at -45 °C, TiCl₄ (2.4 mL, 3.4 equiv.) was slowly added followed by Et₃N (2.8 mL, 4.0 equiv.). The reaction was kept at -45 °C for 45 min before being warmed up to 0 °C and kept at this temperature for an additional 1 h. The reaction was quenched with water, and the organic layer was separated, and the aqueous layer was washed three times with dichloromethane. The combined organic layers were subsequently washed with water and brine, dried over MgSO₄, filtered, and concentrated under reduced pressure to furnish the crude mixture as an orange oil. The crude product was purified by flash chromatography (gradient 1 to 30% EtOAc in hexane) to afford 930 mg (85%) of the beta keto ester product **4a** as an orange oil; *R_f* = 0.60 (7:3 hexanes: EtOAc). The keto ester **4a** (900 mg, 1.0 equiv.) was then added to a stirred solution of triethylamine (0.70 mL, 1.20 equiv) in CH₃CN (15 mL). Tosyl azide (0.90 mL, 1.0 equiv) in CH₃CN (10 mL) was transferred via cannula into the flask, and the reaction was stirred for 12 h. The reaction was monitored by TLC and LCMS for the formation of the new product and upon reaction completion, the crude mixture was concentrated *in vacuo* followed by purification via flash chromatography (gradient elution 9:1 then 8:2 hexane/EtOAc) to afford the desired product **5a** as a yellow oil (910 mg, 67%); *R_f* = 0.46 (7:3 hexanes: EtOAc). ¹H NMR (500 MHz, CDCl₃) δ 7.48 – 7.41 (m, 1H), 7.26 (dd, *J* = 7.8, 1.6 Hz, 1H), 7.18 – 7.11 (m, 2H), 3.71 (s, 3H). ¹³C NMR (126 MHz, CDCl₃) δ 185.7, 160.9, 137.8, 132.0, 130.4, 128.5, 124.8, 118.4, 52.4. (N.B.: the ¹³C signal for the diazo carbon was not detected due to quadrupolar broadening.) HRMS (ESI) calcd for C₁₀H₇N₅O₃ [M]⁺ 245.0549, found 245.0549.

Methyl 3-(2-azido-4-fluorophenyl)-2-diazo-3-oxopropanoate (**5b**)



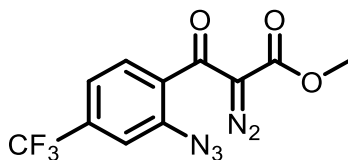
The title compound was prepared analogously to **5a** starting from 2-azido-4-fluorobenzoic acid; isolated as reddish oil (10 mg, 62% yield from the beta keto ester intermediate **4b**); $R_f = 0.56$ (7:3 hexanes: EtOAc). $^1\text{H NMR}$ (700 MHz, CDCl_3) δ 7.32 (dd, $J = 9.1, 5.9$ Hz, 1H), 6.94 – 6.88 (m, 2H), 3.77 (s, 3H). $^{13}\text{C NMR}$ (176 MHz, CDCl_3) δ 184.7, 164.7 (d, $J = 253.4$ Hz), 160.9, 140.2 (d, $J = 9.0$ Hz), 130.7 (d, $J = 9.9$ Hz), 126.6 (d, $J = 3.6$ Hz), 112.3 (d, $J = 22.1$ Hz), 106.0 (d, $J = 25.2$ Hz), 52.5. (N.B.: the ^{13}C signal for the diazo carbon was not detected due to quadrupolar broadening.) HRMS (ESI) calcd for $\text{C}_{10}\text{H}_6\text{FN}_5\text{O}_3\text{Na}$ $[\text{M}+\text{Na}]^+$ 286.0347, found 286.0344.

Methyl 3-(2-azido-3,5-dichlorophenyl)-2-diazo-3-oxopropanoate (**5c**)



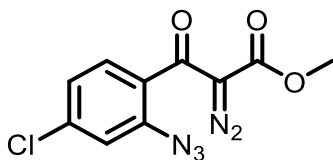
The title compound was prepared analogously to **5a** using 2-azido-3,5-dichlorobenzoic acid; isolated as bright yellow oil (400 mg, 63% from the beta keto ester intermediate **4c**); $R_f = 0.57$ (7:3 hexanes: EtOAc). $^1\text{H NMR}$ (400 MHz, CDCl_3) δ 7.39 (d, $J = 2.3$ Hz, 1H), 7.31 (d, $J = 2.4$ Hz, 1H), 3.82 (s, 3H). $^{13}\text{C NMR}$ (101 MHz, CDCl_3) δ 185.5, 161.2, 143.4, 133.2, 129.9, 121.0, 119.8, 119.4, 52.7. (N.B.: the ^{13}C signal for the diazo carbon was not detected due to quadrupolar broadening.) HRMS (ESI) calcd for $\text{C}_{10}\text{H}_5\text{Cl}_2\text{N}_5\text{O}_3\text{Na}$ $[\text{M}+\text{Na}]^+$ 335.9662, found 335.9660.

Methyl 3-(2-azido-4-(trifluoromethyl)phenyl)-2-diazo-3-oxopropanoate (**5d**)



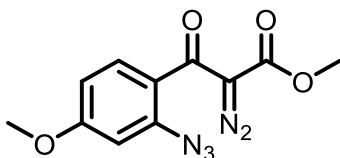
The title compound was prepared analogously to **5a** using 2-azido-4-(trifluoromethyl) benzoic acid; isolated as red oil (50 mg, 46% from the beta keto ester intermediate **4d**) ; $R_f = 0.50$ (7:3 hexanes: EtOAc). $^1\text{H NMR}$ (500 MHz, CDCl_3) δ 7.45 (ddd, $J = 7.9, 1.6, 0.8$ Hz, 1H), 7.42 – 7.38 (m, 2H), 3.77 (s, 3H). $^{13}\text{C NMR}$ (126 MHz, CDCl_3) δ 184.8, 160.6, 138.7, 133.8 (q), 129.0, 124.0, 122.5, 121.7 (q), 115.4 (q), 52.6. (N.B.: the ^{13}C signal for the diazo carbon was not detected due to quadrupolar broadening.) HRMS (ESI) calcd for $\text{C}_{11}\text{H}_6\text{F}_3\text{N}_5\text{O}_3\text{Na}$ $[\text{M}+\text{Na}]^+$ 336.0315, found 336.0316.

Methyl 3-(2-azido-4-chlorophenyl)-2-diazo-3-oxopropanoate (**5e**)



The title compound was prepared analogously to **5a** using 2-azido-4-chlorobenzoic acid; isolated as yellow oil (1.5 g, 62% from the beta keto ester intermediate **4e**) ; $R_f = 0.69$ (7:3 hexanes: EtOAc). $^1\text{H NMR}$ (500 MHz, CDCl_3) δ 7.26 – 7.21 (m, 1H), 7.16 (d, $J = 6.8$ Hz, 2H), 3.76 (s, 3H). $^{13}\text{C NMR}$ (126 MHz, CDCl_3) δ 184.7, 160.8, 139.2, 137.8, 129.7, 128.8, 125.2, 118.6, 52.4. (N.B.: the ^{13}C signal for the diazo carbon was not detected due to quadrupolar broadening.) HRMS (ESI) calcd for $\text{C}_{10}\text{H}_6\text{ClN}_5\text{O}_3\text{Na}$ $[\text{M}+\text{Na}]^+$ 302.0051, found 302.0051.

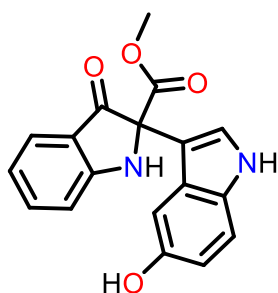
Methyl 3-(2-azido-4-methoxyphenyl)-2-diazo-3-oxopropanoate (**5f**)



The title compound was prepared analogously to **5a** using 2-azido-4-methoxybenzoic acid; isolated as red oil (250 mg, 54% from the beta keto ester intermediate **4f**) ; $R_f = 0.69$ (7:3 hexanes: EtOAc). $^1\text{H NMR}$ (500 MHz, CDCl_3) δ 7.31 (d, $J = 8.6$ Hz, 1H), 6.72 (dd, $J = 8.6, 2.3$ Hz, 1H), 6.68 (d, $J = 2.3$ Hz, 1H), 3.86 (s, 3H), 3.78 (s, 3H). $^{13}\text{C NMR}$ (126 MHz, CDCl_3) δ 184.8, 162.9, 161.3, 139.9, 130.9, 123.1, 110.4, 104.2, 55.7, 52.4. (N.B.: the ^{13}C signal for the diazo carbon was not detected due to quadrupolar broadening.) HRMS (ESI) calcd for $\text{C}_{11}\text{H}_9\text{N}_5\text{O}_4\text{Na}$ $[\text{M}+\text{Na}]^+$ 298.0547, found 298.0550.

2.4.1.2 Representative Procedure for the Synthesis of the Bis(Indole) Compounds (**6a-e** and **10a-e**)

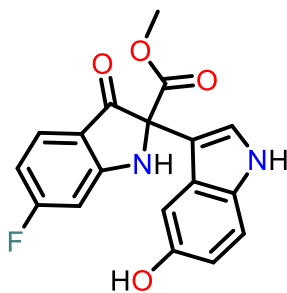
Synthesis of methyl 2-(5-hydroxy-1H-indol-3-yl)-3-oxoindoline-2-carboxylate (**6a**)



To an oven dried round-bottomed flask, a solution of 5-hydroxyindole (221 mg, 0.60 mmol) in DCM (25 mL) and $\text{Cu}(\text{OTf})_2$ (6.50 mg, 0.031 mmol) were stirred for 5 min followed by the addition of a solution of diazo-azide **5a** (75 mg, 0.31 mmol) via a syringe pump over 1 h at room temperature. Once the addition was completed, the reaction was monitored by TLC for consumption of starting material **5a**. After 24 h, the starting material was completely consumed,

and the reaction mixture was concentrated under reduced pressure and purified by flash chromatography (silica gel, gradient elution 8:2 then 7:3 hexane/EtOAc) to afford the bis-indole product **6a** as a yellow oil (90 mg, 91%); $R_f = 0.24$ (7:3 hexanes: EtOAc). ^1H NMR (500 MHz, CDCl_3) δ 8.08 (s, 1H), 7.69 (d, $J = 7.8$ Hz, 1H), 7.53 (ddd, $J = 8.3, 7.1, 1.4$ Hz, 1H), 7.37 (d, $J = 2.7$ Hz, 1H), 7.22 (dd, $J = 8.7, 0.6$ Hz, 1H), 7.03 – 6.97 (m, 2H), 6.93 (ddd, $J = 7.9, 7.1, 0.8$ Hz, 1H), 6.78 (dd, $J = 8.7, 2.4$ Hz, 1H), 5.69 (s, 1H), 4.55 (s, 1H), 3.81 (s, 3H). ^{13}C NMR (126 MHz, CDCl_3) δ 194.6, 168.9, 161.0, 149.9, 137.9, 131.8, 126.1, 125.4, 124.5, 120.4, 119.9, 113.6, 112.6, 112.3, 111.0, 104.2, 72.4, 53.8. HRMS (ESI) calcd for $\text{C}_{18}\text{H}_{13}\text{N}_2\text{O}_4$ $[\text{M}-\text{H}]^-$ 321.0881; found 321.0879.

Methyl 6-fluoro-2-(5-hydroxy-1H-indol-3-yl)-3-oxoindoline-2-carboxylate (**6b**)

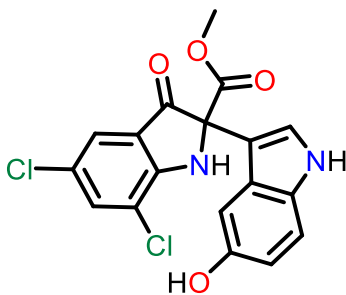


The title compound was prepared analogously to **6a**, but using (0.16 mmol) of **5b** instead of **5a**, and the product was purified by flash chromatography following the previously mentioned procedure and was isolated as yellow oil in 73% yield; $R_f = 0.22$ (7:3 hexanes: EtOAc). ^1H NMR (500 MHz, CDCl_3) δ 8.12 (s, 1H), 7.68 (ddd, $J = 9.1, 5.7, 0.7$ Hz, 1H), 7.36 (d, $J = 2.9$ Hz, 1H), 7.23 (dd, $J = 8.7, 0.6$ Hz, 1H), 7.02 – 6.91 (m, 2H), 6.82 – 6.76 (m, 1H), 6.63 (ddd, $J = 8.9, 6.8, 2.1$ Hz, 2H), 5.80 (s, 1H), 3.82 (s, 3H). ^{13}C NMR (126 MHz, CDCl_3) δ 192.7, 168.8 (d, $J = 5.8$ Hz), 162.5 (d, $J = 14.1$ Hz), 150.1, 131.9, 128.9, 127.9 (d, $J = 12.4$ Hz), 12.50, 126.1, 124.6, 116.3,

112.6 (d, $J = 42.3$ Hz), 110.8, 109.2 (d, $J = 24.7$ Hz), 104.21, 100.0 (d, $J = 26.0$ Hz), 73.0, 54.0.

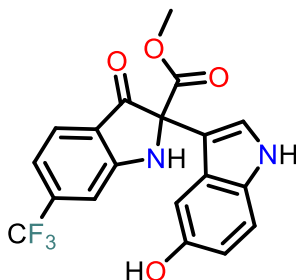
HRMS (ESI) calcd for $C_{18}H_{12}FN_2O_4$ $[M-H]^-$ 339.0787; found 339.0787.

Methyl 5,7-dichloro-2-(5-hydroxy-1H-indol-3-yl)-3-oxoindoline-2-carboxylate (**6c**)



The title compound was prepared analogously to **6a**, but using (0.14 mmol) of **5c** instead of **5a**, and the product was isolated as yellow oil in 84% yield; $R_f = 0.20$ (7:3 hexanes: EtOAc). 1H NMR (500 MHz, $CDCl_3$) δ 8.14 (s, 1H), 7.55 (dd, $J = 12.6, 2.0$ Hz, 2H), 7.35 (d, $J = 2.8$ Hz, 1H), 7.23 (d, $J = 8.7$ Hz, 1H), 7.01 (d, $J = 2.4$ Hz, 1H), 6.80 (dd, $J = 8.7, 2.4$ Hz, 1H), 5.83 (s, 1H), 3.83 (s, 3H). ^{13}C NMR (126 MHz, $CDCl_3$) δ 192.8, 167.8, 155.6, 150.0, 136.4, 131.8, 125.7, 125.5, 124.5, 123.2, 121.6, 119.2, 112.8, 112.4, 109.9, 104.2, 73.3, 54.0. HRMS (ESI) calcd for $C_{18}H_{12}Cl_2N_2O_4$ $[M+H]^+$ 389.0101; found 389.0095.

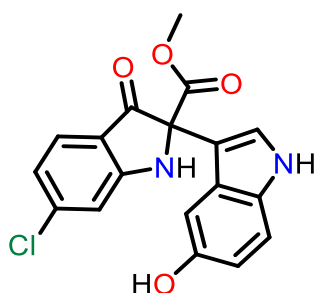
Methyl 2-(5-hydroxy-1H-indol-3-yl)-3-oxo-6-(trifluoromethyl)indoline-2-carboxylate (**6d**)



The title compound was carried out on a small scale (18 mg, 0,060 mmol of the intermediate **5d**), prepared and purified analogously to **6a**, and the product was isolated as yellow oil in 68 % yield;

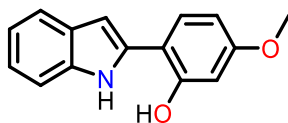
$R_f = 0.24$ (7:3 hexanes: EtOAc). $^1\text{H NMR}$ (500 MHz, CDCl_3) δ 8.11 (s, 1H), 7.78 (d, $J = 8.1$ Hz, 1H), 7.36 (d, $J = 2.8$ Hz, 1H), 7.24 (d, $J = 8.8$ Hz, 2H), 7.15 (d, $J = 5.2$ Hz, 1H), 7.08 – 6.94 (m, 2H), 6.80 (dd, $J = 8.7, 2.4$ Hz, 1H), 5.86 (s, 1H), 3.82 (s, 3H). HRMS (ESI) calcd for $\text{C}_{19}\text{H}_{13}\text{F}_3\text{N}_2\text{O}_4\text{Na}$ $[\text{M}+\text{Na}]^+$ 413.0720; found 413.0720. (Due to small scale of the reaction, no ^{13}C data was obtained.)

Methyl 6-chloro-2-(5-hydroxy-1H-indol-3-yl)-3-oxoindoline-2-carboxylate (**6e**)



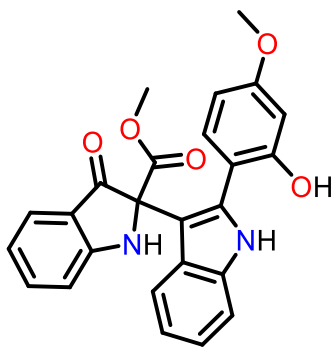
The title compound was prepared analogously to **6a** but using (1.7 mmol) of **5e** instead of **5a**, and the product was isolated as yellow oil in 98% yield; $R_f = 0.22$ (7:3 hexanes: EtOAc). $^1\text{H NMR}$ (700 MHz, CDCl_3) δ 8.11 (s, 1H), 7.60 (d, $J = 8.4$ Hz, 1H), 7.35 (d, $J = 2.7$ Hz, 1H), 7.22 (d, $J = 8.7$ Hz, 1H), 6.98 (dd, $J = 3.8, 2.0$ Hz, 3H), 6.89 (dd, $J = 8.2, 1.7$ Hz, 1H), 6.79 (dd, $J = 8.7, 2.4$ Hz, 1H), 5.75 (s, 1H), 3.82 (s, 3H). $^{13}\text{C NMR}$ (176 MHz, CDCl_3): δ 192.9, 168.0, 155.8, 150.1, 136.5, 131.9, 125.9, 125.6, 124.6, 123.4, 121.7, 119.4, 112.9, 112.5, 110.0, 104.3, 73.4, 54.1. HRMS (ESI) calcd for $\text{C}_{18}\text{H}_{14}\text{ClN}_2\text{O}_4$ $[\text{M}+\text{H}]^+$ 357.0637; found 357.064.

2-(1H-Indol-2-yl)-5-methoxyphenol (**9**)



Phenyl hydrazine (3 mL, 30 mmol) was added to a stirred solution of 2'-hydroxy-4'-methoxyacetophenone (5 g, 30 mmol) in absolute EtOH (30 mL), followed by 5 drops of HOAc. The reaction mixture was heated at 80 °C for 1 h. The reaction was allowed to cool to rt, and then the solvent was removed under reduced pressure. Polyphosphoric acid (PPA, 10 mL) was added to the residue, and the mixture was heated slowly to 130 °C and kept for 1 h. The reaction mixture was poured on ice and neutralised with 2 M NaOH. After neutralization, the greyish solid formed was filtered, washed with water (3 x 100 mL) and purified by flash chromatography (gradient 5 to 20% EtOAc in hexane) to afford the desired compound **9** as yellow- grey solid (4.9 g, 68%). ¹H NMR (500 MHz, DMSO-*d*₆) δ 10.96 (s, 1H), 10.20 (s, 1H), 7.65 (d, *J* = 8.6 Hz, 1H), 7.46 (dd, *J* = 7.8, 1.2 Hz, 1H), 7.41 (dd, *J* = 8.0, 1.0 Hz, 1H), 7.01 (ddd, *J* = 8.1, 6.9, 1.2 Hz, 1H), 6.94 (ddd, *J* = 8.0, 7.0, 1.1 Hz, 1H), 6.82 (d, *J* = 0.9 Hz, 1H), 6.56 (d, *J* = 2.5 Hz, 1H), 6.52 (dd, *J* = 8.6, 2.6 Hz, 1H), 3.75 (s, 3H). ¹³C NMR (126 MHz, DMSO-*d*₆) δ 159.4, 155.5, 136.0, 135.5, 128.4, 128.3, 120.4, 119.2, 118.7, 112.1, 111.0, 105.3, 101.8, 99.2, 55.0. HRMS (ESI) calcd for C₁₅H₁₃O₂ [M-H]⁻ 238.0874; found 238.0872.

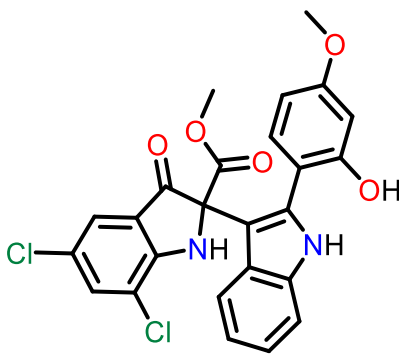
Methyl 2-(2-(2-hydroxy-4-methoxyphenyl)-1H-indol-3-yl)-3-oxoindoline-2-carboxylate (**10a**)



The title compound was prepared analogously to **6a** but using 2.0 equiv of compound **9** in place of 5-hydroxyindole and (0.017 mmol) of **5a**, **10a** was isolated as yellow semisolid in 52% yield;

$R_f = 0.31$ (7:3 hexanes: EtOAc). ^1H NMR (500 MHz, CDCl_3) δ 8.07 (s, 1H), 7.63 (dd, $J = 7.8, 1.3$ Hz, 1H), 7.57 (ddd, $J = 8.4, 7.1, 1.4$ Hz, 1H), 7.35 – 7.29 (m, 2H), 7.18 (ddd, $J = 8.1, 7.1, 1.1$ Hz, 1H), 7.13 (d, $J = 8.4$ Hz, 1H), 7.04 – 6.90 (m, 3H), 6.56 (d, $J = 2.5$ Hz, 1H), 6.52 (dd, $J = 8.4, 2.5$ Hz, 1H), 5.69 (s, 1H), 3.80 (s, 3H), 3.29 (s, 3H). (N.B.: the ^1H signal for the phenolic proton was not detected). ^{13}C NMR (126 MHz, CDCl_3) δ 196.6, 168.3, 162.1, 160.8, 156.8, 138.3, 135.6, 132.3, 131.8, 126.1, 125.6, 122.9, 120.5, 120.5, 119.8, 119.3, 113.1, 111.2, 111.0, 110.3, 106.8, 102.1, 73.3, 55.4, 53.3. HRMS (ESI) calcd for $\text{C}_{25}\text{H}_{20}\text{N}_2\text{O}_5\text{Na}$ $[\text{M}+\text{Na}]^+$ 451.1264; found 451.1257.

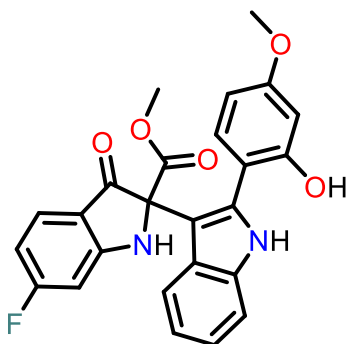
Methyl 5,7-dichloro-2-(2-(2-hydroxy-4-methoxyphenyl)-1H-indol-3-yl)-3-oxoindoline-2-carboxylate (**10b**)



The title compound was prepared analogously to **10a**, and the product was isolated as yellow oil in 67% yield; $R_f = 0.40$ (7:3 hexanes: EtOAc). ^1H NMR (500 MHz, CDCl_3) δ 8.11 (s, 1H), 7.57 – 7.51 (m, 1H), 7.48 (dd, $J = 2.0, 0.7$ Hz, 1H), 7.38 – 7.32 (m, 1H), 7.28 – 7.19 (m, 2H), 7.14 – 7.03 (m, 2H), 6.56 – 6.49 (m, 2H), 3.81 (s, 3H), 3.38 (s, 3H). (N.B.: the ^1H signal for the phenolic and indolinone protons were not detected). ^{13}C NMR (126 MHz, CDCl_3) δ 194.6, 167.6, 162.4, 156.5, 155.5, 136.7, 135.7, 132.3, 131.9, 126.1, 125.6, 123.3, 123.3, 121.3, 120.9, 119.6, 119.0, 111.4,

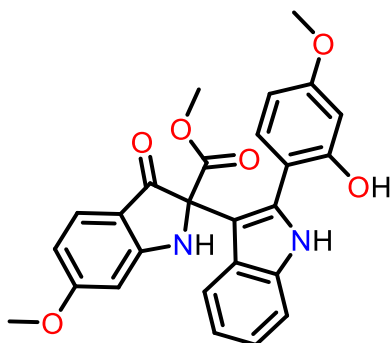
110.9, 109.8, 107.1, 102.0, 74.1, 55.6, 53.7. HRMS (ESI) calcd for $C_{25}H_{18}Cl_2N_2O_5Na$ $[M+Na]^+$ 519.0485; found 518.0482.

Methyl 6-fluoro-2-(2-(2-hydroxy-4-methoxyphenyl)-1H-indol-3-yl)-3-oxoindoline-2-carboxylate
(10d)



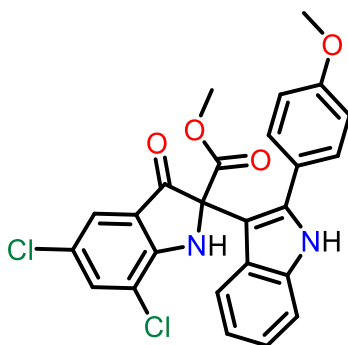
The title compound was prepared analogously to **10a** but using (0.18 mmol) of **5d** instead of **5a**, and the product was isolated as yellow oil in 58% yield; $R_f = 0.30$ (7:3 hexanes: EtOAc). 1H NMR (500 MHz, $CDCl_3$) δ 8.06 (s, 1H), 7.66 – 7.60 (m, 1H), 7.37 – 7.28 (m, 3H), 7.23 – 7.16 (m, 1H), 7.13 (d, $J = 8.4$ Hz, 1H), 7.06 – 6.99 (m, 1H), 6.64 (dd, $J = 9.1, 7.5$ Hz, 2H), 6.57 (d, $J = 2.5$ Hz, 1H), 6.53 (dd, $J = 8.4, 2.5$ Hz, 1H), 5.79 (s, 1H), 3.81 (s, 3H), 3.30 (s, 3H). ^{13}C NMR (126 MHz, $CDCl_3$) 194.6, 168.1, 162.3 (d, $J = 3.3$ Hz), 156.9, 135.7, 132.4, 131.9, 128.2 (d, $J = 12.5$ Hz), 126.1, 123.2, 120.7, 119.8, 115.9, 111.2 (d, $J = 4.1$ Hz), 110.1, 109.3 (d, $J = 24.7$ Hz), 107.0, 102.3, 99.6 (d, $J = 26.2$ Hz), 74.0, 55.5, 53.5. (N.B.: three carbon resonance ^{13}C were missing and could not be properly assigned). HRMS (ESI) calcd for $C_{25}H_{18}FN_2O_5$ $[M-H]^-$ 445.1205; found 445.1194.

Methyl 2-(2-(2-hydroxy-4-methoxyphenyl)-1H-indol-3-yl)-6-methoxy-3-oxoindoline-2-carboxylate (**10e**)



The title compound was prepared analogously to **10a** but using (2.0 mmol) of **5e** instead of **5a**, and the product was isolated as yellow oil in 69% yield; $R_f = 0.30$ (7:3 hexanes: EtOAc). ^1H NMR (500 MHz, CDCl_3) δ 8.03 (s, 1H), 7.55 (d, $J = 8.7$ Hz, 1H), 7.37 – 7.30 (m, 2H), 7.21 – 7.11 (m, 2H), 7.00 (ddd, $J = 8.2, 7.1, 1.0$ Hz, 1H), 6.59 (d, $J = 2.5$ Hz, 1H), 6.52 (td, $J = 8.6, 2.3$ Hz, 2H), 6.41 (d, $J = 2.1$ Hz, 1H), 5.69 (s, 1H), 3.90 (s, 3H), 3.81 (s, 3H), 3.25 (s, 3H). (N.B.: the ^1H signal for the phenolic proton was not detected). ^{13}C NMR (126 MHz, CDCl_3) δ 194.3, 168.8, 168.6, 163.3, 162.2, 157.3, 135.7, 132.4, 131.9, 127.3, 126.2, 123.0, 120.6, 120.0, 112.7, 111.5, 111.1, 110.5, 106.9, 102.5, 95.3, 73.9, 55.9, 55.5, 53.3. HRMS (ESI) calcd for $\text{C}_{26}\text{H}_{22}\text{N}_2\text{O}_6\text{Na}$ $[\text{M}+\text{Na}]^+$ 481.1370; found 481.1370.

Methyl 6-chloro-2-(2-(4-methoxyphenyl)-1H-indol-3-yl)-3-oxoindoline-2-carboxylate (**11**)



The title compound was prepared analogously to **10a** but using 2.0 equiv of 2-(4-methoxyphenyl) indole in place of compound **9**. The product was purified by gradient elution (8:2 then 7:3 hexane/EtOAc) and the product was isolated as yellow semisolid in 62% yield; $R_f = 0.40$ (7:3 hexanes: EtOAc). $^1\text{H NMR}$ (400 MHz, CDCl_3) δ 8.14 (s, 1H), 7.50 (dd, $J = 23.3, 2.0$ Hz, 2H), 7.34 (t, $J = 9.0$ Hz, 3H), 7.23 – 7.15 (m, 2H), 7.06 (ddd, $J = 8.1, 7.2, 1.1$ Hz, 1H), 6.88 (d, $J = 8.6$ Hz, 2H), 5.69 (s, 1H), 3.83 (s, 3H), 3.38 (s, 3H). HRMS (ESI) calcd for $\text{C}_{25}\text{H}_{18}\text{Cl}_2\text{N}_2\text{O}_4\text{Na}$ $[\text{M}+\text{Na}]^+$ 503.0536; found 503.0538. (Due to small scale that was used for this reaction, no ^{13}C data was obtained.)

2.4.2 Computational Details

2.4.2.1 Preparation of the Target Protein for MD Simulations

The cryo-electron microscopy structure of the RSV L protein bound to the tetrameric P protein (PDB ID: 6PZK) was used for our study. Initially, we started by building up the missing residues (609-626) using Prime implemented in the Schrödinger Small Molecule Discovery Suite.^{31, 38} The Protein Preparation Wizard module was used to add hydrogen atoms, minimize energy, and create appropriate protonation states for amino acid side chains and was then subjected to three stages of energy minimization. The AMBERff14SB force field parameters were assigned to the protein.³⁹ The protein was then solvated in a cubic box of TIP3P water.⁴⁰ The solvated system was then neutralized with the addition of Na^+/Cl^- counterions at a concentration of 0.15 M physiological ionic concentration using tleap in AmberTools18.^(ref) The system was then carried forward for subsequent MD simulation. Details on the MD simulations are discussed below.

2.4.2.2 Binding site identification

MD simulation trajectory for the RSV L protein were used to identify potential allosteric pockets. Three different tools were employed to search for those pockets, including fPocket²⁴, Site

Finder implemented in MOE⁴¹, and the SiteMap utility implement in Schrödinger.²⁵ Agreement between the three tools regarding pocket size and druggability scores were the main criteria for pocket selection.

2.4.2.3 Molecular docking

The 2D chemical structures of the ligands were built using ChemDraw version 19.0 and the structures were prepared using LigPrep wizard implemented in Schrödinger. Protonation states at pH 7.0 ± 2.0 for each ligand were assigned using Epik and the ligands' tautomers and conformations were calculated using the OPLS3e force field.^{42, 43} The docking grid box was defined in the center of residues Asn 895, Asp 899, Asp16, Lys 20 and Lys 1145 with a center coordinates of 149.41, 118.59, and 140.67. The Glide scoring function at extra precision (XP) was used for the docking simulations.³² A maximum of 10 poses were generated for each compound, and the top scoring pose was selected for each ligand.

2.4.2.4 MD Simulations and MM-GBSA Rescoring

Complexes preparation followed the above-described method. The force field parameters for the ligands were obtained using the GAFF force field⁴⁴ and Antechamber⁴⁵ and the AM1-BCC charges were assigned for the ligands.⁴⁶ The MD simulations were performed in pmemd.cuda: an initial minimization steps were performed in order to relax the water and ionic positions using 1000 steps of steepest descent and 1000 steps of conjugate gradients minimization, keeping all the complex atoms fixed through an harmonic restraint with a force constant of $500 \text{ kcal/mol/\AA}^2$. This step was followed by 2000 steps of steepest descent followed by 3000 steps of conjugate gradients without restraints. The systems were then heated gradually up from 0 to 300K in 100 ps using Langevin dynamics. During the heating process, the backbone of the protein and the heavy atoms of the ligand were restrained, and a time step of 0.5 fs and periodic volume conditions have been

employed during this phase. The time step has been set to 2 fs, and periodic pressure conditions (1 atm) have been imposed and the restraints have been gradually released in four phases of 50 ps each. The simulations were then continued for 60 ns of production. Analysis of the MD trajectory were carried out using CPPTRAJ.⁴⁷ Plots were generated using Gnuplot (version 5.4) and figures were generated using PyMol.

For MD snapshots extracted from the production simulations, we calculated the enthalpic portion of the binding energy using the Molecular Mechanics/Generalized Born Surface Area (MM/GBSA) method implemented in the MMPBSA.py script.⁴⁸ In MM/GBSA, the free energy change due to ligand binding is calculated as:

$$\Delta G_{\text{bind}} = \Delta E_{\text{MM}} + \Delta G_{\text{solv}} - T\Delta S \quad (1)$$

Where ΔE_{MM} , is the summation of non-bonded and bonded interaction energies. The solvation energy, ΔG_{solv} , is the sum of the polar and non-polar contributions of solvation, where the polar solvation terms are calculated using a Generalized-Born model (igb= 5) and the non-polar terms are computed based on the size of the solvent-accessible surface area. The ($T\Delta S$) portion of the equation refers to the entropic contribution and is computationally expensive and, therefore, is neglected. The pairwise decomposition analyses (idecomp = 4) using the MD trajectories were also carried out to identify the key ligand–residue energetic contributors to the binding free energy of the complexes.

2.4.3 Virological Assays

2.4.3.1 Cells and Virus

Henrietta Lack's (HeLa) cells from American Type Culture Collection (ATCC, CCL2) were grown in Dulbecco's modified Eagle's medium (DMEM) containing L-glutamine, glucose,

and sodium pyruvate with 10% heat inactivated fetal bovine serum (FBS). Human airway epithelial (1HAEO-) cells were grown in minimum essential medium (MEM) supplemented with 10% heat inactivated FBS. All cell lines were incubated at 37°C with 5% CO₂.

2.4.3.2 Compounds Evaluation and Infectious RSV Quantification

Confluent 1HAEO- cells were preincubated with the compounds for 1 h at 10 µM, followed by infection with RSV-A2-GFP at an MOI of 1 for 2 h. At 2 h post-infection, infectious medium was removed from wells to prevent carry over of infectious virus into progeny collections. Cells were fixed and permeabilized with methanol:acetone (1:1), blocked with PBS + 5% FBS, and stained with goat polyclonal anti-RSV antibody (1:1000 dilution), followed by the addition of an anti-goat secondary antibody conjugated to β-galactosidase (1:2000 dilution). Infected cells were stained blue upon the addition of X-Gal substrate (5-bromo-4-chloro-3-indoyl-β-galactopyranoside) in PBS containing 3 mM potassium ferricyanide, 3 mM potassium ferrocyanide and 1 mM magnesium chloride. The cleavage of the X-Gal substrate by β-galactosidase generates an insoluble blue precipitate which indicates RSV infection. Blue stained cells were manually counted as RSV focus-forming units by light microscopy using the EVOS FL Auto Cell Imaging System (Invitrogen).

2.4.3.3 Viral RNA Quantification by qRT-PCR

1HAEO- cells were preincubated with the inhibitors at 10 µM concentration for 1 h followed by infection with RSV-A2-GFP at an MOI of 1 for 24hr in the presence of the inhibitors. Samples worked up with Qiagen RNeasy + mini kit and qPCR straight from RNA with Quanta Qscript XLT 1-step ToughMix (QuantaBio, Beverly, MA, USA). Treatments were done in biological triplicate and qPCR was done in technical duplicate. RNA was quantified relative to *HPRT*.

2.5 References

1. Collins, P. L.; Graham, B. S., Viral and Host Factors in Human Respiratory Syncytial Virus Pathogenesis. *J. Virol.* **2008**, *82*, 2040.
2. Hall, C. B.; Weinberg, G. A.; Iwane, M. K.; Blumkin, A. K.; Edwards, K. M.; Staat, M. A.; Auinger, P.; Griffin, M. R.; Poehling, K. A.; Erdman, D.; Grijalva, C. G.; Zhu, Y.; Szilagyi, P., The burden of respiratory syncytial virus infection in young children. *N Engl J Med* **2009**, *360*, 588-98.
3. Falsey, A. R.; Hennessey, P. A.; Formica, M. A.; Cox, C.; Walsh, E. E., Respiratory syncytial virus infection in elderly and high-risk adults. *N Engl J Med* **2005**, *352*, 1749-59.
4. Resch, B., Burden of respiratory syncytial virus infection in young children. *World J Clin Pediatr* **2012**, *1*, 8-12.
5. Piedimonte, G.; Perez, M. K., Respiratory syncytial virus infection and bronchiolitis. *Piedimonte G, Perez MK. Respiratory syncytial virus infection and bronchiolitis [published correction appears in Pediatr Rev. 2015 Feb;36(2):85]. Pediatr Rev.* **2014**, *35*, 519-530.
6. Pérez-Yarza, E. G.; Moreno, A.; Lázaro, P.; Mejías, A.; Ramilo, O., The association between respiratory syncytial virus infection and the development of childhood asthma: a systematic review of the literature. *Pediatr Infect Dis J* **2007**, *26*, 733-739.
7. Xu, L.; Gao, H.; Zeng, J.; Liu, J.; Lu, C.; Guan, X.; Qian, S.; Xie, Z., A fatal case associated with respiratory syncytial virus infection in a young child. *BMC infect. Dis.* **2018**, *18*, 217.
8. Blount, R. E., Jr.; Morris, J. A.; Savage, R. E., Recovery of cytopathogenic agent from chimpanzees with coryza. *Proc Soc Exp Biol Med* **1956**, *92*, 544-9.
9. Wegzyn, C.; Toh, L. K.; Notario, G.; Biguenet, S.; Unnebrink, K.; Park, C.; Makari, D.; Norton, M., Safety and Effectiveness of Palivizumab in Children at High Risk of Serious Disease Due to Respiratory Syncytial Virus Infection: A Systematic Review. *Infect Dis Ther* **2014**, *3*, 133-58.
10. Turner, T. L.; Kopp, B. T.; Paul, G.; Landgrave, L. C.; Hayes, D., Jr.; Thompson, R., Respiratory syncytial virus: current and emerging treatment options. *Clinicoecon Outcomes Res* **2014**, *6*, 217-25.
11. Jeffree, C. E.; Rixon, H. W. M.; Brown, G.; Aitken, J.; Sugrue, R. J., Distribution of the attachment (G) glycoprotein and GM1 within the envelope of mature respiratory syncytial virus filaments revealed using field emission scanning electron microscopy. *Virology* **2003**, *306*, 254-267.
12. Fields, B. N.; Knipe, D. M.; Howley, P. M., *Fields virology*. Wolters Kluwer Health/Lippincott Williams & Wilkins: Philadelphia, 2013.
13. Hacking, D.; Hull, J., Respiratory syncytial virus: viral biology and the host response. *J Infect* **2002**, *45*, 18-24.
14. Morin, B.; Kranzusch, P. J.; Rahmeh, A. A.; Whelan, S. P. J., The polymerase of negative-stranded RNA viruses. *Curr. Opin. Virol.* **2013**, *3*, 103-110.
15. Collins, P. L.; Fearn, R.; Graham, B. S., Respiratory syncytial virus: virology, reverse genetics, and pathogenesis of disease. *Curr. Top. Microbiol. Immunol.* **2013**, *372*, 3-38.

16. Noton, S. L.; Deflubé, L. R.; Tremaglio, C. Z.; Fearn, R., The Respiratory Syncytial Virus Polymerase Has Multiple RNA Synthesis Activities at the Promoter. *PLoS Pathog.* **2012**, *8*, e1002980.
17. Khattar, S. K.; Yunus, A. S.; Samal, S. K., Mapping the domains on the phosphoprotein of bovine respiratory syncytial virus required for N–P and P–L interactions using a minigenome system. *J. Gen. Virol.* **2001**, *82*, 775-779.
18. Gilman, M. S. A.; Liu, C.; Fung, A.; Behera, I.; Jordan, P.; Rigaux, P.; Ysebaert, N.; Tcherniuk, S.; Sourimant, J.; Eléouët, J.-F.; Sutto-Ortiz, P.; Decroly, E.; Roymans, D.; Jin, Z.; McLellan, J. S., Structure of the Respiratory Syncytial Virus Polymerase Complex. *Cell* **2019**, *179*, 193-204.e14.
19. Elawar, F.; Oraby, A. K.; Kieser, Q.; Jensen, L. D.; Culp, T.; West, F. G.; Marchant, D. J., Pharmacological targets and emerging treatments for respiratory syncytial virus bronchiolitis. *Pharmacology & Therapeutics* **2021**, *220*, 107712.
20. Atienza, B. J. P.; Jensen, L. D.; Noton, S. L.; Ansalem, A. K. V.; Hobman, T.; Fearn, R.; Marchant, D. J.; West, F. G., Dual Catalytic Synthesis of Antiviral Compounds Based on Metallocarbene–Azide Cascade Chemistry. *The Journal of Organic Chemistry* **2018**, *83*, 6829-6842.
21. Schrödinger, L. & DeLano, W., 2020. PyMOL, Available at: <http://www.pymol.org/pymol>.
22. Sutto-Ortiz, P.; Tcherniuk, S.; Ysebaert, N.; Abeywickrema, P.; Noël, M.; Decombe, A.; Debart, F.; Vasseur, J.-J.; Canard, B.; Roymans, D.; Rigaux, P.; Eléouët, J.-F.; Decroly, E., The methyltransferase domain of the Respiratory Syncytial Virus L protein catalyzes cap N7 and 2'-O-methylation. *PLoS Pathogens* **2021**, *17*, e1009562.
23. Battles, M. B.; Langedijk, J. P.; Furmanova-Hollenstein, P.; Chaiwatpongsakorn, S.; Costello, H. M.; Kwanten, L.; Vranckx, L.; Vink, P.; Jaensch, S.; Jonckers, T. H. M.; Koul, A.; Arnoult, E.; Peeples, M. E.; Roymans, D.; McLellan, J. S., Molecular mechanism of respiratory syncytial virus fusion inhibitors. *Nat. Chem. Biol.* **2016**, *12*, 87-93.
24. Le Guilloux, V.; Schmidtke, P.; Tuffery, P., Fpocket: An open source platform for ligand pocket detection. *BMC Bioinformatics* **2009**, *10*, 168.
25. Halgren, T., New Method for Fast and Accurate Binding-site Identification and Analysis. *Chemical Biology & Drug Design* **2007**, *69*, 146-148.
26. Halgren, T. A., Identifying and Characterizing Binding Sites and Assessing Druggability. *Journal of Chemical Information and Modeling* **2009**, *49*, 377-389.
27. Krivák, R.; Hoksza, D., Improving protein-ligand binding site prediction accuracy by classification of inner pocket points using local features. *Journal of Cheminformatics* **2015**, *7*, 12.
28. Lu, X.; McDonald, S. M.; Tortorici, M. A.; Tao, Y. J.; Vasquez-Del Carpio, R.; Nibert, M. L.; Patton, J. T.; Harrison, S. C., Mechanism for coordinated RNA packaging and genome replication by rotavirus polymerase VP1. *Structure* **2008**, *16*, 1678-88.
29. Cao, D.; Gao, Y.; Roesler, C.; Rice, S.; D'Cunha, P.; Zhuang, L.; Slack, J.; Domke, M.; Antonova, A.; Romanelli, S.; Keating, S.; Forero, G.; Juneja, P.; Liang, B., Cryo-EM structure of the respiratory syncytial virus RNA polymerase. *Nat Commun* **2020**, *11*, 368.

30. De Vivo, M.; Masetti, M.; Bottegoni, G.; Cavalli, A., Role of Molecular Dynamics and Related Methods in Drug Discovery. *Journal of Medicinal Chemistry* **2016**, *59*, 4035-4061.
31. Jacobson, M. P.; Pincus, D. L.; Rapp, C. S.; Day, T. J. F.; Honig, B.; Shaw, D. E.; Friesner, R. A., A hierarchical approach to all-atom protein loop prediction. *Proteins: Structure, Function, and Bioinformatics* **2004**, *55*, 351-367.
32. Friesner, R. A.; Murphy, R. B.; Repasky, M. P.; Frye, L. L.; Greenwood, J. R.; Halgren, T. A.; Sanschagrin, P. C.; Mainz, D. T., Extra Precision Glide: Docking and Scoring Incorporating a Model of Hydrophobic Enclosure for Protein–Ligand Complexes. *Journal of Medicinal Chemistry* **2006**, *49*, 6177-6196.
33. Wang, E.; Liu, H.; Wang, J.; Weng, G.; Sun, H.; Wang, Z.; Kang, Y.; Hou, T., Development and Evaluation of MM/GBSA Based on a Variable Dielectric GB Model for Predicting Protein–Ligand Binding Affinities. *Journal of Chemical Information and Modeling* **2020**, *60*, 5353-5365.
34. Chen, J.; Wang, J.; Zhang, Q.; Chen, K.; Zhu, W., Probing Origin of Binding Difference of inhibitors to MDM2 and MDMX by Polarizable Molecular Dynamics Simulation and QM/MM-GBSA Calculation. *Scientific Reports* **2015**, *5*, 17421.
35. Weng, Y. L.; Naik, S. R.; Dingelstad, N.; Lugo, M. R.; Kalyaanamoorthy, S.; Ganesan, A., Molecular dynamics and in silico mutagenesis on the reversible inhibitor-bound SARS-CoV-2 main protease complexes reveal the role of lateral pocket in enhancing the ligand affinity. *Scientific Reports* **2021**, *11*, 7429.
36. Misaki, T.; Nagase, R.; Matsumoto, K.; Tanabe, Y., Ti-Crossed-Claisen Condensation between Carboxylic Esters and Acid Chlorides or Acids: A Highly Selective and General Method for the Preparation of Various β -Keto Esters. *Journal of the American Chemical Society* **2005**, *127*, 2854-2855.
37. Jiang, X.; Hu, F., One-Pot Highly Regioselective Synthesis of Indole-Fused Pyridazino[4,5-b][1,4]benzoxazepin-4(3H)-ones by a Smiles Rearrangement. *Synlett* **2018**, *29*, 1207-1210.
38. Jacobson, M. P.; Friesner, R. A.; Xiang, Z.; Honig, B., On the Role of the Crystal Environment in Determining Protein Side-chain Conformations. *Journal of Molecular Biology* **2002**, *320*, 597-608.
39. Maier, J. A.; Martinez, C.; Kasavajhala, K.; Wickstrom, L.; Hauser, K. E.; Simmerling, C., ff14SB: Improving the Accuracy of Protein Side Chain and Backbone Parameters from ff99SB. *Journal of Chemical Theory and Computation* **2015**, *11*, 3696-3713.
40. Mark, P.; Nilsson, L., Structure and Dynamics of the TIP3P, SPC, and SPC/E Water Models at 298 K. *The Journal of Physical Chemistry A* **2001**, *105*, 9954-9960.
41. Vilar, S.; Cozza, G.; Moro, S., Medicinal chemistry and the molecular operating environment (MOE): application of QSAR and molecular docking to drug discovery. *Curr Top Med Chem* **2008**, *8*, 1555-72.
42. Shelley, J. C.; Cholleti, A.; Frye, L. L.; Greenwood, J. R.; Timlin, M. R.; Uchimaya, M., Epik: a software program for pK_a prediction and protonation state generation for drug-like molecules. *Journal of Computer-Aided Molecular Design* **2007**, *21*, 681-691.

43. Roos, K.; Wu, C.; Damm, W.; Reboul, M.; Stevenson, J. M.; Lu, C.; Dahlgren, M. K.; Mondal, S.; Chen, W.; Wang, L.; Abel, R.; Friesner, R. A.; Harder, E. D., OPLS3e: Extending Force Field Coverage for Drug-Like Small Molecules. *Journal of Chemical Theory and Computation* **2019**, *15*, 1863-1874.
44. Wang, J.; Wang, W.; Kollman, P. A.; Case, D. A., Automatic atom type and bond type perception in molecular mechanical calculations. *J Mol Graph Model* **2006**, *25*, 247-60.
45. Wang, J.; Wolf, R. M.; Caldwell, J. W.; Kollman, P. A.; Case, D. A., Development and testing of a general amber force field. *J Comput Chem* **2004**, *25*, 1157-74.
46. Jakalian, A.; Jack, D. B.; Bayly, C. I., Fast, efficient generation of high-quality atomic charges. AM1-BCC model: II. Parameterization and validation. *Journal of Computational Chemistry* **2002**, *23*, 1623-1641.
47. Roe, D. R.; Cheatham, T. E., PTRAJ and CPPTRAJ: Software for Processing and Analysis of Molecular Dynamics Trajectory Data. *Journal of Chemical Theory and Computation* **2013**, *9*, 3084-3095.
48. Miller, B. R.; McGee, T. D.; Swails, J. M.; Homeyer, N.; Gohlke, H.; Roitberg, A. E., MMPBSA.py: An Efficient Program for End-State Free Energy Calculations. *Journal of Chemical Theory and Computation* **2012**, *8*, 3314-3321.

Chapter 3:

Development of RespVirex: an Allosteric Inhibitor of SARS-CoV-2 Polymerase

3.1 Introduction

Coronaviruses (CoVs) comprise a large family of positive-sense RNA viruses causing respiratory disease in humans and animals.¹ Two highly pathogenic coronaviruses, severe acute respiratory syndrome (SARS-CoV) and the Middle East respiratory syndrome coronavirus (MERS-CoV), have emerged in 2002 and 2012, respectively, causing severe respiratory illness with high mortality rates.^{2, 3} Among this family, a novel severe acute respiratory syndrome coronavirus 2 (SARS-CoV-2) has emerged in 2019 causing a pandemic of the disease known as COVID-19.^{4, 5} The novel virus is characterised by high transmission efficiency leading to severe illness and ultimately death in many cases, specially with the emergence of several variants of concern.⁶

The emergence of SARS-CoV-2 has created an urgent need for the development of new antiviral drugs to combat the virus with higher efficiency and safety profiles. The race to find a cure for SARS-CoV-2 began with drug repositioning to find an effective therapeutic and/or prophylactic drug which represented an effective and rapid approach to identify new use of existing drugs.⁷ Antiviral agents could be developed to target the host-cell machinery essential for viral infection and/or replication, and as direct-acting antivirals (DAAs), targeting viral proteins.⁸ As the replication of the virus depends on the efficient synthesis of viral RNA, the replication complex of the virus represented an attractive therapeutic target for inhibition of virus infection. The RNA-dependant RNA Polymerase (RdRp) is one of the most frequently targeted viral proteins due to its crucial role in viral replication and production of viral RNA. Targeting viral proteins has proven

to be very successful approach in the inhibition of many RNA viruses as seen in the case of using DAAs in the treatment of hepatitis C virus (HCV).^{9, 10} Remdesivir (RDV) is the only FDA-approved drug for the treatment of patients with COVID-19.^{11, 12} RDV is a nucleotide analogue prodrug with a broad-spectrum antiviral activity targeting the RdRp of several RNA viruses.¹³⁻¹⁵ Since RDV is only given intravenously, this route of administration represents a great burden in the large-scale use of the drug. In this context, Pfizer has developed an oral bioavailable drug, PF-07321332, which targets the viral main protease (M^{pro},3CL^{pro}).¹⁶ The drug completely protected the tested animals against variants of concern and reduced the risk of hospitalization in humans and was approved by the FDA in December 2021 as the first orally administered anti-SARS-CoV-2 drug. Although there has been a great progress in the fight against COVID-19, especially regarding vaccines and antivirals development, the need for broad-spectrum antivirals is essential in the preparedness for future pandemics involving unknown viral pathogens.

Non-nucleoside inhibitors represent another class of direct-acting antivirals which target allosteric sites on the viral protein. The key reason for the lack of potent allosteric and non-nucleoside polymerase inhibitors is the absence of structural data where a co-crystallized ligand with the protein could be studied, which represent a great challenge for medicinal chemistry efforts. Therefore, computational tools have proved to be advantageous in many cases, including our work on developing respiratory syncytial virus polymerase inhibitors discussed in Chapter 2.

In this context, we expanded on our drug discovery campaign on a novel class of antiviral agents, which we named RespVirex, based on our lead compound **1**. (**Figure 3.1**) These compounds showed potential antiviral activity against several RNA viruses including Zika and respiratory syncytial virus (RSV).¹⁷ Molecular docking and molecular dynamics (MD) simulations were carried out to explore possible allosteric binding sites on the SARS-CoV-2 polymerase.

Following a detailed analysis of the proposed binding site, a new library of compounds with several modifications was designed, synthesized, and tested *in vitro* to evaluate the activity of this class of inhibitors as non-nucleoside polymerase inhibitors and potential broad-spectrum antivirals.

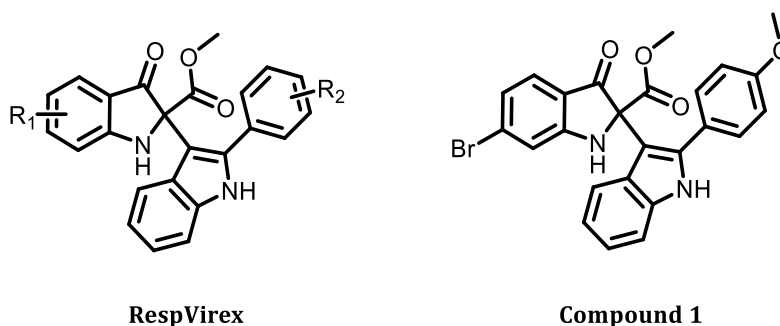


Figure 3.1: Core structure of RespVirex and its derivative compound **1**.

3.2 Results and Discussion:

3.2.1 RespVirex Inhibits SARS-CoV-2 RNA Synthesis

Our previous screening for antiviral small molecules introduced RespVirex as a promising lead compound with a broad-spectrum activity against positive and negative sense RNA viruses.¹⁷ The antiviral activity of RespVirex against SARS-CoV-2 polymerase was first determined using two analogues of RespVirex, compounds **1** and **2** (**Figure 3.2A**). Preliminary evaluation of the antiviral activity revealed that lower levels of SARS-CoV-2 viral genome was detected by qRT-PCR at a concentration of 10 μM (**Figure 3.2B**). Although compound **2** showed more inhibition of viral RNA than compound **1**, the activity observed was mainly due to the cytotoxic effect of the compound on the cells during the treatment which explains the observed lower RNA production. For further validation of the mode of action, the RNA synthesis by SARS-CoV-2 polymerase was monitored using purified SARS-CoV-2 RdRp complex composed of the proteins nsp7, nsp8, and nsp12. The results of this assay revealed that both derivatives significantly inhibited RNA synthesis at a concentration of 10 μM and provided evidence that this class of compounds is

targeting the RdRp complex of SARS-CoV-2 (**Figure 3.2C**). However, the exact binding site of these inhibitors needed to be investigated to design compounds with higher potency.

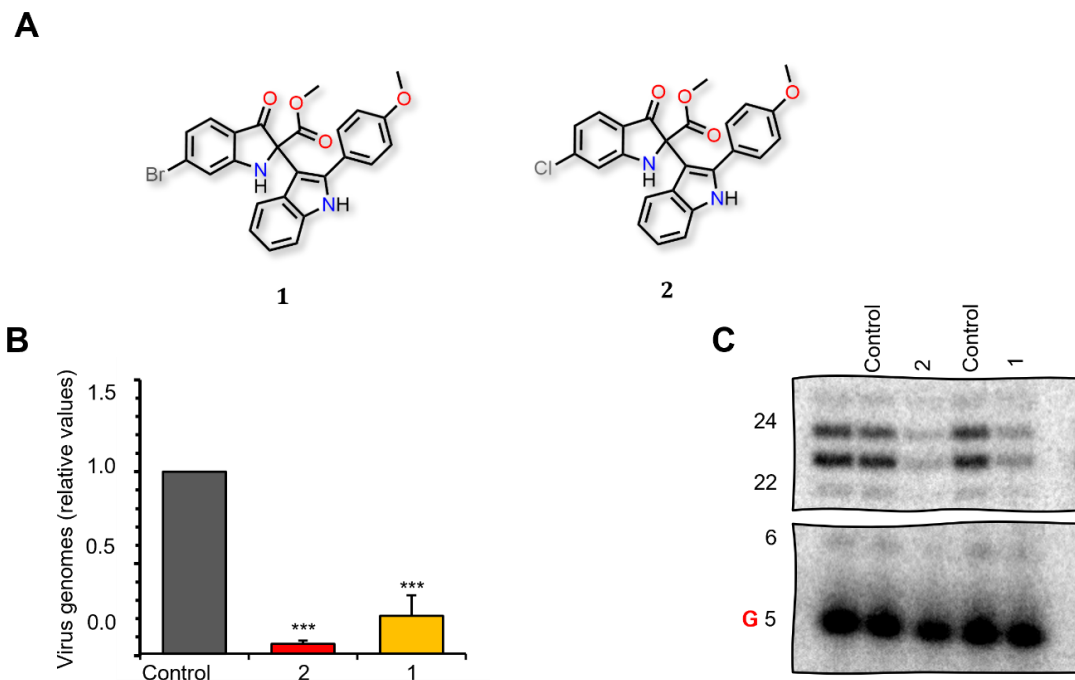


Figure 3.2: Activity of Bis(indole) derivatives on SARS-CoV-2. **A.** Structures of compounds **1** and **2**. **B.** Inhibition of viral RNA by RespVirex analogues. **C.** RNA synthesis inhibition by the tested compounds showing viral RNA product inhibition by RespVirex.

3.2.2 Computational Investigation of Druggable Binding Pockets in the SARS-CoV-2 Polymerase Identifies a Possible Allosteric Site

The RNA-dependant RNA polymerase (RdRp) of SARS-CoV-2 is composed of three subunits: the catalytic subunit known as nsp12 and two accessory subunits known as nsp7 and nsp8.^{18, 19} While nucleotide analog inhibitors target the active site of polymerase complexes, investigating how non-nucleoside inhibitors target allosteric binding sites can be very challenging in the absence of a high-resolution structure of a co-crystallized ligand with the protein of interest. To understand how RespVirex is inhibiting the replication of SARS-CoV-2, we began with a clear objective of identifying the putative binding pocket targeted by this class of compounds using the

published cryo-EM structures of the SARS-CoV-2 RdRp protein (PDB ID: 6M71 and 7AAP).²⁰,²¹ Computational tools were employed to investigate druggable binding sites within the nsp12 of SARS-CoV-2 including the fpocket script, Site Finder implemented in MOE and SiteMap utility implemented in Schrödinger discovery suite.²²⁻²⁵ This approach identified a large druggable binding site within the RdRp domain, denoted as pocket 2, located in close proximity to the active site, the Nidovirus associated nucleotidyl transferase domain (NiRAN) and the fingers domain of nsp12 (**Figure 3.3**). We decided to evaluate the druggability of this pocket using MD simulations.

To evaluate the dynamics and stability of the SARS-CoV-2 polymerase, a 100 ns long MD simulation was run using the cryo-EM structure (PDB ID: 7AAP), which is resolved at a resolution of 2.50 Å. The selected structure had the inhibitor favipiravir ribonucleoside triphosphate resolved in complex with the RdRp. Although other SARS-CoV-2 RdRp structures were used for the docking and evaluation of our compounds as potential inhibitors, we selected this structure in our study because of its high resolution. The stability of the protein was assessed during the MD simulation through the root mean square deviation (RMSD) of the protein backbone. The protein equilibrated around 20 ns of the simulation time with a little deviation from its starting coordinate with an RMSD of 2.4 Å (**Figure 3.4A**). Pocket 2 is formed by residues Val 315 to Phe 326, Phe 326 to Pro 328, Arg 457 to Pro 461, and Asn 628 to Val 675, Lys 676 and Pro 677.

The stability of pocket 2 residues was also assessed and showed an average RMSD value of 1.5 Å during the 100 ns simulation time. The flexibility of the protein residues was analyzed using the atomic fluctuation of the protein backbone atoms. Analysis of the atomic fluctuation data showed that the protein showed several regions with high rigidity, while the N-terminal β -harpin, and NiRAN subdomains showed the most flexibility among all RdRp domains (**Figure 3.4B**). To examine the accessibility of pocket 2 to potential inhibitors, the water hydration of the pocket was

studied by counting the number of water molecules within the first and second hydration shells throughout the MD trajectory. Pocket 2 allowed up to 20 water molecules to enter in the first hydration shell while allowing up to 130 water molecules in the second hydration shell (**Figure 3.4C**).

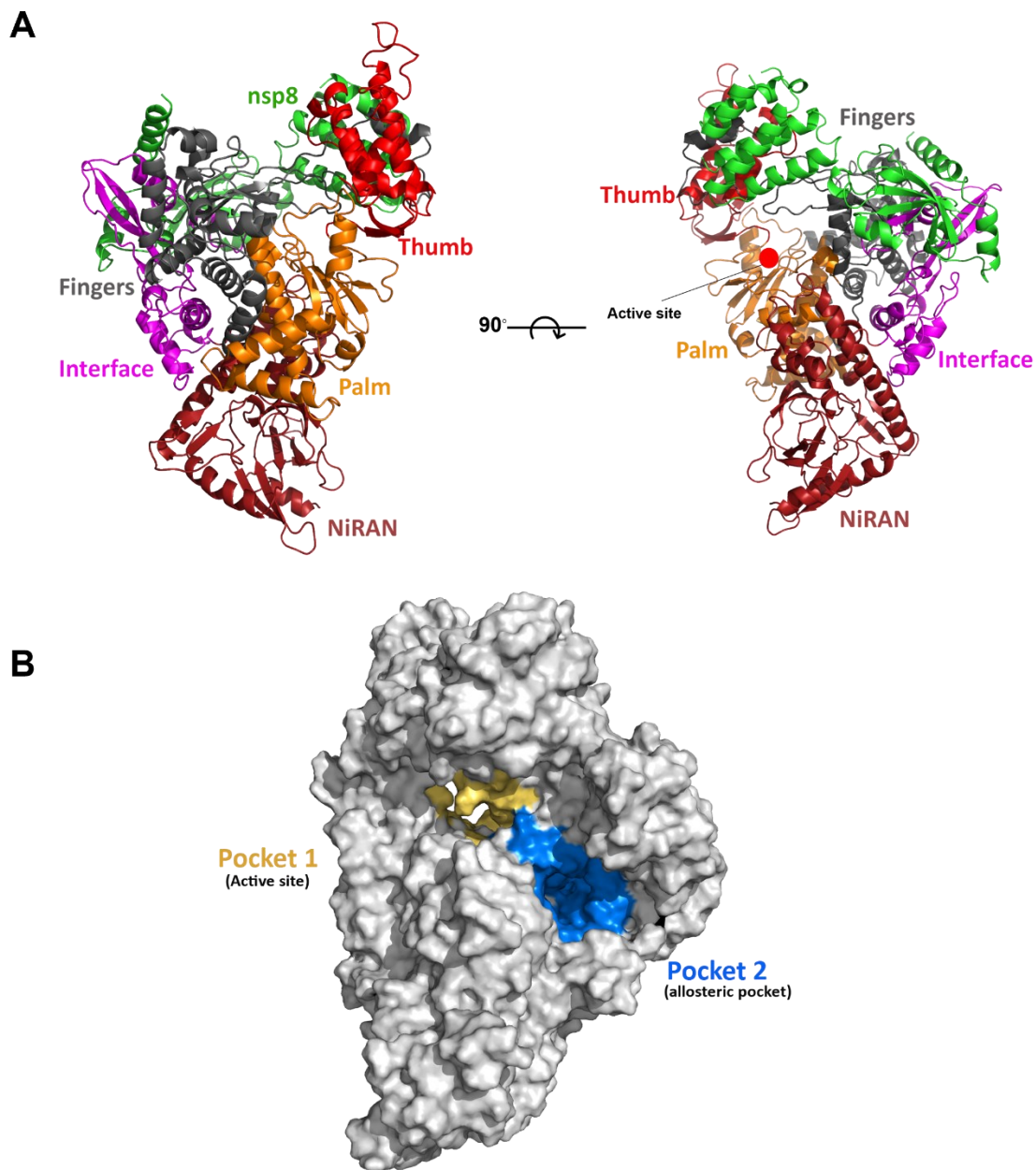


Figure 3.3: Structure of the SARS-CoV-2 replication complex. **A.** Two views of the SARS-CoV-2 polymerase structure related by 90° rotation showing color coded nsp12 and nps8 subunits of the RdRp. **B.** Surface representation

of the SARS-CoV-2 RdRp showing the active site (pocket 1) and the allosteric site (pocket 2). Figures generated using PyMOL.

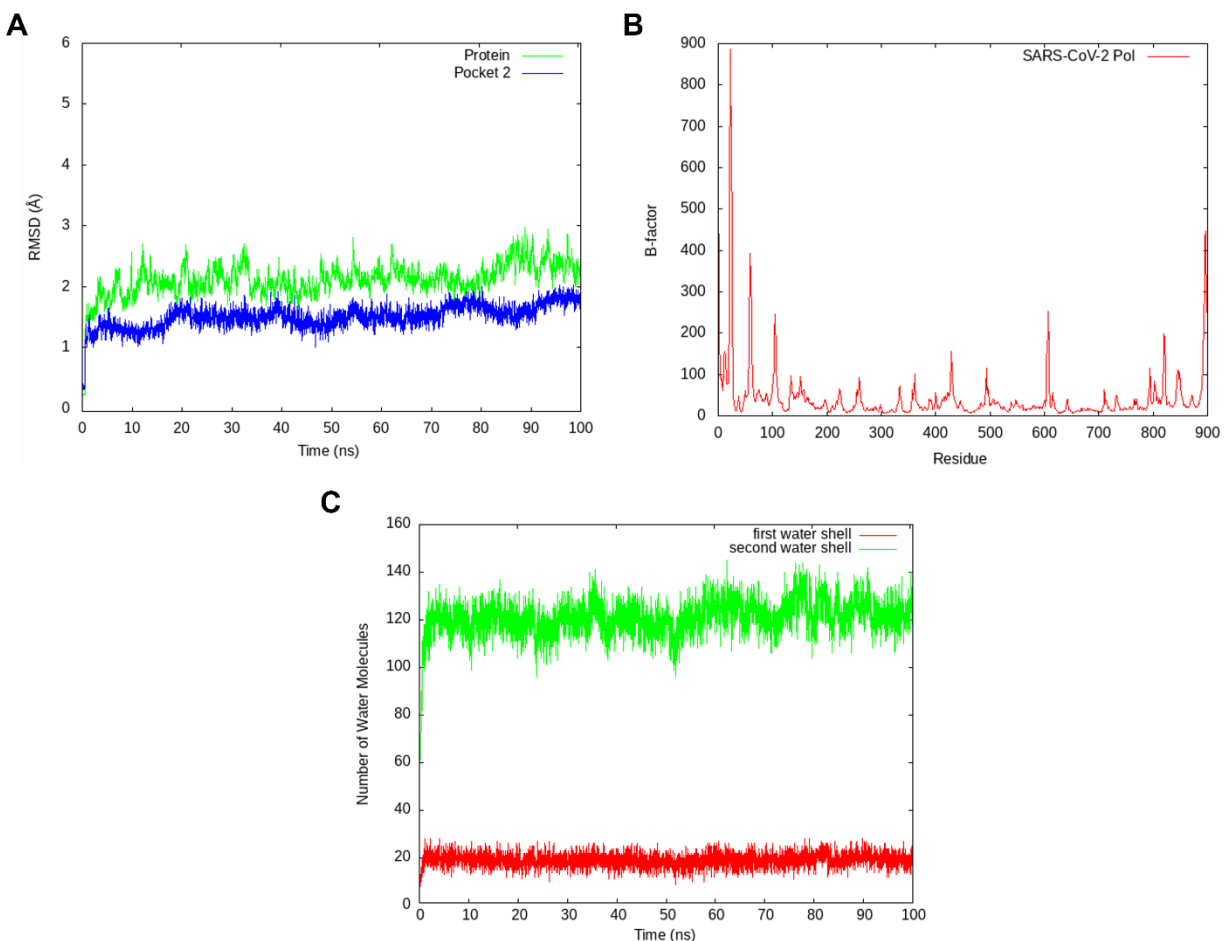


Figure 3.4: MD analysis of SARS-CoV-2 polymerase. **A.** RMSD of the backbone atoms of apo RdRp of SARS-CoV-2 (PDB ID: 7AAP). **B.** Atomic fluctuations of RdRp domain. **C.** Water shell analysis showing the number of water molecules accessing pocket 2 during the 100 ns MD simulation in the first and second water shells.

To further validate our selection of pocket 2 as the putative allosteric site, an MD trajectory analysis of the druggable pockets was conducted. The MDpocket tool is among the best tools to detect pockets and estimate their volume based on MD trajectories.²⁶ Analysis of the MD trajectories revealed that pocket 2 is the most druggable pocket among the investigated pockets with a volume of around $\sim 700 \text{ \AA}^3$ and a druggability score of 0.90 on a zero to one scale. The pocket size and water accessibility in addition to the computationally calculated druggability

scores support the potential of this pocket to be targeted by small molecule inhibitors. Further analysis of this binding site will be discussed.

3.2.3 Investigation of Compound 1 Putative Binding Pose

Based on the inhibitory activity observed against SARS-CoV-2 polymerase, compound **1** was used as a docking control to evaluate the possibility of binding this class of compounds to the identified pocket. To explore the potential binding poses, compound **1** was docked to the allosteric pocket 2 and the poses were ranked based on their favorable interactions and docking scores. Analysis of the binding poses revealed that the compound could potentially bind to the identified pocket with a docking score of -9.54 kcal/mol using the Glide extra precision (XP) scoring function implemented in Schrödinger Suite and -9.01 kcal/mol using the Lamarckian Genetic Algorithm in AutoDock.^{27, 28} Moreover, compound **2** was also docked and showed a docking score of -9.24 kcal/mol. The best scoring poses generated from the docking were subjected to 50 ns long simulations to further assess the stability in complexation with the SARS-CoV-2 polymerase. MD trajectory analysis showed that the complexes were stable in the bound state with an average RMSD of 2.1 and 3.0 Å for compound **1** and compound **2**, respectively (**Figure 3.5**). Both systems equilibrated after 25-30 ns of the simulation; however, the complex of compound **1** with the SARS-CoV-2 polymerase complex was found to be more stable, which could be explained based on the interactions displayed by each compound as will be discussed below.

Analysis of the protein-ligand interactions revealed that the indole fragment of both compounds **1** and **2** fitted into a hydrophobic cleft formed by Pro 461, Leu 460, and Val 675. The compounds also formed a highly stable hydrogen bond interaction between the indole (-NH) and the backbone oxygen of ASN 459 as assessed during the 50 ns MD simulation (**Figure 3.5**). The compounds were further stabilized inside the binding pocket through the formation of another

hydrogen bond between the ester carbonyl oxygen and the guanidinium side chain of ARG 349. Interestingly, compound **2** formed a halogen bond between the chlorine atom and the backbone oxygen of THR 319, contrary to compound **1**, which has bromine instead of chlorine, and did not form any halogen bonds with neighboring residues. We hypothesized that engaging this allosteric site could increase the inhibitor affinity and potency toward the nsp12 by changing the protein dynamics leading to a decrease in the polymerase turnover.

3.2.4 Design of New Analogues Based on the Lead Compound

To improve the potency of the lead compound, we sought to leverage the structure-based drug design principle and design molecules that can effectively engage our computationally proposed binding pocket. Examination of the binding mode of compound **1**, it was obvious that a steric clash between the methoxy group at C4 of the methoxyphenyl indole of compound **1** and the side chain of THR 394 hindered a possible hydrogen bond interaction at that position. Considering that the removal of the methoxy group could reduce this steric clash, a structure-based drug design approach was employed to explore this possibility. It was expected that enhancement of potency could be achieved by introducing a hydrogen bond donor at the C3 position instead of a methoxy group, which we thought could build a hydrogen bond with THR 394 and stabilize the compound (**Figure 3.6A**).

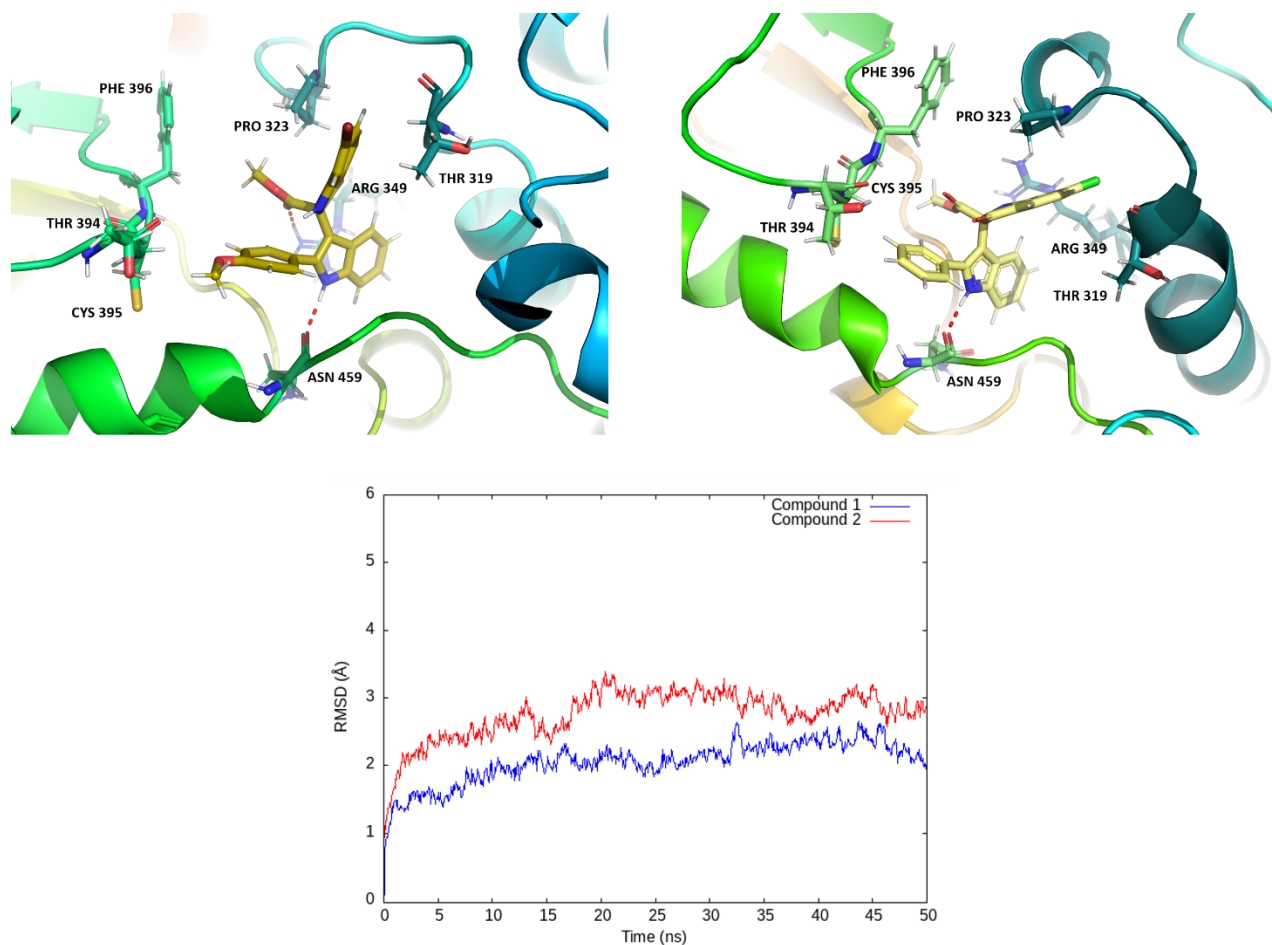


Figure 3.5: MD snapshot of 1 (top left) and 2 (top right) binding to the allosteric pocket of SARS-CoV-2. RMSD of the backbone atoms of compound 1 and 2 complexes with the nsp12 protein (bottom).

The suitability of the proposed modifications was assessed through a Poisson-Boltzmann electrostatic map of the binding site generated using Molecular Operating Environment (MOE).²⁹ Examination of the electrostatic map confirmed the suitability of adding a hydrogen bond donor (HBD) at the C3 position. Further analysis revealed that modification at this position could also contribute to another interaction by acting as a hydrogen bond acceptor through the interaction with the backbone NH of PHE 396 (**Figure 3.6B**). Based upon these analyses, we envisioned that adding a hydroxyl group at this position would potentially capture hydrogen bond interactions with the side chain of THR 394 and the backbone nitrogen of PHE 396, respectively.

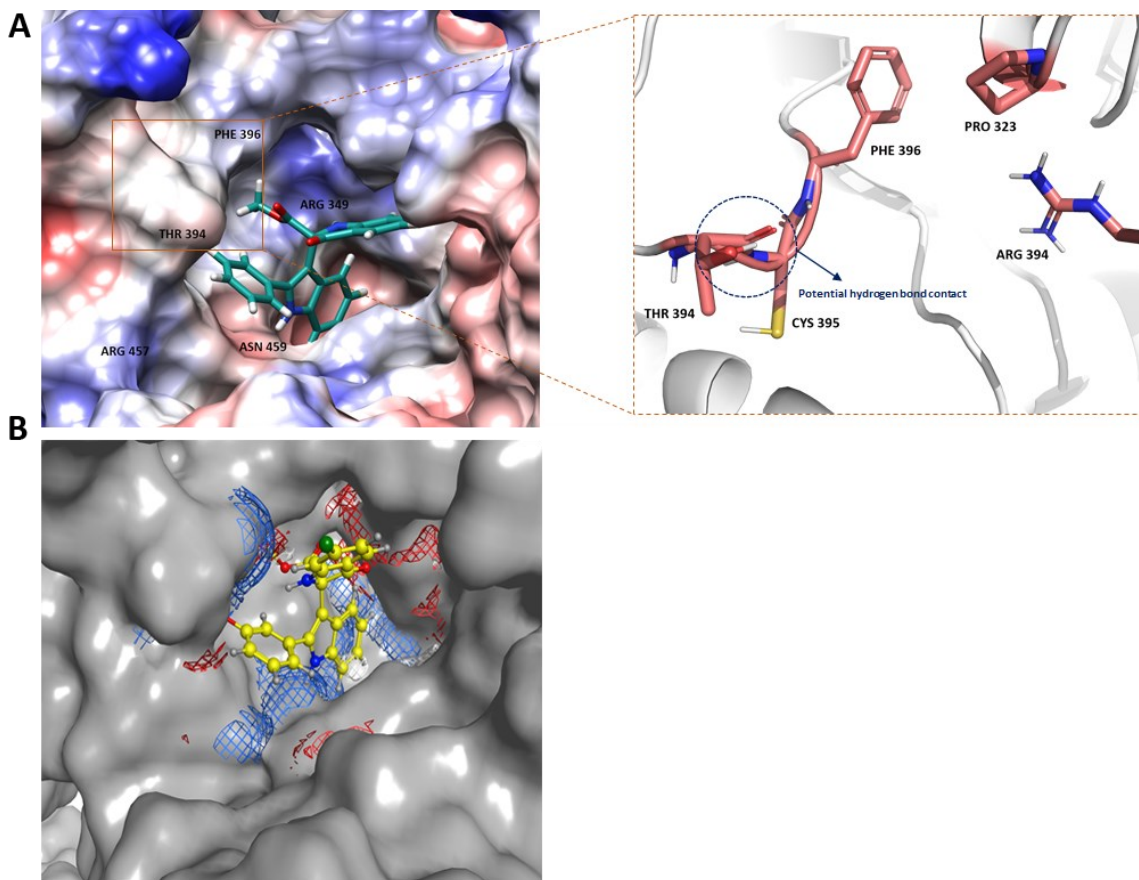


Figure 3.6: Allosteric site analysis. **A.** Putative binding site of the bis-indole based compounds in SARS-CoV-2 polymerase. **B.** Poisson-Boltzmann electrostatic feature maps of the allosteric binding site of SARS-CoV-2 polymerase. Blue, red, and white colors indicate zones where donor, acceptor, and hydrophobic probe atoms show a potential of -2 kcal/mol, respectively.

Given these precedents, the computational results inspired the synthesis of a new library that incorporated a phenolic hydroxyl group at C3 of the 2-phenylindole (**Figure 3.7**). Another set of modifications was considered based on the electrostatic map of the binding site, including protecting the nitrogen of the indole with an acyl group to evaluate the importance of the hydrogen bond formed between the indole ($-\text{NH}$) and ASN 459. The effect of such modification on the activity of the lead compound could be used as a proof-of-concept to validate our computational model. The first library of compounds was designed to incorporate several substitutions on the indolinone ring while maintaining a hydroxyl group at the C3 of the indole fragment. These

modifications were first evaluated computationally to inform the synthesis decision on which modifications could be carried out further.

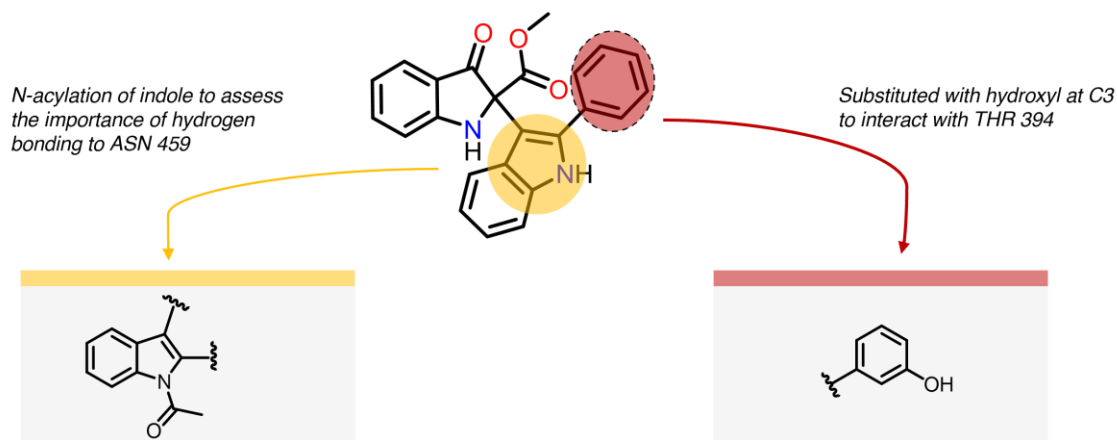


Figure 3.7: The design of new bis-indole derivatives based on compound 1.

3.2.5 Computational Evaluation of the Newly Designed Ligands using MD Simulations

Molecular dynamics (MD) simulations of protein-ligand complexes have proved to be a very useful tool in drug discovery.³⁰ Based on the proposed binding mode, several alternate substitutions on the indolinone fragment were designed and computationally evaluated. The stability of the ligands was assessed in their putative binding site using a 50 ns long MD simulation, and enantiomers of some compounds were evaluated to determine which isomer to carry forward to the antiviral evaluation.

Among the designed compounds were compounds **5** and **6** where both have chlorine atoms at alternating positions on the indolinone moiety, and both compounds showed a stable hydrogen bond between the indole (-NH) and the backbone oxygen of ASN 495. As expected, in compound **5**, the hydroxyl group at the C3 of the 2-phenylindole formed two hydrogen bonds with the backbone oxygen of THR 394 and the backbone nitrogen of PHE 396 (**Figure 3.8A**). In the case of compound **6**, the same

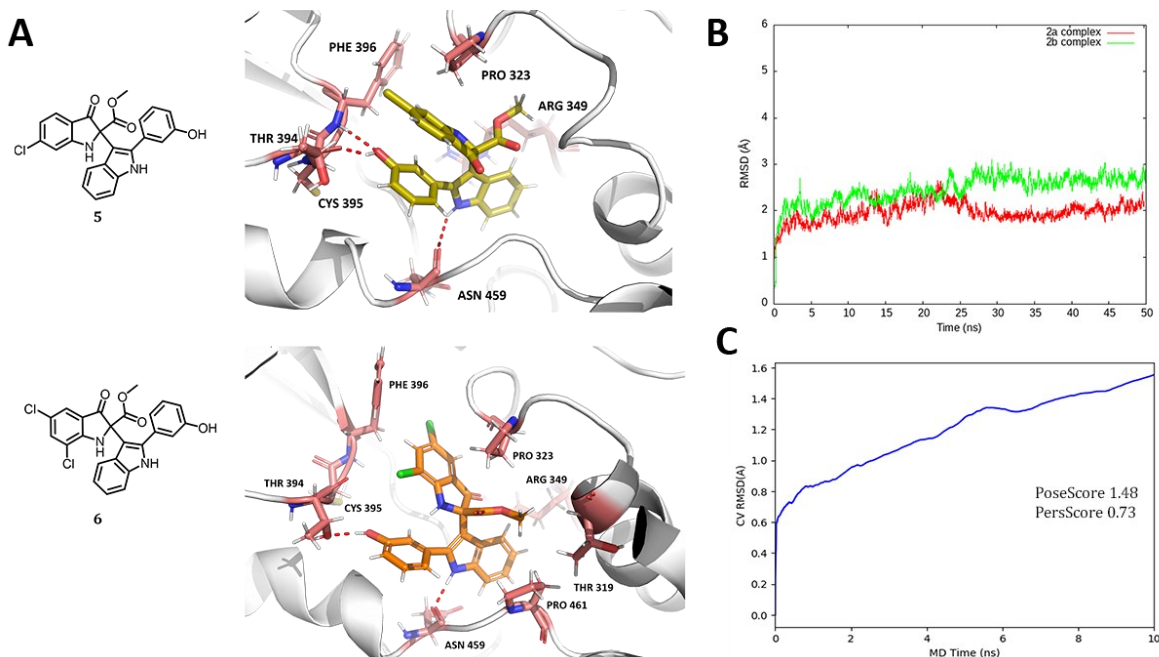


Figure 3.8: **A.** MD snapshot of **5** and **6** complexes showing ligands (the *S* configuration) putative binding poses in the allosteric binding site. **B.** RMSD of the backbone atoms of compounds **5** and **6** in complex with nsp12 protein (N.B.: **2a** refers to **5b** while **2b** refers to **6b**). **C.** Plot of RMSD estimate averaged over all ten trials of BPMD vs. simulation time for compound **6b** in complex with SARS-CoV-2 polymerase.

hydrogen bonds were observed, except that the interaction was observed with the side-chain oxygen of THR 394, and the hydrogen bond to the backbone nitrogen of PHE 396 was not established (**Figure 3.8A**). The stability of both complexes was assessed by the backbone RMSD in which both systems reached equilibrium around 30 ns of the simulation time. with an average fluctuation from the initial coordinates of 1.7 Å and 2.5 Å for **5** and **6** complexes, respectively (**Figure 3.8B**).

Although the structural flexibility of a biological system can be studied with MD simulations, an enhanced sampling method, such as metadynamics³¹, has proven to be more useful in predicting the ligand binding pose.³²⁻³⁴ This method enables sampling of the complex free-energy landscape by introducing bias into the system as a function of a chosen collective variable (CV). This will facilitate the exploration of the entire free-energy landscape and prevent the system from revisiting previously sampled regions.³⁵ Binding Pose MetaDynamics (BPMD) is an

automated, enhanced sampling, metadynamics-based protocol. This technique involves forcing the ligand to move around its binding pose.^{35, 36} The higher mobility of the ligand under a biasing potential is a sign of the binding mode instability. In this work, BPMD was used to validate the binding pose obtained from docking experiments, and compound **6** was used for this experiment. In this simulation, RMSD of the ligand heavy atoms was chosen as the collective variable (CV) and ten independent metadynamics simulations of 10 ns each were performed. The results were assessed for pose stability based on the PoseScore, that is, the RMSD of the ligand with respect to the initial ligand heavy atoms coordinates. The BPMD provides three scores: PoseScore, PersistenceScore (PersScore), and CompositeScore (CompScore). These scores reflect the stability of the ligand during the MD simulation. A detailed description of the key concepts and scores is discussed in the experimental section **3.4.1.5**. Briefly, a PoseScore $\leq 2\text{\AA}$ was considered a stable.³⁵ The results of the BPMD supported the docking poses obtained from docking and MD simulations with a PoseScore of 1.48. In addition, the binding pose had a PersScore of 0.73 which indicates that hydrogen bonds identified between the ligand and the protein at the beginning of the metadynamics are kept for $\sim 70\%$ during the averaged time of the simulation. These results suggest that the binding pose of compound **6** is highly stable under the BPMD bias, supporting our hypothesis that the compounds were accurately modeled in the allosteric binding site of SARS-CoV-2 RdRp (**Figure 3.8C**). To further computationally investigate the affinity of the designed compounds to the SARS-CoV-2 polymerase, the Molecular Mechanics/Generalized Born Surface area (MM/GBSA) method has been employed to estimate the relative binding free energy and the ligands' contributions to the binding.³⁷ The *S* configuration of compound **6**, (**6b**), displayed the best binding affinity with a score of -52.80 ± 3.5 kcal/mol followed by the *S* configuration of compound **5**, (**5b**), which exhibited ΔG of -49.94 ± 2.6 kcal/mol indicating a nano to low

micromolar inhibitors. The *R* enantiomers, compounds **5a** and **6a**, exhibited excellent binding affinity to pocket 2 with scores of -48.43 ± 2.5 and -48.96 ± 3.5 kcal/mol, respectively.

The MM/GBSA for some derivatives from the proposed library shown in (**Figure 3.9**) were also assessed and summarized in Table 3.1; however, we decided to evaluate the first set of derivatives as a proof-of-concept in the process of the lead optimization before synthesizing the rest of the suggested library.

Compound	ΔG_{bind} (kcal/mol)
5a	-48.43 ± 2.5
5b	-49.94 ± 2.6
6a	-48.96 ± 3.5
6b	-52.80 ± 3.5
7a	-33.08 ± 2.6
8a	-30.75 ± 2.8

Table 3.1: summary of MM/GBSA results showing the relative binding free energy of the proposed new compounds. Compounds 5b and 6b showed the highest binding affinity to the SARS-CoV-2 RdRp.

3.2.6 Chemical Synthesis

In Chapter 2, we reported the synthesis of the first- and second-generation antiviral inhibitors against Respiratory Syncytial Virus (RSV), in which several structural modifications of the parent bis-indole RespVirex were synthesized. In this chapter, our computational studies guided specific modifications on the parent molecule compound **1** to extensively investigate the structure-activity relationships of this class of compounds and to further validate our model.

Following the proposed binding poses of the compounds in the allosteric site of SARS-CoV-2 polymerase, series III compounds have the lead compound's methoxy group at C4 of the 2-phenylindole removed and replaced by a hydroxyl group at C3 to establish a potential hydrogen

bond with the protein amino acid residue at that position. This series also comprise different halogen substitutions at alternating positions of the indolinone fragment as could be seen in compounds **5**, **6**, **7**, **8**, **11**, and **12** (**Figure 3.9**).

The synthesis of the titled compounds followed the synthetic route depicted in Scheme 3.1. As described previously in Chapter 2, the targeted compounds were obtained through the reaction of the commercially available anthranilic acid derivatives with sodium azide to produce the intermediate azido anthranilic acid. The beta-keto ester compound (**3**) was formed, according to the Ti-crossed-Claisen condensation reported by Misaki *et al.*, from the reaction of the anthranilic acid derivative with trichloroacetyl chloride and methyl acetate promoted by TiCl₄ and *N*-methylimidazole at -45 °C to furnish this intermediate in good yields.³⁸ The Regitz-diazo transfer was the key step to produce the diazo-azide intermediate (**4**) by the reaction of (**3**) with tosyl azide in the presence of triethylamine at room temperature for 12 h. The intermediate **4** was then subjected to the reaction with Cu(OTf)₂ in DCM to catalytically produce copper metallocarbenes after an *in-situ* reduction of copper (II) precatalyst to copper(I) followed by a Friedel-Crafts alkylation by the indole. This step furnished the titled compounds in good to moderate yields.

We were intrigued by the prospect of testing structurally similar analogues of **5**. Our initial synthetic efforts aimed at enhancing the inhibitory activity of RespVirex while maintaining a good physicochemical profile and enhancing the solubility by modulating some structural features. Therefore, the second round of optimization involved the synthesis of **16**, which had the phenolic hydroxyl group replaced with a primary amine to facilitate a hydrochloric acid salt formation.

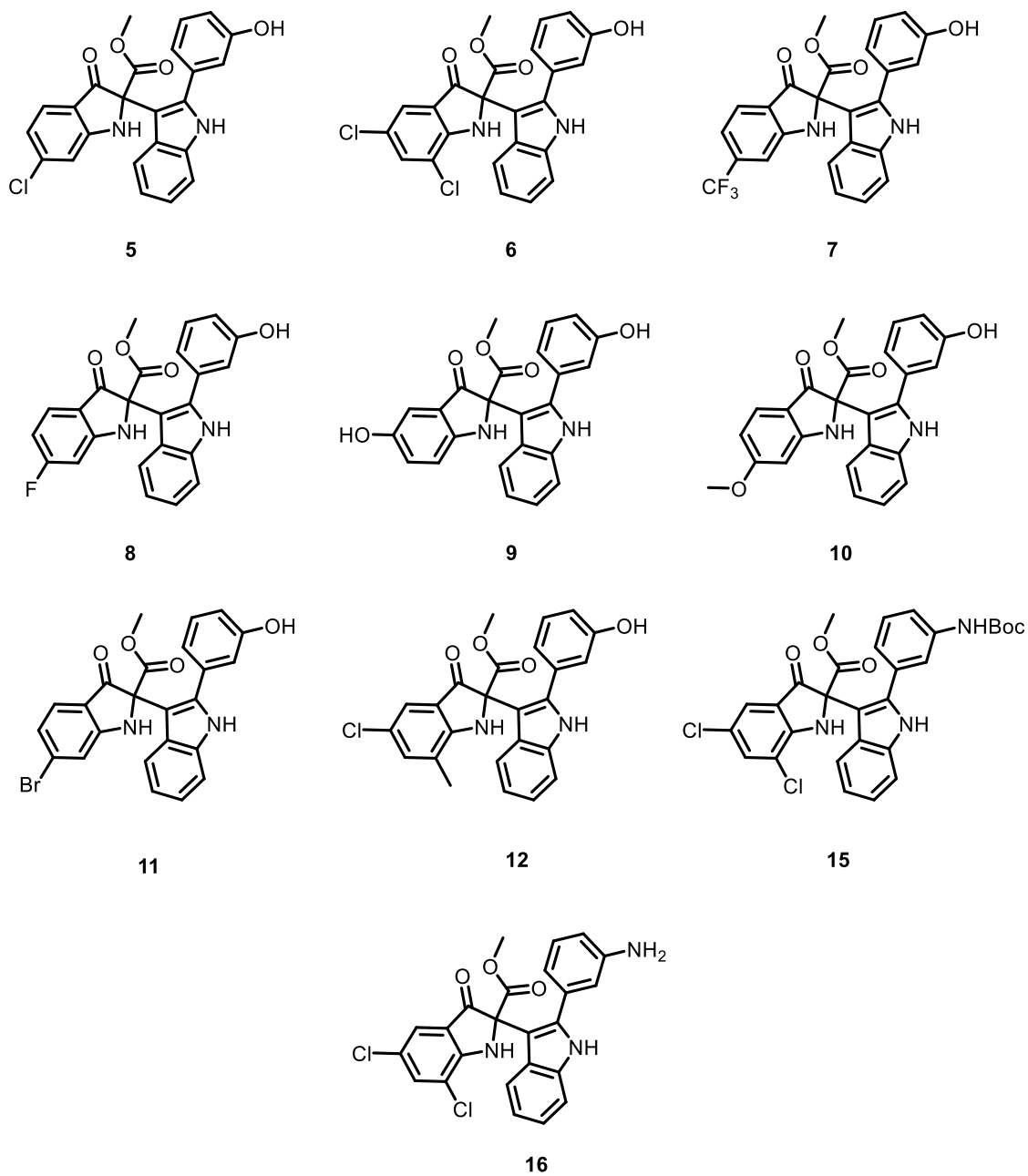
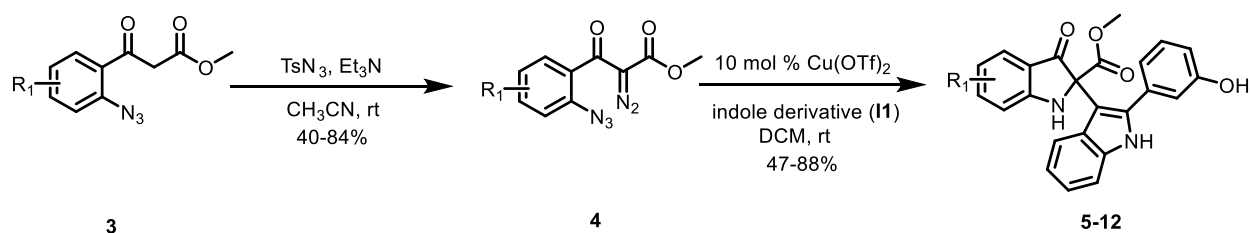
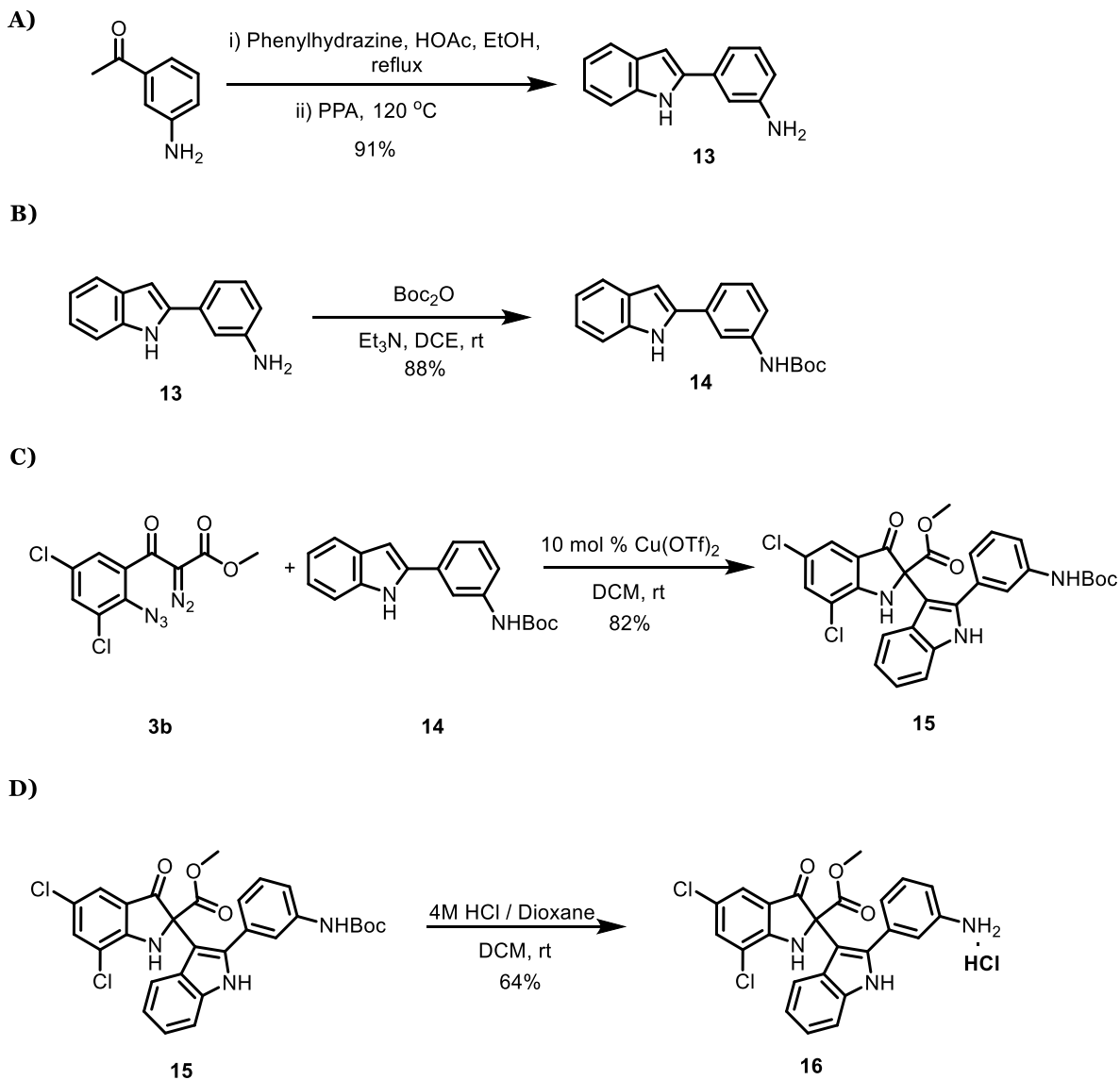


Figure 3.9: Structures of the designed SARS-CoV-2 polymerase inhibitors.



Scheme 3.1: Synthesis of Targeted Compounds.

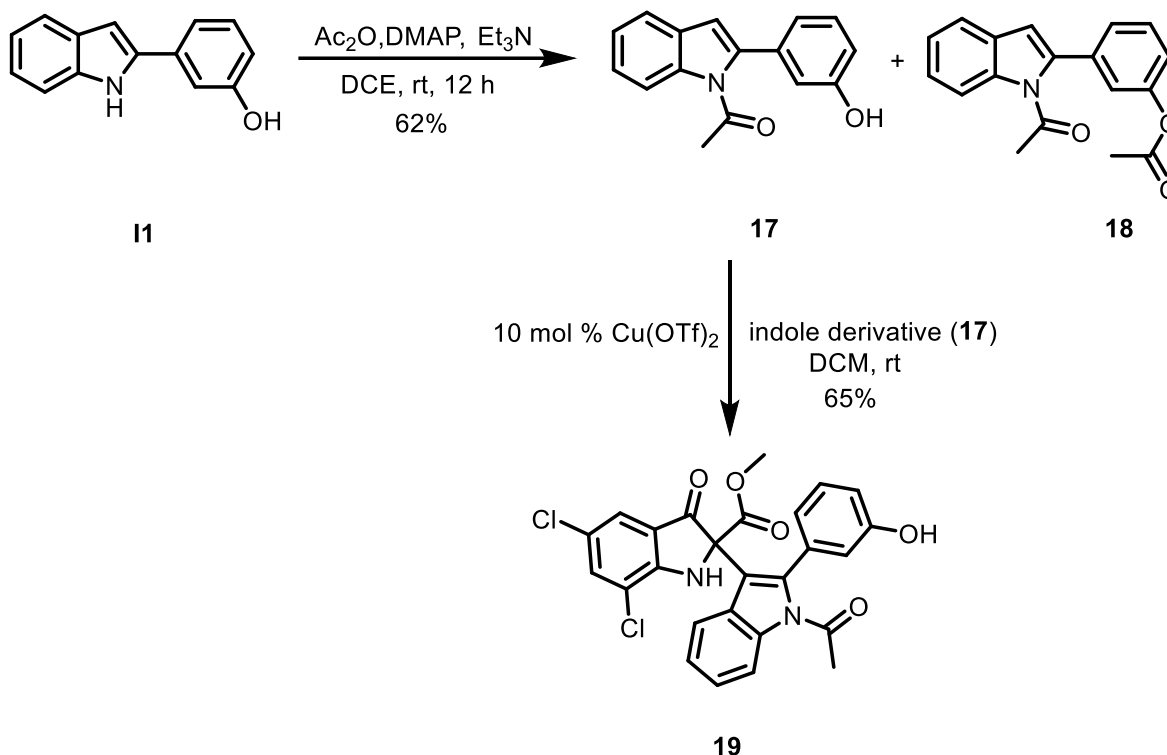
The synthetic route started by Boc protection of the primary amine at C3 of the 2-phenylindole. The intermediate indole **13** was synthesized via the Fischer indole synthesis by the reaction of 3-aminoacetophenone with phenylhydrazine under acidic conditions to yield the desired compound in 91% yield, as shown in Scheme 3.2. The primary amine was then protected by di-tert-butyl dicarbonate to yield compound **14**. Following the Boc protection of the primary amine, **15** was then synthesized by the reaction of **4b** with **14** using catalytic Cu(OTf)₂ in DCM to furnish the desired product. It was decided to keep compound **15** for antiviral screening and generate the free amine version of the compound by the deprotection of Boc using 4 M HCl in dioxane to produce compound **16** in 64% yield. Building on the compounds binding poses in the allosteric pocket 2, we thought of masking the indole nitrogen by synthesizing an *N*-acylated indole. Compound **17** was accessed through the acylation of the indole nitrogen intermediate (**I1**) using acetic anhydride under basic conditions.



Scheme 3.2: Synthesis of Compounds **13** to **16**.

Following the protection of the secondary amine, compound **19** was synthesized under the same conditions previously described in Chapter 2 as depicted in Scheme 3.3. Since proteins are often enantioselective towards drugs, the stereochemistry of small molecules proved to be very crucial in drug discovery.^{39, 40} Our computational model suggested that one enantiomer of RespVirex could be more potent than the other, raising the need to evaluate each enantiomer for

its antiviral activity. Based on the virological evaluations of series III compounds in a racemate form, compound **6** was chosen for separation of enantiomers.



Scheme 3.3: Synthesis of compound **19**.

The compound's antiviral activity governing this choice will be discussed later in this chapter. To resolve the racemic mixture and separate single enantiomers, a chiral HPLC separation was performed using ChiralPak IG column and 20% IPA in hexane as a mobile phase, thus separating each isomer. The compounds were originally synthesized at a small scale; hence, efforts to crystallize both enantiomers to obtain an X-ray structure were very challenging, and all attempts resulted in an amorphous powder. Thus, as an alternative, we envisioned that the electronic circular dichroism (ECD) could be a potential solution. ECD is a well-established approach in assigning the absolute configuration of chiral organic molecules.⁴¹ The ECD of **6a** aligned with the DFT

computed spectrum and the absolute configuration of **6** was assigned based on the comparison with the experimental spectra of the two enantiomers as shown in **Figure 3.10**.

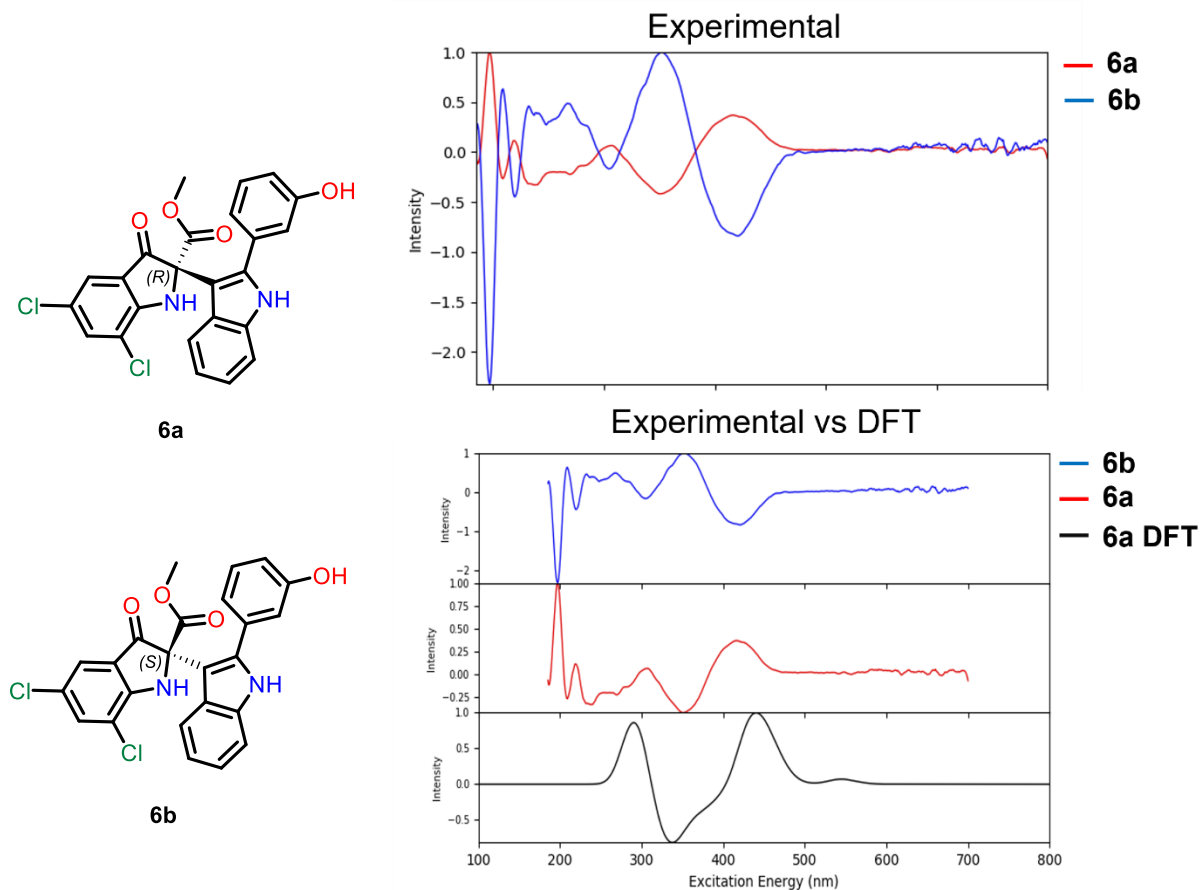


Figure 3.10: Calculated vs Experimental ECD. Chemical structures of compound **6** enantiomers (left), experimental ECD (top right), and experimental vs. calculated ECD spectra at the B3LYP/LACVP** level of theory for **6a** (bottom right).

3.2.7 RespVirex Inhibits SARS-CoV-2 Replication in Cell Culture

To investigate the antiviral activity of RespVirex derivatives, three cell lines were used to identify cells capable of sustaining robust SARS-CoV-2 replication. These cell lines included the African Green Monkey kidney cell line (Vero-E6), HEK293T-human ACE2 cells, and the human airway epithelial cell line (1HAEO-). (**Figure 3.11**)

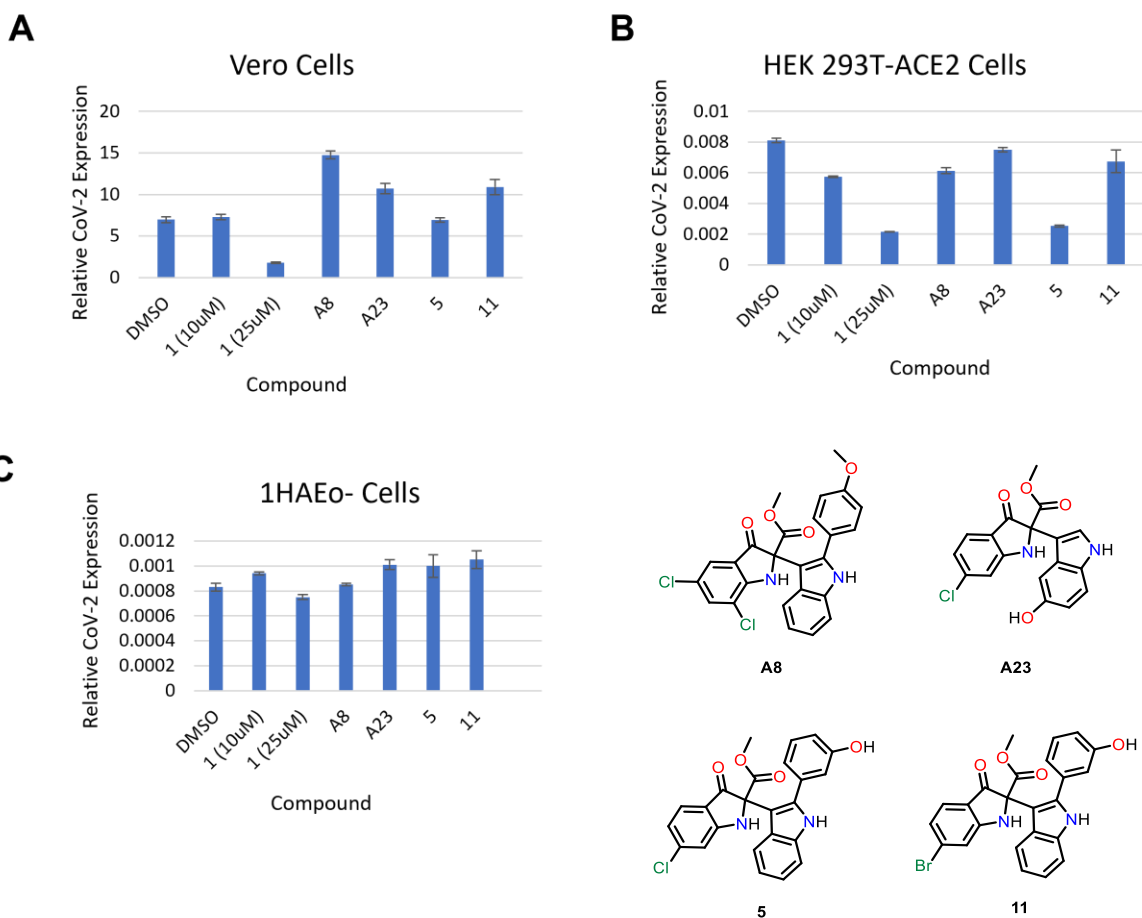


Figure 3.11: Activity of RespVirex analogues on SARS-CoV-2 in **A.** Vero E6 cell, **B.** HEK 293T cells, and **C.** 1HAEO- cells. Compound **1** was used in 10 μ M and 25 μ M while the rest of the compounds were tested at 10 μ M. Compound **5** showed the most promising activity when compared to the lead compound.

The antiviral activity of the designed compounds was assessed in all three cell lines using DMSO as a negative control. Five compounds were selected for the initial screening including **1** as a positive control, compound **A8** and **A23** as representative compounds from the first and second generations discussed in Chapter 2, and the newly designed compounds **5** and **11**. We reasoned that selection for examining the SAR of this class of compounds and to explore whether these compounds would have a broad-spectrum antiviral activity. Compound **1**, the lead compound, did not exhibit any cytotoxicity with a half-maximal cytotoxic concentration (CC_{50}) value of $\sim 60 \mu\text{M}$, allowing for a reasonable window of concentrations to be tested. Although the rest of the compounds were tested at $10 \mu\text{M}$ concentration, compound **1** was tested in two concentrations (10 and $25 \mu\text{M}$) to confirm its efficacy as a lead anti-SARS-CoV-2 RdRp (**Figure 3.11**). Upon examination of the antiviral activity in Vero-E6 cells, compound **1** at $25 \mu\text{M}$ exhibited a substantial activity against SARS-CoV-2 as observed by the relative SARS-CoV-2 expression (**Figure 3.11A**). With a closer look into the activity observed by the selected compounds, compound **5** showed an inhibition pattern similar to the lead compound. However, the results were inconclusive because the inhibition for both compounds was comparable to that of the negative control. It is worth noting that, at this point, we were in the stage of designing a screen for the identification of SARS-CoV-2 antiviral compounds, and the variation of the antiviral results observed in each cell line can be normally expected. These results diverted our focus to another cell line, HEK 293T expressing angiotensin-converting enzyme 2 (ACE2), a vital receptor in the SARS-CoV-2 viral entry.^{42, 43} Intriguingly, compound **5** exhibited an inhibition pattern at $10 \mu\text{M}$ similar to that of compound **1** at $25 \mu\text{M}$ suggesting the importance and effectiveness of the introduced modification(s) (**Figure 3.11B**). This result is in good agreement with our computational model predicting the activity of compound **5**. The human airway epithelial cell line (1HAEO-) did not

seem permissive enough for the virus for our screening purposes, as can be demonstrated by the SARS-CoV-2 expression where the expression of the virus in the presence of the negative control (DMSO) matched that for all compounds in the testing pool and it was decided to exclude this cell line from our screening design.

Notably, although compound **11** carries only a single modification from the parent compound where a hydroxyl group was introduced at C3 instead of a methoxy group at C4 of the 2-phenylindole, the activity of the compound was diminished entirely as shown in **Figure 3.11A and B**. Taken together, the computationally proposed modifications of RespVirex were very crucial in our lead optimization efforts where only a single substitution on RespVirex core structure enhanced the antiviral activity against SARS-CoV-2.

3.2.8 RespVirex Targets the RdRp Enzyme of SARS-CoV-2

Based on our initial screening, several compounds were carried forward to investigate their mechanism of action. A biochemical assay was performed using purified SARS-CoV-2 RdRp enzyme consisting of the replication complex proteins nsp7, nsp8, and nsp12.⁴⁴ The viral RNA synthesis was monitored in the presence of the compounds **1**, **5**, and **11** using two reaction setups. We rationalized the use of compound **11** here due to its similarity with compound **1**. In reaction setup A (**Figure 3.12C**): a 4-mer primer with [α -³²P] GTP was used to initiate RNA synthesis with SARS-CoV-2 RdRp enzyme (**Figure 3.12A**). The inhibitors were added for 10 minutes before the addition of the NTPs and MgCl₂ to start the reaction (**Figure 3.12B**). A dose-dependant inhibition of the RNA synthesis product was observed in the presence of compounds **5** and **6** at concentrations of 0.1, 1, 10, 100 μ M. Although compound **1** exhibited potent inhibitory activity in our previous assays, the compound suffered a low solubility profile leading to unexpected lower activity during this biochemical assay. As setup A was meant to directly assess the effect of the compounds on

3.2.9 RespVirex Can be Used in Combination with Nucleotide Inhibitors

Expanding on our previous work, we designed and synthesized a small library of RespVirex analogues to screen for their polymerase inhibition. A cellular-based assay was developed to evaluate the efficacy of this small library in Vero-E6 cells. For comparison purposes, the FDA-approved drug for the treatment of COVID-19, Remdesivir (RDV), was used as a positive control at 0.3 μM concentration. It is worth noting that RDV is very potent and was used at this concentration to avoid masking the activity of other compounds being screened. Several compounds from our library were evaluated for their antiviral activity, including the eastern fragment of the bis (indole), compound **11**, to validate our modelling studies and explore the minimum structural requirements for viral RNA inhibition. Viral RNA was measured by RT-qPCR as a measure of replication of infectious SARS-CoV-2.

As expected, compound **1** exhibited significant inhibition on the viral RNA produced in Vero-E6 cells. Interestingly, the *R* configuration (**5a**) remarkably inhibited the viral RNA below detection levels (**Figure 3.13**). Meanwhile, treatment with the *S* configuration (**5b**) showed less inhibition of the viral RNA compared to the *R* configuration. Moreover, the combination of RDV with **5a** showed the same level of viral RNA loads compared to that of **5a** alone. Surprisingly, the racemate, compound **6**, showed a comparable level of viral RNA inhibition to that of **5a** (**Figure 3.13**). The structure-activity relationship (SAR) of this class was further investigated through the evaluation of different structural iterations of series I discussed in Chapter 2 and series III discussed herein.

Compounds **A23** is among the tested compounds from the RSV inhibitors discussed in Chapter 2 and it did not have significant effect on viral RNA production at 10 μM when compared to RDV. We also thought of exploring the activity of the indole intermediate (**11**). As expected,

the compound did not exert any significant action against the virus, as shown in **Figure 3.13**, which emphasizes keeping the bis(indole) intact to retain activity during further lead optimization processes.

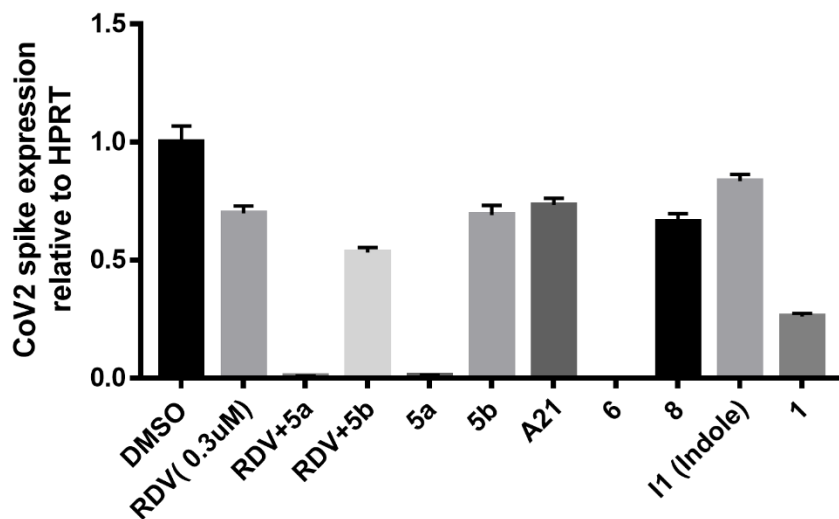


Figure 3.13: Effect of RespVirex analogues on SARS-CoV-2 replication showing inhibition of the viral RNA after treatment with RespVirex derivatives in the presence of DMSO and RDV as negative and positive controls, respectively. Compound **A21** denotes compound **6c** from Chapter 2.

Although several compounds showed good activity, compound **5a** exhibited a potent viral inhibition with an IC_{50} of 3 μM with a $CC_{50} > 300 \mu M$ and a therapeutic index (TI) ~ 211 (**Figure 3.14A**). Compound **6** which only differs from **5** by the presence of two chlorine atoms at the indolinone fragment showed an IC_{50} of 2 μM (**Figure 3.14C**). To confirm the potency of our inhibitors and their effect on the inhibition of viral RNA, a second round of screening was performed in a focused manner where compound **6** was tested at its 50% inhibitory concentration of 2 μM and showed a percentage inhibition of around 30% of viral RNA produced (**Figure 3.14D**). We asked the question whether the combination of our compounds with RDV would have any synergistic activity against the virus. Our results showed that the combination of RDV and **6**

exhibited a 40% reduction in viral RNA production determined via signal normalization (%) of the full template-length product of RNA synthesis in the presence of the compounds to the signal obtained in the absence of the compounds. While the activity of RDV at 0.3 μM showed similar inhibition percentage to that of **5a** at 3 μM , the combination of both inhibitors reduced the virus expression by $\sim 40\%$. While the *S* configuration of compound **5**, **5b**, showed a potent inhibition of the virus by 48%, the combination of **5b** with RDV did not significantly reduce the viral RNA as can be drawn from their percentage inhibition of 52% (**Figure 3.14D**).

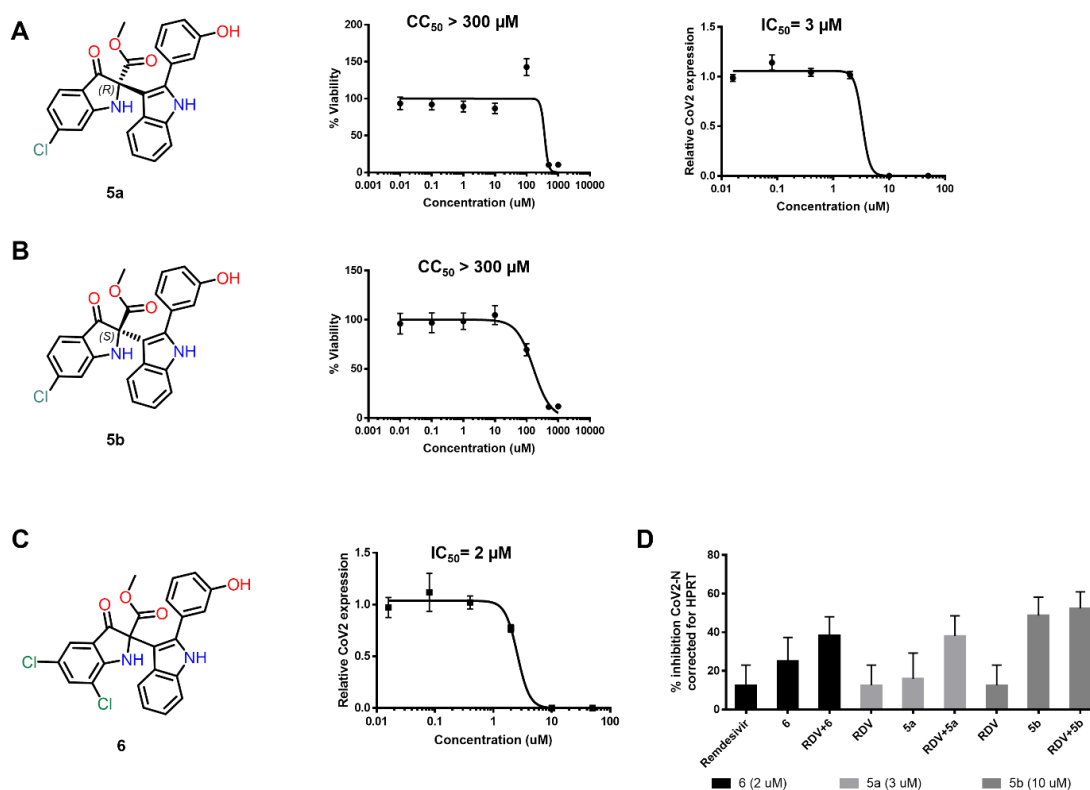


Figure 3.14: Cytotoxicity and IC_{50} values for compounds **5** and **6**. **A.** Chemical structures of the *R* enantiomer of compound **5** (**5a**), MTT, and IC_{50} values. **B.** Chemical structures of the *S* enantiomer of **5b** along with the cytotoxicity assay (N.B.: IC_{50} has not been determined for this enantiomer). **C.** IC_{50} value for compound **6** (racemic). **D.** Percent inhibition of SARS-CoV-2 by RespVirex derivatives in Vero E6 cells. SARS-CoV-2 transcripts were corrected for HPRT1 expression and then compared by treatment group.

The results of these in vitro assays nicely agreed with our computational model, which explains the importance of substitution with halogens on the indolinone fragment. This study revealed two new compounds with high potency and IC₅₀ values in the low micromolar range. Although in this assay the *R* enantiomer showed less inhibitory activity against the viral RNA compared to the *S* enantiomer, this could be attributed mainly to the difference in the test concentration used for both compounds. It is also important to mention that the enantiomers of compound **6** are still under investigation.

3.2.10 Inhibition of RNA Synthesis by Compound 5 Enantiomers

To further evaluate the antiviral effect observed by compound **5** enantiomers, the RNA synthesis in the presence of the inhibitors was monitored. A template with a longer stretch of uridines was used. Significant SARS-CoV-2 RdRp RNA synthesis inhibition was noted after the treatment with **5a**, which reduced the product signal by 50% (**Figure 3.15**). A more potent inhibition was observed when **5b** was added to the replication complex where the full template-length product signal was only 13% which translates to 87% inhibition of the RNA synthesis product. These results confirmed the potency of our compounds against the RdRp of SARS-CoV-2 with direct evidence that the compounds are targeting the viral protein. Building on the precedent results, we demonstrated that our inhibitors exert significant inhibition on the primer extension reactions by the RdRp enzyme. The results of this study show that RespVirex is a good candidate antiviral with demonstrated potent activity.

3.3 Conclusions

The COVID-19 pandemic has changed our perspective on viral infections and the preparedness for such situations. The race for curative therapies has been on the rise since then. These therapeutics included the search for an effective vaccines that can boost human immunity

and overcome viral resistance. However, the emergence of viral variants with limited drug treatment options has created an even more urgent need for the development of new antiviral drugs.

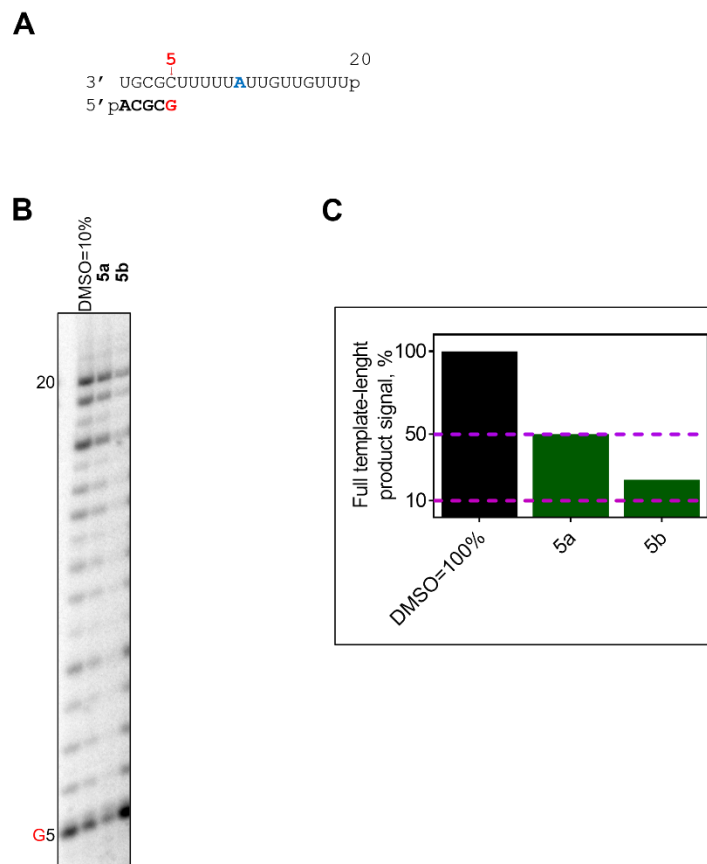


Figure 3.15: SARS-CoV-2 RdRp-catalyzed RNA synthesis in presence of compounds 5a and 5b. **A.** RNA primer/template. G indicates incorporation of [α - 32 P]-GTP at position 5. **B.** RNA synthesis catalyzed by SARS-CoV-2 RdRp complex in the presence of the inhibitors. Bands corresponding to the first incorporated nucleotide (G5) and to the full template-length products (20) are indicated on the left. **C.** Graphical representation of the data shown on the left horizontal purple dashed lines illustrate 50% and 90% inhibition, respectively.

In Chapter 3, we employed computational drug discovery approaches to investigate the possible binding site and modes of interactions of our lead compound. We assessed the antiviral activity of our previously published lead compound **1** on SARS-CoV-2 and the compound exhibited substantial activity against the viral polymerase protein. Herein, we performed a detailed analysis of the SARS-CoV-2 polymerase complex to identify possible allosteric sites and to predict the putative binding pose of our lead compound **1**. The results of these computational efforts

identified an allosteric binding site located near the catalytic active site for which the stability of the binding residues was assessed for potential druggability with small molecules. A structure-based investigation of the identified allosteric binding site revealed a possible room for improvement of our ligands through establishing a strong network of hydrogen bond interactions which led to the design of several derivatives bearing a hydroxyl group instead of a methoxy to establish the desired hydrogen bond with residue THR 394. Molecular dynamics simulations were carried out for the newly designed compounds in complex with the SARS-CoV-2 polymerase and the introduced modifications on the compounds suggested a stable complex with the viral polymerase with demonstrated range of interactions and high binding affinity values.

All designed compounds were synthesized via our established dual catalytic metallocarbene-azide cascade chemistry. The antiviral activity of the synthesized compounds was assessed *in vitro* using a fully replicating SARS-CoV-2 virus strain and biochemically using the RdRp enzyme. The FDA-approved drug for the treatment of SARS-CoV-2, remdesivir (RDV), was used as a positive control and the combination of RDV with RespVirex derivative, **5**, exhibited a synergistic effect and enhanced the antiviral activity of RDV. The results of Chapter 3 identified two compounds, **5** and **6**, with a pronounced antiviral activity compared to the lead compound. The *R* enantiomer **5a** exhibited an IC₅₀ value of 3 μM while the anti-SARS-CoV-2 activity of compound **6** was measured using the racemic compound and exhibited a potent activity with an IC₅₀ value of 2 μM. These results suggest that the presence of a phenolic hydroxyl group at the 2-aryl indole was very critical to enhance the antiviral properties of these compounds by interacting with the side chain of THR 394. A direct biochemical assessment of the activity of compound **5** enantiomers on the SARS-CoV-2 RdRp polymerase suggested that the *S* configuration exhibited more potent antiviral activity as demonstrated by the inhibition of the full-length RNA product

produced by the RdRp of SARS-CoV-2. Although the activity of compound **6** enantiomers along with several RespVirex derivatives are still under investigation, the preliminary results of this class of compounds are promising with the potential for the development of a nanomolar antiviral inhibitors.

To conclude, we designed and synthesized a new series of RespVirex derivatives using a structure-based approach and a detailed *in silico* investigations which yielded a set of derivatives with demonstrated superior antiviral activity and physicochemical properties compared to the lead compound. The results of this study may lead to the development of a new class of direct acting broad-spectrum antivirals, along with our investigated compounds in Chapter 2, with strong chemical and biological properties for the treatment, and potentially the containment, of SARS-CoV2 and other viral respiratory infections by blocking their polymerase complexes.

3.4 Experimental‡

3.4.1 Computational Details

3.4.1.1 Preparation of the SARS-CoV-2 Polymerase for MD simulation

The cryo-electron microscopy structure of the SARS-CoV-2 polymerase complex (nsp7, nsp8, and nsp12) bound to a primer RNA duplex and the inhibitor favipiravir-RTP (PDB ID: 7AAP) was used for our study. Initially, the RNA and the inhibitor were removed for the protein preparation. The Protein Preparation Wizard was used to add hydrogen atoms, minimize energy, and create appropriate protonation states for amino acid side chains and was then subjected to three stages of energy minimization. The AMBERff14SB force field parameters were assigned to the

* I was responsible for the design and synthesis of all compounds in addition to designing and performing all the computational experiments. Leanne Bilawchuk was responsible for conducting *in vitro* virological assays, and Dr. Egor Tchesnokov expressed and purified SARS-CoV-2 RdRp complex and conducted the biochemical assays.

protein.⁴⁵⁻⁴⁷ The protein was then solvated in a cubic box of TIP3P water.⁴⁸ The solvated system was then neutralized with the addition of Na⁺/Cl⁻ counterions at a concentration of 0.15 M physiological ionic concentration using tleap in AmberTools18. The system was then carried forward for subsequent MD simulation. A detailed description of the MD simulations is discussed below.

3.4.1.2 Allosteric Binding Site Identification

The prepared cryo-EM structure and the MD trajectory of the apo SARS-CoV-2 were analyzed for druggable allosteric binding sites identification. We employed three tools to search for these allosteric binding sites including fPocket²², Site Finder implemented in MOE²⁹, and the SiteMap utility implement in Schrödinger.²³

The MDpocket tools was also used to examine the trajectories for shallow allosteric site. The agreement between the tools regarding pocket size, druggability scores were the main criteria for pocket selection.

3.4.1.3 Molecular Docking

The 2D chemical structures of the ligands were built using ChemDraw version 19.0 and the structures were prepared using LigPrep wizard implemented in Schrödinger. Protonation states at pH 7.0 ± 2.0 for each ligand were assigned using Epik and the ligands' tautomers and conformations were calculated using the OPLS3e force field.^{49, 50} The docking grid box was defined in the center of residues Thr 394, Arg 457, Asn 459, Asn 628 and Pro 677 with a center coordinates of 113.74, 108.82, and 110.45. The Glide scoring function at extra precision (XP) was used for the docking simulations²⁷ A maximum of 10 poses were generated for each compound, and the top scoring pose was selected for each ligand.

3.4.1.4 MD Simulations and MM-GBSA Rescoring

Complexes preparation for MD simulations followed the above-described method in section 3.4.1.1. The force field parameters for the ligands were obtained using the GAFF force field⁵¹ and Antechamber⁵² and the AM1-BCC charges were assigned for the ligands.⁵³ The MD simulations were performed in pmemd.cuda: an initial minimization steps were performed in order to relax the water and ionic positions using 5000 steps of steepest descent and 5000 steps of conjugate gradients minimization, keeping all the complex atoms fixed through an harmonic restraint with a force constant of 500 kcal/mol/Å². This step was followed by 2000 steps of steepest descent followed by 3000 steps of conjugate gradients without restraints. The systems were then heated gradually up from 0 to 300K in 100 ps using Langevin dynamics. During the heating process, the backbone of the protein and the heavy atoms of the ligand were restrained, and a time step of 0.5 fs and periodic volume conditions have been employed during this phase. The time step has been set to 2 fs, and periodic pressure conditions (1 atm) have been imposed and the restraints have been gradually released in four phases of 50 ps each. The simulations were then continued for 100 ns of production for the apo protein and 50 ns for the ligand-protein complexes. Analysis of the MD trajectory were carried out using CPPTRAJ.⁵⁴ Plots were generated using Gnuplot (version 5.4) and figures were generated using PyMOL.

For MD snapshots extracted from the production simulations, we calculated the enthalpic portion of the binding energy using the Molecular Mechanics/Generalized Born Surface Area (MM/GBSA) method implemented in the MMPBSA.py script.⁵⁵ In MM/GBSA, the free energy change due to ligand binding is calculated as:

$$\Delta G_{\text{bind}} = \Delta E_{\text{MM}} + \Delta G_{\text{solv}} - T\Delta S \quad (1)$$

Where ΔE_{MM} , is the summation of non-bonded and bonded interaction energies. The solvation energy, ΔG_{solv} , is the sum of the polar and non-polar contributions of solvation, where the polar solvation terms are calculated using a Generalized-Born model and the non-polar terms are computed based on the size of the solvent-accessible surface area. The $(T\Delta S)$ portion of the equation refers to the entropic contribution and is computationally expensive, therefore, it was neglected.

3.4.1.5 Binding Pose Metadynamics

The BPMD consists of three scores: (1) PoseScore: which reflects the average RMSD of the ligand from the starting coordinates where a huge increase in the RMSD indicates unstable ligands that have not been accurately modeled. (2) PersistenceScore (PersScore): which provides a measurement of hydrogen bond persistence calculated during the last 2 ns of the simulation and compare the same hydrogen bonds provided in the input structure, averaged over all the 10 repeat simulations. Low PersScore generally means that hydrogen bond contact is weakened by the BPMD bias. It ranges between 0, which indicates that either the ligand at the start did not have any interaction with the protein or that the interactions were lost during the simulation, and 1, indicates that the interactions between the starting ligand binding mode and the last 2 ns of the simulations are fully kept. (3) The CompositeScore (CompScore): represents a linear combination of PoseScore and PersScore calculated as follows:

$$\text{CompScore} = \text{PoseScore} - 5 \times \text{PersScore}.$$

Binding Pose metadynamics simulations were performed using Desmond module implemented in Schrödinger Suite.⁵⁶ The BPMD is a variation of metadynamics simulation in which 10 independent metadynamics simulations of 10 ns are performed using collective variable (CV) as the measure of the RMSD of the ligand heavy atoms relative to their starting position. A 20 ns

unbiased simulation was used as a reference for the metadynamics production. The MD simulation was performed using compound **6** in complex with the SARS-CoV-2 polymerase. Briefly, the system was solvated in a box of TIP3P water and neutralized by Na⁺ and Cl⁻ ions at a concentration of 0.15 M. The system was then minimized, and restrained MD steps allowed the system to gradually reach the desired temperature of 300 K. The unbiased simulation was then used to compare the stability of the ligand binding pose. The three aforementioned scores were then used to evaluate the metadynamics results.

3.4.1.6 Theoretical ECD Spectra Calculations

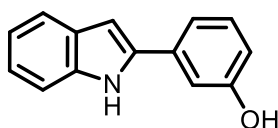
The theoretical ECD spectra were modeled using computational VCD standard workflow by Jaguar implemented in Schrödinger. Conformational analyses were carried out using in MacroModel using the OPLS3e forcefield.⁵⁰ The ECD spectrum of the (*R*) enantiomer of compound **6** was carried out in Jaguar at the B3LYP-D3/LACVP** level of theory. The calculated spectrum was then Boltzmann-averaged and normalized to produce the final spectrum which was then aligned to the experimental spectra of the *R* and *S* enantiomers.

3.4.2 Chemical Synthesis

3.4.2.1 Synthesis of RespVirex Analogues

The compounds were synthesized according to the procedure previously described in Chapter 2.

2-(3-hydroxyphenyl)indole (**II**)



Phenyl hydrazine (1.31 mL, 13 mmol) was added to a stirred solution of 3'-hydroxyacetophenone (2.0 g, 14 mmol) in absolute EtOH (30 mL), followed by 5 drops of HOAc. The reaction mixture

was heated at 80 °C for 1h. After cooling to room temperature, the solvent was evaporated. Polyphosphoric acid (PPA, 10 mL) was added then heated slowly to 130 °C and kept for 1 h. The reaction mixture was poured on ice and neutralised with 2 M NaOH. After neutralization, the greyish solid formed was filtered, washed with water (3 x 100 mL) and purified by flash chromatography (gradient elution 1 to 20% EtOAc in hexane) to afford the desired compound **II** as yellow solid (2.5 g, 81%). ¹H NMR (400 MHz, DMSO-*d*₆): δ 11.42 (s, 1H), 9.53 (s, 1H), 7.51 (d, *J* = 7.8 Hz, 1H), 7.38 (dd, *J* = 8.1, 1.0 Hz, 1H), 7.30 – 7.21 (m, 3H), 7.08 (ddd, *J* = 8.1, 7.0, 1.2 Hz, 1H), 7.01 – 6.96 (m, 1H), 6.79 (d, *J* = 1.9 Hz, 1H), 6.73 (ddd, *J* = 7.6, 2.4, 1.3 Hz, 1H). ¹³C NMR (101 MHz, DMSO-*d*₆): δ 157.7, 137.8, 136.9, 133.4, 129.8, 128.5, 121.3, 119.9, 119.2, 115.9, 114.5, 111.8, 111.2, 98.4. HRMS (ESI) calcd for C₁₄H₁₁NO [M-H]⁻ 208.0768; found 208.0767.

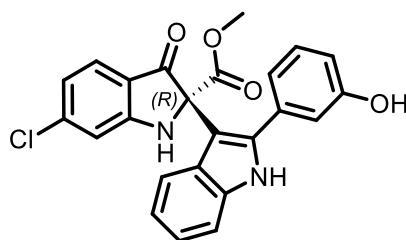
Methyl 6-chloro-2-(2-(3-hydroxyphenyl)-1H-indol-3-yl)-3-oxoindoline-2-carboxylate (**5**)



The title compound was prepared according to our previously described procedure in Chapter 2 using **II** as the indole trap. The product was purified via flash chromatography (gradient elution 9:1 then 8:2 hexane/EtOAc) to furnish **5** as yellow semisolid in 84% yield; *R*_f = 0.22 (7:3 hexanes: EtOAc). ¹H NMR (500 MHz, CDCl₃) 8.33 (s, 1H), 7.61 (d, *J* = 8.2 Hz, 1H), 7.35 (d, *J* = 8.2 Hz, 1H), 7.32 (s, 2H), 7.27 – 7.20 (m, 3H), 7.12 – 7.06 (m, 1H), 7.01 (d, *J* = 1.6 Hz, 1H), 6.99 – 6.93 (m, 3H), 6.90 – 6.86 (m, 1H), 3.34 (s, 3H). ¹³C NMR (126 MHz, CDCl₃): δ 194.6, 168.7, 161.1, 156.0, 144.9, 138.0, 135.4, 133.6, 129.7, 126.7, 126.3, 122.9, 121.5, 121.3, 120.7, 119.4, 118.4,

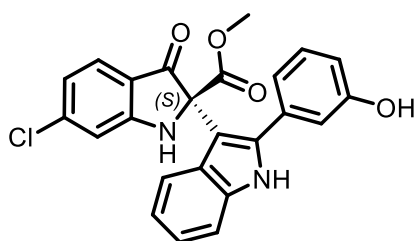
116.4, 116.2, 113.1, 111.5, 107.2, 73.9, 53.5. HRMS (ESI) calcd for C₂₄H₁₆ClN₂O₄ [M-H]⁻ 431.0804; found 431.0799.

Methyl (*R*)-6-chloro-2-(2-(3-hydroxyphenyl)-1H-indol-3-yl)-3-oxoindoline-2-carboxylate (**5a**)



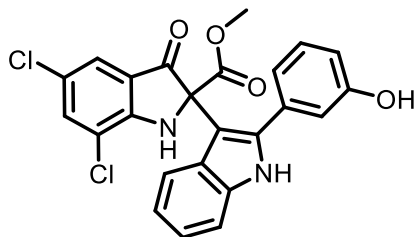
Following the previous procedure, the (*R*) enantiomer, **5a**, was separated using chiral HPLC (6.6 mg): ChiralPak IG column (20% IPA in hexane, 1.5 mL/min), *t_r*= 4.3 min. [α]_D²⁰ = 135.53 (c = 0.63, CHCl₃). Spectroscopic data were in agreement with those described for racemic **5**.

Methyl (*S*)-6-chloro-2-(2-(3-hydroxyphenyl)-1H-indol-3-yl)-3-oxoindoline-2-carboxylate (**5b**)



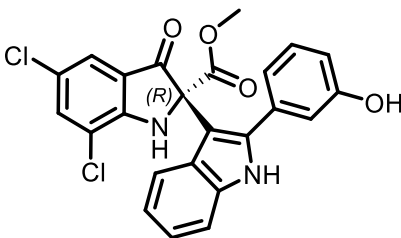
Following the previous procedure, the (*S*) enantiomer, **5b**, was separated using chiral HPLC (6.3 mg): ChiralPak IG column (20% IPA in hexane, 1.5 mL/min), *t_r*= 5.9 min. [α]_D²⁰ = -134.12 (c = 0.66, CHCl₃)

Methyl 5,7-dichloro-2-(2-(3-hydroxyphenyl)-1H-indol-3-yl)-3-oxoindoline-2-carboxylate (**6**)



The title compound was prepared analogously to compound **5** and the product was isolated as yellow semisolid in 75% yield; $R_f = 0.20$ (7:3 hexanes: EtOAc). $^1\text{H NMR}$ (500 MHz, CDCl_3) δ 8.28 (s, 1H), 7.55 (d, $J = 1.9$ Hz, 1H), 7.50 (d, $J = 2.0$ Hz, 1H), 7.34 – 7.28 (m, 1H), 7.24 – 7.15 (m, 3H), 7.06 (ddd, $J = 8.0, 7.0, 1.1$ Hz, 1H), 6.91 (ddd, $J = 7.5, 1.6, 1.0$ Hz, 1H), 6.89 – 6.81 (m, 2H), 5.76 (s, 1H), 3.35 (s, 3H). $^{13}\text{C NMR}$ (126 MHz, CDCl_3) δ 193.9, 168.0, 155.9, 155.4, 137.8, 136.5, 135.4, 133.7, 129.9, 126.6, 125.5, 123.1, 123.0, 121.8, 121.7, 120.9, 119.4, 119.0, 116.4, 116.3, 111.4, 106.9, 74.2, 53.6. HRMS (ESI) calcd for $\text{C}_{24}\text{H}_{16}\text{Cl}_2\text{N}_2\text{O}_4$ $[\text{M}-\text{H}]^-$ 465.0414; found 465.0407.

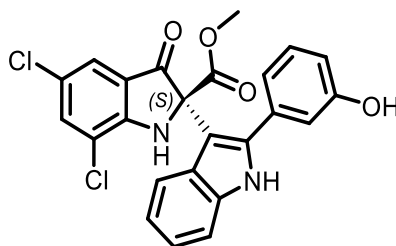
Methyl (*R*)-5,7-dichloro-2-(2-(3-hydroxyphenyl)-1H-indol-3-yl)-3-oxoindoline-2-carboxylate (**6a**)



Following the previous procedure, the (*R*) enantiomer, **6a**, was separated using chiral HPLC: ChiralPak IG column (20% IPA in hexane, 1.5 mL/min), $t_r = 6.8$ min. $[\alpha]_D^{20} = 81.30$ ($c = 0.188$, CHCl_3). Spectroscopic data were in agreement with those described for racemic **6**.

Methyl (*S*)-5,7-dichloro-2-(2-(3-hydroxyphenyl)-1H-indol-3-yl)-3-oxoindoline-2-carboxylate

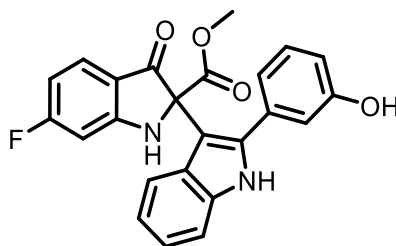
(**6b**)



Following the previous procedure, the (*S*) enantiomer, **6b**, was separated using chiral HPLC: ChiralPak IG column (20% IPA in hexane, 1.5 mL/min), t_r = 15.9 min.

$[\alpha]_D^{20} = -81.23$ ($c = 0.184$, CHCl_3). Spectroscopic data were in agreement with those described for racemic **6**.

Methyl 6-fluoro-2-(2-(3-hydroxyphenyl)-1H-indol-3-yl)-3-oxoindoline-2-carboxylate (**8**)

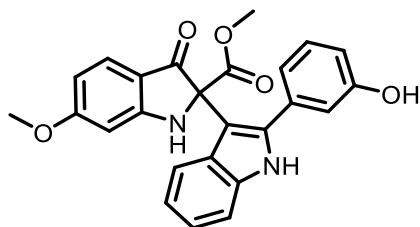


The title compound was prepared analogously to compound **5** and the product was isolated as yellow semisolid in 69% yield; $R_f = 0.19$ (7:3 hexanes: EtOAc). ^1H NMR (500 MHz, CDCl_3) δ 8.29 (s, 1H), 7.62 (dd, $J = 8.5, 5.6$ Hz, 1H), 7.30 – 7.26 (m, 2H), 7.21 – 7.12 (m, 3H), 7.06 – 6.99 (m, 1H), 6.89 (dd, $J = 8.4, 1.7$ Hz, 2H), 6.85 – 6.79 (m, 1H), 6.66 – 6.54 (m, 2H), 3.27 (s, 3H). (N.B.: the indolinone proton was not detected). ^{13}C NMR (126 MHz, CDCl_3): δ 193.8, 168.8 (d, $J = 20.9$ Hz), 162.4 (d, $J = 14.2$ Hz), 156.0, 137.9, 135.4, 133.6, 129.8, 127.8 (d, $J = 12.4$ Hz), 126.7, 122.9, 121.6, 120.8, 119.4, 116.5, 116.2, 111.4, 109.2 (d, $J = 24.7$ Hz), 107.5, 99.6 (d, $J = 26.0$

Hz), 74.0, 53.4 (N.B.: two carbon resonance ^{13}C were missing and could not be properly assigned).

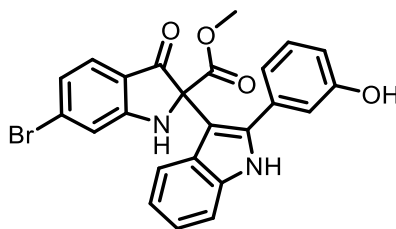
HRMS (ESI) calcd for $\text{C}_{24}\text{H}_{17}\text{FN}_2\text{O}_4$ $[\text{M}-\text{H}]^-$ 415.1110; found 415.1097.

Methyl 2-(2-(3-hydroxyphenyl)-1H-indol-3-yl)-6-methoxy-3-oxoindoline-2-carboxylate (**10**)



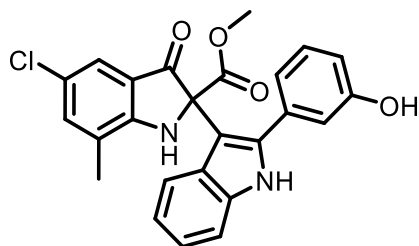
The title compound was prepared analogously to compound **5** and the product was isolated as yellow semisolid in 47% yield; $R_f = 0.24$ (7:3 hexanes: EtOAc). ^1H NMR (500 MHz, CDCl_3) δ 8.47 (s, 1H), 7.61 (d, $J = 8.7$ Hz, 1H), 7.33 (s, 1H), 7.28 – 7.22 (m, 2H), 7.20 – 7.11 (m, 2H), 7.10 – 7.00 (m, 1H), 6.91 – 6.85 (m, 2H), 6.84 – 6.78 (m, 1H), 6.55 (dd, $J = 8.7, 2.1$ Hz, 1H), 6.40 (d, $J = 2.1$ Hz, 1H), 5.78 (s, 1H), 3.90 (s, 3H), 3.27 (s, 3H). ^{13}C NMR (126 MHz, CDCl_3) δ 193.5, 169.3, 168.7, 163.5, 156.2, 138.1, 135.4, 133.6, 129.6, 126.97, 126.93, 122.7, 121.5, 120.6, 119.5, 116.3, 116.1, 113.5, 111.4, 110.6, 107.7, 95.5, 74.01, 55.87, 53.3. HRMS (ESI) calcd for $\text{C}_{25}\text{H}_{20}\text{N}_2\text{O}_5\text{Na}$ $[\text{M}+\text{Na}]^+$ 451.1264; found 451.1263.

Methyl 6-bromo-2-(2-(3-hydroxyphenyl)-1H-indol-3-yl)-3-oxoindoline-2-carboxylate (**11**)



The title compound was prepared analogously to compound **5** and the product was isolate as yellow semisolid in 88% yield; $R_f = 0.22$ (7:3 hexanes: EtOAc). $^1\text{H NMR}$ (400 MHz, CDCl_3) δ 8.46 (s, 1H), 7.49 (d, $J = 8.2$ Hz, 1H), 7.31 (s, 1H), 7.29 – 7.22 (m, 1H), 7.21 – 7.11 (m, 4H), 7.10 – 7.01 (m, 2H), 6.91 – 6.84 (m, 2H), 6.86 – 6.78 (m, 1H), 3.28 (s, 3H). (N.B.: the indolinone proton was not detected). $^{13}\text{C NMR}$ (126 MHz, CDCl_3) δ 195.0, 168.7, 161.1, 156.0, 138.1, 135.4, 133.9, 133.5, 129.7, 126.7, 126.3, 124.0, 122.8, 121.5, 120.7, 119.3, 118.6, 116.3, 116.26, 116.24, 111.6, 107.0, 73.8, 53.5. HRMS (ESI) calcd for $\text{C}_{24}\text{H}_{17}\text{BrN}_2\text{O}_4\text{Na}$ $[\text{M}+\text{Na}]^+$ 499.0264; found 499.0264.

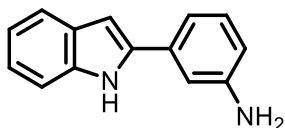
Methyl 5-chloro-2-(2-(3-hydroxyphenyl)-1H-indol-3-yl)-7-methyl-3-oxoindoline-2-carboxylate (**12**)



The title compound was prepared analogously to compound **5** and the product was isolate as yellow semisolid in 81% yield; $R_f = 0.18$ (7:3 hexanes: EtOAc). $^1\text{H NMR}$ (500 MHz, CDCl_3) δ 8.21 (s, 1H), 7.47 – 7.43 (m, 1H), 7.43 – 7.30 (m, 2H), 7.25 – 7.18 (m, 3H), 7.17 (d, $J = 1.1$ Hz, 1H), 7.08 – 7.01 (m, 1H), 6.94 (d, $J = 7.6$ Hz, 1H), 6.90 – 6.82 (m, 2H), 5.38 (s, 1H), 3.34 (s, 3H), 2.21 (s, 3H). $^{13}\text{C NMR}$ (126 MHz, CDCl_3) δ 194.7, 168.7, 158.4, 155.8, 137.7, 137.5, 135.4, 133.9, 129.9,

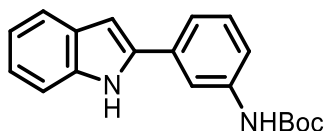
126.8, 125.8, 124.3, 123.0, 121.8, 121.7, 120.8, 120.6, 119.7, 116.5, 116.1, 111.3, 107.7, 73.9, 53.5, 15.6. HRMS (ESI) calcd for C₂₅H₂₀ClN₂O₄ [M+H]⁺ 447.1106; found 447.1113.

3-(1H-indol-2-yl)aniline (**13**)



The title compound was prepared analogously to compound **11**, using 3'-aminoacetophenone and the product was purified by column chromatography (gradient elution 1 to 20% EtOAc in hexane) as an off-white solid in 78% yield; $R_f = 0.3$ (7:3 hexanes: EtOAc). ¹H NMR (500 MHz, DMSO-*d*₆) δ 11.34 (s, 1H), 7.49 (dd, $J = 8.0, 1.1$ Hz, 1H), 7.36 (dd, $J = 8.1, 1.0$ Hz, 1H), 7.12 – 6.94 (m, 6H), 6.68 (dd, $J = 2.3, 0.9$ Hz, 1H), 6.54 (ddd, $J = 8.0, 2.2, 1.0$ Hz, 1H), 5.26 (s, 2H). ¹³C NMR (126 MHz, DMSO-*d*₆): δ 148.6, 138.5, 136.8, 132.7, 129.3, 128.5, 121.1, 119.7, 119.1, 113.6, 113.2, 111.1, 110.6, 97.8. HRMS (ESI) calcd for C₁₄H₁₃N₂ [M+H]⁺ 209.1019; found 209.1016.

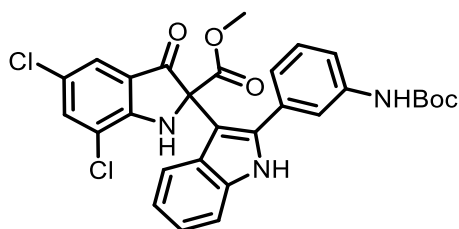
Tert-butyl (3-(1H-indol-2-yl)phenyl)carbamate (**14**)



To a solution of **13** (100 mg, 0.48 mmol) in DCE, triethylamine (8.0 μ L, 0.61 mmol) was added followed by the addition of di-tert-butyl dicarbonate (14 μ L, 0.61 mmol). The reaction was stirred at room temperature and followed by TLC for the formation of the product. Saturated solution of NH₄Cl was added to the reaction mixture and extracted with DCM, dried over Na₂SO₄ and the residue was concentrated under reduced pressure, purified using silica gel chromatography (5-20% EtOAc-Hexane) to afford the product as yellow oil in 88% yield; $R_f = 0.55$ (7:3 hexanes:

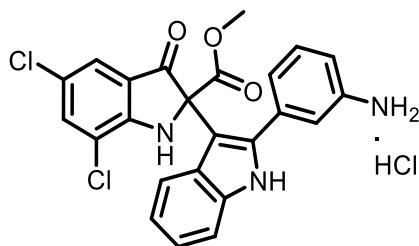
EtOAc). ^1H NMR (500 MHz, CDCl_3) δ 8.55 (s, 1H), 7.87 (s, 1H), 7.62 (dd, $J = 7.8, 1.2$ Hz, 1H), 7.41 – 7.29 (m, 3H), 7.19 (ddd, $J = 8.2, 7.1, 1.2$ Hz, 1H), 7.18 – 7.07 (m, 2H), 6.82 (dd, $J = 2.1, 1.0$ Hz, 1H), 6.62 (s, 1H), 1.56 (s, 9H). ^{13}C NMR (126 MHz, CDCl_3): 152.9, 139.1, 137.7, 136.9, 133.4, 129.6, 129.2, 122.4, 120.7, 120.3, 120.2, 117.6, 114.9, 111.1, 100.3, 80.9, 28.5 (3C). HRMS (ESI) calcd for $\text{C}_{19}\text{H}_{21}\text{N}_2\text{O}_2$ $[\text{M}+\text{H}]^+$ 309.1598; found 309.1597.

Methyl 2-(2-(3-((tert-butoxycarbonyl)amino)phenyl)-1H-indol-3-yl)-5,7-dichloro-3-oxoindoline-2-carboxylate (**15**)



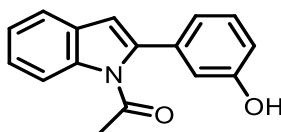
The title compound was prepared analogously to compound **5** but using compound **13** in place of **11**. Isolated as yellow semisolid in 82% yield; $R_f = 0.20$ (7:3 hexanes: EtOAc). ^1H NMR (500 MHz, CDCl_3) δ 8.30 (s, 1H), 7.57 – 7.48 (m, 3H), 7.38 – 7.28 (m, 3H), 7.23 – 7.16 (m, 2H), 7.11 – 7.03 (m, 2H), 6.47 (s, 1H), 5.94 (s, 1H), 3.35 (s, 3H), 1.53 (s, 9H). ^{13}C NMR (126 MHz, CDCl_3) δ 193.4, 167.9, 155.7, 152.5, 138.7, 137.9, 136.3, 135.5, 133.2, 129.3, 126.7, 125.3, 123.5, 123.0, 122.9, 121.9, 120.8, 119.6, 119.5, 119.2, 118.6, 111.4, 107.4, 74.2, 53.6, 28.4 (3C). HRMS (ESI) calcd for $\text{C}_{29}\text{H}_{25}\text{Cl}_2\text{N}_3\text{O}_5\text{Na}$ $[\text{M}+\text{Na}]^+$ 588.1063; found 588.1063.

Methyl 2-(2-(3-aminophenyl)-1H-indol-3-yl)-5,7-dichloro-3-oxoindoline-2-carboxylate (**16**)



A solution of HCl in dioxane (5.0 mL, 4M) was added to a solution of **15** (19 mg) in DCM (2.0 mL) and the reaction was stirred for 12 h. The solvent was then evaporated under reduced pressure. The residue was then washed with DCM and purified via preparative TLC (6:4 hexane/EtOAc) to furnish the product as yellowish powder in 64% yield. ¹H NMR (500 MHz, CD₃OD) δ 7.65 (d, *J* = 2.1 Hz, 1H), 7.45 (d, *J* = 2.0 Hz, 1H), 7.39 – 7.32 (m, 1H), 7.13 – 7.05 (m, 2H), 7.03 – 6.96 (m, 1H), 6.92 (ddd, *J* = 8.1, 6.9, 1.0 Hz, 1H), 6.85 – 6.77 (m, 2H), 6.72 (ddd, *J* = 8.1, 2.3, 1.0 Hz, 1H), 3.30 (s, 3H) (N.B.: the ¹H signal for the amine, indole, and indolinone protons were not detected). ¹³C NMR (126 MHz, CD₃OD) δ 196.9, 169.3, 157.6, 148.9, 140.7, 137.6, 137.1, 135.1, 129.9, 128.0, 124.7, 123.4, 122.7, 122.3, 120.5, 120.1, 120.0, 119.5, 117.2, 116.3, 112.3, 106.4, 75.9, 53.4. HRMS (ESI) calcd for C₂₄H₁₈Cl₂N₃O₃ [M+H]⁺ 466.0720; found 466.0727.

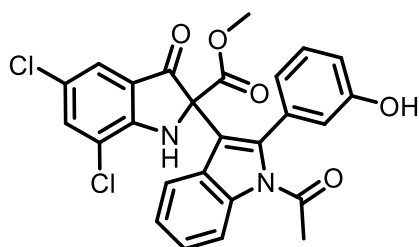
1-(2-(3-hydroxyphenyl)-1H-indol-1-yl)ethan-1-one (**17**)



To a solution of **11** (400 mg, 1.9 mmol) in DCE, triethylamine (3.0 equiv., 0.80 mL) was added followed by the addition of 4-dimethylaminopyridine (0.40 equiv., 88 mg) and acetic anhydride (4.0 equiv., 780 mg). The reaction was stirred at room temperature for 24 h. The reaction mixture was then purified by silica gel chromatography (gradient elution 1 to 20% EtOAc in hexane) to afford the product as yellow oil in 62% yield. ¹H NMR (500 MHz, CDCl₃) δ 8.33 (s, 1H), 7.63 (ddt, *J* = 8.0, 1.3, 0.7 Hz, 1H), 7.50 (ddd, *J* = 7.8, 1.7, 1.0 Hz, 1H), 7.42 (t, *J* = 7.9 Hz, 1H), 7.40 – 7.35 (m, 2H), 7.21 (ddd, *J* = 8.2, 7.0, 1.2 Hz, 1H), 7.13 (ddd, *J* = 8.0, 7.1, 1.0 Hz, 1H), 7.04 (ddd, *J* = 8.0, 2.3, 1.0 Hz, 1H), 6.81 (dd, *J* = 2.2, 0.9 Hz, 1H), 2.35 (s, 3H). ¹³C NMR (126 MHz, CDCl₃)

δ 169.6, 151.4, 137.0, 137.0, 134.1, 130.1, 129.2, 122.7, 122.7, 120.9, 120.8, 120.5, 118.5, 111.1, 100.8, 21.3. HRMS (ESI) calcd for $C_{16}H_{12}NO_2$ $[M-H]^-$ 250.0874; found 250.0874.

Methyl 2-(1-acetyl-2-(3-hydroxyphenyl)-1H-indol-3-yl)-5,7-dichloro-3-oxoindoline-2-carboxylate (**19**)



The title compound was prepared analogously to compound **5** but using compound **17** instead of **11** and the product was isolated as yellow semisolid in 65% yield; $R_f = 0.25$ (7:3 hexanes: EtOAc). 1H NMR (500 MHz, $CDCl_3$) δ 8.28 (s, 1H), 7.56 – 7.47 (m, 2H), 7.43 – 7.34 (m, 2H), 7.29 (dt, $J = 7.7, 1.3$ Hz, 1H), 7.25 – 7.19 (m, 2H), 7.18 – 7.12 (m, 2H), 7.08 (ddd, $J = 8.0, 7.0, 1.0$ Hz, 1H), 3.38 (s, 3H), 2.30 (s, 3H). (N.B.: the indolinone proton was not detected). ^{13}C NMR (126 MHz, $CDCl_3$) δ 193.2, 169.3, 167.8, 155.3, 150.7, 136.8, 136.3, 135.5, 133.8, 129.6, 127.1, 126.6, 125.5, 123.25, 123.20, 122.8, 122.4, 121.9, 121.0, 119.6, 119.1, 111.4, 107.6, 74.0, 53.7, 21.2. HRMS (ESI) calcd for $C_{26}H_{18}Cl_2N_2O_5Na$ $[M+Na]^+$ 531.0485; found 531.0491.

3.4.3 Virological Assays

3.4.3.1 SARS-CoV2 Replication Assay

Confluent Vero E6 cells (gift from Dr. David Evans, University of Alberta) were pre-treated with growth media (Cytiva DMEM + 10% heat inactivated FBS) containing Penicillin/Streptomycin containing drug dissolved in DMSO for 1 hour in biological duplicate or triplicate. SARS-CoV2 conditioned media (“V2/Canada/VIDO/2020”) was then added at an MOI

of 0.1 and the infection was allowed to proceed for 1 hour at which point the infectious media was removed and fresh media containing drug was added. At 24 hours post-infection, monolayers were washed with PBS and then harvested for total RNA isolation as per Qiagen RNeasy + mini kit (74136). Total RNA was quantified using a Nanodrop and equalized to 10 ng/μl before performing a one-step qRT-PCR assay in triplicate technical replicates. Reverse-transcription and amplification were both performed in the same reaction using Quanta qScript XLT One-Step RT-qPCR ToughMix, (95132-02K). TaqMan primer/probes were purchased from ThermoFisher Scientific/Life Technologies: 2019-nCoV (A-47532-FAM), human HPRT1 housekeeping control (HS02800695_m1 - VIC). The RNA was run on a CFX96™ Real-Time system, C1000 Touch Thermal Cycler by Bio-Rad, with cycling conditions as follows: cDNA synthesis at 50 °C for 10 min, initial denaturation at 95 °C for 1 min, and 45 amplification cycles (95 °C for 10 sec, then 60 °C for 60 sec). SARS-CoV2 transcripts were corrected for HPRT1 expression and then compared by treatment group.

3.4.4 RdRp Assay

3.4.4.1 Protein Expression and Purification

The SARS-CoV-2 RdRp complex composed of the three proteins (nsp7, nsp8, and nsp12) was expressed and purified according to a previously published procedure.^{44, 57} Briefly, The pFastBac-1 (Invitrogen, Burlington, Ontario, Canada) plasmid with the codon-optimized synthetic DNA sequences (GenScript, Piscataway, NJ) coding for a portion of lab polyprotein of SARS-CoV-2 (NCBI: QHD43415.1) containing only nsp5, nsp7, nsp8, and nsp12 was used as a starting material for protein expression in insect cells (Sf9, Invitrogen). The MultiBac (Geneva Biotech, Geneva, Switzerland) system was employed for protein expression in insect cells (Sf9, Invitrogen).⁵⁸ The SARS-CoV-2 RdRp complex was then purified using Ni-NTA affinity

chromatography of the nsp8 N-terminal eight-histidine tag according to the manufacturer's specifications (Thermo Scientific, Rockford, IL, USA).

3.4.4.2 RNA Synthesis Inhibition Assay

Serial dilutions of the tested compounds were pre-incubated with 300 nM of SARS-CoV-2 RdRp complex in the presence of 5 mM MgCl₂ and 25 mM Tris-HCl (pH 8) for 10 minutes at the ambient temperature during the aliquoting and 10 or 60 minutes at 30 °C. The RNA synthesis was initiated by addition of a mixture containing 200 μM RNA primer, 2 μM RNA template, 0.1 μM [α -³²P]-GTP, and 0.1 μM NTP. A final concentration of 10% DMSO was used. The reactions were started by incubating (15 μL) of the mixture for 45 minutes at 30 °C and then stopped by the addition of 15 μL of formamide/EDTA (25 mM) mixture then incubated at 95 °C for 10 min. The reaction samples (3 μL) were subjected to denaturing 8 M urea 20% polyacrylamide gel electrophoresis to resolve products of RNA synthesis followed by signal quantification (ImageQuant 5.2, GE Healthcare Biosciences, Uppsala, Sweden) through phosphorimaging (Amerhsham Typhoon 5, Cytivia, Marlborough, MA, USA). The signal corresponding to the full template-length product of RNA synthesis in the presence of a compound was normalized (%) to the signal obtained in the absence of the compound. The normalized values of RNA synthesis were plotted versus compound concentrations and fitted to a log(inhibitor)-versus-normalized-response (variable slope) equation using GraphPad Prism 7.0 (GraphPad Software, Inc., San Diego, CA, USA) to determine the IC₅₀ values for the inhibition of RNA synthesis by a given compound. Suramin was used as positive control.

3.5 References

1. Van Der Hoek, L., Human Coronaviruses: What Do They Cause? *Antiviral Therapy* **2005**, *12*, 651-658.
2. LeDuc, J. W.; Barry, M. A., SARS, the First Pandemic of the 21st Century. *Emerg Infect Dis* **2004**, *10*, e26-e26.
3. Ramadan, N.; Shaib, H., Middle East respiratory syndrome coronavirus (MERS-CoV): A review. *Germs* **2019**, *9*, 35-42.
4. Zhou, P.; Yang, X.-L.; Wang, X.-G.; Hu, B.; Zhang, L.; Zhang, W.; Si, H.-R.; Zhu, Y.; Li, B.; Huang, C.-L.; Chen, H.-D.; Chen, J.; Luo, Y.; Guo, H.; Jiang, R.-D.; Liu, M.-Q.; Chen, Y.; Shen, X.-R.; Wang, X.; Zheng, X.-S.; Zhao, K.; Chen, Q.-J.; Deng, F.; Liu, L.-L.; Yan, B.; Zhan, F.-X.; Wang, Y.-Y.; Xiao, G.-F.; Shi, Z.-L., A pneumonia outbreak associated with a new coronavirus of probable bat origin. *Nature* **2020**, *579*, 270-273.
5. Wu, F.; Zhao, S.; Yu, B.; Chen, Y.-M.; Wang, W.; Song, Z.-G.; Hu, Y.; Tao, Z.-W.; Tian, J.-H.; Pei, Y.-Y.; Yuan, M.-L.; Zhang, Y.-L.; Dai, F.-H.; Liu, Y.; Wang, Q.-M.; Zheng, J.-J.; Xu, L.; Holmes, E. C.; Zhang, Y.-Z., A new coronavirus associated with human respiratory disease in China. *Nature* **2020**, *579*, 265-269.
6. Hadj Hassine, I., Covid-19 vaccines and variants of concern: A review. *Reviews in Medical Virology* **2021**, *n/a*, e2313.
7. Pushpakom, S.; Iorio, F.; Eyers, P. A.; Escott, K. J.; Hopper, S.; Wells, A.; Doig, A.; Guilliams, T.; Latimer, J.; McNamee, C.; Norris, A.; Sanseau, P.; Cavalla, D.; Pirmohamed, M., Drug repurposing: progress, challenges and recommendations. *Nature Reviews Drug Discovery* **2019**, *18*, 41-58.
8. Geraghty, R. J.; Aliota, M. T.; Bonnac, L. F., Broad-Spectrum Antiviral Strategies and Nucleoside Analogues. *Viruses* **2021**, *13*.
9. Gentile, I.; Maraolo, A. E.; Buonomo, A. R.; Zappulo, E.; Borgia, G., The discovery of sofosbuvir: a revolution for therapy of chronic hepatitis C. *Expert Opinion on Drug Discovery* **2015**, *10*, 1363-1377.
10. Asselah, T.; Boyer, N.; Saadoun, D.; Martinot-Peignoux, M.; Marcellin, P., Direct-acting antivirals for the treatment of hepatitis C virus infection: optimizing current IFN-free treatment and future perspectives. *Liver International* **2016**, *36*, 47-57.
11. Teoh, S. L.; Lim, Y. H.; Lai, N. M.; Lee, S. W. H., Directly Acting Antivirals for COVID-19: Where Do We Stand? *Frontiers in Microbiology* **2020**, *11*.
12. Beigel, J. H.; Tomashek, K. M.; Dodd, L. E.; Mehta, A. K.; Zingman, B. S.; Kalil, A. C.; Hohmann, E.; Chu, H. Y.; Luetkemeyer, A.; Kline, S.; Lopez de Castilla, D.; Finberg, R. W.; Dierberg, K.; Tapsen, V.; Hsieh, L.; Patterson, T. F.; Paredes, R.; Sweeney, D. A.; Short, W. R.; Touloumi, G.; Lye, D. C.; Ohmagari, N.; Oh, M.-d.; Ruiz-Palacios, G. M.; Benfield, T.; Fätkenheuer, G.; Kortepeter, M. G.; Atmar, R. L.; Creech, C. B.; Lundgren, J.; Babiker, A. G.; Pett, S.; Neaton, J. D.; Burgess, T. H.; Bonnett, T.; Green, M.; Makowski, M.; Osinusi, A.; Nayak, S.; Lane, H. C., Remdesivir for the Treatment of Covid-19 — Final Report. *New England Journal of Medicine* **2020**, *383*, 1813-1826.

13. Lo, M. K.; Jordan, R.; Arvey, A.; Sudhamsu, J.; Shrivastava-Ranjan, P.; Hotard, A. L.; Flint, M.; McMullan, L. K.; Siegel, D.; Clarke, M. O.; Mackman, R. L.; Hui, H. C.; Perron, M.; Ray, A. S.; Cihlar, T.; Nichol, S. T.; Spiropoulou, C. F., GS-5734 and its parent nucleoside analog inhibit Filo-, Pneumo-, and Paramyxoviruses. *Scientific Reports* **2017**, *7*, 43395.
14. Kokic, G.; Hillen, H. S.; Tegunov, D.; Dienemann, C.; Seitz, F.; Schmitzova, J.; Farnung, L.; Siewert, A.; Höbartner, C.; Cramer, P., Mechanism of SARS-CoV-2 polymerase stalling by remdesivir. *Nature Communications* **2021**, *12*, 279.
15. Gordon, C. J.; Lee, H. W.; Tchesnokov, E. P.; Perry, J. K.; Feng, J. Y.; Bilello, J. P.; Porter, D. P.; Götte, M., Efficient incorporation and template-dependent polymerase inhibition are major determinants for the broad-spectrum antiviral activity of remdesivir. *Journal of Biological Chemistry* **2022**, 298.
16. Abdelnabi, R.; Foo, C. S.; Jochmans, D.; Vangeel, L.; De Jonghe, S.; Augustijns, P.; Mols, R.; Weynand, B.; Wattanakul, T.; Hoglund, R. M.; Tarning, J.; Mowbray, C. E.; Sjö, P.; Escudie, F.; Scandale, I.; Chatelain, E.; Neyts, J., The oral protease inhibitor (PF-07321332) protects Syrian hamsters against infection with SARS-CoV-2 variants of concern. *Nature Communications* **2022**, *13*, 719.
17. Atienza, B. J. P.; Jensen, L. D.; Noton, S. L.; Ansalem, A. K. V.; Hobman, T.; Fearn, R.; Marchant, D. J.; West, F. G., Dual Catalytic Synthesis of Antiviral Compounds Based on Metallocarbene–Azide Cascade Chemistry. *The Journal of Organic Chemistry* **2018**, *83*, 6829-6842.
18. Ahn, D.-G.; Choi, J.-K.; Taylor, D. R.; Oh, J.-W., Biochemical characterization of a recombinant SARS coronavirus nsp12 RNA-dependent RNA polymerase capable of copying viral RNA templates. *Archives of Virology* **2012**, *157*, 2095-2104.
19. Kirchdoerfer, R. N.; Ward, A. B., Structure of the SARS-CoV nsp12 polymerase bound to nsp7 and nsp8 co-factors. *Nature Communications* **2019**, *10*, 2342.
20. Gao, Y.; Yan, L.; Huang, Y.; Liu, F.; Zhao, Y.; Cao, L.; Wang, T.; Sun, Q.; Ming, Z.; Zhang, L.; Ge, J.; Zheng, L.; Zhang, Y.; Wang, H.; Zhu, Y.; Zhu, C.; Hu, T.; Hua, T.; Zhang, B.; Yang, X.; Li, J.; Yang, H.; Liu, Z.; Xu, W.; Guddat, L. W.; Wang, Q.; Lou, Z.; Rao, Z., Structure of the RNA-dependent RNA polymerase from COVID-19 virus. *Science* **2020**, *368*, 779-782.
21. Naydenova, K.; Muir, K. W.; Wu, L. F.; Zhang, Z.; Coscia, F.; Peet, M. J.; Castro-Hartmann, P.; Qian, P.; Sader, K.; Dent, K.; Kimanius, D.; Sutherland, J. D.; Lowe, J.; Barford, D.; Russo, C. J., Structure of the SARS-CoV-2 RNA-dependent RNA polymerase in the presence of favipiravir-RTP. *Proc Natl Acad Sci USA* **2021**, *118*.
22. Le Guilloux, V.; Schmidtke, P.; Tuffery, P., Fpocket: An open source platform for ligand pocket detection. *BMC Bioinformatics* **2009**, *10*, 168.
23. Halgren, T., New Method for Fast and Accurate Binding-site Identification and Analysis. *Chemical Biology & Drug Design* **2007**, *69*, 146-148.
24. Halgren, T. A., Identifying and Characterizing Binding Sites and Assessing Druggability. *Journal of Chemical Information and Modeling* **2009**, *49*, 377-389.

25. Krivák, R.; Hoksza, D., Improving protein-ligand binding site prediction accuracy by classification of inner pocket points using local features. *Journal of Cheminformatics* **2015**, *7*, 12.
26. Schmidtke, P.; Bidon-Chanal, A.; Luque, F. J.; Barril, X., MDpocket: open-source cavity detection and characterization on molecular dynamics trajectories. *Bioinformatics* **2011**, *27*, 3276-3285.
27. Friesner, R. A.; Murphy, R. B.; Repasky, M. P.; Frye, L. L.; Greenwood, J. R.; Halgren, T. A.; Sanschagrin, P. C.; Mainz, D. T., Extra Precision Glide: Docking and Scoring Incorporating a Model of Hydrophobic Enclosure for Protein–Ligand Complexes. *Journal of Medicinal Chemistry* **2006**, *49*, 6177-6196.
28. Morris, G. M.; Goodsell, D. S.; Halliday, R. S.; Huey, R.; Hart, W. E.; Belew, R. K.; Olson, A. J., Automated docking using a Lamarckian genetic algorithm and an empirical binding free energy function. *Journal of Computational Chemistry* **1998**, *19*, 1639-1662.
29. Vilar, S.; Cozza, G.; Moro, S., Medicinal chemistry and the molecular operating environment (MOE): application of QSAR and molecular docking to drug discovery. *Curr Top Med Chem* **2008**, *8*, 1555-72.
30. De Vivo, M.; Masetti, M.; Bottegoni, G.; Cavalli, A., Role of Molecular Dynamics and Related Methods in Drug Discovery. *Journal of Medicinal Chemistry* **2016**, *59*, 4035-4061.
31. Barducci, A.; Bonomi, M.; Parrinello, M., Metadynamics. *WIREs Computational Molecular Science* **2011**, *1*, 826-843.
32. Gervasio, F. L.; Laio, A.; Parrinello, M., Flexible Docking in Solution Using Metadynamics. *Journal of the American Chemical Society* **2005**, *127*, 2600-2607.
33. Russo, S.; Callegari, D.; Incerti, M.; Pala, D.; Giorgio, C.; Brunetti, J.; Bracci, L.; Vicini, P.; Barocelli, E.; Capoferri, L.; Rivara, S.; Tognolini, M.; Mor, M.; Lodola, A., Exploiting Free-Energy Minima to Design Novel EphA2 Protein–Protein Antagonists: From Simulation to Experiment and Return. *Chemistry – A European Journal* **2016**, *22*, 8048-8052.
34. Söderhjelm, P.; Tribello Gareth, A.; Parrinello, M., Locating binding poses in protein-ligand systems using reconnaissance metadynamics. *Proceedings of the National Academy of Sciences* **2012**, *109*, 5170-5175.
35. Fusani, L.; Palmer, D. S.; Somers, D. O.; Wall, I. D., Exploring Ligand Stability in Protein Crystal Structures Using Binding Pose Metadynamics. *Journal of Chemical Information and Modeling* **2020**, *60*, 1528-1539.
36. Clark, A. J.; Tiwary, P.; Borrelli, K.; Feng, S.; Miller, E. B.; Abel, R.; Friesner, R. A.; Berne, B. J., Prediction of Protein–Ligand Binding Poses via a Combination of Induced Fit Docking and Metadynamics Simulations. *Journal of Chemical Theory and Computation* **2016**, *12*, 2990-2998.
37. Wang, E.; Sun, H.; Wang, J.; Wang, Z.; Liu, H.; Zhang, J. Z. H.; Hou, T., End-Point Binding Free Energy Calculation with MM/PBSA and MM/GBSA: Strategies and Applications in Drug Design. *Chemical Reviews* **2019**, *119*, 9478-9508.
38. Misaki, T.; Nagase, R.; Matsumoto, K.; Tanabe, Y., Ti-Crossed-Claisen Condensation between Carboxylic Esters and Acid Chlorides or Acids: A Highly Selective and General Method for the Preparation of Various β -Keto Esters. *Journal of the American Chemical Society* **2005**, *127*, 2854-2855.

39. Brooks, W. H.; Guida, W. C.; Daniel, K. G., The significance of chirality in drug design and development. *Current topics in medicinal chemistry* **2011**, *11*, 760-770.
40. McConathy, J.; Owens, M. J., Stereochemistry in Drug Action. *Prim Care Companion J Clin Psychiatry* **2003**, *5*, 70-73.
41. Pescitelli, G., ECD exciton chirality method today: a modern tool for determining absolute configurations. *Chirality* **2022**, *34*, 333-363.
42. Yang, J.; Petitjean, S. J. L.; Koehler, M.; Zhang, Q.; Dumitru, A. C.; Chen, W.; Derclaye, S.; Vincent, S. P.; Soumillion, P.; Alsteens, D., Molecular interaction and inhibition of SARS-CoV-2 binding to the ACE2 receptor. *Nature Communications* **2020**, *11*, 4541.
43. Beyerstedt, S.; Casaro, E. B.; Rangel, É. B., COVID-19: angiotensin-converting enzyme 2 (ACE2) expression and tissue susceptibility to SARS-CoV-2 infection. *European Journal of Clinical Microbiology & Infectious Diseases* **2021**, *40*, 905-919.
44. Tchesnokov, E. P.; Gordon, C. J.; Woolner, E.; Kocinkova, D.; Perry, J. K.; Feng, J. Y.; Porter, D. P.; Götte, M., Template-dependent inhibition of coronavirus RNA-dependent RNA polymerase by remdesivir reveals a second mechanism of action. *Journal of Biological Chemistry* **2020**, *295*, 16156-16165.
45. Jacobson, M. P.; Pincus, D. L.; Rapp, C. S.; Day, T. J. F.; Honig, B.; Shaw, D. E.; Friesner, R. A., A hierarchical approach to all-atom protein loop prediction. *Proteins: Structure, Function, and Bioinformatics* **2004**, *55*, 351-367.
46. Jacobson, M. P.; Friesner, R. A.; Xiang, Z.; Honig, B., On the Role of the Crystal Environment in Determining Protein Side-chain Conformations. *Journal of Molecular Biology* **2002**, *320*, 597-608.
47. Maier, J. A.; Martinez, C.; Kasavajhala, K.; Wickstrom, L.; Hauser, K. E.; Simmerling, C., ff14SB: Improving the Accuracy of Protein Side Chain and Backbone Parameters from ff99SB. *Journal of Chemical Theory and Computation* **2015**, *11*, 3696-3713.
48. Mark, P.; Nilsson, L., Structure and Dynamics of the TIP3P, SPC, and SPC/E Water Models at 298 K. *The Journal of Physical Chemistry A* **2001**, *105*, 9954-9960.
49. Shelley, J. C.; Cholleti, A.; Frye, L. L.; Greenwood, J. R.; Timlin, M. R.; Uchimaya, M., Epik: a software program for pK_a prediction and protonation state generation for drug-like molecules. *Journal of Computer-Aided Molecular Design* **2007**, *21*, 681-691.
50. Roos, K.; Wu, C.; Damm, W.; Reboul, M.; Stevenson, J. M.; Lu, C.; Dahlgren, M. K.; Mondal, S.; Chen, W.; Wang, L.; Abel, R.; Friesner, R. A.; Harder, E. D., OPLS3e: Extending Force Field Coverage for Drug-Like Small Molecules. *Journal of Chemical Theory and Computation* **2019**, *15*, 1863-1874.
51. Wang, J.; Wang, W.; Kollman, P. A.; Case, D. A., Automatic atom type and bond type perception in molecular mechanical calculations. *J Mol Graph Model* **2006**, *25*, 247-60.
52. Wang, J.; Wolf, R. M.; Caldwell, J. W.; Kollman, P. A.; Case, D. A., Development and testing of a general amber force field. *J Comput Chem* **2004**, *25*, 1157-74.
53. Jakalian, A.; Jack, D. B.; Bayly, C. I., Fast, efficient generation of high-quality atomic charges. AM1-BCC model: II. Parameterization and validation. *Journal of Computational Chemistry* **2002**, *23*, 1623-1641.

54. Roe, D. R.; Cheatham, T. E., PTRAJ and CPPTRAJ: Software for Processing and Analysis of Molecular Dynamics Trajectory Data. *Journal of Chemical Theory and Computation* **2013**, *9*, 3084-3095.
55. Miller, B. R.; McGee, T. D.; Swails, J. M.; Homeyer, N.; Gohlke, H.; Roitberg, A. E., MMPBSA.py: An Efficient Program for End-State Free Energy Calculations. *Journal of Chemical Theory and Computation* **2012**, *8*, 3314-3321.
56. Schrödinger Release 2019-3: Maestro, Schrödinger, LLC, New York, NY.
57. Gordon, C. J.; Tchesnokov, E. P.; Woolner, E.; Perry, J. K.; Feng, J. Y.; Porter, D. P.; Götte, M., Remdesivir is a direct-acting antiviral that inhibits RNA-dependent RNA polymerase from severe acute respiratory syndrome coronavirus 2 with high potency. *Journal of Biological Chemistry* **2020**, *295*, 6785-6797.
58. Berger, I.; Garzoni, F.; Chaillet, M.; Haffke, M.; Gupta, K.; Aubert, A., The MultiBac Protein Complex Production Platform at the EMBL. *JoVE* **2013**, e50159.

Chapter 4:

Conformational Shift by A Single Amino Acid Switch in the Respiratory Syncytial Virus Fusion Glycoprotein Causes Global Neutralizing Antibody Evasion[§]

4.1 Introduction

Viral pneumonia is one of the leading causes of illness and death worldwide, and most cases are due to seasonal viruses. One of these is Respiratory Syncytial Virus (RSV), which is the leading cause of infant hospitalizations worldwide.¹ There are no licensed vaccines for RSV and few antiviral therapies. In the absence of vaccines biologics provide a means of passive immunization and the only currently licensed biologic for at-risk premature infants is a monoclonal antibody, Palivizumab (PZMB), that binds to site II on the fusion (RSVF) protein of RSV.² Other monoclonal antibodies with a longer half-life to last the RSV season with one dose (“one and done”) were designed against other sites on RSV-F, and these are currently in late phase clinical trials.³ A better understanding of viral adaptation is required to understand whether RSV will adapt resistance to these new drugs.

There are two types of RSV, types A (RSVA) and B (RSVB). RSVB diverged from RSVA about 350 years ago⁴ and they share about 90% amino acid sequence identity overall. The A and B types can alternate seasons where one type predominates, or they can co-circulate in the

[§] The contents of this chapter have been copied and/or adapted from the following publication: Elawar, F.[‡], Oraby, A.K.[‡], Stojic, A.[‡], McClelland, R.D.; Erwin, K.; Bilawchuk, L.M.; Hazes, B.; Griffiths, C.D.; Culp, T.N.; West, F.G.; Ramilo, O.; McLellan, J.S.; Mejias, A.; Marchant, D.J., Respiratory Syncytial Virus Evolution by Adaptation. (Under review in *Nature Communications*) Preprint: <https://doi.org/10.21203/rs.3.rs-1578243/v1>
[‡]Authors equally contributed to this work.

population and even present as co-infections in the same patient. However, it is not known what evolutionary pressure drove these RSV types apart and why they have seemingly different behaviours in the population.

The most studied of the RSV proteins is the RSV fusion glycoprotein (RSV-F) and it is the principal antibody neutralization determinant on the RSV virion. Its structure has been elucidated and contains six major antibody neutralization epitopes on its surface.⁵⁻⁷ RSV-F exists as a metastable prefusion form on the virus particle. Conversion from prefusion to post-fusion form mediates fusion of virus with the host cell plasma membrane after interactions with its receptor and coreceptor⁸, delivering the viral genome and replication machinery into the cell.

Here we report on key conformational differences between RSV A and B F glycoprotein mediated by amino acid position 305 of RSV-F. We asked whether this single amino acid mutation could lead to an overall conformational shift in viral surface glycoproteins that would alter susceptibility to serum neutralization. We found that the expression of a leucine (L) in RSVA or an isoleucine (I) in RSVB resulted in significant differences in growth kinetics. It also caused an overall change in RSV susceptibility to neutralizing sera and monoclonal antibodies at multiple sites on the RSV-F protein. In directed evolution assays, we found that the L to I mutation at RSV-F residue 305 occurred at evolutionary bottlenecks induced by sterilizing, and not suboptimal, antiviral pressure. These results suggest that RSVA and RSVB diverged due to sterilizing immunity pressure on the parental virus.

4.2 Results

4.2.1 RSV Types A and B have Different Susceptibilities to Antibodies

We have reported on the diversity of RSVA and B isolates from hospitalized patients in Alberta, Canada during the 2013 to 2016 seasons and Children's Medical Center Dallas (CMCD),

Texas (2004 to 2009) and Nationwide Children's Hospital (NCH), Columbus, Ohio (2010 to 2011) (**Figure 4.1a**).⁹ We have since tested the susceptibility of some of these RSV isolates to antibody prophylaxis (**Figure 4.1b,c,d**), which is performed by injection of palivizumab. Palivizumab is a monoclonal anti-RSV antibody targeted to the RSV-F glycoprotein and it is given to premature infants and high-risk pediatric patients during RSV seasons. Canada has a national taxpayer funded healthcare program that administers prophylaxis regularly throughout the year, however, the susceptibility of RSV to palivizumab is not known.

We studied RSV susceptibility to palivizumab via neutralisation assays on virus isolates from patients in Canada and the USA (n= 34). These isolates have been sequenced and published.⁹¹⁰ We found that most isolates of RSV that we tested were less susceptible to palivizumab than the prototypic RSV strain type-A2 (RSV-A2) (**Figure 4.1b and c**). Palivizumab had an inhibitory concentration 50 (IC₅₀) of 11.8 ng/ml against prototypic laboratory adapted strain RSV-A2, consistent with what has been published previously.¹⁰ However, a representative clinical isolate, 1415S (RSV type-A), that we collected during the 2014 - 2015 season^{10, 11} demonstrated a significantly higher IC₅₀ of 92.4 ng/ml in the presence of palivizumab. We grouped RSVA and B IC₅₀s and found that RSVB clinical isolates were more susceptible to palivizumab with a significantly lower mean IC₅₀ compared to the RSVA isolates (**Figure 4.1c**). When we tested the isolates with an anti-RSVA antisera we noted that the RSVA isolates were significantly more susceptible to neutralization than the RSVB isolates (**Figure 4.1d**). This was expected as the antisera was raised against RSVA. Over time (2013 – 2017) we did not detect a changing trend in susceptibility to palivizumab among the RSV isolates tested.

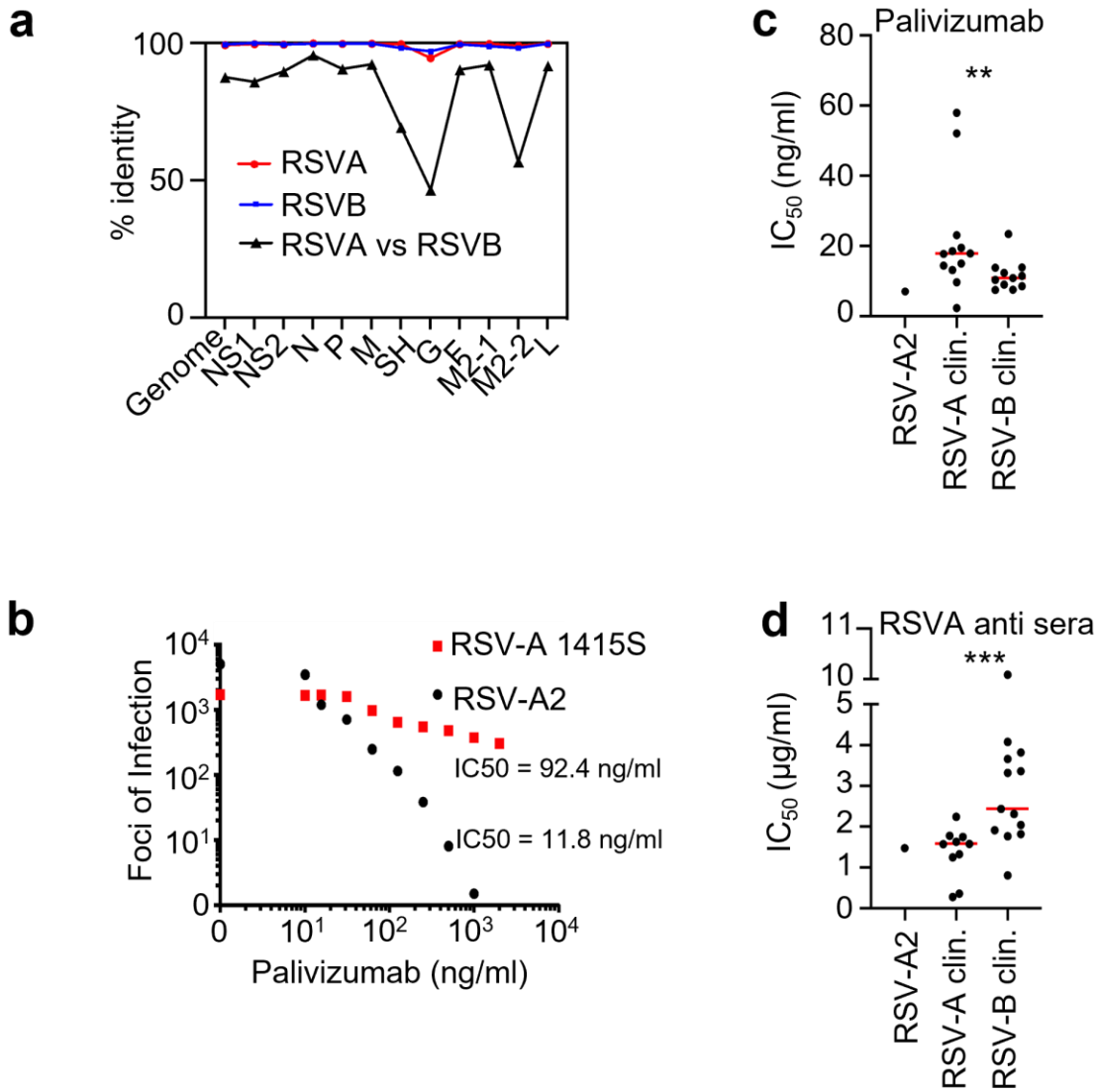


Figure 4.1: Clinical isolates of RSV type-A and B from Alberta, Canada and Ohio, USA share 88 % sequence identity overall and have different susceptibilities to palivizumab. RSV isolates in patient samples were sequenced by next generation sequencing and the genomes were aligned. Whole genome and % identities of the individual RSV genes are shown. The susceptibilities to **b**, **c**, palivizumab monoclonal antibody that targets site II on the RSV fusion glycoprotein (RSV-F) and **d**, RSV type-A antisera of RSV type-A and type-B isolates were tested. RSV-A2; laboratory adapted strain, RSV-A 1415S; RSV type-A clinical isolate. Mann Whitney U test determined significance of parametric data. **, P = 0.0094, ***, P = 0.0003.

4.2.2 RSV-F Site II of RSVA and B Differ at Flanking Amino Acid 305

Palivizumab binds to site II of the RSV-F glycoprotein (**Figure 4.2a-c, Table 4.1**). We found that the palivizumab binding sites of both RSVA and B isolates were identical in their amino acid sequences as previously shown.¹² However, all of the RSVA isolates contained a leucine at amino acid position 305, located in the antigenic site MPE8 (positions 44 – 50, 305 – 310) that flanks downstream of site II (positions 255 - 275). All RSVB isolates contained an isoleucine at this position (**Figure 4.2a,b**) as noted by others previously.¹² However, the functional significance of an L or an I amino acid at position 305 is yet to be reported.

There is a subtle difference in the chemical structure between L and I residues in the position of a methyl group on their amino side chain (**Figure 4.2b**). Therefore, we asked whether an L305I mutation could alter the shape of RSV-F site II (**Figure 4.2c**). To model RSV-F, we used dynamic computational modelling over 0.5 μ s to predict the shape of RSV-F with an L or an I at position 305. Here we noted that residue 305 was positioned directly behind the palivizumab binding site (**Figure 4.2d,e and Figure 4.4**). I305 caused site II to bulge outward (**Figure 4.2d**) compared to L305. We also noted that the overall shape of the RSV-F glycoprotein protomer with I305 shifted compared to the L305-containing protomer (**Figure 4.2e**).

a

AA	300	301	302	303	304	305	306	307	308	309	310
RSV A	V	V	Q	L	P	L	Y	G	V	I	D
RSV B	V	V	Q	L	P	I	Y	G	V	I	D

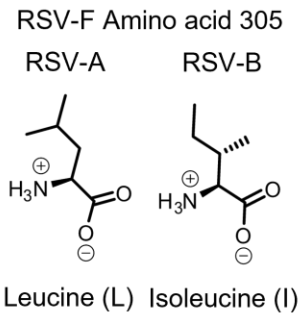
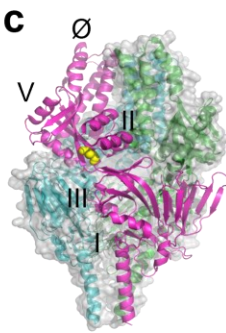
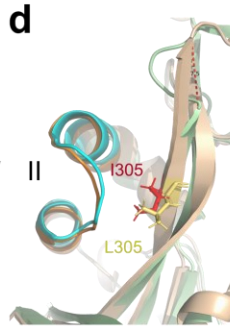
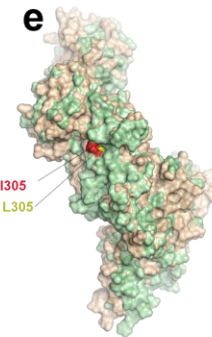
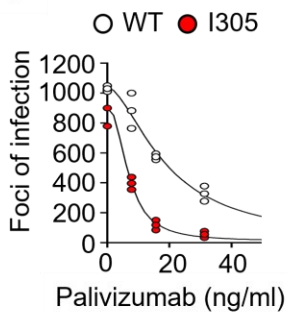
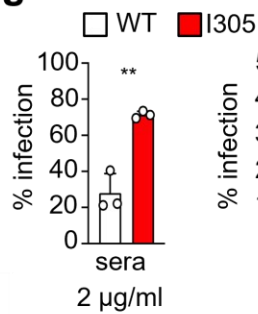
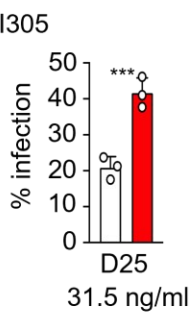
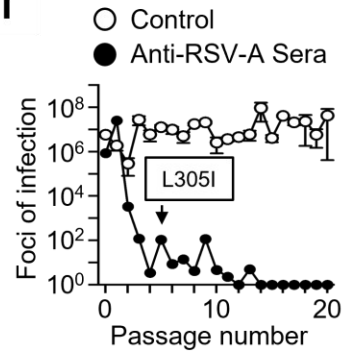
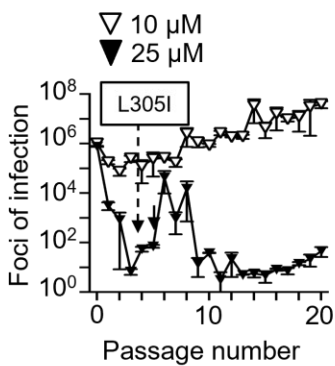
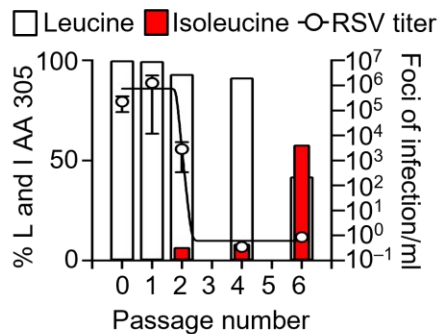
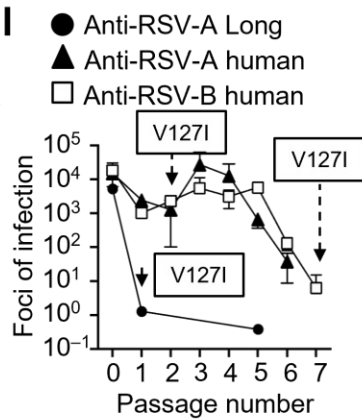
b**c****d****e****f****g****h****i****j****k****l**

Figure 4.2: Mutation in RSV-F at amino acid position 305 occurs at evolutionary bottlenecks and changes the shape and antibody neutralization sensitivity of RSV. **a, b** Amino acids leucine and Isoleucine occupy position 305 in the RSV-F protein of RSV type-A and B, respectively. **c**, Schematic of RSV-F trimer with the positions of the five principal neutralization sites from I – V shown on a protomer of RSV-F. **d**, Overlay of RSV-F Site-II, and the **e**, RSV-F protomer with Leucine (yellow) and Isoleucine (red) at position 305 with a protein-wide shift after all atom

alignment. **f**, Titration curves of recombinant WT-rgRSV and I305-rgRSV in the presence of increasing concentrations of anti-site II antibody palivizumab, **g**, RSV type-A antisera, and **h**, a monoclonal antibody against site Ø (D25). **i**, WT-RSV was grown in the presence of RSV type-A antisera or control sera, and **j**, an RSV polymerase inhibitor in a bronchial epithelial cell line in culture. Virus was sampled daily, quantified by qRT-PCR, and the genomes were sequenced by Illumina next generation sequencing. The passage number at which there was a mutation is indicated in boxed text. **k**, the proportion of RSV quasi-species sequencing reads with Leucine and Isoleucine at position 305 were plotted alongside RSV titer. **l**, the same experiment as described in **i** was performed on an RSVB clinical isolate B127 in the presence of anti-RSV type-A sera, human anti-RSVA and human RSVB sera. The harvested virus particles were quantified by qRT-PCR and sequenced by Illumina next generation sequencing.

4.2.3 Recombinant I305 RSV type-A is More Susceptible to Palivizumab

Given the morphological differences in site II of RSV F when L and I are at amino acid position 305, we asked if an L305I substitution would affect susceptibility of RSV to antibody neutralization. To test this, we used a recombinant genetic model of RSVA (rgRSV)¹³ where amino acid at position 305 was changed to isoleucine as found in RSV B. I305-RSV growth characteristics were measured (**Figure 4.3a**) along with its response to coreceptor blocking (**Figure 4.3b**) because this site II is where the RSV coreceptor NCL binds RSV F.¹⁴ We found that I305-rgRSV was no more or less susceptible to blocking the NCL interaction than the parent WT-rgRSVA virus. We hypothesized that the genetically engineered I305 rgRSV type-A virus model would become more susceptible to palivizumab, similar to RSV B isolates (**Figure 4.1c**). As we expected, I305 rgRSV was significantly more susceptible to palivizumab than the parental rgRSV (**Figure 4.2f**). Furthermore, like RSVB isolates, we found that I305 rgRSV was significantly less susceptible to RSVA antisera (**Figure 4.2g**).

We then asked if other neutralization sites on RSV-F would be altered by an L to I amino acid change at position 305. We hypothesized that the overall shape shift we observed of RSV-F with I305 (**Figure 4.2d,e and Figure 4.4**) could change the ability for monoclonal antibodies (mAb) to bind to other sites on RSV-F and neutralize infection.

a

RSV type- isolate name	RSV-F amino acid 247 – 305 sequence (Palivizumab binding site is in bold font)
A- B (1516)	STYMLTNSSELL SLINDMPITNDQKKLM SSNVQIVRQQSYSIMSIKEEVLAYVVQLPL
A- B (1617)	STYMLTNSSELL SLINDMPITNDQKKLM SSNVQIVRQQSYSIMSIKEEVLAYVVQLPL
A- BBB (1516)	STYMLTNSSELL SLINDMPITNDQKKLM SSNVQIVRQQSYSIMSIKEEVLAYVVQLPL
A- DD (1516)	STYMLTNSSELL SLINDMPITNDQKKLM SSNVQIVRQQSYSIMSIKEEVLAYVVQLPL
A- E (1617)	STYMLTNSSELL SLINDMPITNDQKKLM SSNVQIVRQQSYSIMSIKEEVLAYVVQLPL
A- F (1617)	STYMLTNSSELL SLINDMPITNDQKKLM SSNVQIVRQQSYSIMSIKEEVLAYVVQLPL
A- GFP (1516)	STYMLTNSSELL SLINDMPITNDQKKLM SSNVQIVRQQSYSIMSIKEEVLAYVVQLPL
A- I (1415)	STYMLTNSSELL SLINDMPITNDQKKLM SSNVQIVRQQSYSIMSIKEEVLAYVVQLPL
A- J (1415)	STYMLTNSSELL SLINDMPITNDQKKLM SSNVQIVRQQSYSIMSIKEEVLAYVVQLPL
A- K2 (1415)	STYMLTNSSELL SLINDMPITNDQKKLM SSNVQIVRQQSYSIMSIKEEVLAYVVQLPL
A- TT (1516)	STYMLTNSSELL SLINDMPITNDQKKLM SSNVQIVRQQSYSIMSIKEEVLAYVVQLPL
A- M (1415)	STYMLTNSSELL SLINDMPITNDQKKLM SSNVQIVRQQSYSIMSIKEEVLAYVVQLPL
A- O (1516)	STYMLTNSSELL SLINDMPITNDQKKLM SSNVQIVRQQSYSIMSIKEEVLAYVVQLPL
A- S (1415)	STYMLTNSSELL SLINDMPITNDQKKLM SSNVQIVRQQSYSIMSIKEEVLAYVVQLPL
A- A2 (1415)	STYMLTNSSELL SLINDMPITNDQKKLM SSNVQIVRQQSYSIMSIKEEVLAYVVQLPL
B- C (1617)	STYMLTNSSELL SLINDMPITNDQKKLM SSNVQIVRQQSYSIMSIKEEVLAYVVQLPI
B- E (1415)	STYMLTNSSELL SLINDMPITNDQKKLM SSNVQIVRQQSYSIMSIKEEVLAYVVQLPI
B- E (1516)	STYMLTNSSELL SLINDMPITNDQKKLM SSNVQIVRQQSYSIMSVIKEEVLAYVVQLPI
B- FF (1516)	STYMLTNSSELL SLINDMPITNDQKKLM SSNVQIVRQQSYSIMSIKEEVLAYVVQLPI
B- FFF (1516)	STYMLTNSSELL SLINDMPITNDQKKLM SSNVQIVRQQSYSIMSIKEEVLAYVVQLPI
B-F2 (1415)	STYMLTNSSELL SLINDMPITNDQKKLM SSNVQIVRQQSYSIMSIKEEVLAYVVQLPI
B- H (1617)	STYMLTNSSELL SLINDMPITNDQKKLM SSNVQIVRQQSYSIMSIKEEVLAYVVQLPI
B- J (1516)	STYMLTNSSELL SLINDMPITNDQKKLM SSNVQIVRQQSYSIMSIKEEVLAYVVQLPI
B- JJJ (1516)	STYMLTNSSELL SLINDMPITNDQKKLM SSNVQIVRQQSYSIMSIKEEVLAYVVQLPI
B- O (1415)	STYMLTNSSELL SLINDMPITNDQKKLM SSNVQIVRQQSYSIMSIKEEVLAYVVQLPI
B- L (1617)	STYMLTNSSELL SLINDMPITNDQKKLM SSNVQIVRQQSYSIMSIKEEVLAYVVQLPI
B- MM (1516)	STYMLTNSSELL SLINDMPITNDQKKLM SSNVQIVRQQSYSIMSIKEEVLAYVVQLPI
B- N2 (1415)	STYMLTNSSELL SLINDMPITNDQKKLM SSNVQIVRQQSYSIMSIKEEVLAYVVQLPI
B- N (1415)	STYMLTNSSELL SLINDMPITNDQKKLM SSNVQIVRQQSYSIMSIKEEVLAYVVQLPI
B- S (1617)	STYMLTNSSELL SLINDMPITNDQKKLM SSNVQIVRQQSYSIMSIKEEVLAYVVQLPI
B- X (1516)	STYMLTNSSELL SLINDMPITNDQKKLM SSNVQIVRQQSYSIMSIKEEVLAYVVQLPI
B- Y (1415)	STYMLTNSSELL SLINDMPITNDQKKLM SSNVQIVRQQSYSIMSIKEEVLAYVVQLPI
B- U (1516)	STYMLTNSSELL SLINDMPITNDQKKLM SSNVQIVRQQSYSIMSIKEEVLAYVVQLPI
B- Z (1415)	STYMLTNSSELL SLINDMPITNDQKKLM SSNVQIVRQQSYSIMSIKEEVLAYVVQLPI

b

RSV gene	RSV A	RSV B	*RSV A vs B
Whole genomes	99.4%	99.5%	87.6%
NS1	99.7%	100%	85.9%
NS2	99.5%	99.5%	89.7%
N	99.95%	99.8%	95.7%
P	99.8%	99.8%	90.6%
M	99.9%	99.8%	92.4%
SH	99.7%	98.3%	69.4%
G	94.6%	97.0%	46.6%
F	99.7%	99.6%	90.4%
M2-1	99.8%	98.9%	92.1%
M2-2	99.0%	98.3%	56.8%
L	99.8%	99.8%	91.8%

Table 4.1: RSV F sequence alignment and identity. **a.** RSV F protein sequence alignment of clinical isolates. **b.** Sequence identity between RSV subtypes A and B.

To study this, we tested the susceptibility to neutralization at a different site. We tested mAb D25 which binds to site Ø at the apex of RSV-F (**Figure 4.2b**). Here, I305 rgRSV was significantly less susceptible to neutralization by D25 than the parental L305 rgRSV (**Figure 4.2h**). In summary, we found that the alteration in the shape of the RSV-F protomer caused by L305I could affect the susceptibility of RSV to palivizumab, anti-sera, and D25 mAb which binds to a different site on RSV-F (site Ø) than palivizumab (site II).

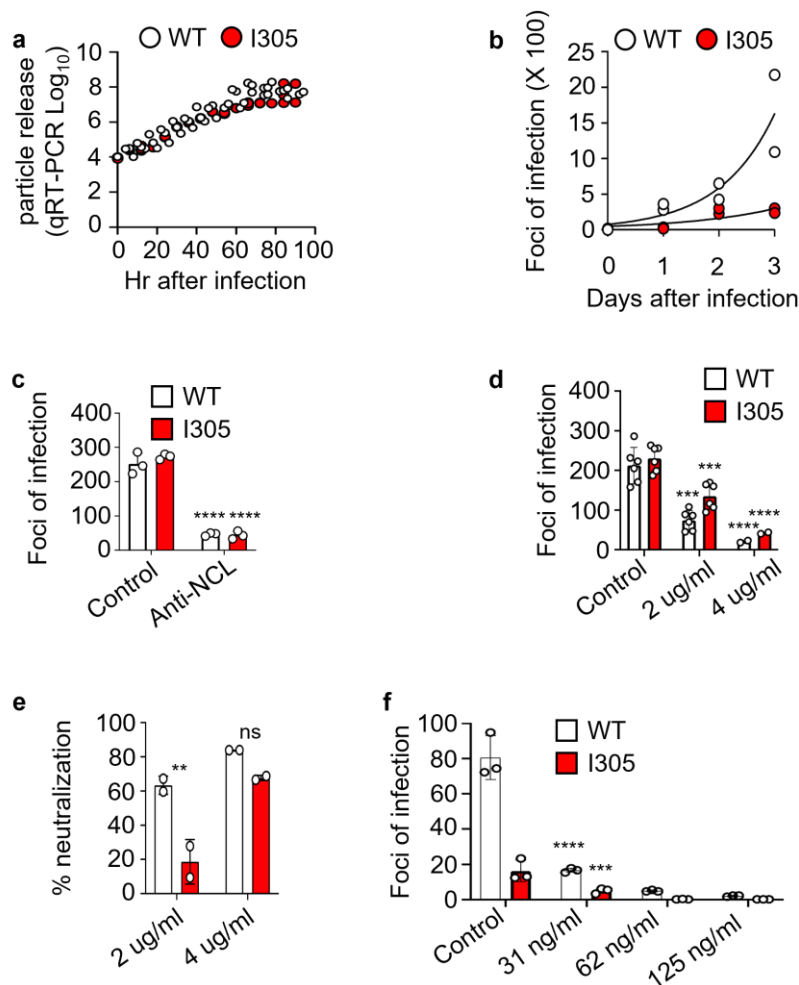


Figure 4.3: L305I is less susceptible to polyclonal antisera and D25 monoclonal antibody but produces less infectious particles. **a**, WT-RSV (L305) and I305-RSV were grown in Hep-2 pharyngeal cells and viral genomes were detected by qRT-PCR, or **b**, harvested at the indicated days after infection and infectivity of the cell conditioned media detected on Hep-2 cells. **c**, susceptibility to NCL blocking with AS14111 aptamer was tested on L and I305 viruses. **d**, Neutralization susceptibility of genetically engineered WT-RSV (L305) and I305-RSV were tested with anti-RSVA neutralizing sera, **e**, percent neutralization is derived from the data in **(d)**, **f**, Neutralization susceptibility of genetically engineered WT-RSV (L305) and I305-RSV were tested with D25 monoclonal antibody.

4.2.4 Amino Acid Substitution at Position 305 Causes a Significant Change in RSV-F Protomer Conformation

Others have shown that the RSV-F trimer ‘breathes’ on the surface of the RSV virion particle.¹⁵ Trimer ‘breathing’ alters the accessibility of antibodies to trimerized RSV-F glycoproteins. We wanted to know whether amino substitutions at position 305 could affect the RSV-F trimer conformation as a measure of breathing, just like it changes the shape. To look at this aspect of RSV-F trimer behaviour, we evaluated the dynamicity of the RSV-F trimer with L and I at AA position 305.

The $C\alpha$ of both systems containing either L and I at position 305 each equilibrated around 200 ns of the simulation time with an average RMSD of 2.3 Å and 2.8 Å for the wild type and the L305I mutant, respectively (**Figure 4.4d**). Therefore, we expect the RSV-F trimer to breathe the same amount with either an L or I at position 305. We also investigated the flexibility of the system residues which were analyzed using the atomic fluctuations expressed at beta factors of the protein backbone atoms for both systems. Interestingly, the majority of the protein residues were stable during the whole simulations with a little flexibility observed in the region 250-305 for the L305I mutant compared to that of the WT with larger flexibility in the 420-450 region and 850-900 region of the WT compared to that of the L305I mutant (**Figure 4.4**).

To better validate our observations, we mutated another residue located away from the palivizumab binding site to investigate conformational changes and the dynamicity of the RSV F protomer. Residue Asn 228 was mutated to Asp 228 (N228D), and we carried out a 270 ns long MD simulation. Clustering of the MD trajectories revealed that the N228D mutant did not show a noticeable conformational shift from the WT. All atoms alignment of the mutant to the WT structure was carried out and showed an RMSD of 2.4Å. (**Figure 4.5a**) The RMSD of both systems

showed a stable structure during the whole simulation with an average RMSD of 2.9 Å and 2.7 Å for the WT and N228D, respectively. (**Figure 4.5b**) We also analyzed the atomic fluctuation as a means for obtaining an idea about the regions flexibility of the structures and our results indicates a similar trend in region flexibility between the RSV WT and mutant indicating no conformation changes observed as a result of this mutation (**Figure 4.5c**). These results further support our modelling data for the L305I mutant by inducing and simulating another mutant on the RSV F as a negative control.

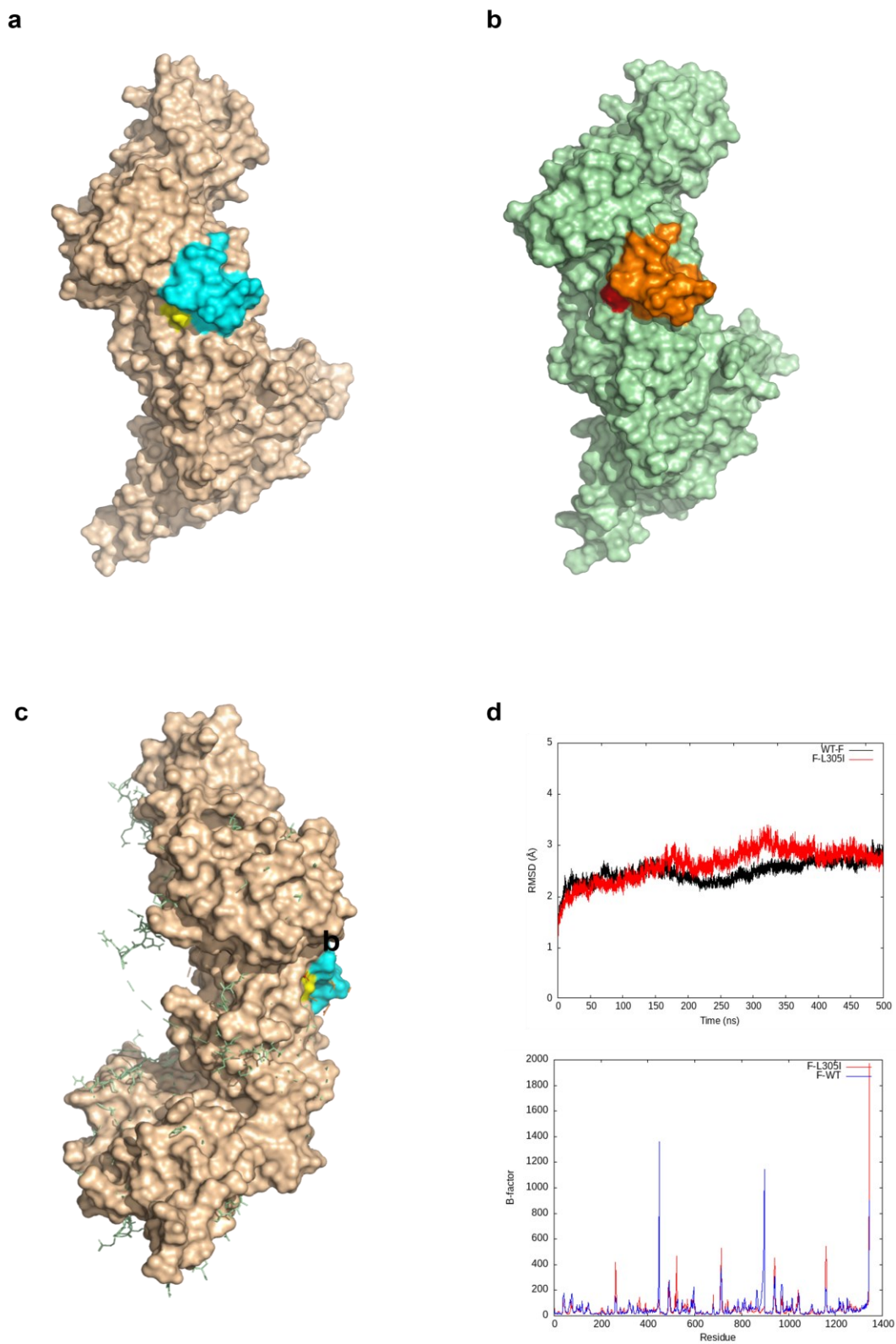
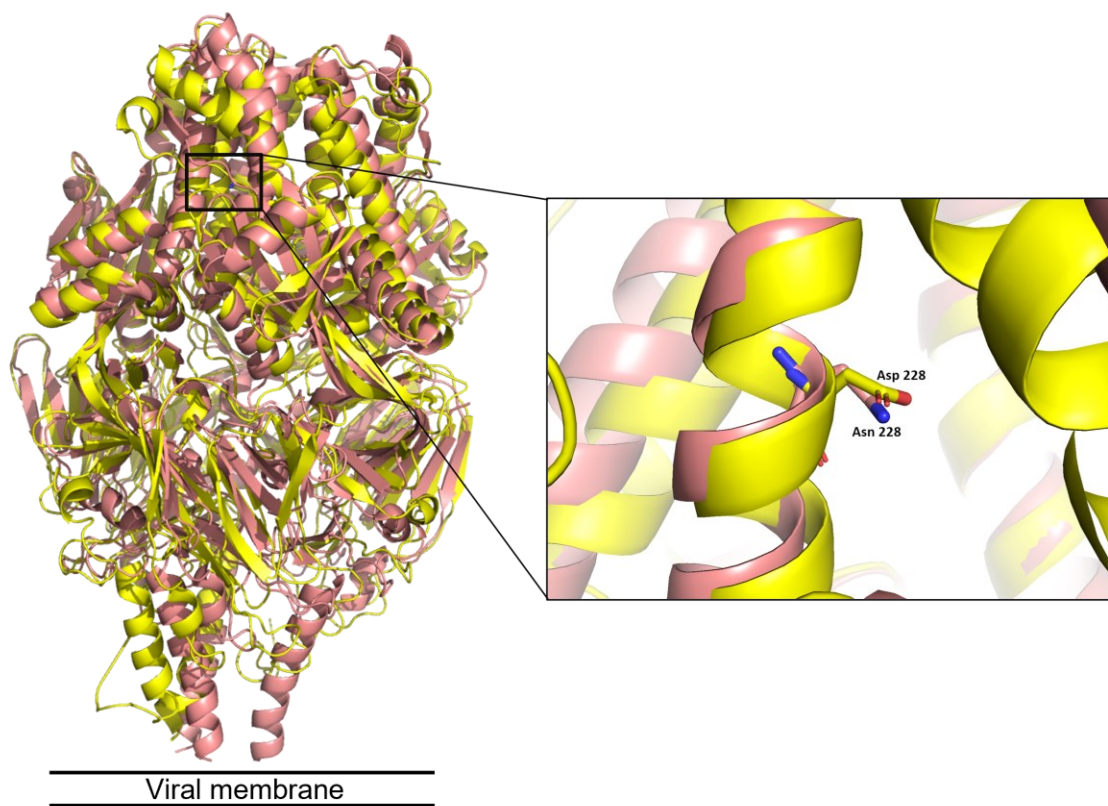
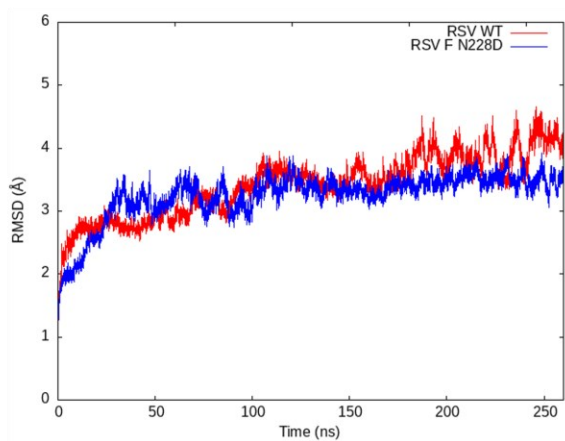


Figure 4.4: Conformational changes in the RSV F protein. **a.** RSV F WT, residue Leu 305 (yellow) and site II (cyan). **b.** RSV F L305I showing Ile 305 (red) and site II (orange). **c.** overlay of the two structures. **d.** MD trajectory analysis for both systems represented by the RMSD trends (top) and B factor (bottom).

a



b



c

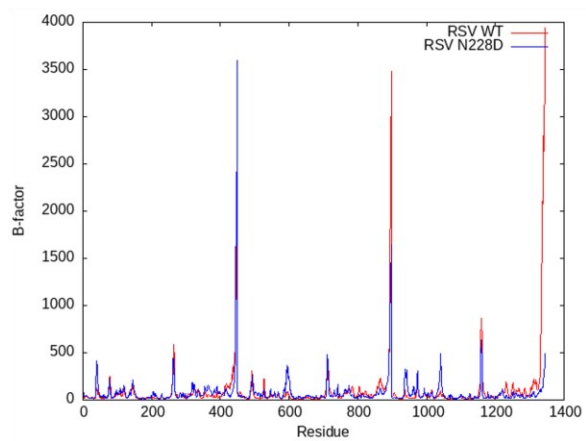


Figure 4.5: MD analysis of N228D mutant. **a.** Structure alignment of the WT and the N228D mutant. **b.** RMSD trends. **c.** RMSF showing similar atoms motion for both structures.

4.2.5 MD Simulations Predicted RSV F Breathing upon Nirsevimab (MEDI8897) Binding

The McLellan group have previously shown that binding of CR9501 antibody to the RSV F protein enhances the opening of the prefusion-stabilized RSV F trimer.¹⁶ To test whether we could observe the trimer breathing using MD simulations, the structure of the RSV trimer was obtained from the crystal structure of RSV F bound to Nirsevimab MEDI8897 (PDB ID: 5UDC).¹⁷ Although the X-ray structure was solved with three units of MEDI8897 antibody, we decided to remove all antibodies and redock only two units of the antibody to facilitate breath observation and validate our model. Our results showed that after 200 ns MD simulation there were an obvious breathing and a shape shift in the complex conformation as observed by the measurement between the two antibodies subunits where the solved and docked complexes showed a distance between the antibody subunits of ~ 28 Å before the MD simulation, while this distance increased to ~ 50 Å after 200 ns MD along with a general shape shift in the RSV protomer (**Figure 4.6 a and b**). We also observed this drastic change in the RMSD of the C α of the complex where the whole system equilibrated around 120 ns of the simulation with an average RMSD of 7 Å from the starting coordinates (**Figure 4.6c**). These results support the previous reports of RSV trimer breathing observed by computational methods; however, very long MD simulations need to be performed in order to observe the complete opening and dissociation of the RSV F protein. Overall, clustering of the MD trajectories indicated a shape shift induced by the L to I mutation at the 305 position, however, our observations indicated that trimer breathing was likely not involved in the differences in antibody neutralization susceptibility

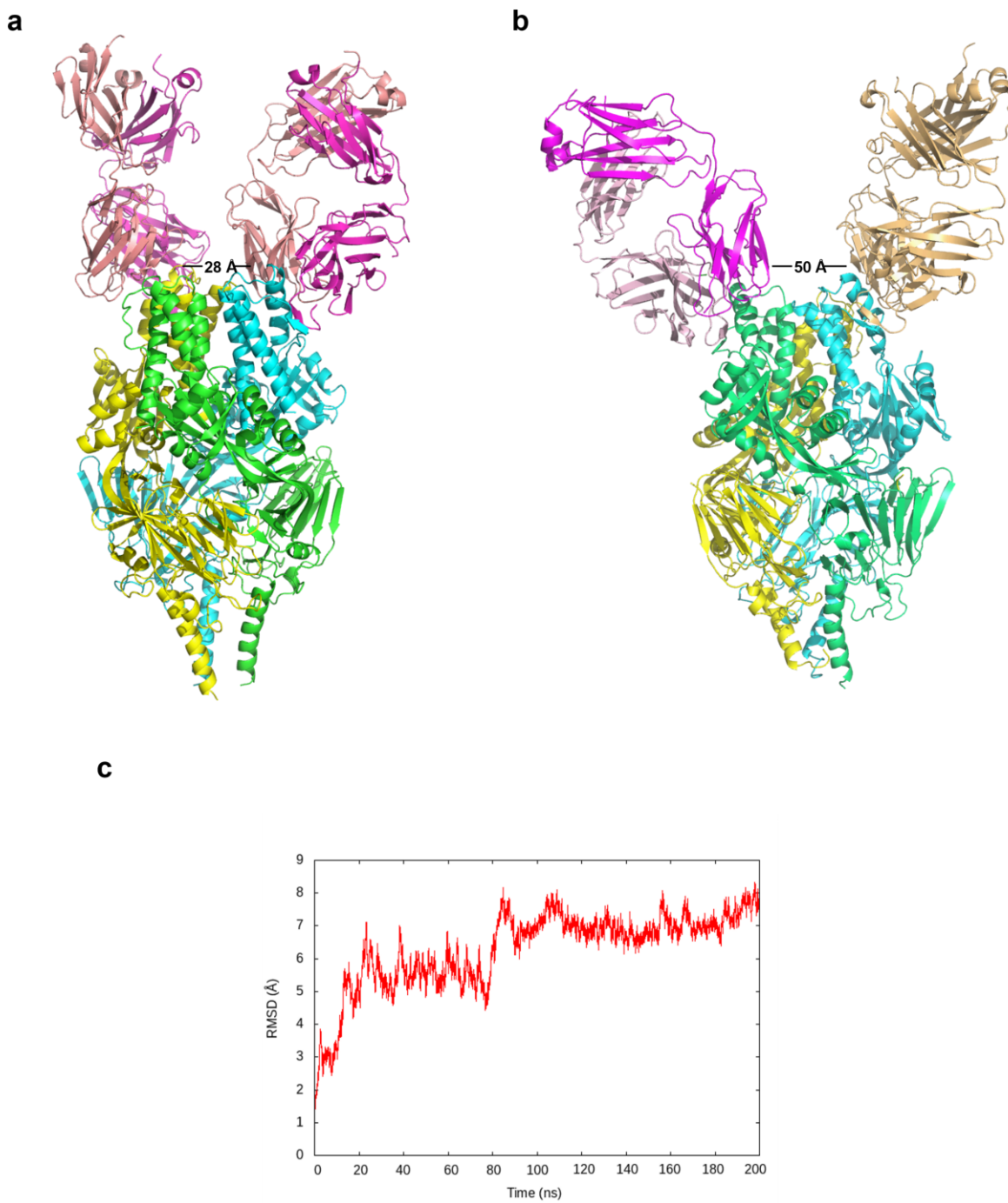


Figure 4.6: Conformational analysis of RSV F bound to MEDI8897. **a.** MEDI8897 bound to RSV F. **b.** Low energy structure of the protein-antibody complex extracted from the 200 ns MD simulation. **c.** RMSD of the C α atoms of the RSV F- MEDI8897 complex.

4.2.6 RSV-F with Leucine and Isoleucine 305 have Different Binding Affinities to Neutralizing Sera and Monoclonal Antibodies

We immobilized L and I305 rgRSV virion particles, as well as recombinant proteins WT and I305 prefusion-stabilized DS-CAV1 RSV-F4 on surface plasmon resonance (SPR) sensor chips. SPR detected rgRSV-F (**Figure 4.7**) and DS-CAV1 RSV-F (**Figure 4.8**) binding by antisera and antibodies and calculated the binding affinities by reporting the dissociation constants (K_D). We found that the K_D measured for D25 binding to rgRSV was similar to what has been published for Nirsevimab (MEDI8897) that binds to the same site, site Ø, on RSV-F¹⁸ (Table 4.2). The RSVB isolate (RSVB 9320) that is reported in this work is typical of RSV type-B in that it has an I at amino acid position 305 and, as predicted, it is bound by MEDI8897 with lower affinity than RSV A, as we observed with D25 binding to I305 rgRSV A (Table 4.2). Further, we found that the antibody binding affinities to L and I305 rgRSV corresponded to the antibodies' abilities to neutralize L or I305 rgRSV virus infections (Table 4.2).

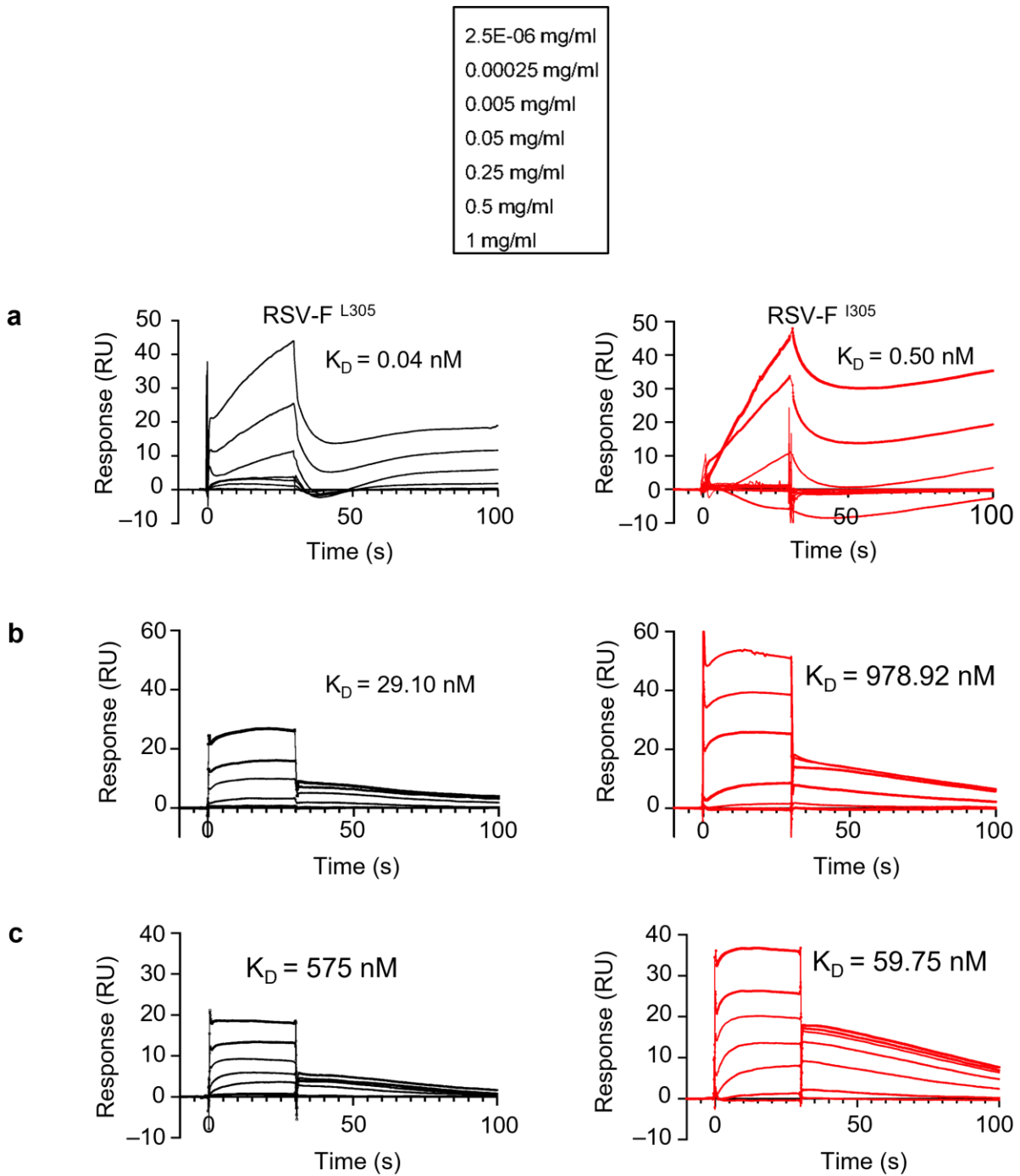


Figure 4.7: Example surface plasmon resonance traces of antibody binding to L305 and I305 rgRSV virions. Plasmon surface resonance traces of **a**, RSVA antisera, **b**, D25 monoclonal antibody, and **c**, palivizumab, binding to L305 (left) and I305 (right).

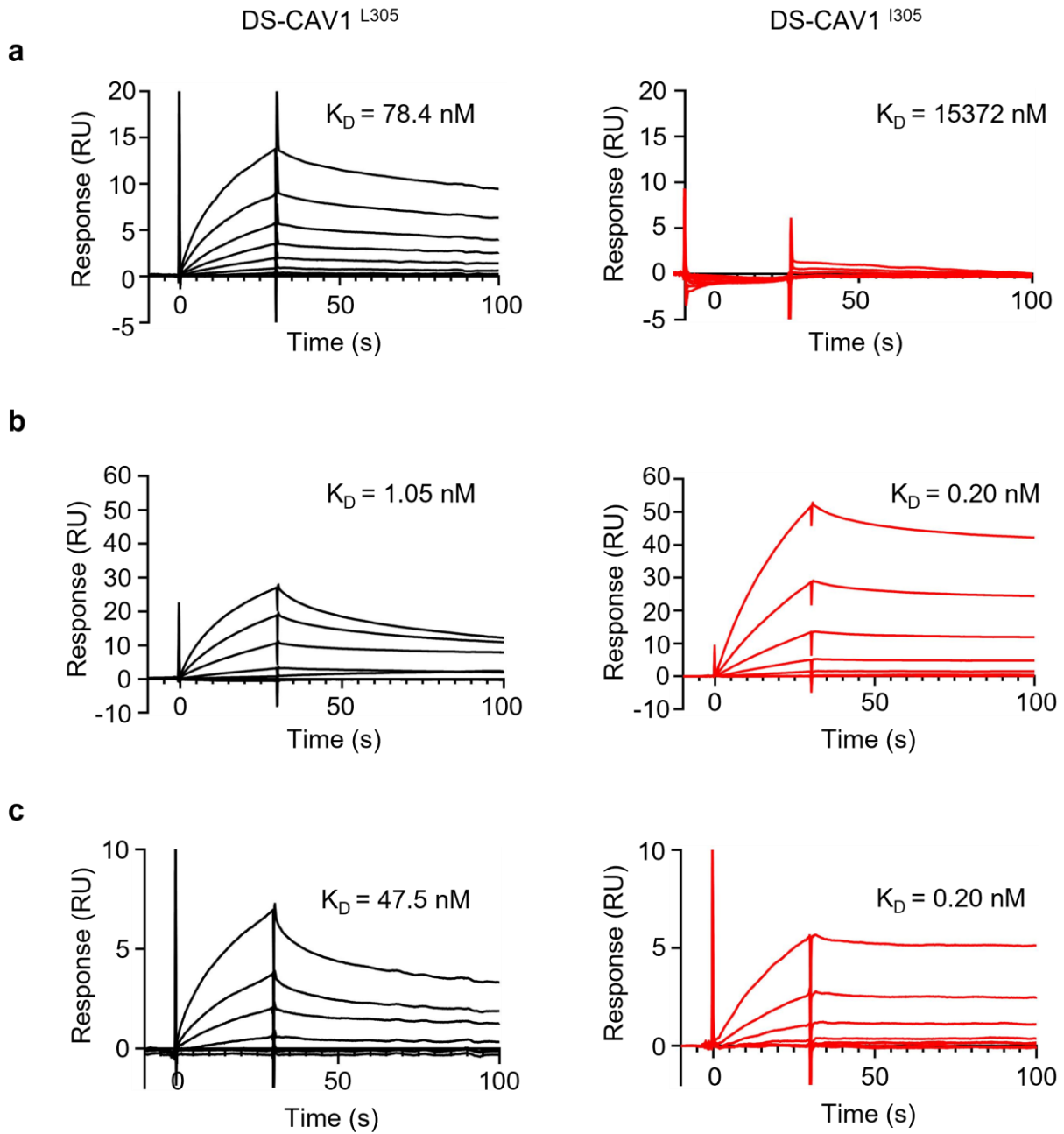


Figure 4.8: Example surface plasmon resonance traces of antibody binding to L305 and I305 DS-CAV1 RSV-F recombinant proteins. Plasmon surface resonance traces of **a**, D25 monoclonal antibody **b**, Palivizumab and **c**, 101F monoclonal antibody, binding to L305 (left) and I305 (right).

nAb site		Leucine 305	Isoleucine 305
Anti-RSVA sera	IC ₅₀ (µg/ml)	1.395	2.341
	K _D (M)	5.97E-11 ± 3.91E-11	5.03E-10 ± 4.47E-10
D25 (site Ø)	IC ₅₀ (ng/ml)	7.04	18.21
	K _D (M)	2.91E-08 ± 2.08E-08	1.46E-06 ± 1.56E-07
Palivizumab (site II)	IC ₅₀ (ng/ml)	21	7
	K _D (M)	1.28E-06 ± 9.91E-07	8.68E-08 ± 5.41E-08

IC₅₀= Inhibitory concentration 50, K_D = Dissociation Constant. Data are the result of three independent experiments. Mean ± standard deviation.

DS-CAV1 molar dissociation constants (K_D) of antibodies to sites Ø, II and IV

nAb site		Leucine 305	Isoleucine 305
D25 (site Ø)	K _D (M)	7.84E-08 ± 2.56E-09	1.54E-05 ± 2.14E-05
Palivizumab (site II)	K _D (M)	1.05E-09 ± 6.81E-10	1.96E-10 ± 2.12E-10
101F (site IV)	K _D (M)	4.75E-08 ± 6.37E-08	1.99E-10 ± 2.19E-10

K_D= Dissociation Constant. Data are the result of three independent experiments. Mean ± standard deviation.

Table 4.2: Inhibitory concentration 50 and Molar dissociation constants (K_D) of antibodies to sites Ø and II.

4.2.7 Mutation at RSVA-F Amino Acid Position 305 and RSVB-F Amino Acid Position 127 Occurs at Evolutionary Bottlenecks Caused by Anti-RSV Sera

While RSVA and B share about 90% percent amino acid sequence identity and co-circulate in the population, they remain distinct virus types. It is estimated that RSVA and B diverged about 350 years ago; however, the selective pressure that led to this divergence is not known.⁴

We performed a longitudinal viral evolution assay in the presence of neutralizing antisera to understand how selective pressure on RSV would affect both its mutation in culture, as well as the conditions from which the L305I mutation occurs in RSV. Viruses and antisera were added to cultures of human bronchial epithelial cells and virus was collected every two days for 20 passages (40 days) (**Figure 4.2i**). The viral titer produced in infected cells was measured and the whole viral genomes were determined by Illumina sequencing.

We found that the L305I mutation occurred when RSV titer approached its lowest point, due to the presence of either sera or an RSV polymerase inhibitor (**Figure 4.2j**) that we developed.¹⁹ An increase in the proportion of I305 was associated with a rebound in titer (**Figure 4.2k**). When either sera or inhibitor were added at lower doses, so that RSV could replicate relatively unchecked in culture, the sequence of RSV-F remained stable. Altogether, these data suggest that the L305I mutation emerges at evolutionary bottlenecks when otherwise dominant strains are depleted by sterilizing immunity.

4.2.8 Identification of New Mutations in RSV B

In a parallel experiment, we treated RSVB clinical isolate, B127, with anti-RSVA and anti-RSVB serum (**Figure 4.2I**). As with RSVA, we identified mutations that occurred in the RSVB F glycoprotein at evolutionary bottlenecks by sterilizing neutralization pressure. The theory of mutation as proposed by Mueller's Ratchet is that mutation invariably leads to loss of fitness and moves in only one direction; this precludes I305 from reverting to an L in RSVB. Indeed, we found that RSVB remained I305 but we identified a new mutation, V127I, that occurred. Interestingly, the mutation happened at both evolutionary bottlenecks and in the presence of sub-optimal non-sterilizing doses of anti-RSVB human sera. Therefore, we predict that V127I will arise more readily under mild neutralizing pressure.

4.2.9 WT and L305I rgRSV Viruses have Different Susceptibilities to RSVA and B Patient Sera

To this point, our data suggest that the sensitivity of recombinant RSV to sera can be switched by an amino acid mutation at position 305 of RSV-F. Accordingly, we then asked whether we could observe corresponding susceptibility of WT (L305) and I305 rRSV to sera from pediatric patients infected with confirmed RSVA or RSVB. Infants were selected to prevent confounding of results from older patients which are complicated by immune memory to previous RSV infections. WT and I305 rRSV viruses were treated with serial dilutions of serum from 3 patients infected with RSVA, and 3 infected with RSVB. As expected, WT rRSV was more susceptible to RSVA sera than I305 rRSV and I305 rRSV was more susceptible to one of the RSVB sera (**Figure 4.9**). Overall, the WT and I305 rRSV viruses had different profiles of neutralization to all of the different sera we tested.

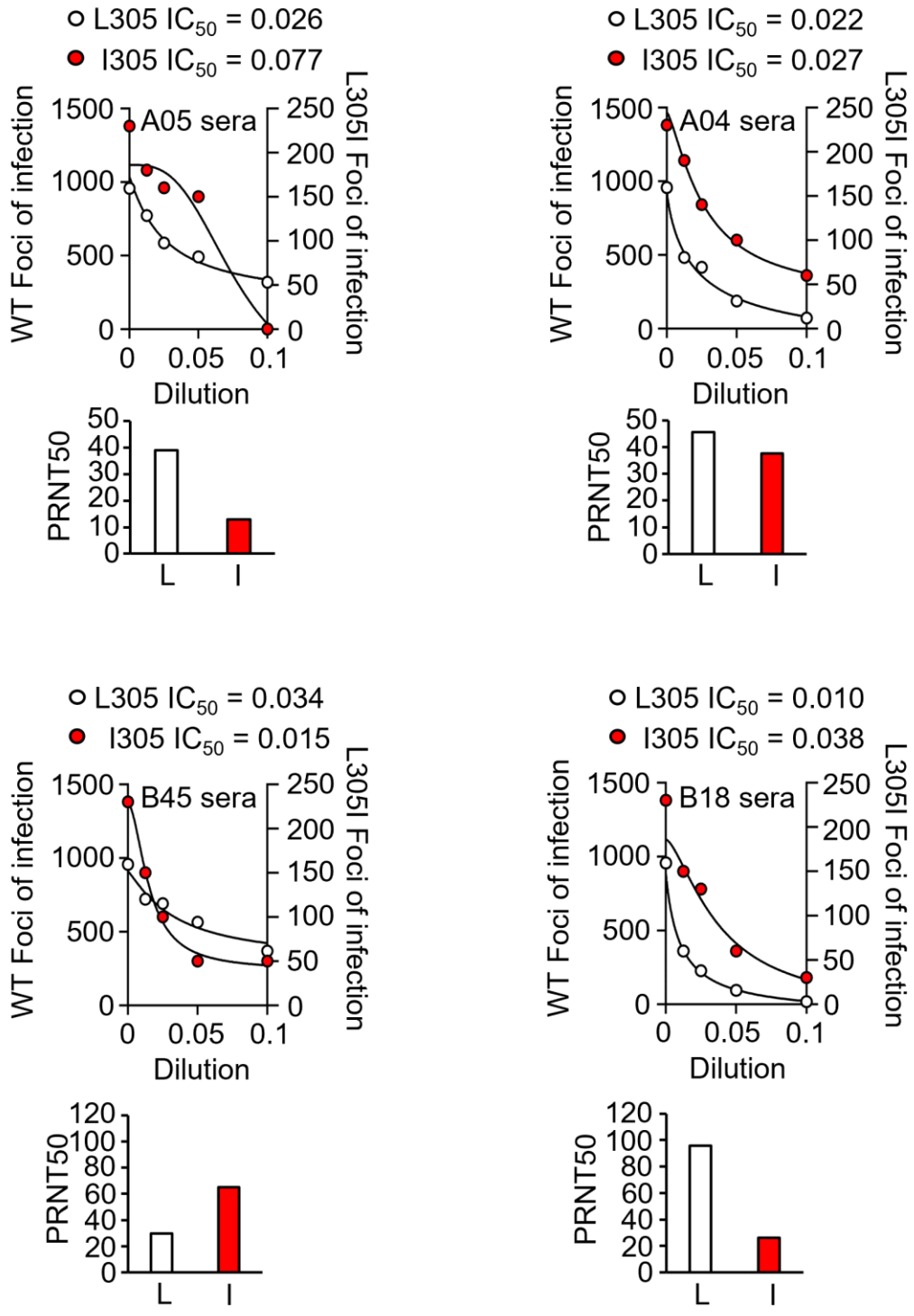


Figure 4.9: Leucine 305-RSVs are more susceptible to RSV antisera from infants infected with RSV A and B. Neutralization susceptibility of genetically engineered WT-RSV (L305) and I305-RSV were tested with neutralizing sera from RSV type-A and type-B infected infants. IHAE bronchial epithelial cells were infected and the infectious titers were determined by direct immunostaining for RSV infection. (Bar graphs) PRNT50 was calculated from serum titrations as a measure of serum ability to neutralize RSV.

4.3 Discussion

In this study we found that a single amino acid mutation could cause a conformational switch in the RSV-F glycoprotein, leading to an overall change in susceptibility to antibody neutralization all sites we tested on RSV-F and there was a loss of fitness. This is a demonstration of Muller's Ratchet during RSV mutation.^{20, 21} We suggest that mutation at amino acid 305 may have been the basis of RSVA and B divergence about 350 years ago; 'the first click' of Muller's genetic ratchet that led to RSV divergence. We found that this mutation was the first to arise in evolutionary bottlenecks brought on by both serum and drug neutralization of infection. Muller's Ratchet states that mutation inevitably results in loss of fitness.²¹ Consistent with this, we found that I305 rgRSV grew more slowly than L305 rgRSV and that RSVB clinical isolates, with few exceptions, we have found grow more slowly and to lower titer in culture than RSV A isolates.⁶ This reduced fitness in RSV may have been a trade-off for survival in the presence of evolutionary pressure from a sterilizing immune response. Conditions under which RSVA L305 viral load was suppressed thereby removed the competition that allowed RSVB I305 to grow. This would suggest that I305 arises normally but is outcompeted in the presence of L305. Since the emergence of I305, compensatory mutations have resulted in some RSVB infections growing to levels equivalent to that of RSVA.¹⁰ To summarize, the loss of competition from otherwise dominant strains during evolutionary bottlenecks allows mutants to grow that would otherwise be less fit and outgrown by dominant strains.

4.4 Conclusion

This study represents a critical advance in understanding the potential of any future therapeutic breakthrough by viruses. In the absence of vaccines, therapeutic antibodies are the only preventative measure against infection. Currently, there are 3 preventative biologic monoclonal antibodies for RSV in late-phase clinical trials.⁹ Vaccines that provide protection from RSV continue to be studied, however, their development lags behind that of biologics. While between-isolate comparisons have not shown mutations at amino acid position 305, we predict that sufficient pressure from a vaccine or therapeutic could lead to emergence of mutation at L305 in RSVA and V127 in RSVB, conferring resistance. Interestingly we found that V127 more readily emerged in the presence of less than sterilizing immunity. In summary, RSVA is more likely to adapt if biologics, vaccines, and therapeutics provide sterilizing levels of immunity to RSV infection. We expect that V127 will emerge more in the future. Thus, these results present a paradox: therapeutics effective enough to be sterilizing may lead to outgrowth of viral resistance, however, this resistance mutation is accompanied by the trade-off of reduced RSV replicative fitness.

4.5 Experimental Details ^{**}

4.5.1 Cell Culture

Henrietta Lack's (HeLa) cells from American Type Culture Collection (ATCC, CCL2) were grown in Dulbecco's modified Eagle's medium (DMEM) containing L-glutamine, glucose, and sodium pyruvate with 10% heat inactivated fetal bovine serum (FBS). Human airway epithelial (1HAEO-) cells (a gift from D.Gruenert, University of California, San Francisco, CA,

^{**} I was responsible for designing and performing the computational experiments. Farah Elawar, Aleksandra Stojic, Leanne Bilawchuk and Kaci Erwin carried out the virological experiments.

USA) were grown in minimum essential medium (MEM) supplemented with 10% heat inactivated FBS. All immortalized cell lines were incubated at 37°C with 5% CO₂.

4.5.2 Antibodies, Antisera, and DNA Aptamers (Reagents)

The following antibodies were used: anti-F (RSV) D25 (Cambridge Bio, 01-07-0120), anti-F (RSV) 101F (Cambridge Bio, 01-07-0140), anti-RSV polyclonal (Meridian, B65860G1), anti-goat IgG H&L (β -galactosidase) (Abcam, ab136712), and Palivizumab (Synagis[®]). Palivizumab was provided by the Stollery Children's hospital neonatal intensive care unit in Edmonton Alberta, Canada. The following reagents were used: 0.5mg/ml 5-Bromo-4-chloro-3-indolyl- β -D-galactopyranoside (X-Gal) (ThermoFisher, BP1615-1) and Yellow Substrate (PBS containing 3mM potassium ferricyanide III, 3mM potassium ferrocyanide trihydrate, and 1mM magnesium chloride hexahydrate). Polyclonal anti-RSVA sera No. B65860G (Meridian Life Science, Memphis, TN, USA), Human infant RSV-positive nasopharyngeal samples were provided by Drs. Asuncion Mejias and Octavio Romario. Stabilized RSV-F DS-CAV1 WT and L305I proteins were provided by Drs. Jason McLellan and Kaci Erwin and expressed as previously described.⁷ AS14111 and CON nucleotide aptamers were ordered and prepared as described previously.²²

4.5.3 Virus Isolation, Propagation, and Purification

Clinical samples were tested with a NxTAG[®] Respiratory Virus Panel (RVP, Luminex, Austin, TX, USA) and samples positive for RSV-A or RSV-B were subject to further analysis. Clinical strains of RSV were isolated from patient nasopharyngeal samples as previously described⁸. Briefly, NP samples diluted in 1mL DMEM + 10% FBS + 1X Penicillin/Streptomycin (P/S) were added to sub-confluent HeLa cells and incubated at 37°C with 5% CO₂. After 4 hours, fresh media was added to the cells and the virus was left to propagate for 96 hours. Virus media was harvested and stored in liquid nitrogen. Recombinant lab adapted strain RSV type-A2 expressing green

fluorescent protein (GFP) (rgRSV RW30) was a gift from M.E. Peeples (Children's Research Institute, Columbus, OH, USA). Lab strain A2 and the RSV L305 mutant were purified by sucrose density gradient purification as described previously.^{7, 22} Briefly, virus was precipitated from conditioned media by stirring with 10% Polyethylene glycol (PEG)-6000 on ice for 90 min. The virus was pelleted by centrifugation at 4,300 x g at 4°C for 30 min, the pellets resuspended in NT buffer (0.15 M NaCl, 0.05 M tris, pH 7.5) and overlaid on a discontinuous sucrose gradient (35%, 45%, 60% sucrose in NT buffer) as previously described.²² The sucrose purified RSV band was spun for 4 h at 217,290× g at 4°C, harvested, then aliquoted and stored in liquid nitrogen.

4.5.4 Construction of the RSV L305I Mutant

The rgRSV-L305I mutant was constructed by inserting a CTA to ATA mutation at amino acid position 305 into the rgRSV RW30 vector via Gibson Cloning.²² To clone the RSV-L305I mutant, 6 primers were designed using SnapGene Software, a forward and reverse primer for each of the 3 complementary PCR fragments that were created, with one of the primers containing the CTA to ATA mutation. The online ThermoFisher Multiple Primer Analyzer was used for primer analysis. Each PCR fragment was created separately using the Q5[®] High-Fidelity DNA polymerase protocol. Briefly, dNTPs (NEB, N0446S), template plasmid RSV RW30 DNA, forward and reverse primers, Q5[®] Reaction Buffer (NEB, B9027S) and Q5[®] High-Fidelity DNA polymerase (NEB, M0491S) were combined on ice. PCR reactions were carried out in a thermocycler under the following settings: 98°C for 30s, [98°C for 10s, 55°C for 30s, 72°C for 21s] for 35 cycles, 72°C for 5 min, and set to hold at 10°C once the reaction was complete. The size of PCR products was confirmed using a 1% agarose gel stained with SYBR[®] Safe DNA gel stain (ThermoFisher, #S33102). DNA was extracted according to the Qiaex II Gel Extraction Kit (Qiagen, #20051) and purified using the QIAquick PCR purification kit (Qiagen, #28104). The

purified products were annealed together using the NEBuilder HiFi DNA Assembly Master Mix and accompanying protocol (NEB, #E2621L) by combining the Master Mix with the purified PCR fragments and incubating them at 50°C for 15 min in the thermocycler. Annealed viral plasmid DNA was used to transform competent NEB10-beta E.coli (NEB, #C3019) according to the High Efficiency Transformation Protocol (NEB). Briefly, assembled plasmid and competent cells were incubated on ice for 30 min and heat shocked at 42°C for 30s, SOC media was added and incubated on a shaker for 1 hour at room temperature. Bacteria were plated on YT + 10µg/mL tetracycline selection plates, incubated overnight at 37°C, and the following day individual colonies were selected and grown in YT broth overnight at 37°C. Bacteria were pelleted by centrifugation at 500 x g for 10 mins and plasmid DNA was isolated using the QIAprep[®] Spin Miniprep Kit (Qiagen, #27106). Extracted plasmid DNA size was confirmed on a 1% agarose gel as described above and plasmids were sent for sequencing to the Molecular Biology Service Unit (MBSU, University of Alberta, Edmonton, AB, Canada) to confirm the presence of the L305I mutation.

4.5.5 RSV Reverse Genetics

Full length rgRSV RW30 and mutant L305I RW30 cDNA were rescued into infectious virions in HeLa cells. Briefly, full length rgRSV RW30 or RSV-L305I, support plasmids (RSV N, P, L, and M2-1), and T7 RNA polymerase (a gift from Benhur Lee, Addgene plasmid #65974) were transfected into sub-confluent HeLa cells using TransIT-HeLa MONSTER (Mirus Bio, MIR 2900). After rescue, RSV was propagated in HeLa cells in T75 flasks and harvested as cell-free (clarified) RSV-conditioned DMEM with 10% FBS. RSV-conditioned media was aliquoted and stored in liquid nitrogen. The RSV-L305I mutant was used as media-virus and the rgRSV RW30 was further sucrose purified before use in experiments.

4.5.6 Infectious RSV Quantification

RSV infected cells were detected using a colorimetric immunostaining assay as previously described.²² Briefly, RSV-infected monolayers were fixed and permeabilized with methanol:acetone (1:1 volume) and incubated for 10 min at RT. Cells were blocked with PBS + 10% FBS and incubated for 30 min at RT. Subsequently, cells were stained with primary goat anti-RSV (diluted 1:1000) and incubated overnight at 4°C. The following day cells were treated with secondary rabbit anti-goat antibody conjugated to β -galactosidase (diluted 1:2000) and in the absence of light for 1 hour at RT. Cells were then stained blue with 1:1000 X-gal diluted in PBS containing 3mM potassium ferricyanide III, 3mM potassium ferrocyanide trihydrate, and 1mM magnesium chloride hexahydrate and incubated away from light at 37°C with 5% CO₂ for 2-4 hours until blue spots were fully developed. Foci of infection stained blue and were counted under the EVOS[®] F1 Auto Imaging System (ThermoFisher, AMAFD1000). Viral titre was estimated in focus-forming units (FFU/mL). Note that all antibodies were diluted to appropriate concentrations in PBS + 1% FBS and that cells were washed three times with PBS following all blocking and staining treatments unless otherwise specified.

4.5.7 RSV Evolution Experiment

Using a 75% confluent monolayer of HeLa cells, lab strain RSV A2, and a selected RSVA and RSVB clinical isolate were incubated with RSV polyclonal goat sera, human RSV A sera, and human RSV B sera. The sera were each diluted 1:1000 and after 4 hours in media with the sera they were changed, and the infection was allowed to proceed for 48 hours at 37°C. After 48 hours, viruses were collected, and the process was repeated on a new HeLa cell monolayer. The viruses were passaged twenty times with the respective sera. RNA was harvested for every passage and viral growth was measured by qRT-PCR and a foci counting assay to test infectivity.

4.5.8 Neutralization Assays with Antibodies and Anti-Nucleolin Aptamer using RSV Clinical Isolates

Experiments were conducted as described previously.^{7, 10} Residual palivizumab was provided by Stollery Children's Hospital neonatal intensive care unit in Edmonton, Alberta, Canada.

4.5.9 Whole Genome Sequencing

Whole genome sequencing was done as described in ¹⁰. Briefly, viral RNA from each passage of the evolution experiment was extracted using the QIAamp[®] Viral RNA Mini Kit (Qiagen, 52906). Viral mRNA was isolated by poly-A pulldown with oligo d(T) 25 beads using the NEBNext[®] Poly(A) mRNA Magnetic Isolation Module (NEB, E7490L). The first strand of cDNA was prepared using the High-Capacity cDNA RT Kit (ThermoFisher, 4368814) and the second strand synthesized with the large Klenow fragment of DNA polymerase 1 (NEB, M0210L). cDNA was purified with the MinElute[™] PCR Purification Kit (Qiagen, 28004). Tagmentation and creation of the library was done using the Nextera XT DNA Library Preparation Protocol (Illumina, FC-131-1096). Index adapters used for sample identification were created by MBSU (Molecular Biology Service Unit, University of Alberta, Edmonton, AB, Canada) and libraries were cleaned up using the MagJET NGS Cleanup Kit (ThermoFisher, K2821). Sample concentration was checked using the NanoDrop [™] 8000 Spectrophotometer (ThermoFisher, ND-8000-GL) and sample purity analyzed by the Agilent 2100 Bioanalyzer G2938C (Marshall Scientific, AG-2100C) at the MBSU. Equal amounts of DNA were combined and sent for sequencing to the MBSU for Next Generation Sequencing on the MiSeq[®] System (Illumina, SY-410-1003).

4.5.10 Surface Plasmon Resonance

Experiments were performed using the Biacore T200 Surface Plasmon Resonance System (Cytiva, 28975001). Briefly, whole virion WT-RSV (1.0×10^5 particles) and L305I-RSV (1.0×10^7 particles), and prefusion-stabilized RSV-F DS-CAV1; L305 and I305 (0.5 mg/ml), were diluted with sodium acetate at a 1:3 ratio and covalently immobilized onto the surface of a CM5 sensor chip (Cytiva, BR100530) with an amine coupling kit (Cytiva, BR100050). At least 1600 response units (RUs) of virion and stabilized protein were coupled before proceeding. Phosphate buffered saline (PBS) was used as a buffer and each experiment was run in triplicate under the following conditions: contact time 30s, flow rate $30 \mu\text{L}/\text{min}$, dissociation 300s. Glycine NaOH and 25mM NaOH were used for regeneration of virion and stabilized protein ligands respectively, and under the following conditions: contact time 30s, flow rate $30 \mu\text{L}/\text{min}$, stabilization 60s. 100% FBS, D25 monoclonal antibody, 101F monoclonal antibody, Palivizumab, and Anti-RSVA sera were 2-fold serially diluted 8 times in PBS from the following starting concentrations: 50%, 3333 nM, 125 nM, 31.25 nM, and 12.5 nM respectively. The resulting K_d values were determined and analysed using the Biacore Insight Evaluation Software (Cytiva).

4.5.11 Determining the Percentage Identity and Similarity of RSV Isolates

Amino acid identity and similarity between RSVA and B were determined using Geneious software, Biomatters, New Zealand.

4.5.12 Aligning Multiple Clinical Isolates of RSV and Determine Amino Acid Differences in F Protein

5141 RSV-F protein sequences were downloaded from the NIAID Virus Pathogen Database and Analysis Resource (ViPR) (PMID: 22006842) through the web site at <http://www.viprbrc.org/>. SeqKit (PMID: 27706213) was then used to filter the RSV-F sequences

to include only sequences that are the correct length (574 amino acids), contain no unknown residues, and are identified as RSV type-A or RSV type-B. After this filtering, 2870 sequences remained – 1685 RSV type-A (58.7%) and 1185 RSV type-B (41.3%). The RSV type-A sequences and type-B sequences were aligned separately and together using Clustal Omega (PMID: 30976793) with default settings and analyzed using Jalview 2.11.1.4 (PMID: 19151095). Amino acids with at least 30% greater conservation for both RSV type-A and type-B compared to the combined alignment were marked as being conserved by RSV type.

4.5.13 Computational Details

4.5.13.1 Preparation of Protein for MD simulation

Starting coordinates for the RSV F protein were obtained from the Protein Data Bank for both the monomer (PDB accession: 4MMU) and the protomer (PDB accession: 5UDC). The X-ray structure of the protomer was solved with bound MEDI8897, which was removed to obtain the free protomer. Mutation at residue 305 was performed using the Schrödinger Small Molecule Discovery Suite.²³ The Protein Preparation Wizard module in Schrödinger was used to add hydrogen atoms, minimize energy, fill missing loops, and create the appropriate protonation states of amino acid side chains. The protein structure was then subjected to three stages of energy minimization, all of which utilized the OPLS3 force-field.^{24, 25}

4.5.13.2 Molecular Dynamics Simulations of the RSV F Protomer

The structures of RSV F protein were solvated in a cuboidal box of TIP3P water molecules using AMBER's tLEap tool.²⁶ The ff14SB parameters were assigned for the protein.²⁷ The complexes were then neutralized, solvated in a NaCl salt concentration of 0.15 M with tLEap using the same process described above. The simulations were performed using PMEMD in AMBER18: an initial minimization step was performed in order to relax the water and ionic positions. The

whole system was then minimized and heated gradually up to 300K in 100 ps using Langevin dynamics. During the heating process, we restrained the backbone of the protein and a time step of 0.5 fs and periodic volume conditions have been employed during this phase. The time step has been set to 2 fs, and periodic pressure conditions (1atm) have been imposed and the restraints have been gradually released in four phases of 50 ps each. The production phase of the simulations at the NPT conditions were performed in triplicates for 100, 270 and 500 ns using GPU accelerated version of PMEMD (pmemd.cuda) implemented in AMBER 18.

4.5.13.3 Protein-Protein Docking

Molecular docking between the F protein and MEDI8897 was investigated using two protein-protein docking servers to perform a blind docking: (A) The ClusPro 2.0 protein-protein docking Web server (<http://cluspro.bu.edu/>). (B) HDOCK webserver (<http://hdock.phys.hust.edu.cn/>). The best models were then selected based on the lowest energy clustered structures and the pose matching the crystal structure. ClusPro outperformed HDOCK in this regard.

4.5.13.4 Structural Analysis of Molecular Dynamics Simulations

The CPPTRAJ software in AMBER18 was used to compute the root mean squared deviation (RMSD) of the protein coordinates with respect to the reference X-ray structure along the MD trajectories.²⁸ The coordinates of the models were also clustered using CPPTRAJ with the average-linkage clustering algorithm.

4.5.13.5 Statistical Analysis

Unless otherwise indicated, results are expressed as mean \pm s.d. We compared group means by either two-tailed Student's t-tests or one-way analysis of variance (ANOVA) with Tukey's post hoc analysis, comparing each group with the appropriate control using GraphPad Prism 9 software.

All tests are two-tailed unless otherwise indicated. We considered a P value ≤ 0.05 to be statistically significant. Representative data from a single experiment were confirmed by 3 or more independent repeats.

4.6 References

1. Griffiths, C.; Drews, S. J.; Marchant, D. J., Respiratory Syncytial Virus: Infection, Detection, and New Options for Prevention and Treatment. *Clin Microbiol Rev* **2017**, *30*, 277-319.
2. Elawar, F.; Oraby, A. K.; Kieser, Q.; Jensen, L. D.; Culp, T.; West, F. G.; Marchant, D. J., Pharmacological targets and emerging treatments for respiratory syncytial virus bronchiolitis. *Pharmacol Ther* **2021**, *220*, 107712.
3. Rodriguez-Fernandez, R.; Mejias, A.; Ramilo, O., Monoclonal Antibodies for Prevention of Respiratory Syncytial Virus Infection. *Pediatr Infect Dis J* **2021**, *40*, S35-S39.
4. Zlateva, K. T.; Lemey, P.; Moes, E.; Vandamme, A. M.; Van Ranst, M., Genetic variability and molecular evolution of the human respiratory syncytial virus subgroup B attachment G protein. *J Virol* **2005**, *79*, 9157-67.
5. McLellan, J. S.; Chen, M.; Leung, S.; Graepel, K. W.; Du, X.; Yang, Y.; Zhou, T.; Baxa, U.; Yasuda, E.; Beaumont, T.; Kumar, A.; Modjarrad, K.; Zheng, Z.; Zhao, M.; Xia, N.; Kwong, P. D.; Graham, B. S., Structure of RSV fusion glycoprotein trimer bound to a prefusion-specific neutralizing antibody. *Science* **2013**, *340*, 1113-7.
6. McLellan, J. S., Neutralizing epitopes on the respiratory syncytial virus fusion glycoprotein. *Curr Opin Virol* **2015**, *11*, 70-5.
7. McLellan, J. S.; Yang, Y.; Graham, B. S.; Kwong, P. D., Structure of respiratory syncytial virus fusion glycoprotein in the postfusion conformation reveals preservation of neutralizing epitopes. *J Virol* **2011**, *85*, 7788-96.
8. Griffiths, C. D.; Bilawchuk, L. M.; McDonough, J. E.; Jamieson, K. C.; Elawar, F.; Cen, Y.; Duan, W.; Lin, C.; Song, H.; Casanova, J. L.; Ogg, S.; Jensen, L. D.; Thienpont, B.; Kumar, A.; Hobman, T. C.; Proud, D.; Moraes, T. J.; Marchant, D. J., IGF1R is an entry receptor for respiratory syncytial virus. *Nature* **2020**, *583*, 615-619.
9. Rodriguez-Fernandez, R.; Tapia, L. I.; Yang, C. F.; Torres, J. P.; Chavez-Bueno, S.; Garcia, C.; Jaramillo, L. M.; Moore-Clingenpeel, M.; Jafri, H. S.; Peeples, M. E.; Piedra, P. A.; Ramilo, O.; Mejias, A., Respiratory Syncytial Virus Genotypes, Host Immune Profiles, and Disease Severity in Young Children Hospitalized With Bronchiolitis. *J Infect Dis* **2017**, *217*, 24-34.
10. Elawar, F.; Griffiths, C. D.; Zhu, D.; Bilawchuk, L. M.; Jensen, L. D.; Forss, L.; Tang, J.; Hazes, B.; Drews, S. J.; Marchant, D. J., A Virological and Phylogenetic Analysis of the Emergence of New Clades of Respiratory Syncytial Virus. *Sci Rep* **2017**, *7*, 12232.

11. Phung, E.; Chang, L. A.; Morabito, K. M.; Kanekiyo, M.; Chen, M.; Nair, D.; Kumar, A.; Chen, G. L.; Ledgerwood, J. E.; Graham, B. S.; Ruckwardt, T. J., Epitope-Specific Serological Assays for RSV: Conformation Matters. *Vaccines (Basel)* **2019**, *7*.
12. Hause, A. M.; Henke, D. M.; Avadhanula, V.; Shaw, C. A.; Tapia, L. I.; Piedra, P. A., Sequence variability of the respiratory syncytial virus (RSV) fusion gene among contemporary and historical genotypes of RSV/A and RSV/B. *PLoS One* **2017**, *12*, e0175792.
13. Zhang, L.; Peeples Mark, E.; Boucher Richard, C.; Collins Peter, L.; Pickles Raymond, J., Respiratory Syncytial Virus Infection of Human Airway Epithelial Cells Is Polarized, Specific to Ciliated Cells, and without Obvious Cytopathology. *Journal of Virology* **2002**, *76*, 5654-5666.
14. Mastrangelo, P.; Chin, A. A.; Tan, S.; Jeon, A. H.; Ackerley, C. A.; Siu, K. K.; Lee, J. E.; Hegele, R. G., Identification of RSV Fusion Protein Interaction Domains on the Virus Receptor, Nucleolin. *Viruses* **2021**, *13*.
15. Gilman, M. S. A.; Furmanova-Hollenstein, P.; Pascual, G.; A, B. v. t. W.; Langedijk, J. P. M.; McLellan, J. S., Transient opening of trimeric prefusion RSV F proteins. *Nat Commun* **2019**, *10*, 2105.
16. Gilman, M. S. A.; Furmanova-Hollenstein, P.; Pascual, G.; B. van 't Wout, A.; Langedijk, J. P. M.; McLellan, J. S., Transient opening of trimeric prefusion RSV F proteins. *Nature Communications* **2019**, *10*, 2105.
17. Zhu, Q.; McLellan Jason, S.; Kallewaard Nicole, L.; Ulbrandt Nancy, D.; Palaszynski, S.; Zhang, J.; Moldt, B.; Khan, A.; Svabek, C.; McAuliffe Josephine, M.; Wrapp, D.; Patel Nita, K.; Cook Kimberly, E.; Richter Bettina, W. M.; Ryan Patricia, C.; Yuan Andy, Q.; Suzich JoAnn, A., A highly potent extended half-life antibody as a potential RSV vaccine surrogate for all infants. *Science Translational Medicine* **2017**, *9*, eaaj1928.
18. Zhu, Q.; Lu, B.; McTamney, P.; Palaszynski, S.; Diallo, S.; Ren, K.; Ulbrandt, N. D.; Kallewaard, N.; Wang, W.; Fernandes, F.; Wong, S.; Svabek, C.; Moldt, B.; Esser, M. T.; Jing, H.; Suzich, J. A., Prevalence and Significance of Substitutions in the Fusion Protein of Respiratory Syncytial Virus Resulting in Neutralization Escape From Antibody MEDI8897. *J Infect Dis* **2018**, *218*, 572-580.
19. Atienza, B. J. P.; Jensen, L. D.; Noton, S. L.; Ansalem, A. K. V.; Hobman, T.; Fearn, R.; Marchant, D. J.; West, F. G., Dual Catalytic Synthesis of Antiviral Compounds Based on Metallocarbene-Azide Cascade Chemistry. *J Org Chem* **2018**, *83*, 6829-6842.
20. Chao, L., Fitness of RNA virus decreased by Muller's ratchet. *Nature* **1990**, *348*, 454-5.

21. Muller, H. J., The relation of recombination to mutational advance. *Mutation Research/Fundamental and Molecular Mechanisms of Mutagenesis* **1964**, *1*, 2-9.
22. Bilawchuk, L. M.; Griffiths, C. D.; Jensen, L. D.; Elawar, F.; Marchant, D. J., The Susceptibilities of Respiratory Syncytial Virus to Nucleolin Receptor Blocking and Antibody Neutralization are Dependent upon the Method of Virus Purification. *Viruses* **2017**, *9*.
23. Schrödinger Release 2019-3: Maestro, Schrödinger, LLC, New York, NY.
24. Shelley, J. C.; Cholleti, A.; Frye, L. L.; Greenwood, J. R.; Timlin, M. R.; Uchimaya, M., Epik: a software program for pK_a prediction and protonation state generation for drug-like molecules. *Journal of Computer-Aided Molecular Design* **2007**, *21*, 681-691.
25. Roos, K.; Wu, C.; Damm, W.; Reboul, M.; Stevenson, J. M.; Lu, C.; Dahlgren, M. K.; Mondal, S.; Chen, W.; Wang, L.; Abel, R.; Friesner, R. A.; Harder, E. D., OPLS3e: Extending Force Field Coverage for Drug-Like Small Molecules. *J Chem Theory Comput* **2019**, *15*, 1863-1874.
26. Mark, P.; Nilsson, L., Structure and Dynamics of the TIP3P, SPC, and SPC/E Water Models at 298 K. *The Journal of Physical Chemistry A* **2001**, *105*, 9954-9960.
27. Maier, J. A.; Martinez, C.; Kasavajhala, K.; Wickstrom, L.; Hauser, K. E.; Simmerling, C., ff14SB: Improving the Accuracy of Protein Side Chain and Backbone Parameters from ff99SB. *Journal of Chemical Theory and Computation* **2015**, *11*, 3696-3713.
28. Roe, D. R.; Cheatham, T. E., PTRAJ and CPPTRAJ: Software for Processing and Analysis of Molecular Dynamics Trajectory Data. *Journal of Chemical Theory and Computation* **2013**, *9*, 3084-3095.

Chapter 5:

Summary and Future Directions

In Chapter 1, we comprehensively reviewed the respiratory syncytial virus (RSV) along with its viral proteins and their suitability as drug targets. We also outlined different therapeutic strategies and the progress of some antiviral small molecules and biologics in clinical trials. Despite the current stream of small molecules making their way into clinical trials, the availability of potent antiviral agents to combat RSV infections and other seasonal respiratory viruses is still an unmet need.

In Chapter 2, we employed a computational approach to investigate and evaluate the druggability of various allosteric binding sites on the RSV L protein. A model was developed based on our previously discovered lead compound, compound **1**, for which we analysed the putative binding pose, which is located near the NTP entry path, and the required interactions for a stable protein-ligand complex that will further our drug discovery development of a more potent analogue. We showed that computationally guided design and modifications of the bis(indole) compounds led to the development of compound **6** with potential antiviral activity. The synthesis of the designed compounds followed our previously disclosed metallocarbene azide cascade chemistry which is robust and straightforward. Moreover, when the virus was passaged twenty times with the lead compound **1**, a resistant mutant emerged with an interesting mutation at residue Trp 893. This amino acid was computationally predicted to form a direct hydrogen bond interaction with our compounds. Our findings could lead to the discovery of a new class of antiviral compounds with a novel mechanism of viral protein inhibition.

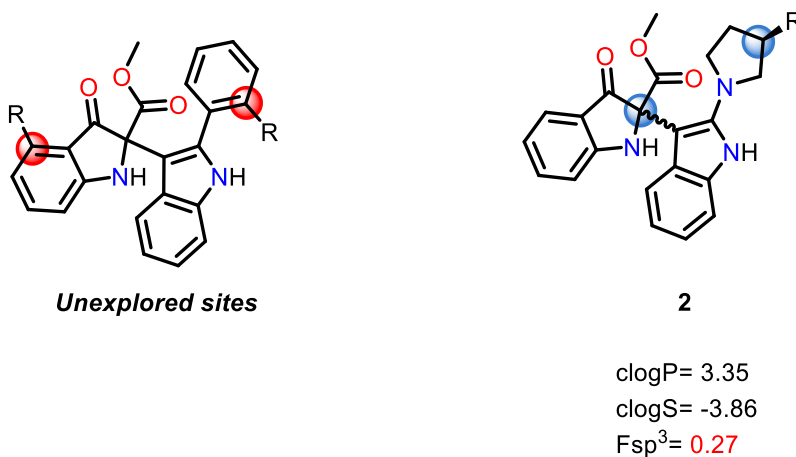
In Chapter 3, we continued to investigate the potential of our bis(indole) compounds as broad-spectrum antiviral agents. We eventually evaluated two previously published compounds from our group, compounds **1** and **2**, against SARS-CoV-2, the virus that caused the global COVID-19 pandemic in 2020. Interestingly, compound **1** showed good activity against the virus with no observed cytotoxicity. Compound **1** was used as a guide towards the design of more potent compounds using our computational modelling approach. Detailed *in silico* investigations provided guidance toward the possible allosteric site on the SARS-CoV-2 polymerase complex. The identified pocket is located near the active site and possibly affecting its dynamics. Visual inspection of the putative binding pocket led to the design of several compounds bearing a single modification on the indole fragment of the parent compound. Extensive analysis of the relative binding free energy of these compounds to the SARS-CoV-2 polymerase using MM/GBSA method suggested that several compounds could exert enhanced antiviral activity by locking the conformation of this binding site. Several derivatives were synthesized and evaluated using cell-based and biochemical assays developed in our collaborators labs, Drs. David Marchant, and Matthias Götte. These efforts led to the discovery of compounds **5** and **6** with substantial antiviral activity (low micromolar) and high selectivity index. *In vitro* evaluation of compound **5** enantiomers revealed that one enantiomer exhibited more pronounced antiviral activity than the other affirming the significance of chirality in drug design.

In Chapter 4, we demonstrated that single amino acid at position 305 in the RSV fusion glycoprotein (RSV F) switches the profile from RSV type A which has a leucine at this position, to RSV type B with an isoleucine at the same position 305. Our computational investigations showed that this single amino acid mutation caused protein-wide shape-shift, altering both antibody and patient serum neutralization susceptibility. Molecular dynamics were carried out for both the wild type (WT) and the mutant protein, and we observed a noticeable conformational change in the antigenic site II of the F protein where the monoclonal antibody (mAb) palivizumab binds. In addition, the alteration in the shape of the RSV F protomer cause by the L305I mutation could affect the susceptibility of RSV to palivizumab and other mAb binding to different sites on the RSV F including D25 mAb which binds to site Ø.

The mutations were engineered in an RSV reverse genetic model that led to a switch in the susceptibility between RSVA and B patient sera. Moreover, this study showed that viral replication in the presence of our RSV polymerase inhibitors, forces mutation at position 305 and was the only mutation occurred in RSV type A at evolutionary bottlenecks. This study is significant as we demonstrate that effective antiviral agents could potentially lead to more rapid virus mutations and immune evasion.

In Future work, several compounds will be tested for their antiviral activity against RSV, SARS-CoV-2 and other respiratory viruses. Most of the compounds described in Chapter 3 are still under investigation including the enantiomers of compound **6** which showed the most potent activity against SARS-CoV-2. We are collaborating with Dr. Joanne Lemieux, Department of Biochemistry and the Li Ka Shing Institute of Virology at the University of Alberta for the co-crystallization of our lead compounds with the RSV L protein and the SARS-CoV-2 nsp12.

Finally, certain properties of our compounds including molecular mass and lipophilicity represent a compelling medicinal chemistry avenues that should be explored. With a robust chemical methodology for the synthesis of the bis (indole) scaffold, other unexplored sites on the parent compound can be one of these avenues to improve its physicochemical properties. Another important aspect that can be explored is increasing the drug-likeness by considering molecular complexity (Scheme 5.1). Two measures can be used to reflect on molecular complexity including the extent of carbon bond saturation as defined by the fraction of sp^3 carbons (F_{sp^3}) along with the number of chiral carbons in the molecule. I envisioned that this complexity can be explored through the introduction of a pyrrolidine ring on the C-2 of the indole fragment. This modification improved the calculated physicochemical properties of the molecule including the $clogP$, $clogS$ and most importantly the F_{sp^3} which increased from 0.08 to 0.27 for compound **2** (Scheme 5.1).



Scheme 5.1: Potential modifications on the lead compound 5 for SAR analysis.

Compiled References

Chapter 1

1. Rima, B.; Collins, P.; Easton, A.; Fouchier, R.; Kurath, G.; Lamb, R. A.; Lee, B.; Maisner, A.; Rota, P.; Wang, L.; Ictv Report, C., ICTV Virus Taxonomy Profile: Pneumoviridae. *J Gen Virol* **2017**, *98*, 2912-2913.
2. Blount, R. E., Jr.; Morris, J. A.; Savage, R. E., Recovery of cytopathogenic agent from chimpanzees with coryza. *Proc Soc Exp Biol Med* **1956**, *92*, 544-9.
3. Chanock, R.; Finberg, L., Recovery from infants with respiratory illness of a virus related to chimpanzee coryza agent (CCA). II. Epidemiologic aspects of infection in infants and young children. *Am J Hyg* **1957**, *66*, 291-300.
4. Andrew, J. D.; Gardner, P. S., Occurrence of Respiratory Syncytial Virus in Acute Respiratory Diseases in Infancy. *Br Med J* **1963**, *2*, 1447-8.
5. Morales, F.; Calder, M. A.; Inglis, J. M.; Murdoch, P. S.; Williamson, J., A study of respiratory infections in the elderly to assess the role of respiratory syncytial virus. *J Infect* **1983**, *7*, 236-47.
6. Marty, F. M.; Chemaly, R. F.; Mullane, K. M.; Lee, D. G.; Hirsch, H. H.; Small, C. B.; Bergeron, A.; Shoham, S.; Ljungman, P.; Waghmare, A.; Blanchard, E.; Kim, Y. J.; McKeivitt, M.; Porter, D. P.; Jordan, R.; Guo, Y.; German, P.; Boeckh, M.; Watkins, T. R.; Chien, J. W.; Dadwal, S. S., A Phase 2b, Randomized, Double-blind, Placebo-Controlled Multicenter Study Evaluating Antiviral Effects, Pharmacokinetics, Safety, and Tolerability of Presatovir in Hematopoietic Cell Transplant Recipients with Respiratory Syncytial Virus (RSV) Infection of the Lower Respiratory Tract. *Clin Infect Dis* **2019**.
7. Ruckwardt, T. J.; Morabito, K. M.; Graham, B. S., Immunological Lessons from Respiratory Syncytial Virus Vaccine Development. *Immunity* **2019**, *51*, 429-442.
8. Jares Baglivo, S.; Polack, F. P., The long road to protect infants against severe RSV lower respiratory tract illness. *F1000Res* **2019**, *8*.
9. Stevens, M.; Rusch, S.; DeVincenzo, J.; Kim, Y. I.; Harrison, L.; Meals, E. A.; Boyers, A.; Fok-Seang, J.; Huntjens, D.; Lounis, N.; Mari, N. K.; Remmerie, B.; Roymans, D.; Koul, A.; Verloes, R., Antiviral Activity of Oral JNJ-53718678 in Healthy Adult Volunteers Challenged With Respiratory Syncytial Virus: A Placebo-Controlled Study. *J Infect Dis* **2018**, *218*, 748-756.

10. Smith, D. W.; Frankel, L. R.; Mathers, L. H.; Tang, A. T.; Ariagno, R. L.; Prober, C. G., A controlled trial of aerosolized ribavirin in infants receiving mechanical ventilation for severe respiratory syncytial virus infection. *N Engl J Med* **1991**, *325*, 24-9.
11. Smith, E. A., "Management of the infant with respiratory syncytial virus". *J Pediatr Nurs* **1991**, *6*, 434.
12. Meert, K. L.; Sarnaik, A. P.; Gelmini, M. J.; Lieh-Lai, M. W., Aerosolized ribavirin in mechanically ventilated children with respiratory syncytial virus lower respiratory tract disease: a prospective, double-blind, randomized trial. *Crit Care Med* **1994**, *22*, 566-72.
13. Law, B. J.; Wang, E. E.; MacDonald, N.; McDonald, J.; Dobson, S.; Boucher, F.; Langley, J.; Robinson, J.; Mitchell, I.; Stephens, D., Does ribavirin impact on the hospital course of children with respiratory syncytial virus (RSV) infection? An analysis using the pediatric investigators collaborative network on infections in Canada (PICNIC) RSV database. *Pediatrics* **1997**, *99*, E7.
14. Hardelid, P.; Verfuenden, M.; McMenam, J.; Smyth, R. L.; Gilbert, R., The contribution of child, family and health service factors to respiratory syncytial virus (RSV) hospital admissions in the first 3 years of life: birth cohort study in Scotland, 2009 to 2015. *Euro Surveill* **2019**, *24*.
15. Robinson, J. L.; Le Saux, N.; Canadian Paediatric Society, I. D.; Immunization, C., Preventing hospitalizations for respiratory syncytial virus infection. *Paediatr Child Health* **2015**, *20*, 321-33.
16. Murray, J.; Bottle, A.; Sharland, M.; Modi, N.; Aylin, P.; Majeed, A.; Saxena, S.; Medicines for Neonates Investigator, G., Risk factors for hospital admission with RSV bronchiolitis in England: a population-based birth cohort study. *PLoS One* **2014**, *9*, e89186.
17. Shi, T.; Denouel, A.; Tietjen, A. K.; Campbell, I.; Moran, E.; Li, X.; Campbell, H.; Demont, C.; Nyawanda, B. O.; Chu, H. Y.; Stoszek, S. K.; Krishnan, A.; Openshaw, P.; Falsey, A. R.; Nair, H.; Investigators, R., Global Disease Burden Estimates of Respiratory Syncytial Virus-Associated Acute Respiratory Infection in Older Adults in 2015: A Systematic Review and Meta-Analysis. *J Infect Dis* **2019**.
18. Chanock, R. M.; Murphy, B. R.; Collins, P. L.; Coelingh, K. V.; Olmsted, R. A.; Snyder, M. H.; Spriggs, M. K.; Prince, G. A.; Moss, B.; Flores, J.; et al., Live viral vaccines for respiratory and enteric tract diseases. *Vaccine* **1988**, *6*, 129-33.
19. Leader, S.; Jacobson, P.; Marcin, J.; Vardis, R.; Sorrentino, M.; Murray, D., A method for identifying the financial burden of hospitalized infants on families. *Value Health* **2002**, *5*, 55-9.
20. Mitchell, I.; Defoy, I.; Grubb, E., Burden of Respiratory Syncytial Virus Hospitalizations in Canada. *Can Respir J* **2017**, *2017*, 4521302.

21. Paes, B.; Mitchell, I.; Li, A.; Lanctot, K. L., Respiratory hospitalizations and respiratory syncytial virus prophylaxis in special populations. *Eur J Pediatr* **2012**, *171*, 833-41.
22. Paes, B. A.; Mitchell, I.; Banerji, A.; Lanctot, K. L.; Langley, J. M., A decade of respiratory syncytial virus epidemiology and prophylaxis: translating evidence into everyday clinical practice. *Can Respir J* **2011**, *18*, e10-9.
23. Nair, H.; Nokes, D. J.; Gessner, B. D.; Dherani, M.; Madhi, S. A.; Singleton, R. J.; O'Brien, K. L.; Roca, A.; Wright, P. F.; Bruce, N.; Chandran, A.; Theodoratou, E.; Sutanto, A.; Sedyaningsih, E. R.; Ngama, M.; Munywoki, P. K.; Kartasasmita, C.; Simoes, E. A.; Rudan, I.; Weber, M. W.; Campbell, H., Global burden of acute lower respiratory infections due to respiratory syncytial virus in young children: a systematic review and meta-analysis. *Lancet* **2010**, *375*, 1545-55.
24. Shi, T.; McAllister, D. A.; O'Brien, K. L.; Simoes, E. A. F.; Madhi, S. A.; Gessner, B. D.; Polack, F. P.; Balsells, E.; Acacio, S.; Aguayo, C.; Alassani, I.; Ali, A.; Antonio, M.; Awasthi, S.; Awori, J. O.; Azziz-Baumgartner, E.; Baggett, H. C.; Baillie, V. L.; Balmaseda, A.; Barahona, A.; Basnet, S.; Bassat, Q.; Basualdo, W.; Bigogo, G.; Bont, L.; Breiman, R. F.; Brooks, W. A.; Broor, S.; Bruce, N.; Bruden, D.; Buchy, P.; Campbell, S.; Carosone-Link, P.; Chadha, M.; Chipeta, J.; Chou, M.; Clara, W.; Cohen, C.; de Cuellar, E.; Dang, D. A.; Dash-Yandag, B.; Deloria-Knoll, M.; Dherani, M.; Eap, T.; Ebruke, B. E.; Echavarria, M.; de Freitas Lazaro Emediato, C. C.; Fasce, R. A.; Feikin, D. R.; Feng, L.; Gentile, A.; Gordon, A.; Goswami, D.; Goyet, S.; Groome, M.; Halasa, N.; Hirve, S.; Homaira, N.; Howie, S. R. C.; Jara, J.; Jroundi, I.; Kartasasmita, C. B.; Khuri-Bulos, N.; Kotloff, K. L.; Krishnan, A.; Libster, R.; Lopez, O.; Lucero, M. G.; Lucion, F.; Lupisan, S. P.; Marcone, D. N.; McCracken, J. P.; Mejia, M.; Moisi, J. C.; Montgomery, J. M.; Moore, D. P.; Moraleda, C.; Moyes, J.; Munywoki, P.; Mutyara, K.; Nicol, M. P.; Nokes, D. J.; Nymadawa, P.; da Costa Oliveira, M. T.; Oshitani, H.; Pandey, N.; Paranhos-Baccala, G.; Phillips, L. N.; Picot, V. S.; Rahman, M.; Rakoto-Andrianarivelo, M.; Rasmussen, Z. A.; Rath, B. A.; Robinson, A.; Romero, C.; Russomando, G.; Salimi, V.; Sawatwong, P.; Scheltema, N.; Schweiger, B.; Scott, J. A. G.; Seidenberg, P.; Shen, K.; Singleton, R.; Sotomayor, V.; Strand, T. A.; Sutanto, A.; Sylla, M.; Tapia, M. D.; Thamthitawat, S.; Thomas, E. D.; Tokarz, R.; Turner, C.; Venter, M.; Waicharoen, S.; Wang, J.; Watthanaworawit, W.; Yoshida, L. M.; Yu, H.; Zar, H. J.; Campbell, H.; Nair, H.; Network, R. S. V. G. E., Global, regional, and national disease burden estimates of acute lower respiratory infections due to respiratory syncytial virus in young children in 2015: a systematic review and modelling study. *Lancet* **2017**, *390*, 946-958.
25. Carrat, F.; Vergu, E.; Ferguson, N. M.; Lemaitre, M.; Cauchemez, S.; Leach, S.; Valleron, A. J., Time lines of infection and disease in human influenza: a review of volunteer challenge studies. *Am J Epidemiol* **2008**, *167*, 775-85.

26. Jefferson, T.; Jones, M. A.; Doshi, P.; Del Mar, C. B.; Hama, R.; Thompson, M. J.; Spencer, E. A.; Onakpoya, I.; Mahtani, K. R.; Nunan, D.; Howick, J.; Heneghan, C. J., Neuraminidase inhibitors for preventing and treating influenza in healthy adults and children. *Cochrane Database Syst Rev* **2014**, CD008965.
27. Bagga, B.; Woods, C. W.; Veldman, T. H.; Gilbert, A.; Mann, A.; Balaratnam, G.; Lambkin-Williams, R.; Oxford, J. S.; McClain, M. T.; Wilkinson, T.; Nicholson, B. P.; Ginsburg, G. S.; Devincenzo, J. P., Comparing influenza and RSV viral and disease dynamics in experimentally infected adults predicts clinical effectiveness of RSV antivirals. *Antivir Ther* **2013**, *18*, 785-91.
28. DeVincenzo, J. P.; Wilkinson, T.; Vaishnav, A.; Cehelsky, J.; Meyers, R.; Nochur, S.; Harrison, L.; Meeking, P.; Mann, A.; Moane, E.; Oxford, J.; Pareek, R.; Moore, R.; Walsh, E.; Studholme, R.; Dorsett, P.; Alvarez, R.; Lambkin-Williams, R., Viral load drives disease in humans experimentally infected with respiratory syncytial virus. *Am J Respir Crit Care Med* **2010**, *182*, 1305-14.
29. El Saleeby, C. M.; Bush, A. J.; Harrison, L. M.; Aitken, J. A.; Devincenzo, J. P., Respiratory syncytial virus load, viral dynamics, and disease severity in previously healthy naturally infected children. *J Infect Dis* **2011**, *204*, 996-1002.
30. Griffiths, C.; Drews, S. J.; Marchant, D. J., Respiratory Syncytial Virus: Infection, Detection, and New Options for Prevention and Treatment. *Clin Microbiol Rev* **2017**, *30*, 277-319.
31. Sloan, C.; Heaton, M.; Kang, S.; Berrett, C.; Wu, P.; Gebretsadik, T.; Sicignano, N.; Evans, A.; Lee, R.; Hartert, T., The impact of temperature and relative humidity on spatiotemporal patterns of infant bronchiolitis epidemics in the contiguous United States. *Health Place* **2017**, *45*, 46-54.
32. Welliver, R. C., Sr., Temperature, humidity, and ultraviolet B radiation predict community respiratory syncytial virus activity. *Pediatr Infect Dis J* **2007**, *26*, S29-35.
33. Janet, S.; Broad, J.; Snape, M. D., Respiratory syncytial virus seasonality and its implications on prevention strategies. *Hum Vaccin Immunother* **2018**, *14*, 234-244.
34. Bilawchuk, L. M.; Griffiths, C. D.; Jensen, L. D.; Elawar, F.; Marchant, D. J., The Susceptibilities of Respiratory Syncytial Virus to Nucleolin Receptor Blocking and Antibody Neutralization are Dependent upon the Method of Virus Purification. *Viruses* **2017**, *9*.
35. Collins, P. L.; Graham, B. S., Viral and host factors in human respiratory syncytial virus pathogenesis. *J Virol* **2008**, *82*, 2040-55.

36. Trento, A.; Casas, I.; Calderon, A.; Garcia-Garcia, M. L.; Calvo, C.; Perez-Brena, P.; Melero, J. A., Ten years of global evolution of the human respiratory syncytial virus BA genotype with a 60-nucleotide duplication in the G protein gene. *J Virol* **2010**, *84*, 7500-12.
37. Elawar, F.; Griffiths, C. D.; Zhu, D.; Bilawchuk, L. M.; Jensen, L. D.; Forss, L.; Tang, J.; Hazes, B.; Drews, S. J.; Marchant, D. J., A Virological and Phylogenetic Analysis of the Emergence of New Clades of Respiratory Syncytial Virus. *Sci Rep* **2017**, *7*, 12232.
38. Morawska, L., Droplet fate in indoor environments, or can we prevent the spread of infection? *Indoor Air* **2006**, *16*, 335-47.
39. Hall, C. B.; Douglas, R. G., Jr.; Geiman, J. M., Possible transmission by fomites of respiratory syncytial virus. *J Infect Dis* **1980**, *141*, 98-102.
40. Hall, C. B.; Douglas, R. G., Jr., Modes of transmission of respiratory syncytial virus. *J Pediatr* **1981**, *99*, 100-3.
41. Kulkarni, H.; Smith, C. M.; Lee Ddo, H.; Hirst, R. A.; Easton, A. J.; O'Callaghan, C., Evidence of Respiratory Syncytial Virus Spread by Aerosol. Time to Revisit Infection Control Strategies? *Am J Respir Crit Care Med* **2016**, *194*, 308-16.
42. Roy, C. J.; Milton, D. K., Airborne transmission of communicable infection--the elusive pathway. *N Engl J Med* **2004**, *350*, 1710-2.
43. Cruz-Sanchez, T. M.; Haddrell, A. E.; Hackett, T. L.; Singhera, G. K.; Marchant, D.; Lekivetz, R.; Meredith, A.; Horne, D.; Knight, D. A.; van Eeden, S. F.; Bai, T. R.; Hegele, R. G.; Dorscheid, D. R.; Agnes, G. R., Formation of a stable mimic of ambient particulate matter containing viable infectious respiratory syncytial virus and its dry-deposition directly onto cell cultures. *Anal Chem* **2013**, *85*, 898-906.
44. Zlateva, K. T.; Lemey, P.; Vandamme, A. M.; Van Ranst, M., Molecular evolution and circulation patterns of human respiratory syncytial virus subgroup a: positively selected sites in the attachment g glycoprotein. *J Virol* **2004**, *78*, 4675-83.
45. Grad, Y. H.; Newman, R.; Zody, M.; Yang, X.; Murphy, R.; Qu, J.; Malboeuf, C. M.; Levin, J. Z.; Lipsitch, M.; DeVincenzo, J., Within-host whole-genome deep sequencing and diversity analysis of human respiratory syncytial virus infection reveals dynamics of genomic diversity in the absence and presence of immune pressure. *J Virol* **2014**, *88*, 7286-93.
46. Martinello, R. A.; Chen, M. D.; Weibel, C.; Kahn, J. S., Correlation between respiratory syncytial virus genotype and severity of illness. *J Infect Dis* **2002**, *186*, 839-42.

47. Laham, F. R.; Mansbach, J. M.; Piedra, P. A.; Hasegawa, K.; Sullivan, A. F.; Espinola, J. A.; Camargo, C. A., Jr., Clinical Profiles of Respiratory Syncytial Virus Subtypes A AND B Among Children Hospitalized with Bronchiolitis. *Pediatr Infect Dis J* **2017**, *36*, 808-810.
48. Walsh, E. E.; McConnochie, K. M.; Long, C. E.; Hall, C. B., Severity of Respiratory Syncytial Virus Infection Is Related to Virus Strain. *JID* **1997**, *175*, 814-820.
49. Fodha, I.; Vabret, A.; Ghedira, L.; Seboui, H.; Chouchane, S.; Dewar, J.; Gueddiche, N.; Trabelsi, A.; Boujaafar, N.; Freymuth, F., Respiratory syncytial virus infections in hospitalized infants: association between viral load, virus subgroup, and disease severity. *J Med Virol* **2007**, *79*, 1951-8.
50. Devincenzo, J. P., Natural infection of infants with respiratory syncytial virus subgroups A and B: a study of frequency, disease severity, and viral load. *Pediatr Res* **2004**, *56*, 914-7.
51. Buckingham, S. C.; Bush, A. J.; Devincenzo, J. P., Nasal quantity of respiratory syncytial virus correlates with disease severity in hospitalized infants. *Pediatr Infect Dis J* **2000**, *19*, 113-7.
52. Barik, S., Respiratory syncytial virus mechanisms to interfere with type 1 interferons. *Curr Top Microbiol Immunol* **2013**, *372*, 173-91.
53. Bitko, V.; Shulyayeva, O.; Mazumder, B.; Musiyenko, A.; Ramaswamy, M.; Look, D. C.; Barik, S., Nonstructural proteins of respiratory syncytial virus suppress premature apoptosis by an NF-kappaB-dependent, interferon-independent mechanism and facilitate virus growth. *J Virol* **2007**, *81*, 1786-95.
54. Wu, W.; Tran, K. C.; Teng, M. N.; Heesom, K. J.; Matthews, D. A.; Barr, J. N.; Hiscox, J. A., The interactome of the human respiratory syncytial virus NS1 protein highlights multiple effects on host cell biology. *J Virol* **2012**, *86*, 7777-89.
55. Zhang, W.; Yang, H.; Kong, X.; Mohapatra, S.; San Juan-Vergara, H.; Hellermann, G.; Behera, S.; Singam, R.; Lockey, R. F.; Mohapatra, S. S., Inhibition of respiratory syncytial virus infection with intranasal siRNA nanoparticles targeting the viral NS1 gene. *Nat Med* **2005**, *11*, 56-62.
56. Vasou, A.; Paulus, C.; Narloch, J.; Gage, Z. O.; Rameix-Welti, M. A.; Eleouet, J. F.; Nevels, M.; Randall, R. E.; Adamson, C. S., Modular cell-based platform for high throughput identification of compounds that inhibit a viral interferon antagonist of choice. *Antiviral Res* **2018**, *150*, 79-92.
57. Collins, P. L.; Melero, J. A., Progress in understanding and controlling respiratory syncytial virus: still crazy after all these years. *Virus Res* **2011**, *162*, 80-99.

58. Tawar, R. G.; Duquerroy, S.; Vonrhein, C.; Varela, P. F.; Damier-Piolle, L.; Castagne, N.; MacLellan, K.; Bedouelle, H.; Bricogne, G.; Bhella, D.; Eleouet, J. F.; Rey, F. A., Crystal structure of a nucleocapsid-like nucleoprotein-RNA complex of respiratory syncytial virus. *Science* **2009**, *326*, 1279-83.
59. Lifland, A. W.; Jung, J.; Alonas, E.; Zurla, C.; Crowe, J. E., Jr.; Santangelo, P. J., Human respiratory syncytial virus nucleoprotein and inclusion bodies antagonize the innate immune response mediated by MDA5 and MAVS. *J Virol* **2012**, *86*, 8245-58.
60. Mogensen, T. H., Pathogen recognition and inflammatory signaling in innate immune defenses. *Clin Microbiol Rev* **2009**, *22*, 240-73, Table of Contents.
61. Yoneyama, M.; Kikuchi, M.; Natsukawa, T.; Shinobu, N.; Imaizumi, T.; Miyagishi, M.; Taira, K.; Akira, S.; Fujita, T., The RNA helicase RIG-I has an essential function in double-stranded RNA-induced innate antiviral responses. *Nat Immunol* **2004**, *5*, 730-7.
62. Yoneyama, M.; Kikuchi, M.; Matsumoto, K.; Imaizumi, T.; Miyagishi, M.; Taira, K.; Foy, E.; Loo, Y. M.; Gale, M., Jr.; Akira, S.; Yonehara, S.; Kato, A.; Fujita, T., Shared and unique functions of the DExD/H-box helicases RIG-I, MDA5, and LGP2 in antiviral innate immunity. *J Immunol* **2005**, *175*, 2851-8.
63. Hornung, V.; Ellegast, J.; Kim, S.; Brzozka, K.; Jung, A.; Kato, H.; Poeck, H.; Akira, S.; Conzelmann, K. K.; Schlee, M.; Endres, S.; Hartmann, G., 5'-Triphosphate RNA is the ligand for RIG-I. *Science* **2006**, *314*, 994-7.
64. Clemens, M. J.; Hershey, J. W.; Hovanessian, A. C.; Jacobs, B. C.; Katze, M. G.; Kaufman, R. J.; Lengyel, P.; Samuel, C. E.; Sen, G. C.; Williams, B. R., PKR: proposed nomenclature for the RNA-dependent protein kinase induced by interferon. *J Interferon Res* **1993**, *13*, 241.
65. Garcia, C. S.; Curiel, R. E.; Mwatibo, J. M.; Pestka, S.; Li, H.; Espinoza-Delgado, I., The antineoplastic agent bryostatin-1 differentially regulates IFN-gamma receptor subunits in monocytic cells: transcriptional and posttranscriptional control of IFN-gamma R2. *J Immunol* **2006**, *177*, 2707-16.
66. Clemens, M. J.; Elia, A., The double-stranded RNA-dependent protein kinase PKR: structure and function. *J Interferon Cytokine Res* **1997**, *17*, 503-24.
67. Groskreutz, D. J.; Babor, E. C.; Monick, M. M.; Varga, S. M.; Hunninghake, G. W., Respiratory syncytial virus limits alpha subunit of eukaryotic translation initiation factor 2 (eIF2alpha) phosphorylation to maintain translation and viral replication. *J Biol Chem* **2010**, *285*, 24023-31.

68. Gilman, M. S. A.; Liu, C.; Fung, A.; Behera, I.; Jordan, P.; Rigaux, P.; Ysebaert, N.; Tcherniuk, S.; Sourimant, J.; Eleouet, J. F.; Sutto-Ortiz, P.; Decroly, E.; Roymans, D.; Jin, Z.; McLellan, J. S., Structure of the Respiratory Syncytial Virus Polymerase Complex. *Cell* **2019**, *179*, 193-204 e14.
69. Hara, K.; Yaita, K.; Khamrin, P.; Kumthip, K.; Kashiwagi, T.; Eleouet, J. F.; Rameix-Welti, M. A.; Watanabe, H., A small fragmented P protein of respiratory syncytial virus inhibits virus infection by targeting P protein. *J Gen Virol* **2020**, *101*, 21-32.
70. Kiss, G.; Holl, J. M.; Williams, G. M.; Alonas, E.; Vanover, D.; Lifland, A. W.; Gudheti, M.; Guerrero-Ferreira, R. C.; Nair, V.; Yi, H.; Graham, B. S.; Santangelo, P. J.; Wright, E. R., Structural analysis of respiratory syncytial virus reveals the position of M2-1 between the matrix protein and the ribonucleoprotein complex. *J Virol* **2014**, *88*, 7602-17.
71. Johnson, S. M.; McNally, B. A.; Ioannidis, I.; Flano, E.; Teng, M. N.; Oomens, A. G.; Walsh, E. E.; Peeples, M. E., Respiratory Syncytial Virus Uses CX3CR1 as a Receptor on Primary Human Airway Epithelial Cultures. *PLoS Pathog* **2015**, *11*, e1005318.
72. Lingemann, M.; McCarty, T.; Liu, X.; Buchholz, U. J.; Surman, S.; Martin, S. E.; Collins, P. L.; Munir, S., The alpha-1 subunit of the Na⁺,K⁺-ATPase (ATP1A1) is required for macropinocytic entry of respiratory syncytial virus (RSV) in human respiratory epithelial cells. *PLoS Pathog* **2019**, *15*, e1007963.
73. Krzyzaniak, M. A.; Zumstein, M. T.; Gerez, J. A.; Picotti, P.; Helenius, A., Host cell entry of respiratory syncytial virus involves macropinocytosis followed by proteolytic activation of the F protein. *PLoS Pathog* **2013**, *9*, e1003309.
74. Malhotra, R.; Ward, M.; Bright, H.; Priest, R.; Foster, M. R.; Hurle, M.; Blair, E.; Bird, M., Isolation and characterisation of potential respiratory syncytial virus receptor(s) on epithelial cells. *Microbes Infect* **2003**, *5*, 123-33.
75. Marchant, D.; Singhera, G. K.; Utokaparch, S.; Hackett, T. L.; Boyd, J. H.; Luo, Z.; Si, X.; Dorscheid, D. R.; McManus, B. M.; Hegele, R. G., Toll-like receptor 4-mediated activation of p38 mitogen-activated protein kinase is a determinant of respiratory virus entry and tropism. *J Virol* **2010**, *84*, 11359-73.
76. Behera, A. K.; Matsuse, H.; Kumar, M.; Kong, X.; Lockey, R. F.; Mohapatra, S. S., Blocking intercellular adhesion molecule-1 on human epithelial cells decreases respiratory syncytial virus infection. *Biochem Biophys Res Commun* **2001**, *280*, 188-95.
77. Tayyari, F.; Marchant, D.; Moraes, T. J.; Duan, W.; Mastrangelo, P.; Hegele, R. G., Identification of nucleolin as a cellular receptor for human respiratory syncytial virus. *Nat Med* **2011**, *17*, 1132-5.

78. McLellan, J. S.; Chen, M.; Leung, S.; Graepel, K. W.; Du, X.; Yang, Y.; Zhou, T.; Baxa, U.; Yasuda, E.; Beaumont, T.; Kumar, A.; Modjarrad, K.; Zheng, Z.; Zhao, M.; Xia, N.; Kwong, P. D.; Graham, B. S., Structure of RSV fusion glycoprotein trimer bound to a prefusion-specific neutralizing antibody. *Science* **2013**, *340*, 1113-7.
79. Karron, R. A.; Buonagurio, D. A.; Georgiu, A. F.; Whitehead, S. S.; Adamus, J. E.; Clements-Mann, M. L.; Harris, D. O.; Randolph, V. B.; Udem, S. A.; Murphy, B. R.; Sidhu, M. S., Respiratory syncytial virus (RSV) SH and G proteins are not essential for viral replication in vitro: clinical evaluation and molecular characterization of a cold-passaged, attenuated RSV subgroup B mutant. *Proc Natl Acad Sci U S A* **1997**, *94*, 13961-6.
80. Bukreyev, A.; Yang, L.; Collins, P. L., The secreted G protein of human respiratory syncytial virus antagonizes antibody-mediated restriction of replication involving macrophages and complement. *J Virol* **2012**, *86*, 10880-4.
81. Bukreyev, A.; Whitehead, S. S.; Murphy, B. R.; Collins, P. L., Recombinant respiratory syncytial virus from which the entire SH gene has been deleted grows efficiently in cell culture and exhibits site-specific attenuation in the respiratory tract of the mouse. *J Virol* **1997**, *71*, 8973-82.
82. Whitehead, S. S.; Bukreyev, A.; Teng, M. N.; Firestone, C. Y.; St Claire, M.; Elkins, W. R.; Collins, P. L.; Murphy, B. R., Recombinant respiratory syncytial virus bearing a deletion of either the NS2 or SH gene is attenuated in chimpanzees. *J Virol* **1999**, *73*, 3438-42.
83. Karron, R. A.; Wright, P. F.; Belshe, R. B.; Thumar, B.; Casey, R.; Newman, F.; Polack, F. P.; Randolph, V. B.; Deatly, A.; Hackell, J.; Gruber, W.; Murphy, B. R.; Collins, P. L., Identification of a recombinant live attenuated respiratory syncytial virus vaccine candidate that is highly attenuated in infants. *J Infect Dis* **2005**, *191*, 1093-104.
84. Selvaraj, M.; Yegambaram, K.; Todd, E.; Richard, C. A.; Dods, R. L.; Pangratiou, G. M.; Trinh, C. H.; Moul, S. L.; Murphy, J. C.; Mankouri, J.; Eleouet, J. F.; Barr, J. N.; Edwards, T. A., The Structure of the Human Respiratory Syncytial Virus M2-1 Protein Bound to the Interaction Domain of the Phosphoprotein P Defines the Orientation of the Complex. *MBio* **2018**, *9*.
85. Bouillier, C.; Cosentino, G.; Leger, T.; Rincheval, V.; Richard, C. A.; Desquesnes, A.; Sitterlin, D.; Blouquit-Laye, S.; Eleouet, J. F.; Gault, E.; Rameix-Welti, M. A., The Interactome analysis of the Respiratory Syncytial Virus protein M2-1 suggests a new role in viral mRNA metabolism post-transcription. *Sci Rep* **2019**, *9*, 15258.
86. Tchesnokov, E. P.; Raeisimakiani, P.; Ngure, M.; Marchant, D.; Gotte, M., Recombinant RNA-Dependent RNA Polymerase Complex of Ebola Virus. *Sci Rep* **2018**, *8*, 3970.

87. Fearn, R.; Collins, P. L., Model for polymerase access to the overlapped L gene of respiratory syncytial virus. *J Virol* **1999**, *73*, 388-97.
88. Noton, S. L.; Deflube, L. R.; Tremaglio, C. Z.; Fearn, R., The respiratory syncytial virus polymerase has multiple RNA synthesis activities at the promoter. *PLoS Pathog* **2012**, *8*, e1002980.
89. Grosfeld, H.; Hill, M. G.; Collins, P. L., RNA replication by respiratory syncytial virus (RSV) is directed by the N, P, and L proteins; transcription also occurs under these conditions but requires RSV superinfection for efficient synthesis of full-length mRNA. *J Virol* **1995**, *69*, 5677-86.
90. Collins, P. L.; Hill, M. G.; Cristina, J.; Grosfeld, H., Transcription elongation factor of respiratory syncytial virus, a nonsegmented negative-strand RNA virus. *Proc Natl Acad Sci U S A* **1996**, *93*, 81-5.
91. Collins, P. L.; Hill, M. G.; Camargo, E.; Grosfeld, H.; Chanock, R. M.; Murphy, B. R., Production of infectious human respiratory syncytial virus from cloned cDNA confirms an essential role for the transcription elongation factor from the 5' proximal open reading frame of the M2 mRNA in gene expression and provides a capability for vaccine development. *Proc Natl Acad Sci U S A* **1995**, *92*, 11563-7.
92. Poch, O.; Sauvaget, I.; Delarue, M.; Tordo, N., Identification of four conserved motifs among the RNA-dependent polymerase encoding elements. *EMBO J* **1989**, *8*, 3867-74.
93. Cowton, V. M.; McGivern, D. R.; Fearn, R., Unravelling the complexities of respiratory syncytial virus RNA synthesis. *J Gen Virol* **2006**, *87*, 1805-21.
94. Barik, S., The structure of the 5' terminal cap of the respiratory syncytial virus mRNA. *J Gen Virol* **1993**, *74* (Pt 3), 485-90.
95. Dupuy, L. C.; Dobson, S.; Bitko, V.; Barik, S., Casein kinase 2-mediated phosphorylation of respiratory syncytial virus phosphoprotein P is essential for the transcription elongation activity of the viral polymerase; phosphorylation by casein kinase 1 occurs mainly at Ser(215) and is without effect. *J Virol* **1999**, *73*, 8384-92.
96. Asenjo, A.; Calvo, E.; Villanueva, N., Phosphorylation of human respiratory syncytial virus P protein at threonine 108 controls its interaction with the M2-1 protein in the viral RNA polymerase complex. *J Gen Virol* **2006**, *87*, 3637-42.
97. Broadbent, L.; Groves, H.; Shields, M. D.; Power, U. F., Respiratory syncytial virus, an ongoing medical dilemma: an expert commentary on respiratory syncytial virus prophylactic and therapeutic pharmaceuticals currently in clinical trials. *Influenza Other Respir Viruses* **2015**, *9*, 169-78.

98. Perron, M.; Stray, K.; Kinkade, A.; Theodore, D.; Lee, G.; Eisenberg, E.; Sangi, M.; Gilbert, B. E.; Jordan, R.; Piedra, P. A.; Toms, G. L.; Mackman, R.; Cihlar, T., GS-5806 Inhibits a Broad Range of Respiratory Syncytial Virus Clinical Isolates by Blocking the Virus-Cell Fusion Process. *Antimicrob Agents Chemother* **2015**, *60*, 1264-73.
99. Mackman, R. L.; Sangi, M.; Sperandio, D.; Parrish, J. P.; Eisenberg, E.; Perron, M.; Hui, H.; Zhang, L.; Siegel, D.; Yang, H.; Saunders, O.; Booramra, C.; Lee, G.; Samuel, D.; Babaoglu, K.; Carey, A.; Gilbert, B. E.; Piedra, P. A.; Strickley, R.; Iwata, Q.; Hayes, J.; Stray, K.; Kinkade, A.; Theodore, D.; Jordan, R.; Desai, M.; Cihlar, T., Discovery of an Oral Respiratory Syncytial Virus (RSV) Fusion Inhibitor (GS-5806) and Clinical Proof of Concept in a Human RSV Challenge Study. *J. Med. Chem.* **2015**, *58*, 1630-1643.
100. Samuel, D.; Xing, W.; Niedziela-Majka, A.; Wong, J. S.; Hung, M.; Brendza, K. M.; Perron, M.; Jordan, R.; Sperandio, D.; Liu, X.; Mackman, R.; Sakowicz, R., GS-5806 inhibits pre- to postfusion conformational changes of the respiratory syncytial virus fusion protein. *Antimicrob Agents Chemother* **2015**, *59*, 7109-12.
101. Mackman, R. L.; Sangi, M.; Sperandio, D.; Parrish, J. P.; Eisenberg, E.; Perron, M.; Hui, H.; Zhang, L.; Siegel, D.; Yang, H.; Saunders, O.; Booramra, C.; Lee, G.; Samuel, D.; Babaoglu, K.; Carey, A.; Gilbert, B. E.; Piedra, P. A.; Strickley, R.; Iwata, Q.; Hayes, J.; Stray, K.; Kinkade, A.; Theodore, D.; Jordan, R.; Desai, M.; Cihlar, T., Discovery of an oral respiratory syncytial virus (RSV) fusion inhibitor (GS-5806) and clinical proof of concept in a human RSV challenge study. *J Med Chem* **2015**, *58*, 1630-43.
102. DeVincenzo, J. P.; Whitley, R. J.; Mackman, R. L.; Scaglioni-Weinlich, C.; Harrison, L.; Farrell, E.; McBride, S.; Lambkin-Williams, R.; Jordan, R.; Xin, Y.; Ramanathan, S.; O'Riordan, T.; Lewis, S. A.; Li, X.; Toback, S. L.; Lin, S. L.; Chien, J. W., Oral GS-5806 activity in a respiratory syncytial virus challenge study. *N Engl J Med* **2014**, *371*, 711-22.
103. Stray, K.; Perron, M.; Porter, D. P.; Anderson, F.; Lewis, S. A.; Perry, J.; Miller, M.; Cihlar, T.; DeVincenzo, J.; Chien, J. W.; Jordan, R., Drug resistance assessment following administration of RSV fusion inhibitor presatovir to participants experimentally infected with respiratory syncytial virus. *J Infect Dis* **2020**.
104. Kim, Y.-I.; Pareek, R.; Murphy, R.; Harrison, L.; Farrell, E.; Cook, R.; DeVincenzo, J., The antiviral effects of RSV fusion inhibitor, MDT-637, on clinical isolates, vs its achievable concentrations in the human respiratory tract and comparison to ribavirin. *Influenza and Other Respiratory Viruses* **2017**, *11*, 525-530.
105. Douglas, J. L.; Panis, M. L.; Ho, E.; Lin, K.-Y.; Krawczyk, S. H.; Grant, D. M.; Cai, R.; Swaminathan, S.; Chen, X.; Cihlar, T., Small Molecules VP-14637 and JNJ-2408068 Inhibit Respiratory Syncytial Virus Fusion by Similar Mechanisms. *Antimicrob. Agents Chemother.* **2005**, *49*, 2460.

106. Douglas, J. L.; Panis, M. L.; Ho, E.; Lin, K.-Y.; Krawczyk, S. H.; Grant, D. M.; Cai, R.; Swaminathan, S.; Cihlar, T., Inhibition of Respiratory Syncytial Virus Fusion by the Small Molecule VP-14637 via Specific Interactions with F Protein. *J. Virol.* **2003**, *77*, 5054.
107. Roymans, D.; De Bondt, H. L.; Arnoult, E.; Geluykens, P.; Gevers, T.; Van Ginderen, M.; Verheyen, N.; Kim, H.; Willebrords, R.; Bonfanti, J.-F.; Bruinzeel, W.; Cummings, M. D.; van Vlijmen, H.; Andries, K., Binding of a potent small-molecule inhibitor of six-helix bundle formation requires interactions with both heptad-repeats of the RSV fusion protein. *Proc. Natl. Acad. Sci. USA* **2010**, *107*, 308.
108. Battles, M. B.; Langedijk, J. P.; Furmanova-Hollenstein, P.; Chaiwatpongsakorn, S.; Costello, H. M.; Kwanten, L.; Vranckx, L.; Vink, P.; Jaensch, S.; Jonckers, T. H. M.; Koul, A.; Arnoult, E.; Peeples, M. E.; Roymans, D.; McLellan, J. S., Molecular mechanism of respiratory syncytial virus fusion inhibitors. *Nat. Chem. Biol.* **2016**, *12*, 87-93.
109. Roymans, D.; Alnajjar, S. S.; Battles, M. B.; Sithicharoenchai, P.; Furmanova-Hollenstein, P.; Rigaux, P.; Berg, J. V. d.; Kwanten, L.; Ginderen, M. V.; Verheyen, N.; Vranckx, L.; Jaensch, S.; Arnoult, E.; Voorzaat, R.; Gallup, J. M.; Larios-Mora, A.; Crabbe, M.; Huntjens, D.; Raboisson, P.; Langedijk, J. P.; Ackermann, M. R.; McLellan, J. S.; Vendeville, S.; Koul, A., Therapeutic efficacy of a respiratory syncytial virus fusion inhibitor. *Nat Commun* **2017**, *8*, 167.
110. Israel, S.; Rusch, S.; DeVincenzo, J.; Boyers, A.; Fok-Seang, J.; Huntjens, D.; Lounis, N.; Mariën, K.; Stevens, M.; Verloes, R., Effect of Oral JNJ-53718678 (JNJ-678) on Disease Severity in Healthy Adult Volunteers Experimentally Inoculated With Live Respiratory Syncytial Virus (RSV): A Placebo-Controlled Challenge Study. *Open Forum Infectious Diseases* **2016**, *3*.
111. Roymans, D.; Alnajjar, S. S.; Battles, M. B.; Sithicharoenchai, P.; Furmanova-Hollenstein, P.; Rigaux, P.; Berg, J. V. D.; Kwanten, L.; Ginderen, M. V.; Verheyen, N.; Vranckx, L.; Jaensch, S.; Arnoult, E.; Voorzaat, R.; Gallup, J. M.; Larios-Mora, A.; Crabbe, M.; Huntjens, D.; Raboisson, P.; Langedijk, J. P.; Ackermann, M. R.; McLellan, J. S.; Vendeville, S.; Koul, A., Therapeutic efficacy of a respiratory syncytial virus fusion inhibitor. *Nat Commun* **2017**, *8*, 167.
112. Bonfanti, J.-F.; Meyer, C.; Doublet, F.; Fortin, J.; Muller, P.; Queguiner, L.; Gevers, T.; Janssens, P.; Szel, H.; Willebrords, R.; Timmerman, P.; Wuyts, K.; van Remoortere, P.; Janssens, F.; Wigerinck, P.; Andries, K., Selection of a Respiratory Syncytial Virus Fusion Inhibitor Clinical Candidate. 2. Discovery of a Morpholinopropylaminobenzimidazole Derivative (TMC353121). *J. Med. Chem.* **2008**, *51*, 875-896.
113. Ispas, G.; Koul, A.; Verbeeck, J.; Sheehan, J.; Sanders-Beer, B.; Roymans, D.; Andries, K.; Rouan, M.-C.; De Jonghe, S.; Bonfanti, J.-F.; Vanstockem, M.; Simmen, K.; Verloes, R., Antiviral Activity of TMC353121, a Respiratory Syncytial Virus (RSV) Fusion Inhibitor, in a Non-Human Primate Model. *PLOS ONE* **2015**, *10*, e0126959.

114. DeVincenzo, J.; Tait, D.; Efthimiou, J.; Mori, J.; Kim, Y. I.; Thomas, E.; Wilson, L.; Harland, R.; Mathews, N.; Cockerill, S.; Powell, K.; Littler, E., A Randomized, Placebo-Controlled, Respiratory Syncytial Virus Human Challenge Study of the Antiviral Efficacy, Safety, and Pharmacokinetics of RV521, an Inhibitor of the RSV-F Protein. *Antimicrob Agents Chemother* **2020**, *64*.
115. Challa, S.; Scott, A. D.; Yuzhakov, O.; Zhou, Y.; Tiong-Yip, C. L.; Gao, N.; Thresher, J.; Yu, Q., Mechanism of action for respiratory syncytial virus inhibitor RSV604. *Antimicrob Agents Chemother* **2015**, *59*, 1080-7.
116. Munday, D. C.; Wu, W.; Smith, N.; Fix, J.; Noton, S. L.; Galloux, M.; Touzelet, O.; Armstrong, S. D.; Dawson, J. M.; Aljabr, W.; Easton, A. J.; Rameix-Welti, M. A.; de Oliveira, A. P.; Simabuco, F. M.; Ventura, A. M.; Hughes, D. J.; Barr, J. N.; Fearn, R.; Digard, P.; Eleouet, J. F.; Hiscox, J. A., Interactome analysis of the human respiratory syncytial virus RNA polymerase complex identifies protein chaperones as important cofactors that promote L-protein stability and RNA synthesis. *J Virol* **2015**, *89*, 917-30.
117. Lam, J. K.; Chow, M. Y.; Zhang, Y.; Leung, S. W., siRNA Versus miRNA as Therapeutics for Gene Silencing. *Mol Ther Nucleic Acids* **2015**, *4*, e252.
118. Gottlieb, J.; Zamora, M. R.; Hodges, T.; Musk, A. W.; Sommerwerk, U.; Dilling, D.; Arcasoy, S.; DeVincenzo, J.; Karsten, V.; Shah, S.; Bettencourt, B. R.; Cehelsky, J.; Nochur, S.; Gollob, J.; Vaishnav, A.; Simon, A. R.; Glanville, A. R., ALN-RSV01 for prevention of bronchiolitis obliterans syndrome after respiratory syncytial virus infection in lung transplant recipients. *J Heart Lung Transplant* **2016**, *35*, 213-21.
119. De Clercq, E.; Li, G., Approved Antiviral Drugs over the Past 50 Years. *Clin Microbiol Rev* **2016**, *29*, 695-747.
120. Lichtman, M. A., A historical perspective on the development of the cytarabine (7days) and daunorubicin (3days) treatment regimen for acute myelogenous leukemia: 2013 the 40th anniversary of 7+3. *Blood Cells Mol Dis* **2013**, *50*, 119-30.
121. De Clercq, E.; Schinazi, R. F., Editorial overview: Antiviral strategies. *Curr Opin Virol* **2016**, *18*, v-vi.
122. DeVincenzo, J. P.; McClure, M. W.; Symons, J. A.; Fathi, H.; Westland, C.; Chanda, S.; Lambkin-Williams, R.; Smith, P.; Zhang, Q.; Beigelman, L.; Blatt, L. M.; Fry, J., Activity of Oral ALS-008176 in a Respiratory Syncytial Virus Challenge Study. *N Engl J Med* **2015**, *373*, 2048-58.
123. Witkowski, J. T.; Robins, R. K.; Sidwell, R. W.; Simon, L. N., Design, synthesis, and broad spectrum antiviral activity of 1-*D*-ribofuranosyl-1,2,4-triazole-3-carboxamide and related nucleosides. *J Med Chem* **1972**, *15*, 1150-4.

124. Kim, Y. I.; Pareek, R.; Murphy, R.; Harrison, L.; Farrell, E.; Cook, R.; DeVincenzo, J., The antiviral effects of RSV fusion inhibitor, MDT-637, on clinical isolates, vs its achievable concentrations in the human respiratory tract and comparison to ribavirin. *Influenza Other Respir Viruses* **2017**, *11*, 525-530.
125. Sudo, K.; Miyazaki, Y.; Kojima, N.; Kobayashi, M.; Suzuki, H.; Shintani, M.; Shimizu, Y., YM-53403, a unique anti-respiratory syncytial virus agent with a novel mechanism of action. *Antiviral Res* **2005**, *65*, 125-31.
126. Chapman, J.; Abbott, E.; Alber, D. G.; Baxter, R. C.; Bithell, S. K.; Henderson, E. A.; Carter, M. C.; Chambers, P.; Chubb, A.; Cockerill, G. S.; Collins, P. L.; Dowdell, V. C.; Keegan, S. J.; Kelsey, R. D.; Lockyer, M. J.; Luongo, C.; Najarro, P.; Pickles, R. J.; Simmonds, M.; Taylor, D.; Tyms, S.; Wilson, L. J.; Powell, K. L., RSV604, a novel inhibitor of respiratory syncytial virus replication. *Antimicrob Agents Chemother* **2007**, *51*, 3346-53.
127. Hong, Z.; Cameron, C. E., Pleiotropic mechanisms of ribavirin antiviral activities. *Prog Drug Res* **2002**, *59*, 41-69.
128. Sidwell, R. W.; Huffman, J. H.; Khare, G. P.; Allen, L. B.; Witkowski, J. T.; Robins, R. K., Broad-spectrum antiviral activity of Virazole: 1-beta-D-ribofuranosyl-1,2,4-triazole-3-carboxamide. *Science* **1972**, *177*, 705-6.
129. Scholtissek, C., Inhibition of influenza RNA synthesis by virazole (ribavirin). *Arch Virol* **1976**, *50*, 349-52.
130. Huffman, J. H.; Sidwell, R. W.; Khare, G. P.; Witkowski, J. T.; Allen, L. B.; Robins, R. K., In vitro effect of 1-beta-D-ribofuranosyl-1,2,4-triazole-3-carboxamide (virazole, ICN 1229) on deoxyribonucleic acid and ribonucleic acid viruses. *Antimicrob Agents Chemother* **1973**, *3*, 235-41.
131. Hruska, J. F.; Bernstein, J. M.; Douglas, R. G., Jr.; Hall, C. B., Effects of ribavirin on respiratory syncytial virus in vitro. *Antimicrob Agents Chemother* **1980**, *17*, 770-5.
132. Feld, J. J.; Liang, T. J., HCV persistence: cure is still a four letter word. *Hepatology* **2005**, *41*, 23-5.
133. Houghton, M., Hepatitis C: the next 25years. *Antiviral Res* **2014**, *110*, 77-8.
134. Tiong-Yip, C. L.; Aschenbrenner, L.; Johnson, K. D.; McLaughlin, R. E.; Fan, J.; Challa, S.; Xiong, H.; Yu, Q., Characterization of a respiratory syncytial virus L protein inhibitor. *Antimicrob Agents Chemother* **2014**, *58*, 3867-73.
135. Noah, J. W.; Severson, W.; Chung, D. H.; Moore, B.; Jia, F.; Xu, X.; Maddox, C.; Rasmussen, L.; Sosa, M. I.; Tower, N. A.; Ananthan, S.; White, E. L.; Jonsson, C.; Matharu, D. S.; Golden, J. E.; Prisinzano,

- T. E.; Aube, J., A Cell Based HTS Approach for the Discovery of New Inhibitors of RSV. In *Probe Reports from the NIH Molecular Libraries Program*, Bethesda (MD), 2010.
136. Coates, M.; Brookes, D.; Kim, Y. I.; Allen, H.; Fordyce, E. A. F.; Meals, E. A.; Colley, T.; Ciana, C. L.; Parra, G. F.; Sherbukhin, V.; Stockwell, J. A.; Thomas, J. C.; Hunt, S. F.; Anderson-Dring, L.; Onions, S. T.; Cass, L.; Murray, P. J.; Ito, K.; Strong, P.; DeVincenzo, J. P.; Rapeport, G., Preclinical Characterization of PC786, an Inhaled Small-Molecule Respiratory Syncytial Virus L Protein Polymerase Inhibitor. *Antimicrob Agents Chemother* **2017**, *61*.
137. Noton, S. L.; Nagendra, K.; Dunn, E. F.; Mawhorter, M. E.; Yu, Q.; Fearn, R., Respiratory Syncytial Virus Inhibitor AZ-27 Differentially Inhibits Different Polymerase Activities at the Promoter. *J Virol* **2015**, *89*, 7786-98.
138. Plant, H.; Stacey, C.; Tiong-Yip, C. L.; Walsh, J.; Yu, Q.; Rich, K., High-Throughput Hit Screening Cascade to Identify Respiratory Syncytial Virus (RSV) Inhibitors. *J Biomol Screen* **2015**, *20*, 597-605.
139. Wang, G.; Deval, J.; Hong, J.; Dyatkina, N.; Prhac, M.; Taylor, J.; Fung, A.; Jin, Z.; Stevens, S. K.; Serebryany, V.; Liu, J.; Zhang, Q.; Tam, Y.; Chanda, S. M.; Smith, D. B.; Symons, J. A.; Blatt, L. M.; Beigelman, L., Discovery of 4'-chloromethyl-2'-deoxy-3',5'-di-O-isobutyryl-2'-fluorocytidine (ALS-8176), a first-in-class RSV polymerase inhibitor for treatment of human respiratory syncytial virus infection. *J Med Chem* **2015**, *58*, 1862-78.
140. Smith, D. B.; Kalayanov, G.; Sund, C.; Winqvist, A.; Maltseva, T.; Leveque, V. J. P.; Rajyaguru, S.; Pogam, S. L.; Najera, I.; Benkestock, K.; Zhou, X.-X.; Kaiser, A. C.; Maag, H.; Cammack, N.; Martin, J. A.; Swallow, S.; Johansson, N. G.; Klumpp, K.; Smith, M., The Design, Synthesis, and Antiviral Activity of Monofluoro and Difluoro Analogues of 4'-Azidocytidine against Hepatitis C Virus Replication: The Discovery of 4'-Azido-2'-deoxy-2'-fluorocytidine and 4'-Azido-2'-dideoxy-2',2'-difluorocytidine. *J. Med. Chem.* **2009**, *52*, 2971-2978.
141. Nelson, D. R.; Zeuzem, S.; Andreone, P.; Ferenci, P.; Herring, R.; Jensen, D. M.; Marcellin, P.; Pockros, P. J.; Rodriguez-Torres, M.; Rossaro, L.; Rustgi, V. K.; Sepe, T.; Sulkowski, M.; Thomason, I. R.; Yoshida, E. M.; Chan, A.; Hill, G., Balapiravir plus peginterferon alfa-2a (40KD)/ribavirin in a randomized trial of hepatitis C genotype 1 patients. *Ann Hepatol* **2012**, *11*, 15-31.
142. Deval, J.; Hong, J.; Wang, G.; Taylor, J.; Smith, L. K.; Fung, A.; Stevens, S. K.; Liu, H.; Jin, Z.; Dyatkina, N.; Prhac, M.; Stoycheva, A. D.; Serebryany, V.; Liu, J.; Smith, D. B.; Tam, Y.; Zhang, Q.; Moore, M. L.; Fearn, R.; Chanda, S. M.; Blatt, L. M.; Symons, J. A.; Beigelman, L., Molecular Basis for the Selective Inhibition of Respiratory Syncytial Virus RNA Polymerase by 2'-Fluoro-4'-Chloromethyl-Cytidine Triphosphate. *PLoS Pathog.* **2015**, *11*, e1004995.

143. Deval, J.; Hong, J.; Wang, G.; Taylor, J.; Smith, L. K.; Fung, A.; Stevens, S. K.; Liu, H.; Jin, Z.; Dyatkina, N.; Prhac, M.; Stoycheva, A. D.; Serebryany, V.; Liu, J.; Smith, D. B.; Tam, Y.; Zhang, Q.; Moore, M. L.; Fearn, R.; Chanda, S. M.; Blatt, L. M.; Symons, J. A.; Beigelman, L., Molecular Basis for the Selective Inhibition of Respiratory Syncytial Virus RNA Polymerase by 2'-Fluoro-4'-Chloromethyl-Cytidine Triphosphate. *PLoS Pathog* **2015**, *11*, e1004995.
144. Beigel, J. H.; Nam, H. H.; Adams, P. L.; Krafft, A.; Ince, W. L.; El-Kamary, S. S.; Sims, A. C., Advances in respiratory virus therapeutics – A meeting report from the 6th isirv Antiviral Group conference. *Antiviral Research* **2019**, *167*, 45-67.
145. Palivizumab, a Humanized Respiratory Syncytial Virus Monoclonal Antibody, Reduces Hospitalization From Respiratory Syncytial Virus Infection in High-risk Infants. *Pediatrics* **1998**, *102*, 531-7.
146. Saez-Llorens, X.; Moreno, M. T.; Ramilo, O.; Sanchez, P. J.; Top, F. H., Jr.; Connor, E. M.; Group, M.-S., Safety and pharmacokinetics of palivizumab therapy in children hospitalized with respiratory syncytial virus infection. *Pediatr Infect Dis J* **2004**, *23*, 707-12.
147. Detalle, L.; Stohr, T.; Palomo, C.; Piedra, P. A.; Gilbert, B. E.; Mas, V.; Millar, A.; Power, U. F.; Stortelers, C.; Allosery, K.; Melero, J. A.; Depla, E., Generation and Characterization of ALX-0171, a Potent Novel Therapeutic Nanobody for the Treatment of Respiratory Syncytial Virus Infection. *Antimicrob Agents Chemother* **2016**, *60*, 6-13.
148. Hultberg, A.; Temperton, N. J.; Rosseels, V.; Koenders, M.; Gonzalez-Pajuelo, M.; Schepens, B.; Ibanez, L. I.; Vanlandschoot, P.; Schillemans, J.; Saunders, M.; Weiss, R. A.; Saelens, X.; Melero, J. A.; Verrips, C. T.; Van Gucht, S.; de Haard, H. J., Llama-derived single domain antibodies to build multivalent, superpotent and broadened neutralizing anti-viral molecules. *PLoS One* **2011**, *6*, e17665.
149. Zhu, Q.; McLellan, J. S.; Kallewaard, N. L.; Ulbrandt, N. D.; Palaszynski, S.; Zhang, J.; Moldt, B.; Khan, A.; Svabek, C.; McAuliffe, J. M.; Wrapp, D.; Patel, N. K.; Cook, K. E.; Richter, B. W. M.; Ryan, P. C.; Yuan, A. Q.; Suzich, J. A., A highly potent extended half-life antibody as a potential RSV vaccine surrogate for all infants. *Sci Transl Med* **2017**, *9*.
150. Domachowske, J. B.; Khan, A. A.; Esser, M. T.; Jensen, K.; Takas, T.; Villafana, T.; Dubovsky, F.; Griffin, M. P., Safety, Tolerability and Pharmacokinetics of MEDI8897, an Extended Half-life Single-dose Respiratory Syncytial Virus Prefusion F-targeting Monoclonal Antibody Administered as a Single Dose to Healthy Preterm Infants. *Pediatr Infect Dis J* **2018**, *37*, 886-892.
151. Griffin, M. P.; Khan, A. A.; Esser, M. T.; Jensen, K.; Takas, T.; Kankam, M. K.; Villafana, T.; Dubovsky, F., Safety, Tolerability, and Pharmacokinetics of MEDI8897, the Respiratory Syncytial Virus Prefusion F-

- Targeting Monoclonal Antibody with an Extended Half-Life, in Healthy Adults. *Antimicrob Agents Chemother* **2017**, *61*.
152. Hall, C. B.; Walsh, E. E.; Long, C. E.; Schnabel, K. C., Immunity to and frequency of reinfection with respiratory syncytial virus. *J Infect Dis* **1991**, *163*, 693-8.
153. Kim, H. W.; Canchola, J. G.; Brandt, C. D.; Pyles, G.; Chanock, R. M.; Jensen, K.; Parrott, R. H., Respiratory syncytial virus disease in infants despite prior administration of antigenic inactivated vaccine. *Am J Epidemiol* **1969**, *89*, 422-34.
154. Baicus, A., History of polio vaccination. *World J Virol* **2012**, *1*, 108-14.
155. Jancar, S.; Sanchez Crespo, M., Immune complex-mediated tissue injury: a multistep paradigm. *Trends Immunol* **2005**, *26*, 48-55.
156. Polack, F. P.; Teng, M. N.; Collins, P. L.; Prince, G. A.; Exner, M.; Regele, H.; Lirman, D. D.; Rabold, R.; Hoffman, S. J.; Karp, C. L.; Kleeberger, S. R.; Wills-Karp, M.; Karron, R. A., A role for immune complexes in enhanced respiratory syncytial virus disease. *J Exp Med* **2002**, *196*, 859-65.
157. Delgado, M. F.; Coviello, S.; Monsalvo, A. C.; Melendi, G. A.; Hernandez, J. Z.; Batalle, J. P.; Diaz, L.; Trento, A.; Chang, H. Y.; Mitzner, W.; Ravetch, J.; Melero, J. A.; Irusta, P. M.; Polack, F. P., Lack of antibody affinity maturation due to poor Toll-like receptor stimulation leads to enhanced respiratory syncytial virus disease. *Nat Med* **2009**, *15*, 34-41.
158. Smith, G.; Raghunandan, R.; Wu, Y.; Liu, Y.; Massare, M.; Nathan, M.; Zhou, B.; Lu, H.; Boddapati, S.; Li, J.; Flyer, D.; Glenn, G., Respiratory syncytial virus fusion glycoprotein expressed in insect cells form protein nanoparticles that induce protective immunity in cotton rats. *PLoS One* **2012**, *7*, e50852.
159. Karron, R. A.; Buchholz, U. J.; Collins, P. L., Live-attenuated respiratory syncytial virus vaccines. *Curr Top Microbiol Immunol* **2013**, *372*, 259-84.
160. Wright, P. F.; Karron, R. A.; Belshe, R. B.; Thompson, J.; Crowe, J. E., Jr.; Boyce, T. G.; Halburnt, L. L.; Reed, G. W.; Whitehead, S. S.; Anderson, E. L.; Wittek, A. E.; Casey, R.; Eichelberger, M.; Thumar, B.; Randolph, V. B.; Udem, S. A.; Chanock, R. M.; Murphy, B. R., Evaluation of a live, cold-passaged, temperature-sensitive, respiratory syncytial virus vaccine candidate in infancy. *J Infect Dis* **2000**, *182*, 1331-42.
161. Malkin, E.; Yogev, R.; Abughali, N.; Sliman, J.; Wang, C. K.; Zuo, F.; Yang, C. F.; Eickhoff, M.; Esser, M. T.; Tang, R. S.; Dubovsky, F., Safety and immunogenicity of a live attenuated RSV vaccine in healthy RSV-seronegative children 5 to 24 months of age. *PLoS One* **2013**, *8*, e77104.

162. Johnson, S.; Oliver, C.; Prince, G. A.; Hemming, V. G.; Pfarr, D. S.; Wang, S. C.; Dormitzer, M.; O'Grady, J.; Koenig, S.; Tamura, J. K.; Woods, R.; Bansal, G.; Couchenour, D.; Tsao, E.; Hall, W. C.; Young, J. F., Development of a humanized monoclonal antibody (MEDI-493) with potent in vitro and in vivo activity against respiratory syncytial virus. *J Infect Dis* **1997**, *176*, 1215-24.
163. Prevention of respiratory syncytial virus infections: indications for the use of palivizumab and update on the use of RSV-IGIV. American Academy of Pediatrics Committee on Infectious Diseases and Committee of Fetus and Newborn. *Pediatrics* **1998**, *102*, 1211-6.
164. Feltes, T. F.; Cabalka, A. K.; Meissner, H. C.; Piazza, F. M.; Carlin, D. A.; Top, F. H., Jr.; Connor, E. M.; Sondheimer, H. M.; Cardiac Synagis Study, G., Palivizumab prophylaxis reduces hospitalization due to respiratory syncytial virus in young children with hemodynamically significant congenital heart disease. *J Pediatr* **2003**, *143*, 532-40.
165. Geskey, J. M.; Thomas, N. J.; Brummel, G. L., Palivizumab: a review of its use in the protection of high risk infants against respiratory syncytial virus (RSV). *Biologics* **2007**, *1*, 33-43.
166. Hampp, C.; Kauf, T. L.; Saidi, A. S.; Winterstein, A. G., Cost-effectiveness of respiratory syncytial virus prophylaxis in various indications. *Arch Pediatr Adolesc Med* **2011**, *165*, 498-505.
167. Banerji, A.; Lanctot, K. L.; Paes, B. A.; Masoud, S. T.; Tam, D. Y.; Macdonald, W. A.; Roberts, A., Comparison of the cost of hospitalization for respiratory syncytial virus disease versus palivizumab prophylaxis in Canadian Inuit infants. *Pediatr Infect Dis J* **2009**, *28*, 702-6.
168. Malley, R.; DeVincenzo, J.; Ramilo, O.; Dennehy, P. H.; Meissner, H. C.; Gruber, W. C.; Sanchez, P. J.; Jafri, H.; Balsley, J.; Carlin, D.; Buckingham, S.; Vernacchio, L.; Ambrosino, D. M., Reduction of respiratory syncytial virus (RSV) in tracheal aspirates in intubated infants by use of humanized monoclonal antibody to RSV F protein. *J Infect Dis* **1998**, *178*, 1555-61.
169. Helmink, B. J.; Ragsdale, C. E.; Peterson, E. J.; Merkel, K. G., Comparison of Intravenous Palivizumab and Standard of Care for Treatment of Respiratory Syncytial Virus Infection in Mechanically Ventilated Pediatric Patients. *J Pediatr Pharmacol Ther* **2016**, *21*, 146-54.
170. Lauring, A. S.; Andino, R., Quasispecies theory and the behavior of RNA viruses. *PLoS Pathog* **2010**, *6*, e1001005.
171. Crowe, J. E.; Firestone, C. Y.; Crim, R.; Beeler, J. A.; Coelingh, K. L.; Barbas, C. F.; Burton, D. R.; Chanock, R. M.; Murphy, B. R., Monoclonal antibody-resistant mutants selected with a respiratory syncytial virus-neutralizing human antibody fab fragment (Fab 19) define a unique epitope on the fusion (F) glycoprotein. *Virology* **1998**, *252*, 373-5.

172. Zhao, X.; Chen, F. P.; Sullender, W. M., Respiratory syncytial virus escape mutant derived in vitro resists palivizumab prophylaxis in cotton rats. *Virology* **2004**, *318*, 608-12.
173. Zhu, Q.; Patel, N. K.; McAuliffe, J. M.; Zhu, W.; Wachter, L.; McCarthy, M. P.; Suzich, J. A., Natural polymorphisms and resistance-associated mutations in the fusion protein of respiratory syncytial virus (RSV): effects on RSV susceptibility to palivizumab. *J Infect Dis* **2012**, *205*, 635-8.
174. Boivin, G.; Caouette, G.; Frenette, L.; Carbonneau, J.; Ouakki, M.; De Serres, G., Human respiratory syncytial virus and other viral infections in infants receiving palivizumab. *J Clin Virol* **2008**, *42*, 52-7.
175. Zhu, Q.; McAuliffe, J. M.; Patel, N. K.; Palmer-Hill, F. J.; Yang, C. F.; Liang, B.; Su, L.; Zhu, W.; Wachter, L.; Wilson, S.; MacGill, R. S.; Krishnan, S.; McCarthy, M. P.; Losonsky, G. A.; Suzich, J. A., Analysis of respiratory syncytial virus preclinical and clinical variants resistant to neutralization by monoclonal antibodies palivizumab and/or motavizumab. *J Infect Dis* **2011**, *203*, 674-82.
176. DeVincenzo, J. P.; Hall, C. B.; Kimberlin, D. W.; Sanchez, P. J.; Rodriguez, W. J.; Jantusch, B. A.; Corey, L.; Kahn, J. S.; Englund, J. A.; Suzich, J. A.; Palmer-Hill, F. J.; Branco, L.; Johnson, S.; Patel, N. K.; Piazza, F. M., Surveillance of clinical isolates of respiratory syncytial virus for palivizumab (Synagis)-resistant mutants. *J Infect Dis* **2004**, *190*, 975-8.
177. Bem, R. A.; Domachowske, J. B.; Rosenberg, H. F., Animal models of human respiratory syncytial virus disease. *Am J Physiol Lung Cell Mol Physiol* **2011**, *301*, L148-56.
178. Taylor, G., Animal models of respiratory syncytial virus infection. *Vaccine* **2017**, *35*, 469-480.
179. Stark, J. M.; McDowell, S. A.; Koenigsnecht, V.; Prows, D. R.; Leikauf, J. E.; Le Vine, A. M.; Leikauf, G. D., Genetic susceptibility to respiratory syncytial virus infection in inbred mice. *J Med Virol* **2002**, *67*, 92-100.
180. Heylen, E.; Neyts, J.; Jochmans, D., Drug candidates and model systems in respiratory syncytial virus antiviral drug discovery. *Biochem Pharmacol* **2017**, *127*, 1-12.
181. Rouan, M. C.; Gevers, T.; Roymans, D.; de Zwart, L.; Nauwelaers, D.; De Meulder, M.; van Remoortere, P.; Vanstockem, M.; Koul, A.; Simmen, K.; Andries, K., Pharmacokinetics-pharmacodynamics of a respiratory syncytial virus fusion inhibitor in the cotton rat model. *Antimicrob Agents Chemother* **2010**, *54*, 4534-9.
182. Atienza, B. J. P.; Jensen, L. D.; Noton, S. L.; Ansalem, A. K. V.; Hobman, T.; Fearn, R.; Marchant, D. J.; West, F. G., Dual Catalytic Synthesis of Antiviral Compounds Based on Metallocarbene–Azide Cascade Chemistry. *The Journal of Organic Chemistry* **2018**, *83*, 6829-6842.

Chapter 2

1. Collins, P. L.; Graham, B. S., Viral and Host Factors in Human Respiratory Syncytial Virus Pathogenesis. *J. Virol.* **2008**, *82*, 2040.
2. Hall, C. B.; Weinberg, G. A.; Iwane, M. K.; Blumkin, A. K.; Edwards, K. M.; Staat, M. A.; Auinger, P.; Griffin, M. R.; Poehling, K. A.; Erdman, D.; Grijalva, C. G.; Zhu, Y.; Szilagyi, P., The burden of respiratory syncytial virus infection in young children. *N Engl J Med* **2009**, *360*, 588-98.
3. Falsey, A. R.; Hennessey, P. A.; Formica, M. A.; Cox, C.; Walsh, E. E., Respiratory syncytial virus infection in elderly and high-risk adults. *N Engl J Med* **2005**, *352*, 1749-59.
4. Resch, B., Burden of respiratory syncytial virus infection in young children. *World J Clin Pediatr* **2012**, *1*, 8-12.
5. Piedimonte, G.; Perez, M. K., Respiratory syncytial virus infection and bronchiolitis. *Piedimonte G, Perez MK. Respiratory syncytial virus infection and bronchiolitis [published correction appears in Pediatr Rev. 2015 Feb;36(2):85]. Pediatr Rev.* **2014**, *35*, 519-530.
6. Pérez-Yarza, E. G.; Moreno, A.; Lázaro, P.; Mejías, A.; Ramilo, O., The association between respiratory syncytial virus infection and the development of childhood asthma: a systematic review of the literature. *Pediatr Infect Dis J* **2007**, *26*, 733-739.
7. Xu, L.; Gao, H.; Zeng, J.; Liu, J.; Lu, C.; Guan, X.; Qian, S.; Xie, Z., A fatal case associated with respiratory syncytial virus infection in a young child. *BMC infect. Dis.* **2018**, *18*, 217.
8. Blount, R. E., Jr.; Morris, J. A.; Savage, R. E., Recovery of cytopathogenic agent from chimpanzees with coryza. *Proc Soc Exp Biol Med* **1956**, *92*, 544-9.
9. Wegzyn, C.; Toh, L. K.; Notario, G.; Biguenet, S.; Unnebrink, K.; Park, C.; Makari, D.; Norton, M., Safety and Effectiveness of Palivizumab in Children at High Risk of Serious Disease Due to Respiratory Syncytial Virus Infection: A Systematic Review. *Infect Dis Ther* **2014**, *3*, 133-58.
10. Turner, T. L.; Kopp, B. T.; Paul, G.; Landgrave, L. C.; Hayes, D., Jr.; Thompson, R., Respiratory syncytial virus: current and emerging treatment options. *Clinicoecon Outcomes Res* **2014**, *6*, 217-25.
11. Jeffree, C. E.; Rixon, H. W. M.; Brown, G.; Aitken, J.; Sugrue, R. J., Distribution of the attachment (G) glycoprotein and GM1 within the envelope of mature respiratory syncytial virus filaments revealed using field emission scanning electron microscopy. *Virology* **2003**, *306*, 254-267.
12. Fields, B. N.; Knipe, D. M.; Howley, P. M., *Fields virology*. Wolters Kluwer Health/Lippincott Williams & Wilkins: Philadelphia, 2013.
13. Hacking, D.; Hull, J., Respiratory syncytial virus: viral biology and the host response. *J Infect* **2002**, *45*, 18-24.
14. Morin, B.; Kranzusch, P. J.; Rahmeh, A. A.; Whelan, S. P. J., The polymerase of negative-stranded RNA viruses. *Curr. Opin. Virol.* **2013**, *3*, 103-110.
15. Collins, P. L.; Fearn, R.; Graham, B. S., Respiratory syncytial virus: virology, reverse genetics, and pathogenesis of disease. *Curr. Top. Microbiol. Immunol.* **2013**, *372*, 3-38.

16. Noton, S. L.; Deflubé, L. R.; Tremaglio, C. Z.; Fearn, R., The Respiratory Syncytial Virus Polymerase Has Multiple RNA Synthesis Activities at the Promoter. *PLoS Pathog.* **2012**, *8*, e1002980.
17. Khattar, S. K.; Yunus, A. S.; Samal, S. K., Mapping the domains on the phosphoprotein of bovine respiratory syncytial virus required for N–P and P–L interactions using a minigenome system. *J. Gen. Virol.* **2001**, *82*, 775-779.
18. Gilman, M. S. A.; Liu, C.; Fung, A.; Behera, I.; Jordan, P.; Rigaux, P.; Ysebaert, N.; Tcherniuk, S.; Sourimant, J.; Eléouët, J.-F.; Sutto-Ortiz, P.; Decroly, E.; Roymans, D.; Jin, Z.; McLellan, J. S., Structure of the Respiratory Syncytial Virus Polymerase Complex. *Cell* **2019**, *179*, 193-204.e14.
19. Elawar, F.; Oraby, A. K.; Kieser, Q.; Jensen, L. D.; Culp, T.; West, F. G.; Marchant, D. J., Pharmacological targets and emerging treatments for respiratory syncytial virus bronchiolitis. *Pharmacology & Therapeutics* **2021**, *220*, 107712.
20. Atienza, B. J. P.; Jensen, L. D.; Noton, S. L.; Ansalem, A. K. V.; Hobman, T.; Fearn, R.; Marchant, D. J.; West, F. G., Dual Catalytic Synthesis of Antiviral Compounds Based on Metallocarbene–Azide Cascade Chemistry. *The Journal of Organic Chemistry* **2018**, *83*, 6829-6842.
21. Schrödinger, L. & DeLano, W., 2020. PyMOL, Available at: <http://www.pymol.org/pymol>.
22. Sutto-Ortiz, P.; Tcherniuk, S.; Ysebaert, N.; Abeywickrema, P.; Noël, M.; Decombe, A.; Debart, F.; Vasseur, J.-J.; Canard, B.; Roymans, D.; Rigaux, P.; Eléouët, J.-F.; Decroly, E., The methyltransferase domain of the Respiratory Syncytial Virus L protein catalyzes cap N7 and 2'-O-methylation. *PLoS Pathogens* **2021**, *17*, e1009562.
23. Battles, M. B.; Langedijk, J. P.; Furmanova-Hollenstein, P.; Chaiwatpongsakorn, S.; Costello, H. M.; Kwanten, L.; Vranckx, L.; Vink, P.; Jaensch, S.; Jonckers, T. H. M.; Koul, A.; Arnoult, E.; Peeples, M. E.; Roymans, D.; McLellan, J. S., Molecular mechanism of respiratory syncytial virus fusion inhibitors. *Nat. Chem. Biol.* **2016**, *12*, 87-93.
24. Le Guilloux, V.; Schmidtke, P.; Tuffery, P., Fpocket: An open source platform for ligand pocket detection. *BMC Bioinformatics* **2009**, *10*, 168.
25. Halgren, T., New Method for Fast and Accurate Binding-site Identification and Analysis. *Chemical Biology & Drug Design* **2007**, *69*, 146-148.
26. Halgren, T. A., Identifying and Characterizing Binding Sites and Assessing Druggability. *Journal of Chemical Information and Modeling* **2009**, *49*, 377-389.
27. Krivák, R.; Hoksza, D., Improving protein-ligand binding site prediction accuracy by classification of inner pocket points using local features. *Journal of Cheminformatics* **2015**, *7*, 12.
28. Lu, X.; McDonald, S. M.; Tortorici, M. A.; Tao, Y. J.; Vasquez-Del Carpio, R.; Nibert, M. L.; Patton, J. T.; Harrison, S. C., Mechanism for coordinated RNA packaging and genome replication by rotavirus polymerase VP1. *Structure* **2008**, *16*, 1678-88.
29. Cao, D.; Gao, Y.; Roesler, C.; Rice, S.; D'Cunha, P.; Zhuang, L.; Slack, J.; Domke, M.; Antonova, A.; Romanelli, S.; Keating, S.; Forero, G.; Juneja, P.; Liang, B., Cryo-EM structure of the respiratory syncytial virus RNA polymerase. *Nat Commun* **2020**, *11*, 368.

30. De Vivo, M.; Masetti, M.; Bottegoni, G.; Cavalli, A., Role of Molecular Dynamics and Related Methods in Drug Discovery. *Journal of Medicinal Chemistry* **2016**, *59*, 4035-4061.
31. Jacobson, M. P.; Pincus, D. L.; Rapp, C. S.; Day, T. J. F.; Honig, B.; Shaw, D. E.; Friesner, R. A., A hierarchical approach to all-atom protein loop prediction. *Proteins: Structure, Function, and Bioinformatics* **2004**, *55*, 351-367.
32. Friesner, R. A.; Murphy, R. B.; Repasky, M. P.; Frye, L. L.; Greenwood, J. R.; Halgren, T. A.; Sanschagrin, P. C.; Mainz, D. T., Extra Precision Glide: Docking and Scoring Incorporating a Model of Hydrophobic Enclosure for Protein–Ligand Complexes. *Journal of Medicinal Chemistry* **2006**, *49*, 6177-6196.
33. Wang, E.; Liu, H.; Wang, J.; Weng, G.; Sun, H.; Wang, Z.; Kang, Y.; Hou, T., Development and Evaluation of MM/GBSA Based on a Variable Dielectric GB Model for Predicting Protein–Ligand Binding Affinities. *Journal of Chemical Information and Modeling* **2020**, *60*, 5353-5365.
34. Chen, J.; Wang, J.; Zhang, Q.; Chen, K.; Zhu, W., Probing Origin of Binding Difference of inhibitors to MDM2 and MDMX by Polarizable Molecular Dynamics Simulation and QM/MM-GBSA Calculation. *Scientific Reports* **2015**, *5*, 17421.
35. Weng, Y. L.; Naik, S. R.; Dingelstad, N.; Lugo, M. R.; Kalyaanamoorthy, S.; Ganesan, A., Molecular dynamics and in silico mutagenesis on the reversible inhibitor-bound SARS-CoV-2 main protease complexes reveal the role of lateral pocket in enhancing the ligand affinity. *Scientific Reports* **2021**, *11*, 7429.
36. Misaki, T.; Nagase, R.; Matsumoto, K.; Tanabe, Y., Ti-Crossed-Claisen Condensation between Carboxylic Esters and Acid Chlorides or Acids: A Highly Selective and General Method for the Preparation of Various β -Keto Esters. *Journal of the American Chemical Society* **2005**, *127*, 2854-2855.
37. Jiang, X.; Hu, F., One-Pot Highly Regioselective Synthesis of Indole-Fused Pyridazino[4,5-b][1,4]benzoxazepin-4(3H)-ones by a Smiles Rearrangement. *Synlett* **2018**, *29*, 1207-1210.
38. Jacobson, M. P.; Friesner, R. A.; Xiang, Z.; Honig, B., On the Role of the Crystal Environment in Determining Protein Side-chain Conformations. *Journal of Molecular Biology* **2002**, *320*, 597-608.
39. Maier, J. A.; Martinez, C.; Kasavajhala, K.; Wickstrom, L.; Hauser, K. E.; Simmerling, C., ff14SB: Improving the Accuracy of Protein Side Chain and Backbone Parameters from ff99SB. *Journal of Chemical Theory and Computation* **2015**, *11*, 3696-3713.
40. Mark, P.; Nilsson, L., Structure and Dynamics of the TIP3P, SPC, and SPC/E Water Models at 298 K. *The Journal of Physical Chemistry A* **2001**, *105*, 9954-9960.
41. Vilar, S.; Cozza, G.; Moro, S., Medicinal chemistry and the molecular operating environment (MOE): application of QSAR and molecular docking to drug discovery. *Curr Top Med Chem* **2008**, *8*, 1555-72.
42. Shelley, J. C.; Cholleti, A.; Frye, L. L.; Greenwood, J. R.; Timlin, M. R.; Uchimaya, M., Epik: a software program for pK_a prediction and protonation state generation for drug-like molecules. *Journal of Computer-Aided Molecular Design* **2007**, *21*, 681-691.

43. Roos, K.; Wu, C.; Damm, W.; Reboul, M.; Stevenson, J. M.; Lu, C.; Dahlgren, M. K.; Mondal, S.; Chen, W.; Wang, L.; Abel, R.; Friesner, R. A.; Harder, E. D., OPLS3e: Extending Force Field Coverage for Drug-Like Small Molecules. *Journal of Chemical Theory and Computation* **2019**, *15*, 1863-1874.
44. Wang, J.; Wang, W.; Kollman, P. A.; Case, D. A., Automatic atom type and bond type perception in molecular mechanical calculations. *J Mol Graph Model* **2006**, *25*, 247-60.
45. Wang, J.; Wolf, R. M.; Caldwell, J. W.; Kollman, P. A.; Case, D. A., Development and testing of a general amber force field. *J Comput Chem* **2004**, *25*, 1157-74.
46. Jakalian, A.; Jack, D. B.; Bayly, C. I., Fast, efficient generation of high-quality atomic charges. AM1-BCC model: II. Parameterization and validation. *Journal of Computational Chemistry* **2002**, *23*, 1623-1641.
47. Roe, D. R.; Cheatham, T. E., PTRAJ and CPPTRAJ: Software for Processing and Analysis of Molecular Dynamics Trajectory Data. *Journal of Chemical Theory and Computation* **2013**, *9*, 3084-3095.
48. Miller, B. R.; McGee, T. D.; Swails, J. M.; Homeyer, N.; Gohlke, H.; Roitberg, A. E., MMPBSA.py: An Efficient Program for End-State Free Energy Calculations. *Journal of Chemical Theory and Computation* **2012**, *8*, 3314-3321.

Chapter 3

1. Van Der Hoek, L., Human Coronaviruses: What Do They Cause? *Antiviral Therapy* **2005**, *12*, 651-658.
2. LeDuc, J. W.; Barry, M. A., SARS, the First Pandemic of the 21st Century. *Emerg Infect Dis* **2004**, *10*, e26-e26.
3. Ramadan, N.; Shaib, H., Middle East respiratory syndrome coronavirus (MERS-CoV): A review. *Germes* **2019**, *9*, 35-42.
4. Zhou, P.; Yang, X.-L.; Wang, X.-G.; Hu, B.; Zhang, L.; Zhang, W.; Si, H.-R.; Zhu, Y.; Li, B.; Huang, C.-L.; Chen, H.-D.; Chen, J.; Luo, Y.; Guo, H.; Jiang, R.-D.; Liu, M.-Q.; Chen, Y.; Shen, X.-R.; Wang, X.; Zheng, X.-S.; Zhao, K.; Chen, Q.-J.; Deng, F.; Liu, L.-L.; Yan, B.; Zhan, F.-X.; Wang, Y.-Y.; Xiao, G.-F.; Shi, Z.-L., A pneumonia outbreak associated with a new coronavirus of probable bat origin. *Nature* **2020**, *579*, 270-273.
5. Wu, F.; Zhao, S.; Yu, B.; Chen, Y.-M.; Wang, W.; Song, Z.-G.; Hu, Y.; Tao, Z.-W.; Tian, J.-H.; Pei, Y.-Y.; Yuan, M.-L.; Zhang, Y.-L.; Dai, F.-H.; Liu, Y.; Wang, Q.-M.; Zheng, J.-J.; Xu, L.; Holmes, E. C.; Zhang, Y.-Z., A new coronavirus associated with human respiratory disease in China. *Nature* **2020**, *579*, 265-269.
6. Hadj Hassine, I., Covid-19 vaccines and variants of concern: A review. *Reviews in Medical Virology* **2021**, *n/a*, e2313.
7. Pushpakom, S.; Iorio, F.; Eyers, P. A.; Escott, K. J.; Hopper, S.; Wells, A.; Doig, A.; Guilliams, T.; Latimer, J.; McNamee, C.; Norris, A.; Sanseau, P.; Cavalla, D.; Pirmohamed, M., Drug repurposing: progress, challenges and recommendations. *Nature Reviews Drug Discovery* **2019**, *18*, 41-58.
8. Geraghty, R. J.; Aliota, M. T.; Bonnac, L. F., Broad-Spectrum Antiviral Strategies and Nucleoside Analogues. *Viruses* **2021**, *13*.

9. Gentile, I.; Maraolo, A. E.; Buonomo, A. R.; Zappulo, E.; Borgia, G., The discovery of sofosbuvir: a revolution for therapy of chronic hepatitis C. *Expert Opinion on Drug Discovery* **2015**, *10*, 1363-1377.
10. Asselah, T.; Boyer, N.; Saadoun, D.; Martinot-Peignoux, M.; Marcellin, P., Direct-acting antivirals for the treatment of hepatitis C virus infection: optimizing current IFN-free treatment and future perspectives. *Liver International* **2016**, *36*, 47-57.
11. Teoh, S. L.; Lim, Y. H.; Lai, N. M.; Lee, S. W. H., Directly Acting Antivirals for COVID-19: Where Do We Stand? *Frontiers in Microbiology* **2020**, *11*.
12. Beigel, J. H.; Tomashek, K. M.; Dodd, L. E.; Mehta, A. K.; Zingman, B. S.; Kalil, A. C.; Hohmann, E.; Chu, H. Y.; Luetkemeyer, A.; Kline, S.; Lopez de Castilla, D.; Finberg, R. W.; Dierberg, K.; Tapson, V.; Hsieh, L.; Patterson, T. F.; Paredes, R.; Sweeney, D. A.; Short, W. R.; Touloumi, G.; Lye, D. C.; Ohmagari, N.; Oh, M.-d.; Ruiz-Palacios, G. M.; Benfield, T.; Fätkenheuer, G.; Kortepeter, M. G.; Atmar, R. L.; Creech, C. B.; Lundgren, J.; Babiker, A. G.; Pett, S.; Neaton, J. D.; Burgess, T. H.; Bonnett, T.; Green, M.; Makowski, M.; Osinusi, A.; Nayak, S.; Lane, H. C., Remdesivir for the Treatment of Covid-19 — Final Report. *New England Journal of Medicine* **2020**, *383*, 1813-1826.
13. Lo, M. K.; Jordan, R.; Arvey, A.; Sudhamsu, J.; Shrivastava-Ranjan, P.; Hotard, A. L.; Flint, M.; McMullan, L. K.; Siegel, D.; Clarke, M. O.; Mackman, R. L.; Hui, H. C.; Perron, M.; Ray, A. S.; Cihlar, T.; Nichol, S. T.; Spiropoulou, C. F., GS-5734 and its parent nucleoside analog inhibit Filo-, Pneumo-, and Paramyxoviruses. *Scientific Reports* **2017**, *7*, 43395.
14. Kokic, G.; Hillen, H. S.; Tegunov, D.; Dienemann, C.; Seitz, F.; Schmitzova, J.; Farnung, L.; Siewert, A.; Höbartner, C.; Cramer, P., Mechanism of SARS-CoV-2 polymerase stalling by remdesivir. *Nature Communications* **2021**, *12*, 279.
15. Gordon, C. J.; Lee, H. W.; Tchesnokov, E. P.; Perry, J. K.; Feng, J. Y.; Bilello, J. P.; Porter, D. P.; Götte, M., Efficient incorporation and template-dependent polymerase inhibition are major determinants for the broad-spectrum antiviral activity of remdesivir. *Journal of Biological Chemistry* **2022**, *298*.
16. Abdelnabi, R.; Foo, C. S.; Jochmans, D.; Vangeel, L.; De Jonghe, S.; Augustijns, P.; Mols, R.; Weynand, B.; Wattanakul, T.; Hoglund, R. M.; Tarning, J.; Mowbray, C. E.; Sjö, P.; Escudié, F.; Scandale, I.; Chatelain, E.; Neyts, J., The oral protease inhibitor (PF-07321332) protects Syrian hamsters against infection with SARS-CoV-2 variants of concern. *Nature Communications* **2022**, *13*, 719.
17. Atienza, B. J. P.; Jensen, L. D.; Noton, S. L.; Ansalem, A. K. V.; Hobman, T.; Fearn, R.; Marchant, D. J.; West, F. G., Dual Catalytic Synthesis of Antiviral Compounds Based on Metallocarbene–Azide Cascade Chemistry. *The Journal of Organic Chemistry* **2018**, *83*, 6829-6842.
18. Ahn, D.-G.; Choi, J.-K.; Taylor, D. R.; Oh, J.-W., Biochemical characterization of a recombinant SARS coronavirus nsp12 RNA-dependent RNA polymerase capable of copying viral RNA templates. *Archives of Virology* **2012**, *157*, 2095-2104.
19. Kirchdoerfer, R. N.; Ward, A. B., Structure of the SARS-CoV nsp12 polymerase bound to nsp7 and nsp8 co-factors. *Nature Communications* **2019**, *10*, 2342.

20. Gao, Y.; Yan, L.; Huang, Y.; Liu, F.; Zhao, Y.; Cao, L.; Wang, T.; Sun, Q.; Ming, Z.; Zhang, L.; Ge, J.; Zheng, L.; Zhang, Y.; Wang, H.; Zhu, Y.; Zhu, C.; Hu, T.; Hua, T.; Zhang, B.; Yang, X.; Li, J.; Yang, H.; Liu, Z.; Xu, W.; Guddat, L. W.; Wang, Q.; Lou, Z.; Rao, Z., Structure of the RNA-dependent RNA polymerase from COVID-19 virus. *Science* **2020**, *368*, 779-782.
21. Naydenova, K.; Muir, K. W.; Wu, L. F.; Zhang, Z.; Coscia, F.; Peet, M. J.; Castro-Hartmann, P.; Qian, P.; Sader, K.; Dent, K.; Kimanius, D.; Sutherland, J. D.; Lowe, J.; Barford, D.; Russo, C. J., Structure of the SARS-CoV-2 RNA-dependent RNA polymerase in the presence of favipiravir-RTP. *Proc Natl Acad Sci USA* **2021**, *118*.
22. Le Guilloux, V.; Schmidtke, P.; Tuffery, P., Fpocket: An open source platform for ligand pocket detection. *BMC Bioinformatics* **2009**, *10*, 168.
23. Halgren, T., New Method for Fast and Accurate Binding-site Identification and Analysis. *Chemical Biology & Drug Design* **2007**, *69*, 146-148.
24. Halgren, T. A., Identifying and Characterizing Binding Sites and Assessing Druggability. *Journal of Chemical Information and Modeling* **2009**, *49*, 377-389.
25. Krivák, R.; Hoksza, D., Improving protein-ligand binding site prediction accuracy by classification of inner pocket points using local features. *Journal of Cheminformatics* **2015**, *7*, 12.
26. Schmidtke, P.; Bidon-Chanal, A.; Luque, F. J.; Barril, X., MDpocket: open-source cavity detection and characterization on molecular dynamics trajectories. *Bioinformatics* **2011**, *27*, 3276-3285.
27. Friesner, R. A.; Murphy, R. B.; Repasky, M. P.; Frye, L. L.; Greenwood, J. R.; Halgren, T. A.; Sanschagrin, P. C.; Mainz, D. T., Extra Precision Glide: Docking and Scoring Incorporating a Model of Hydrophobic Enclosure for Protein-Ligand Complexes. *Journal of Medicinal Chemistry* **2006**, *49*, 6177-6196.
28. Morris, G. M.; Goodsell, D. S.; Halliday, R. S.; Huey, R.; Hart, W. E.; Belew, R. K.; Olson, A. J., Automated docking using a Lamarckian genetic algorithm and an empirical binding free energy function. *Journal of Computational Chemistry* **1998**, *19*, 1639-1662.
29. Vilar, S.; Cozza, G.; Moro, S., Medicinal chemistry and the molecular operating environment (MOE): application of QSAR and molecular docking to drug discovery. *Curr Top Med Chem* **2008**, *8*, 1555-72.
30. De Vivo, M.; Masetti, M.; Bottegoni, G.; Cavalli, A., Role of Molecular Dynamics and Related Methods in Drug Discovery. *Journal of Medicinal Chemistry* **2016**, *59*, 4035-4061.
31. Barducci, A.; Bonomi, M.; Parrinello, M., Metadynamics. *WIREs Computational Molecular Science* **2011**, *1*, 826-843.
32. Gervasio, F. L.; Laio, A.; Parrinello, M., Flexible Docking in Solution Using Metadynamics. *Journal of the American Chemical Society* **2005**, *127*, 2600-2607.
33. Russo, S.; Callegari, D.; Incerti, M.; Pala, D.; Giorgio, C.; Brunetti, J.; Bracci, L.; Vicini, P.; Barocelli, E.; Capoferri, L.; Rivara, S.; Tognolini, M.; Mor, M.; Lodola, A., Exploiting Free-Energy Minima to Design Novel EphA2 Protein-Protein Antagonists: From Simulation to Experiment and Return. *Chemistry – A European Journal* **2016**, *22*, 8048-8052.

34. Söderhjelm, P.; Tribello Gareth, A.; Parrinello, M., Locating binding poses in protein-ligand systems using reconnaissance metadynamics. *Proceedings of the National Academy of Sciences* **2012**, *109*, 5170-5175.
35. Fusani, L.; Palmer, D. S.; Somers, D. O.; Wall, I. D., Exploring Ligand Stability in Protein Crystal Structures Using Binding Pose Metadynamics. *Journal of Chemical Information and Modeling* **2020**, *60*, 1528-1539.
36. Clark, A. J.; Tiwary, P.; Borrelli, K.; Feng, S.; Miller, E. B.; Abel, R.; Friesner, R. A.; Berne, B. J., Prediction of Protein–Ligand Binding Poses via a Combination of Induced Fit Docking and Metadynamics Simulations. *Journal of Chemical Theory and Computation* **2016**, *12*, 2990-2998.
37. Wang, E.; Sun, H.; Wang, J.; Wang, Z.; Liu, H.; Zhang, J. Z. H.; Hou, T., End-Point Binding Free Energy Calculation with MM/PBSA and MM/GBSA: Strategies and Applications in Drug Design. *Chemical Reviews* **2019**, *119*, 9478-9508.
38. Misaki, T.; Nagase, R.; Matsumoto, K.; Tanabe, Y., Ti-Crossed-Claisen Condensation between Carboxylic Esters and Acid Chlorides or Acids: A Highly Selective and General Method for the Preparation of Various β -Keto Esters. *Journal of the American Chemical Society* **2005**, *127*, 2854-2855.
39. Brooks, W. H.; Guida, W. C.; Daniel, K. G., The significance of chirality in drug design and development. *Current topics in medicinal chemistry* **2011**, *11*, 760-770.
40. McConathy, J.; Owens, M. J., Stereochemistry in Drug Action. *Prim Care Companion J Clin Psychiatry* **2003**, *5*, 70-73.
41. Pescitelli, G., ECD exciton chirality method today: a modern tool for determining absolute configurations. *Chirality* **2022**, *34*, 333-363.
42. Yang, J.; Petitjean, S. J. L.; Koehler, M.; Zhang, Q.; Dumitru, A. C.; Chen, W.; Derclaye, S.; Vincent, S. P.; Soumillion, P.; Alsteens, D., Molecular interaction and inhibition of SARS-CoV-2 binding to the ACE2 receptor. *Nature Communications* **2020**, *11*, 4541.
43. Beyerstedt, S.; Casaro, E. B.; Rangel, É. B., COVID-19: angiotensin-converting enzyme 2 (ACE2) expression and tissue susceptibility to SARS-CoV-2 infection. *European Journal of Clinical Microbiology & Infectious Diseases* **2021**, *40*, 905-919.
44. Tchesnokov, E. P.; Gordon, C. J.; Woolner, E.; Kocinkova, D.; Perry, J. K.; Feng, J. Y.; Porter, D. P.; Götte, M., Template-dependent inhibition of coronavirus RNA-dependent RNA polymerase by remdesivir reveals a second mechanism of action. *Journal of Biological Chemistry* **2020**, *295*, 16156-16165.
45. Jacobson, M. P.; Pincus, D. L.; Rapp, C. S.; Day, T. J. F.; Honig, B.; Shaw, D. E.; Friesner, R. A., A hierarchical approach to all-atom protein loop prediction. *Proteins: Structure, Function, and Bioinformatics* **2004**, *55*, 351-367.
46. Jacobson, M. P.; Friesner, R. A.; Xiang, Z.; Honig, B., On the Role of the Crystal Environment in Determining Protein Side-chain Conformations. *Journal of Molecular Biology* **2002**, *320*, 597-608.
47. Maier, J. A.; Martinez, C.; Kasavajhala, K.; Wickstrom, L.; Hauser, K. E.; Simmerling, C., ff14SB: Improving the Accuracy of Protein Side Chain and Backbone Parameters from ff99SB. *Journal of Chemical Theory and Computation* **2015**, *11*, 3696-3713.

48. Mark, P.; Nilsson, L., Structure and Dynamics of the TIP3P, SPC, and SPC/E Water Models at 298 K. *The Journal of Physical Chemistry A* **2001**, *105*, 9954-9960.
49. Shelley, J. C.; Cholleti, A.; Frye, L. L.; Greenwood, J. R.; Timlin, M. R.; Uchimaya, M., Epik: a software program for pK_a prediction and protonation state generation for drug-like molecules. *Journal of Computer-Aided Molecular Design* **2007**, *21*, 681-691.
50. Roos, K.; Wu, C.; Damm, W.; Reboul, M.; Stevenson, J. M.; Lu, C.; Dahlgren, M. K.; Mondal, S.; Chen, W.; Wang, L.; Abel, R.; Friesner, R. A.; Harder, E. D., OPLS3e: Extending Force Field Coverage for Drug-Like Small Molecules. *Journal of Chemical Theory and Computation* **2019**, *15*, 1863-1874.
51. Wang, J.; Wang, W.; Kollman, P. A.; Case, D. A., Automatic atom type and bond type perception in molecular mechanical calculations. *J Mol Graph Model* **2006**, *25*, 247-60.
52. Wang, J.; Wolf, R. M.; Caldwell, J. W.; Kollman, P. A.; Case, D. A., Development and testing of a general amber force field. *J Comput Chem* **2004**, *25*, 1157-74.
53. Jakalian, A.; Jack, D. B.; Bayly, C. I., Fast, efficient generation of high-quality atomic charges. AM1-BCC model: II. Parameterization and validation. *Journal of Computational Chemistry* **2002**, *23*, 1623-1641.
54. Roe, D. R.; Cheatham, T. E., PTRAJ and CPPTRAJ: Software for Processing and Analysis of Molecular Dynamics Trajectory Data. *Journal of Chemical Theory and Computation* **2013**, *9*, 3084-3095.
55. Miller, B. R.; McGee, T. D.; Swails, J. M.; Homeyer, N.; Gohlke, H.; Roitberg, A. E., MMPBSA.py: An Efficient Program for End-State Free Energy Calculations. *Journal of Chemical Theory and Computation* **2012**, *8*, 3314-3321.
56. Schrödinger Release 2019-3: Maestro, Schrödinger, LLC, New York, NY.
57. Gordon, C. J.; Tchesnokov, E. P.; Woolner, E.; Perry, J. K.; Feng, J. Y.; Porter, D. P.; Götte, M., Remdesivir is a direct-acting antiviral that inhibits RNA-dependent RNA polymerase from severe acute respiratory syndrome coronavirus 2 with high potency. *Journal of Biological Chemistry* **2020**, *295*, 6785-6797.
58. Berger, I.; Garzoni, F.; Chaillet, M.; Haffke, M.; Gupta, K.; Aubert, A., The MultiBac Protein Complex Production Platform at the EMBL. *JoVE* **2013**, e50159.

Chapter 4

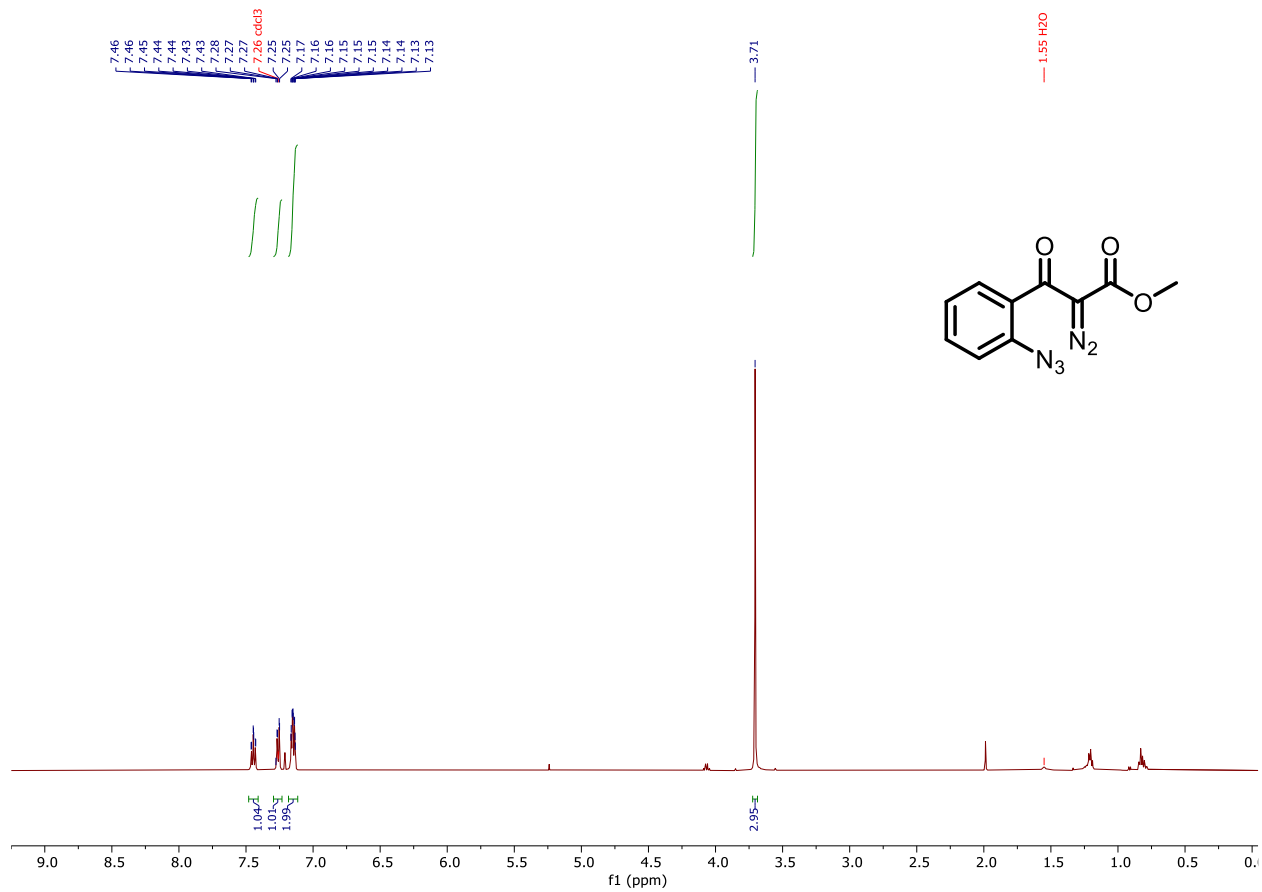
1. Griffiths, C.; Drews, S. J.; Marchant, D. J., Respiratory Syncytial Virus: Infection, Detection, and New Options for Prevention and Treatment. *Clin Microbiol Rev* **2017**, *30*, 277-319.
2. Elawar, F.; Oraby, A. K.; Kieser, Q.; Jensen, L. D.; Culp, T.; West, F. G.; Marchant, D. J., Pharmacological targets and emerging treatments for respiratory syncytial virus bronchiolitis. *Pharmacol Ther* **2021**, *220*, 107712.
3. Rodriguez-Fernandez, R.; Mejias, A.; Ramilo, O., Monoclonal Antibodies for Prevention of Respiratory Syncytial Virus Infection. *Pediatr Infect Dis J* **2021**, *40*, S35-S39.

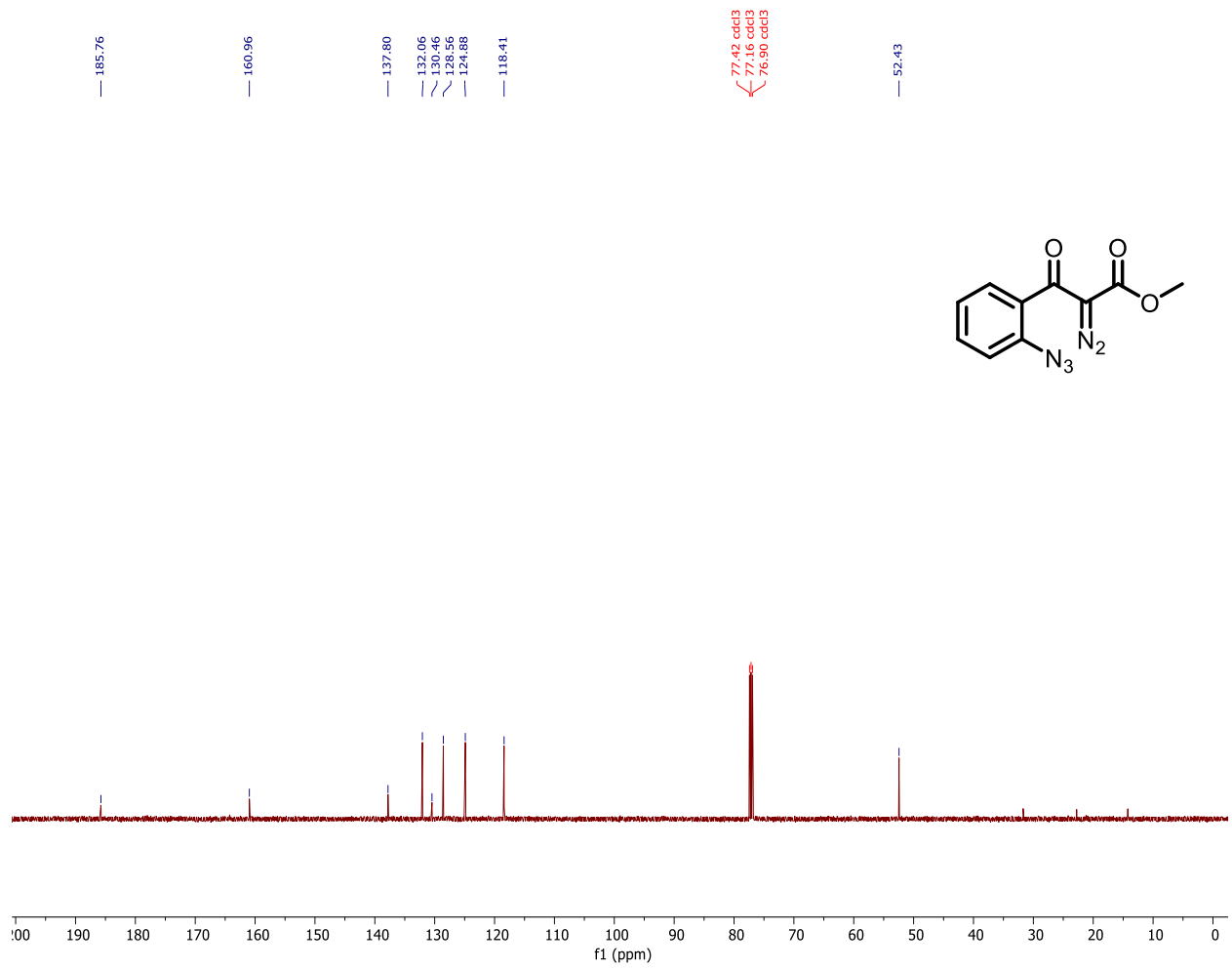
4. Zlateva, K. T.; Lemey, P.; Moes, E.; Vandamme, A. M.; Van Ranst, M., Genetic variability and molecular evolution of the human respiratory syncytial virus subgroup B attachment G protein. *J Virol* **2005**, *79*, 9157-67.
5. McLellan, J. S.; Chen, M.; Leung, S.; Graepel, K. W.; Du, X.; Yang, Y.; Zhou, T.; Baxa, U.; Yasuda, E.; Beaumont, T.; Kumar, A.; Modjarrad, K.; Zheng, Z.; Zhao, M.; Xia, N.; Kwong, P. D.; Graham, B. S., Structure of RSV fusion glycoprotein trimer bound to a prefusion-specific neutralizing antibody. *Science* **2013**, *340*, 1113-7.
6. McLellan, J. S., Neutralizing epitopes on the respiratory syncytial virus fusion glycoprotein. *Curr Opin Virol* **2015**, *11*, 70-5.
7. McLellan, J. S.; Yang, Y.; Graham, B. S.; Kwong, P. D., Structure of respiratory syncytial virus fusion glycoprotein in the postfusion conformation reveals preservation of neutralizing epitopes. *J Virol* **2011**, *85*, 7788-96.
8. Griffiths, C. D.; Bilawchuk, L. M.; McDonough, J. E.; Jamieson, K. C.; Elawar, F.; Cen, Y.; Duan, W.; Lin, C.; Song, H.; Casanova, J. L.; Ogg, S.; Jensen, L. D.; Thienpont, B.; Kumar, A.; Hobman, T. C.; Proud, D.; Moraes, T. J.; Marchant, D. J., IGF1R is an entry receptor for respiratory syncytial virus. *Nature* **2020**, *583*, 615-619.
9. Rodriguez-Fernandez, R.; Tapia, L. I.; Yang, C. F.; Torres, J. P.; Chavez-Bueno, S.; Garcia, C.; Jaramillo, L. M.; Moore-Clingenpeel, M.; Jafri, H. S.; Peeples, M. E.; Piedra, P. A.; Ramilo, O.; Mejias, A., Respiratory Syncytial Virus Genotypes, Host Immune Profiles, and Disease Severity in Young Children Hospitalized With Bronchiolitis. *J Infect Dis* **2017**, *217*, 24-34.
10. Elawar, F.; Griffiths, C. D.; Zhu, D.; Bilawchuk, L. M.; Jensen, L. D.; Forss, L.; Tang, J.; Hazes, B.; Drews, S. J.; Marchant, D. J., A Virological and Phylogenetic Analysis of the Emergence of New Clades of Respiratory Syncytial Virus. *Sci Rep* **2017**, *7*, 12232.
11. Phung, E.; Chang, L. A.; Morabito, K. M.; Kanekiyo, M.; Chen, M.; Nair, D.; Kumar, A.; Chen, G. L.; Ledgerwood, J. E.; Graham, B. S.; Ruckwardt, T. J., Epitope-Specific Serological Assays for RSV: Conformation Matters. *Vaccines (Basel)* **2019**, *7*.
12. Hause, A. M.; Henke, D. M.; Avadhanula, V.; Shaw, C. A.; Tapia, L. I.; Piedra, P. A., Sequence variability of the respiratory syncytial virus (RSV) fusion gene among contemporary and historical genotypes of RSV/A and RSV/B. *PLoS One* **2017**, *12*, e0175792.

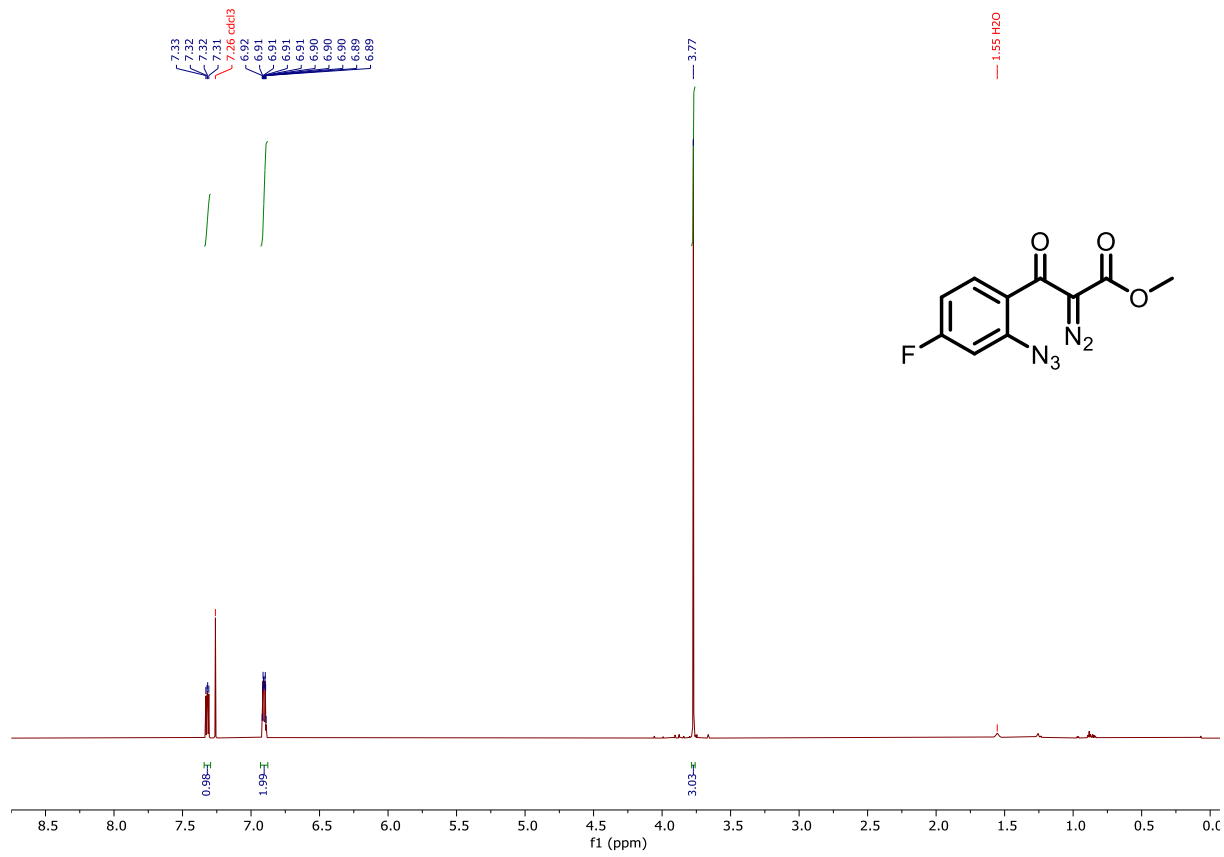
13. Zhang, L.; Peeples Mark, E.; Boucher Richard, C.; Collins Peter, L.; Pickles Raymond, J., Respiratory Syncytial Virus Infection of Human Airway Epithelial Cells Is Polarized, Specific to Ciliated Cells, and without Obvious Cytopathology. *Journal of Virology* **2002**, *76*, 5654-5666.
14. Mastrangelo, P.; Chin, A. A.; Tan, S.; Jeon, A. H.; Ackerley, C. A.; Siu, K. K.; Lee, J. E.; Hegele, R. G., Identification of RSV Fusion Protein Interaction Domains on the Virus Receptor, Nucleolin. *Viruses* **2021**, *13*.
15. Gilman, M. S. A.; Furmanova-Hollenstein, P.; Pascual, G.; A, B. v. t. W.; Langedijk, J. P. M.; McLellan, J. S., Transient opening of trimeric prefusion RSV F proteins. *Nat Commun* **2019**, *10*, 2105.
16. Gilman, M. S. A.; Furmanova-Hollenstein, P.; Pascual, G.; B. van 't Wout, A.; Langedijk, J. P. M.; McLellan, J. S., Transient opening of trimeric prefusion RSV F proteins. *Nature Communications* **2019**, *10*, 2105.
17. Zhu, Q.; McLellan Jason, S.; Kallewaard Nicole, L.; Ulbrandt Nancy, D.; Palaszynski, S.; Zhang, J.; Moldt, B.; Khan, A.; Svabek, C.; McAuliffe Josephine, M.; Wrapp, D.; Patel Nita, K.; Cook Kimberly, E.; Richter Bettina, W. M.; Ryan Patricia, C.; Yuan Andy, Q.; Suzich JoAnn, A., A highly potent extended half-life antibody as a potential RSV vaccine surrogate for all infants. *Science Translational Medicine* **2017**, *9*, eaaj1928.
18. Zhu, Q.; Lu, B.; McTamney, P.; Palaszynski, S.; Diallo, S.; Ren, K.; Ulbrandt, N. D.; Kallewaard, N.; Wang, W.; Fernandes, F.; Wong, S.; Svabek, C.; Moldt, B.; Esser, M. T.; Jing, H.; Suzich, J. A., Prevalence and Significance of Substitutions in the Fusion Protein of Respiratory Syncytial Virus Resulting in Neutralization Escape From Antibody MEDI8897. *J Infect Dis* **2018**, *218*, 572-580.
19. Atienza, B. J. P.; Jensen, L. D.; Noton, S. L.; Ansalem, A. K. V.; Hobman, T.; Fearn, R.; Marchant, D. J.; West, F. G., Dual Catalytic Synthesis of Antiviral Compounds Based on Metallocarbene-Azide Cascade Chemistry. *J Org Chem* **2018**, *83*, 6829-6842.
20. Chao, L., Fitness of RNA virus decreased by Muller's ratchet. *Nature* **1990**, *348*, 454-5.
21. Muller, H. J., The relation of recombination to mutational advance. *Mutation Research/Fundamental and Molecular Mechanisms of Mutagenesis* **1964**, *1*, 2-9.
22. Bilawchuk, L. M.; Griffiths, C. D.; Jensen, L. D.; Elawar, F.; Marchant, D. J., The Susceptibilities of Respiratory Syncytial Virus to Nucleolin Receptor Blocking and Antibody Neutralization are Dependent upon the Method of Virus Purification. *Viruses* **2017**, *9*.
23. Schrödinger Release 2019-3: Maestro, Schrödinger, LLC, New York, NY.

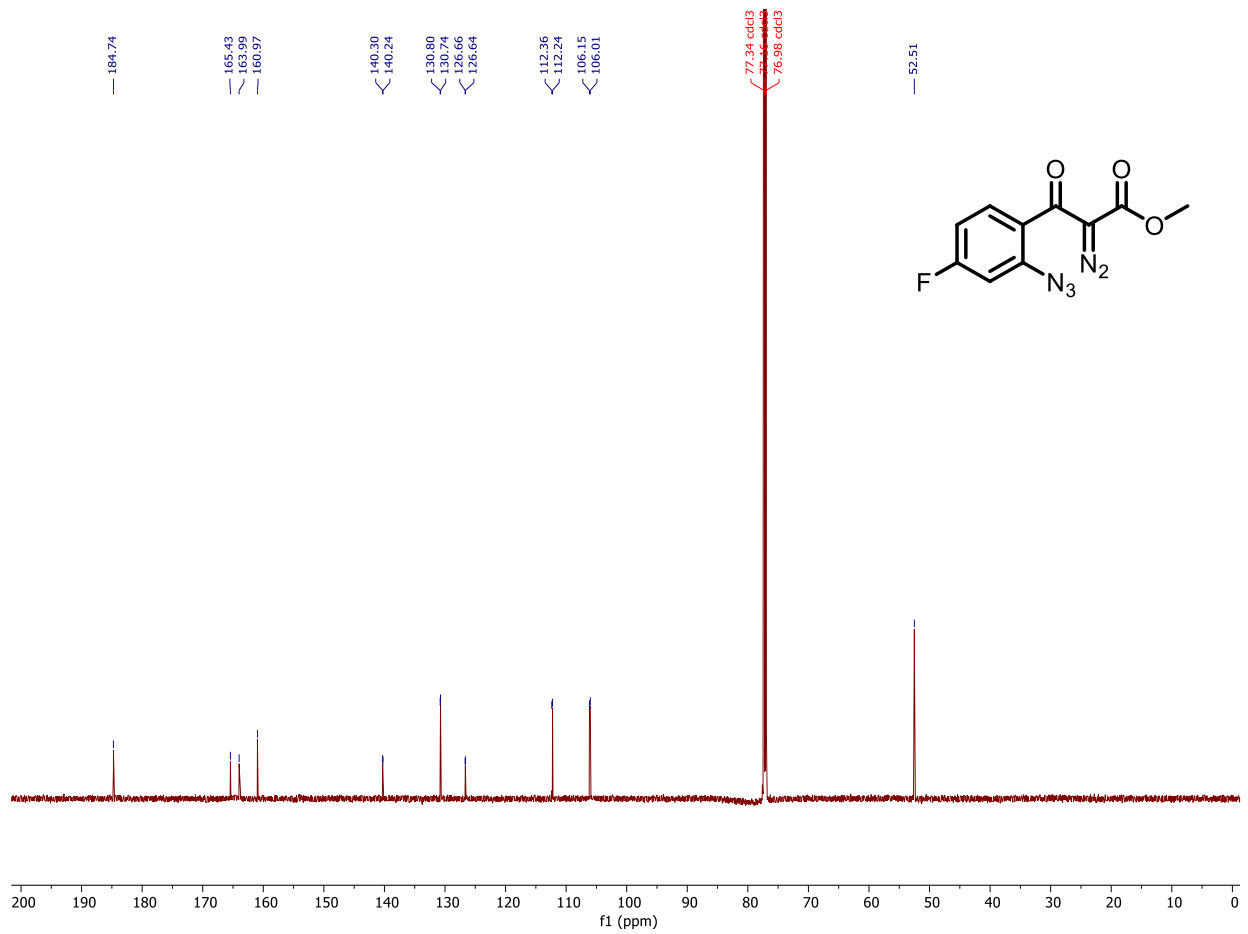
24. Shelley, J. C.; Cholleti, A.; Frye, L. L.; Greenwood, J. R.; Timlin, M. R.; Uchimaya, M., Epik: a software program for pK_a prediction and protonation state generation for drug-like molecules. *Journal of Computer-Aided Molecular Design* **2007**, *21*, 681-691.
25. Roos, K.; Wu, C.; Damm, W.; Reboul, M.; Stevenson, J. M.; Lu, C.; Dahlgren, M. K.; Mondal, S.; Chen, W.; Wang, L.; Abel, R.; Friesner, R. A.; Harder, E. D., OPLS3e: Extending Force Field Coverage for Drug-Like Small Molecules. *J Chem Theory Comput* **2019**, *15*, 1863-1874.
26. Mark, P.; Nilsson, L., Structure and Dynamics of the TIP3P, SPC, and SPC/E Water Models at 298 K. *The Journal of Physical Chemistry A* **2001**, *105*, 9954-9960.
27. Maier, J. A.; Martinez, C.; Kasavajhala, K.; Wickstrom, L.; Hauser, K. E.; Simmerling, C., ff14SB: Improving the Accuracy of Protein Side Chain and Backbone Parameters from ff99SB. *Journal of Chemical Theory and Computation* **2015**, *11*, 3696-3713.
28. Roe, D. R.; Cheatham, T. E., PTRAJ and CPPTRAJ: Software for Processing and Analysis of Molecular Dynamics Trajectory Data. *Journal of Chemical Theory and Computation* **2013**, *9*, 3084-3095.

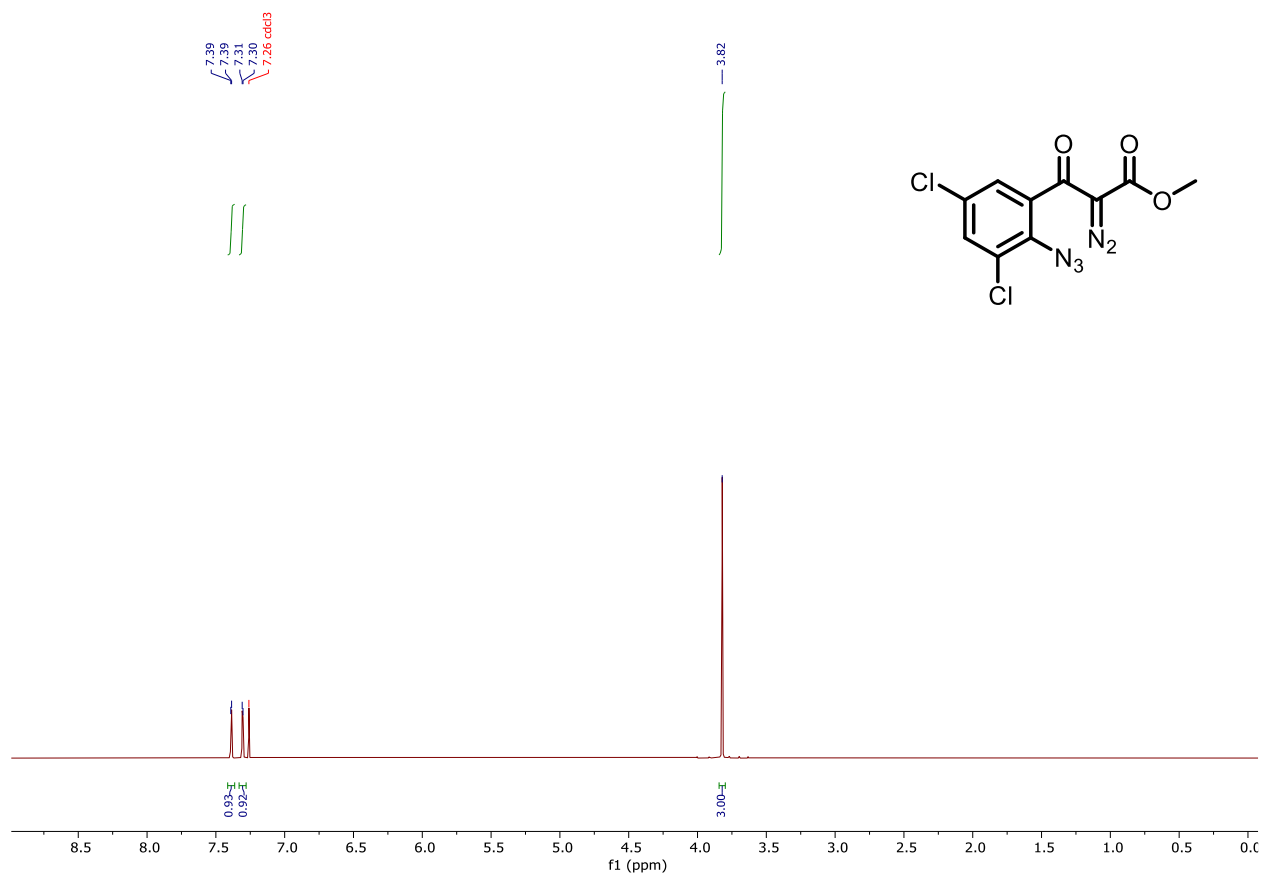
Appendix I
Selected NMR Spectra (Chapter 2)

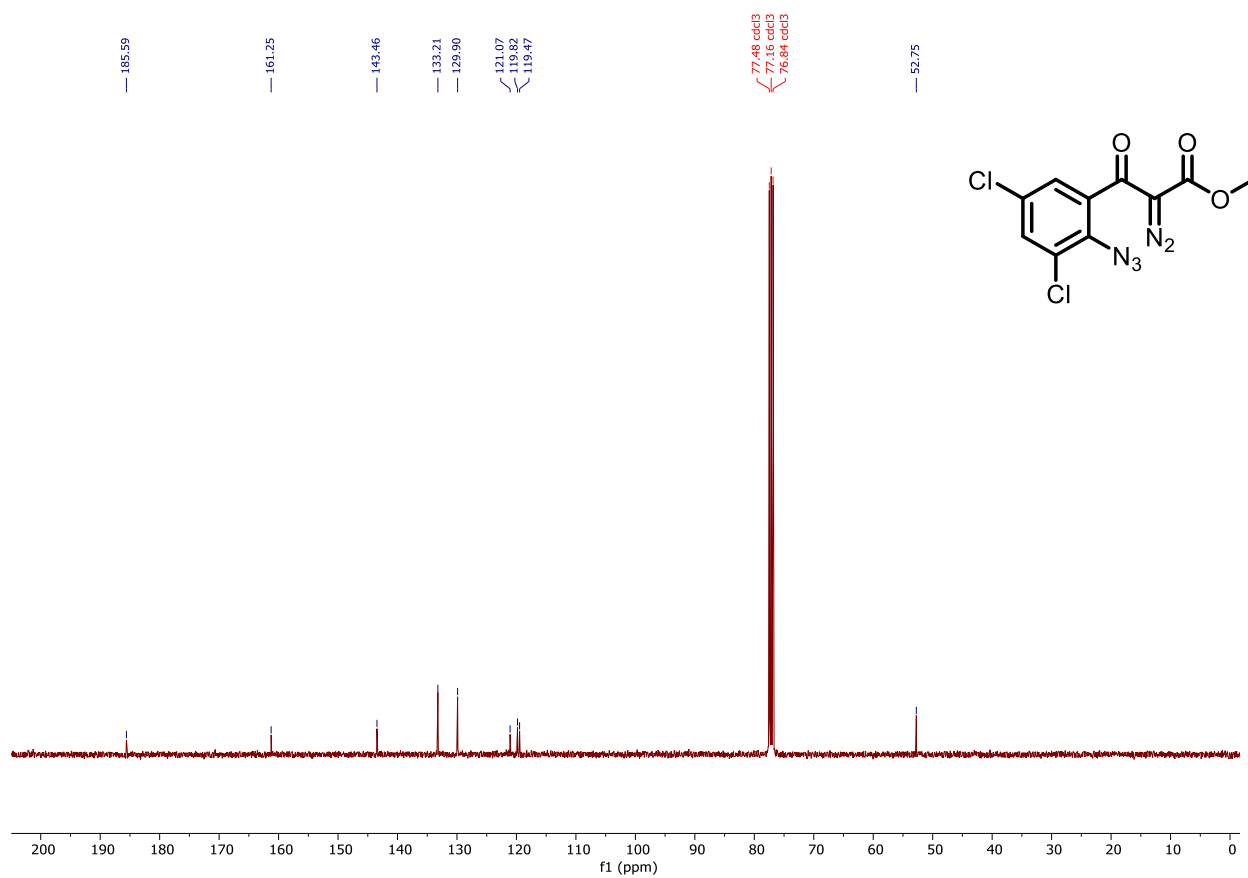


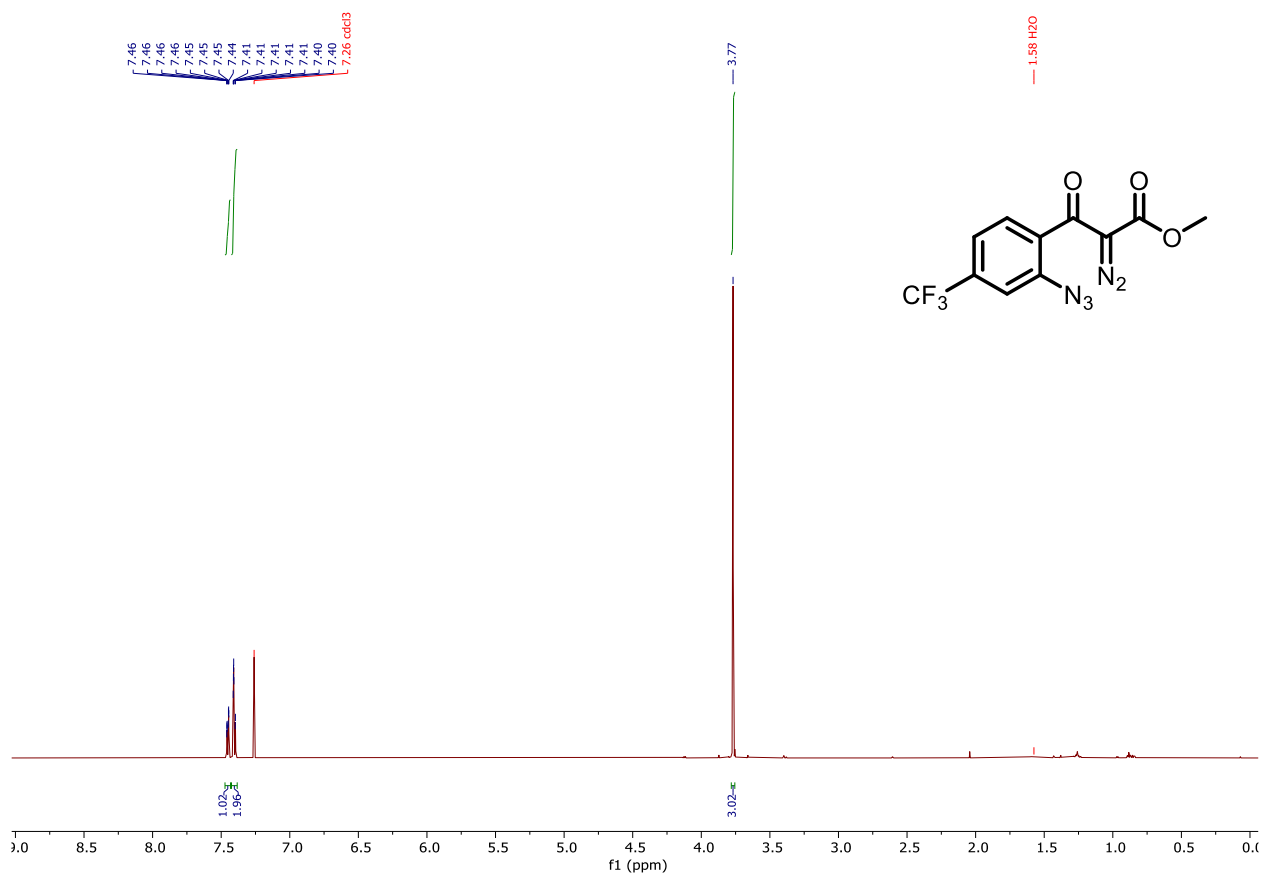


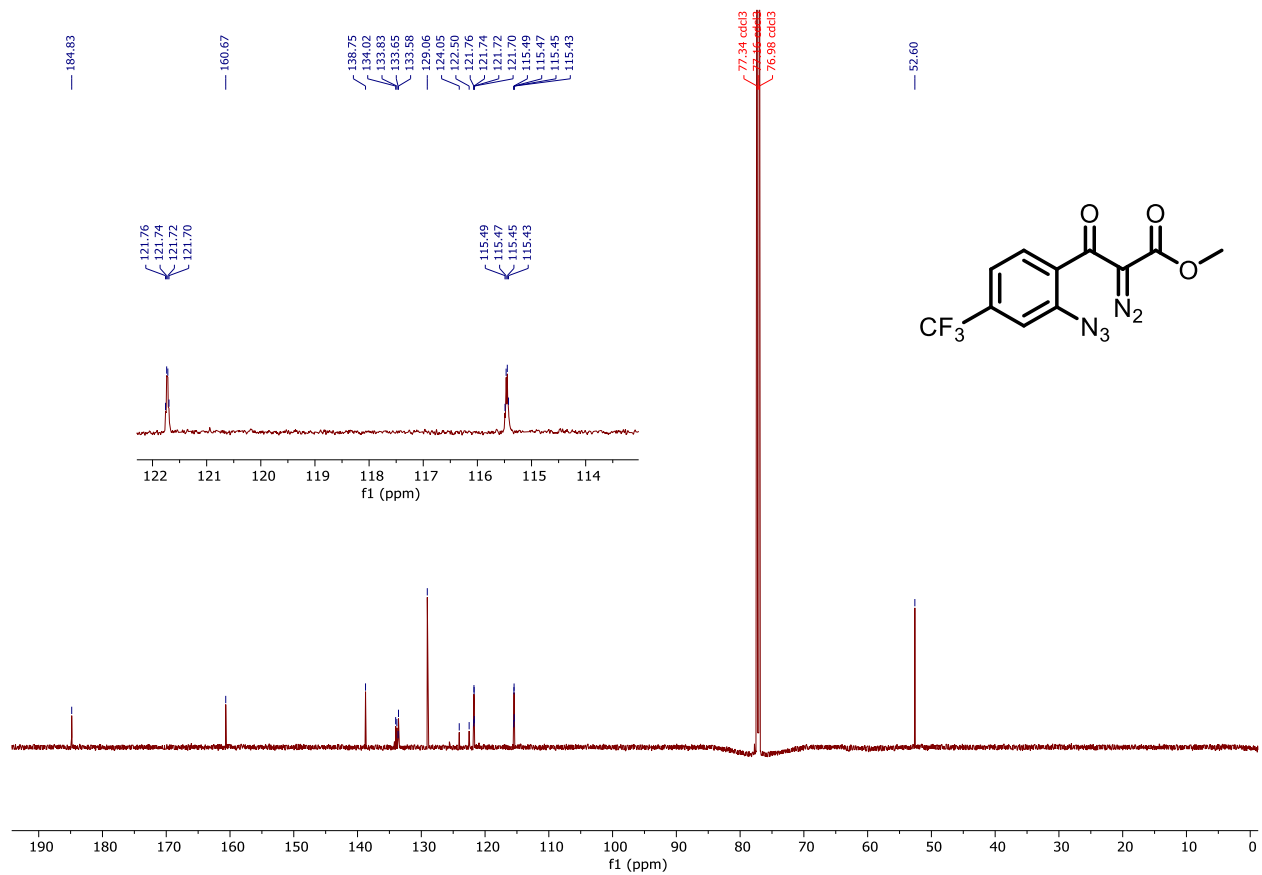


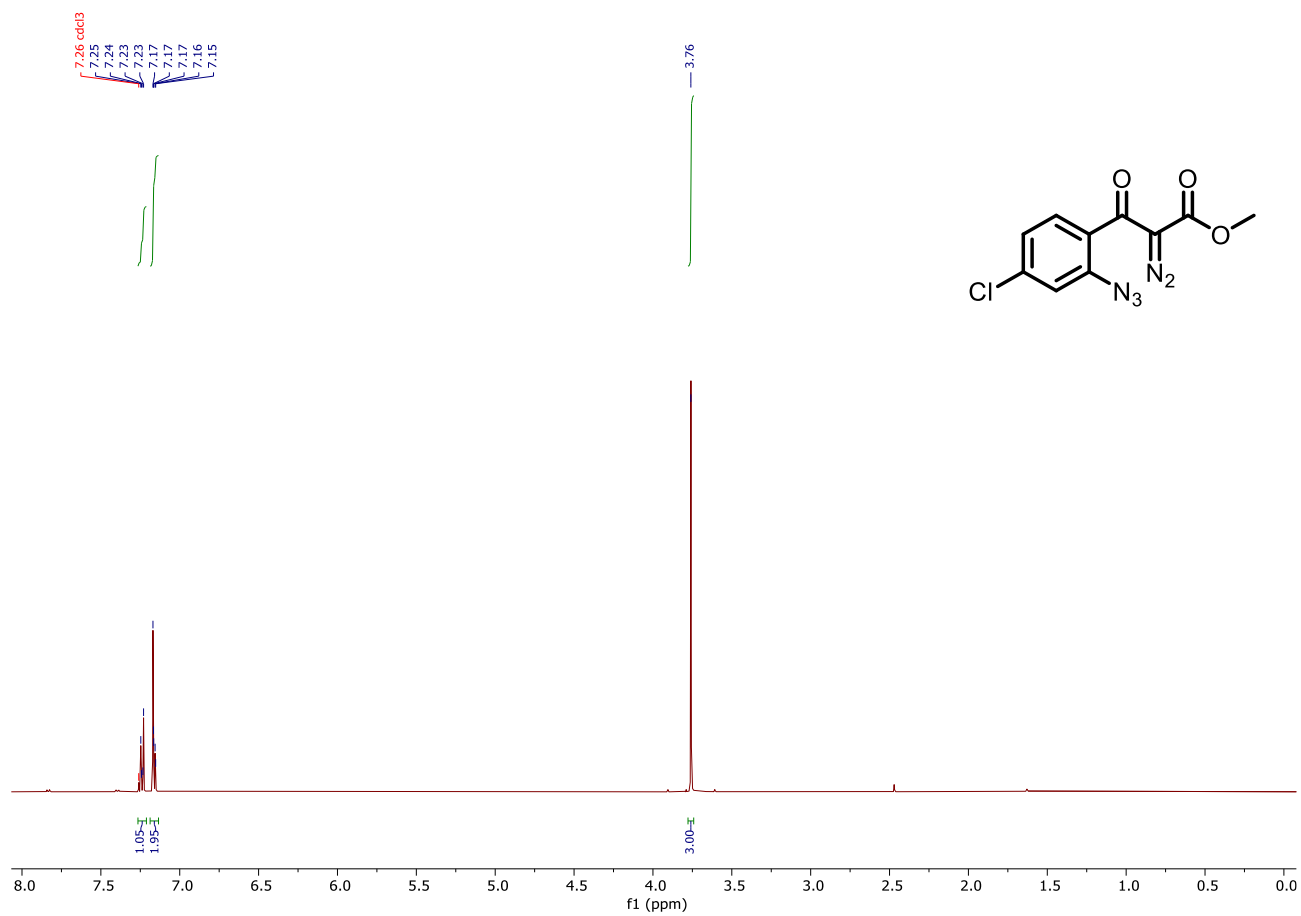


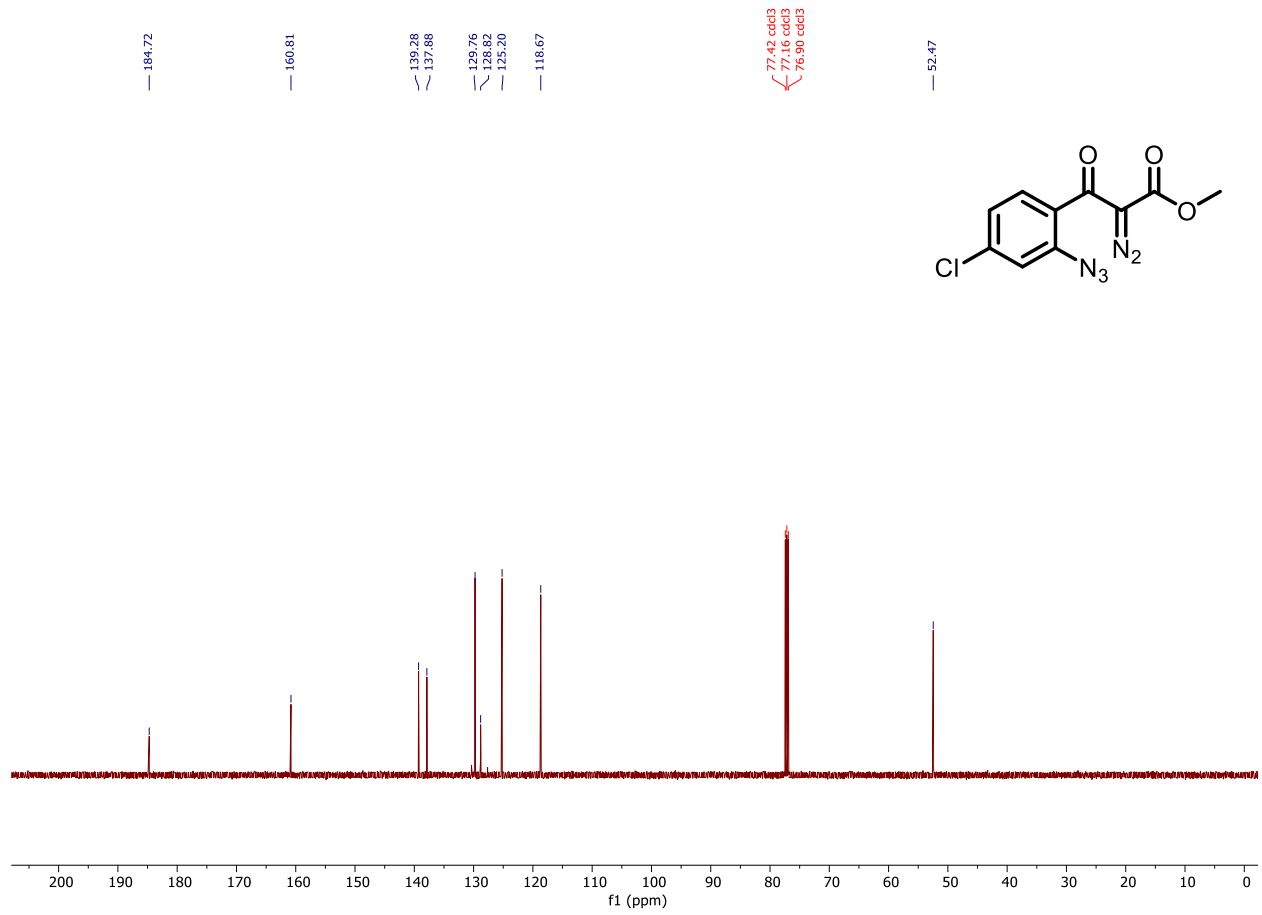


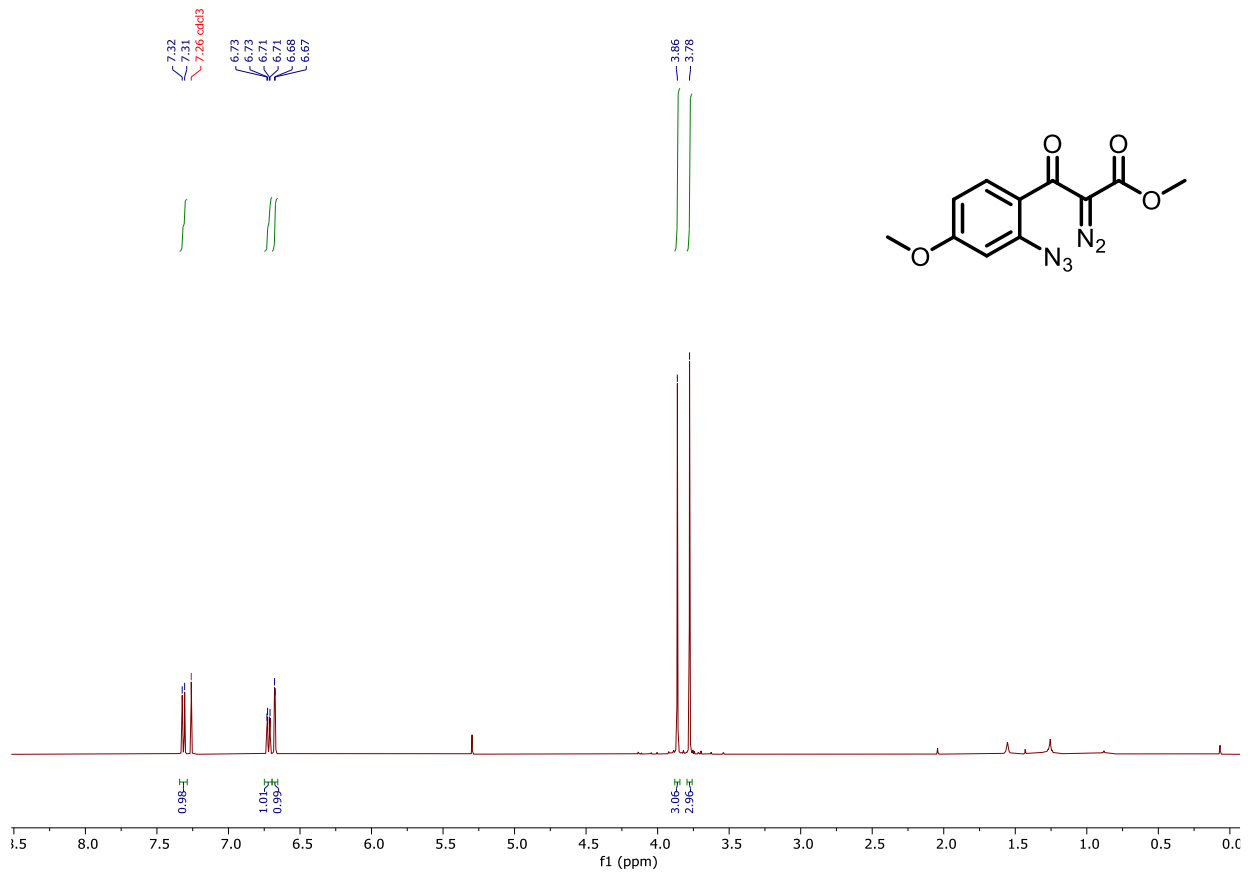


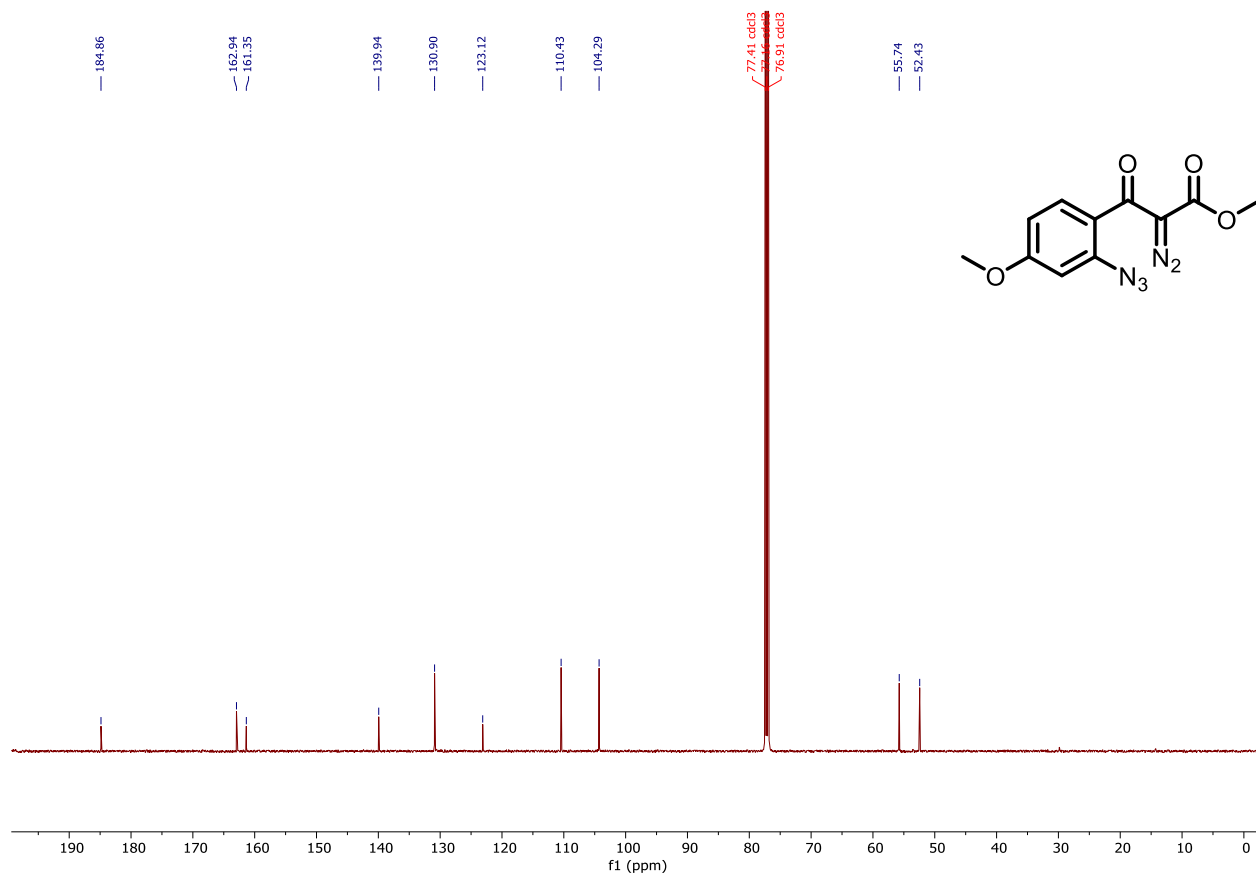


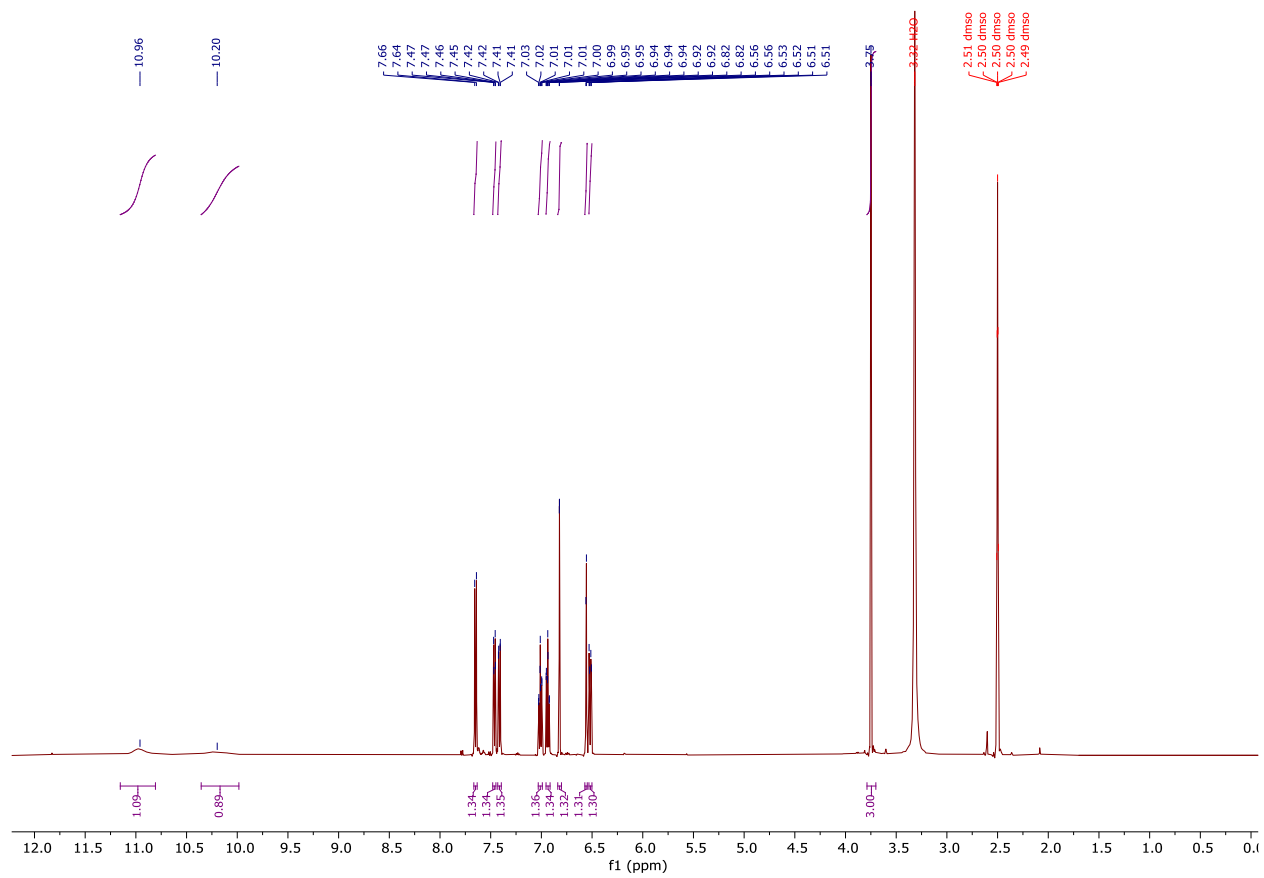


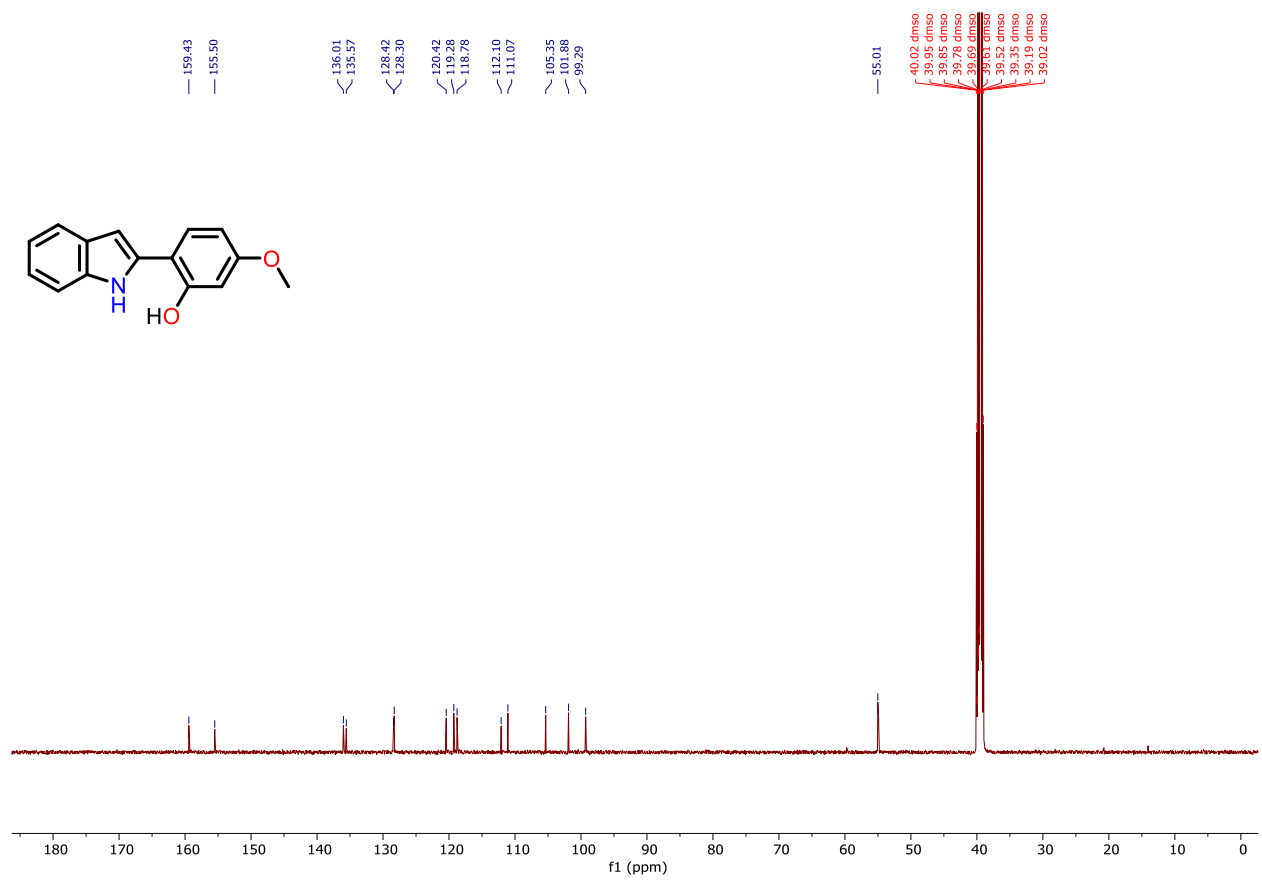


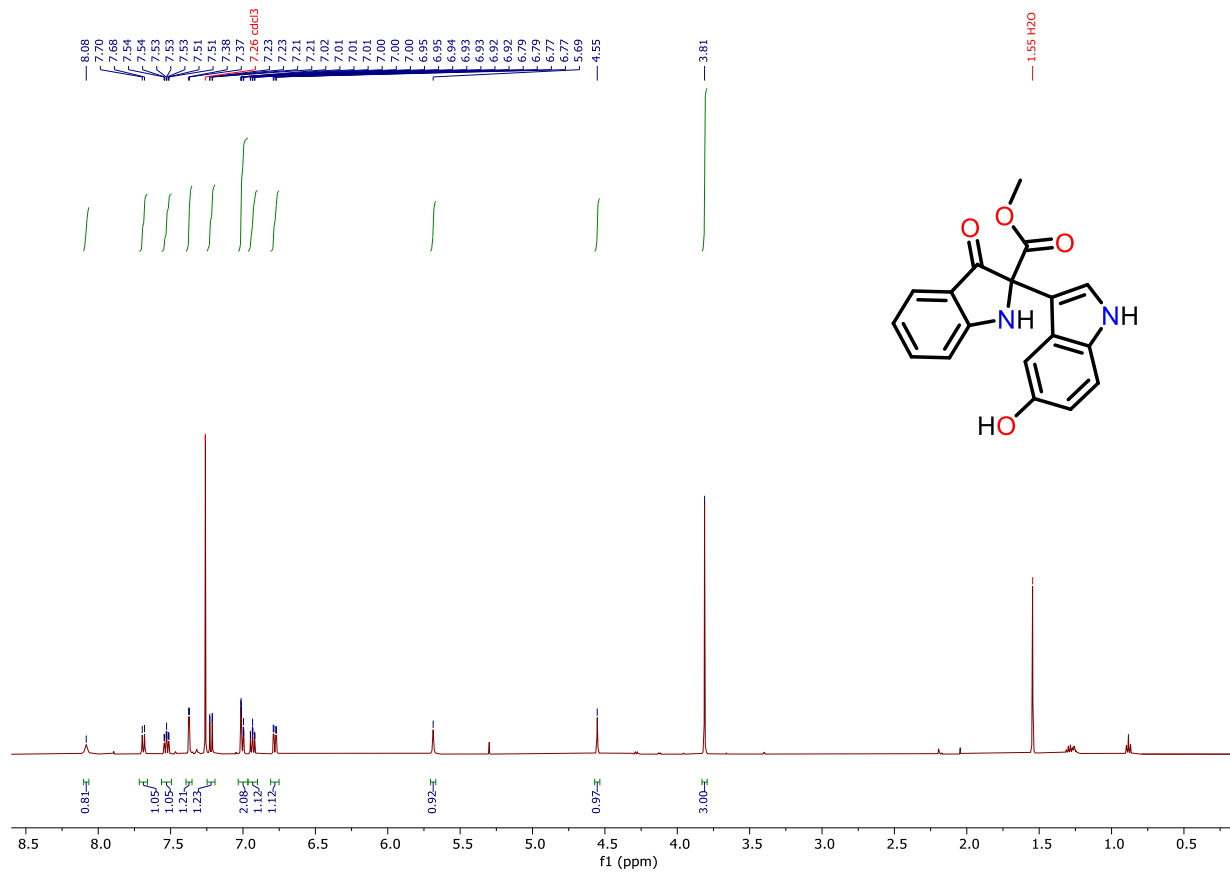


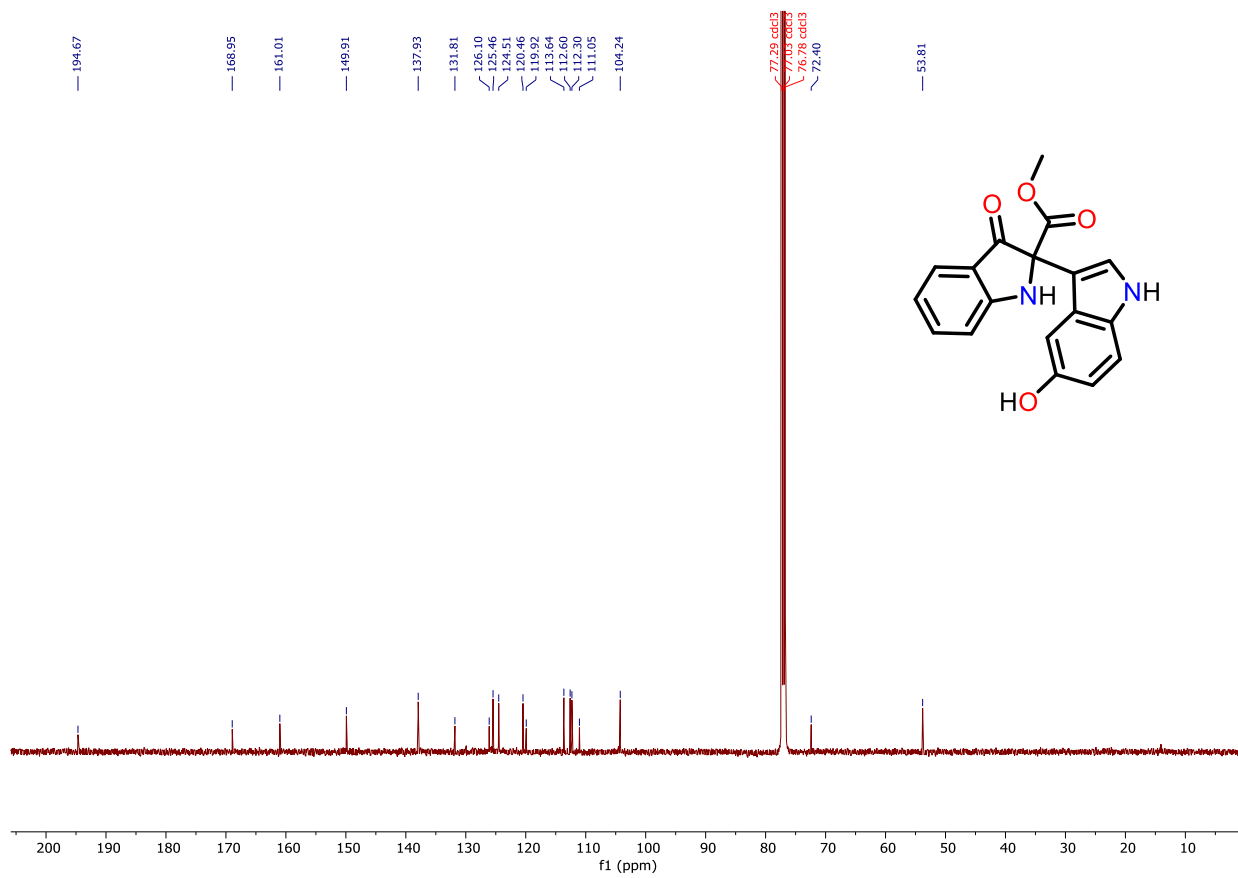


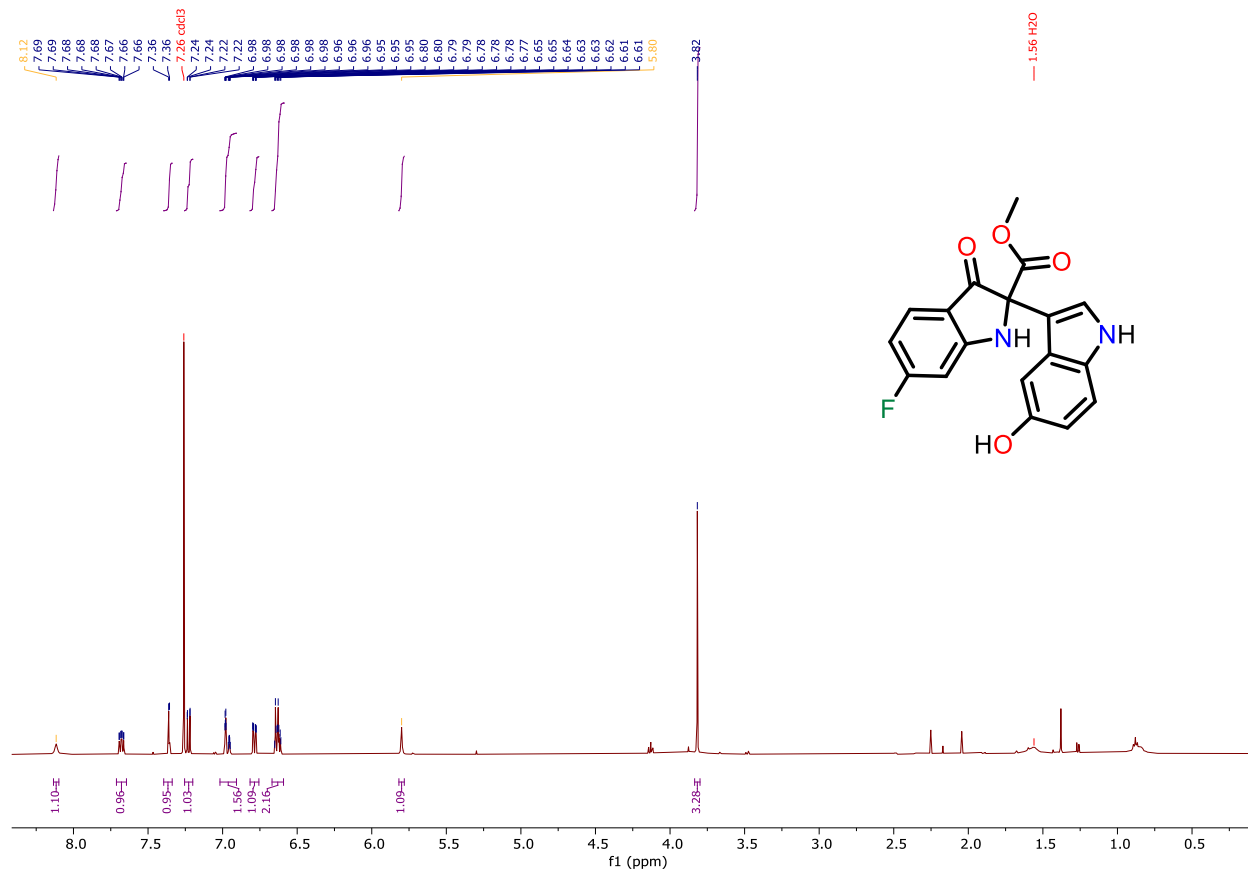


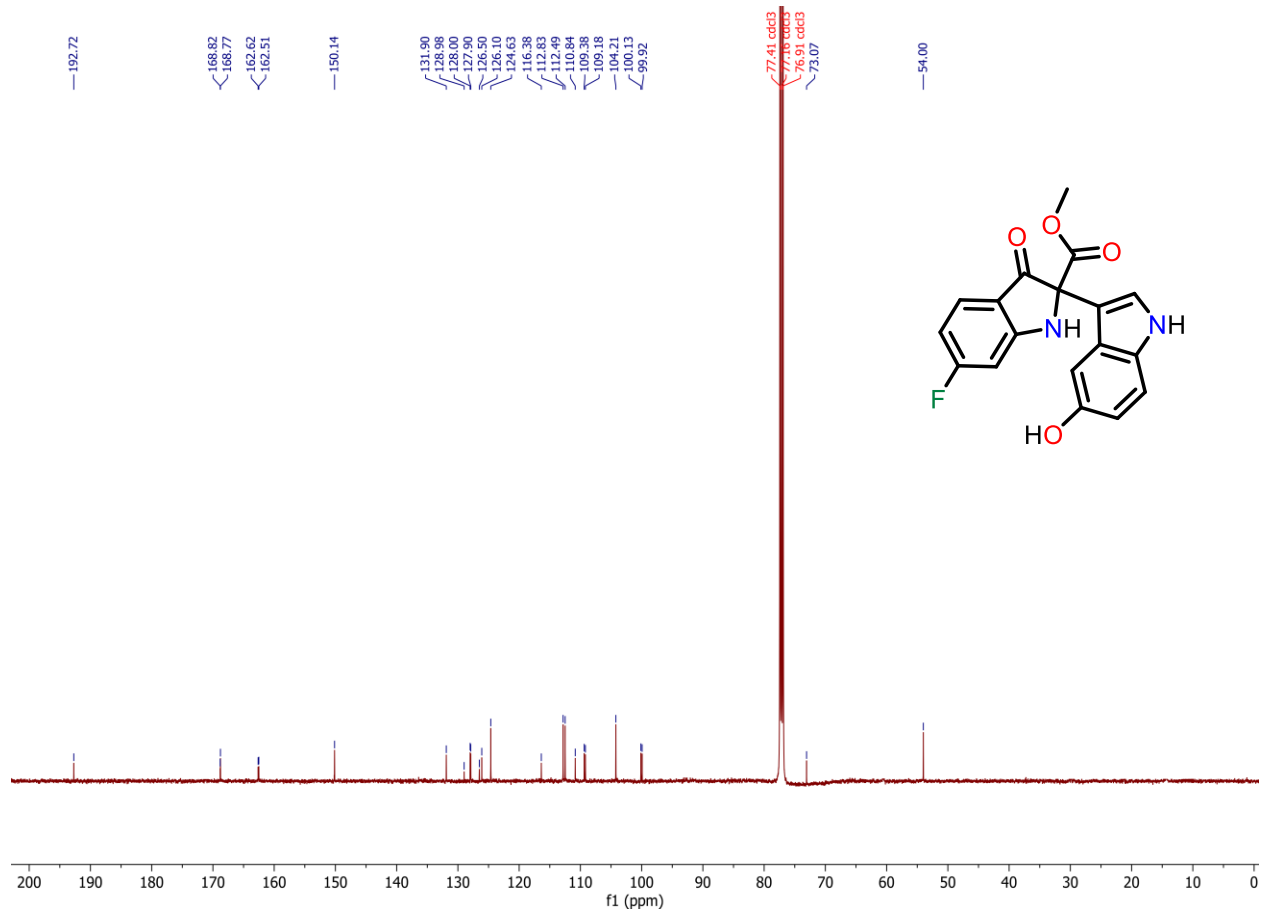


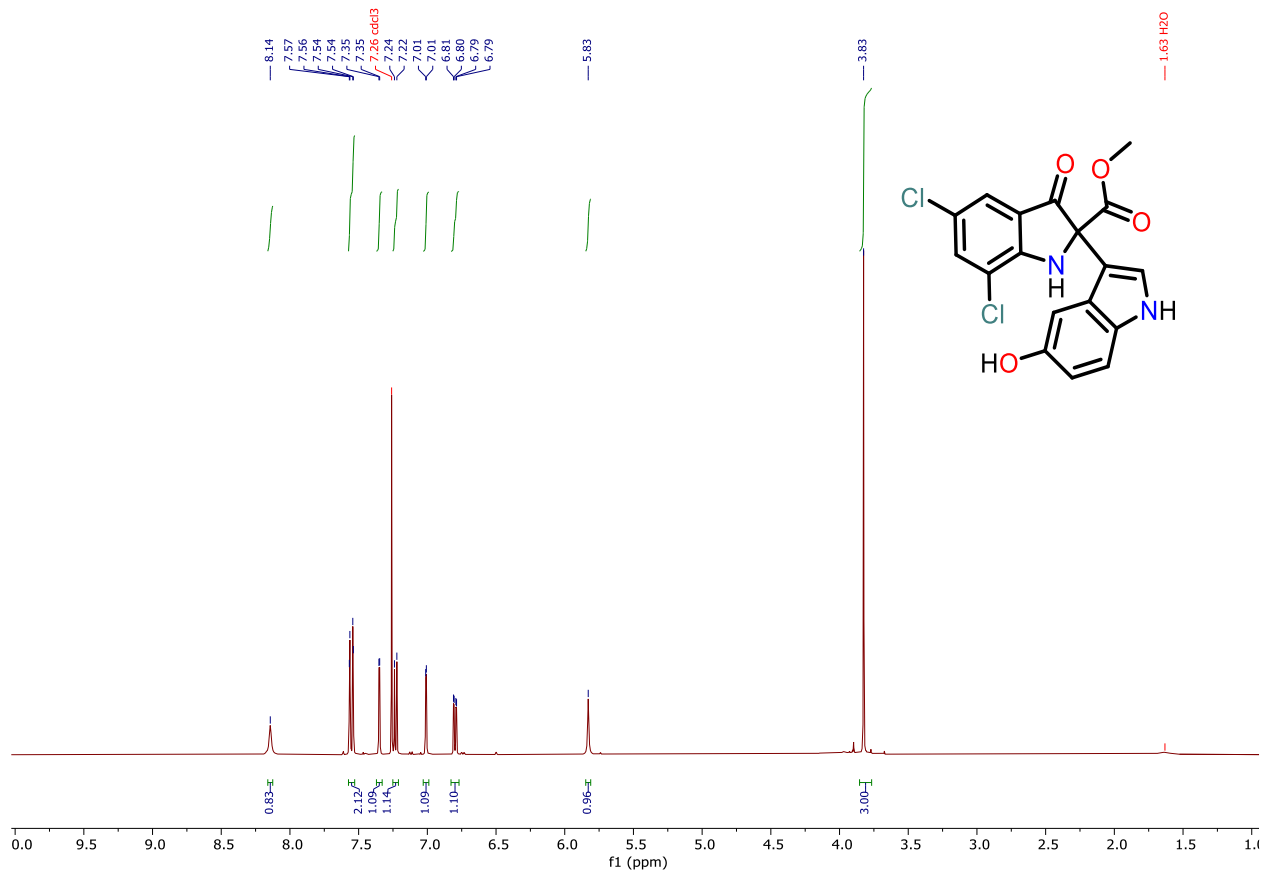


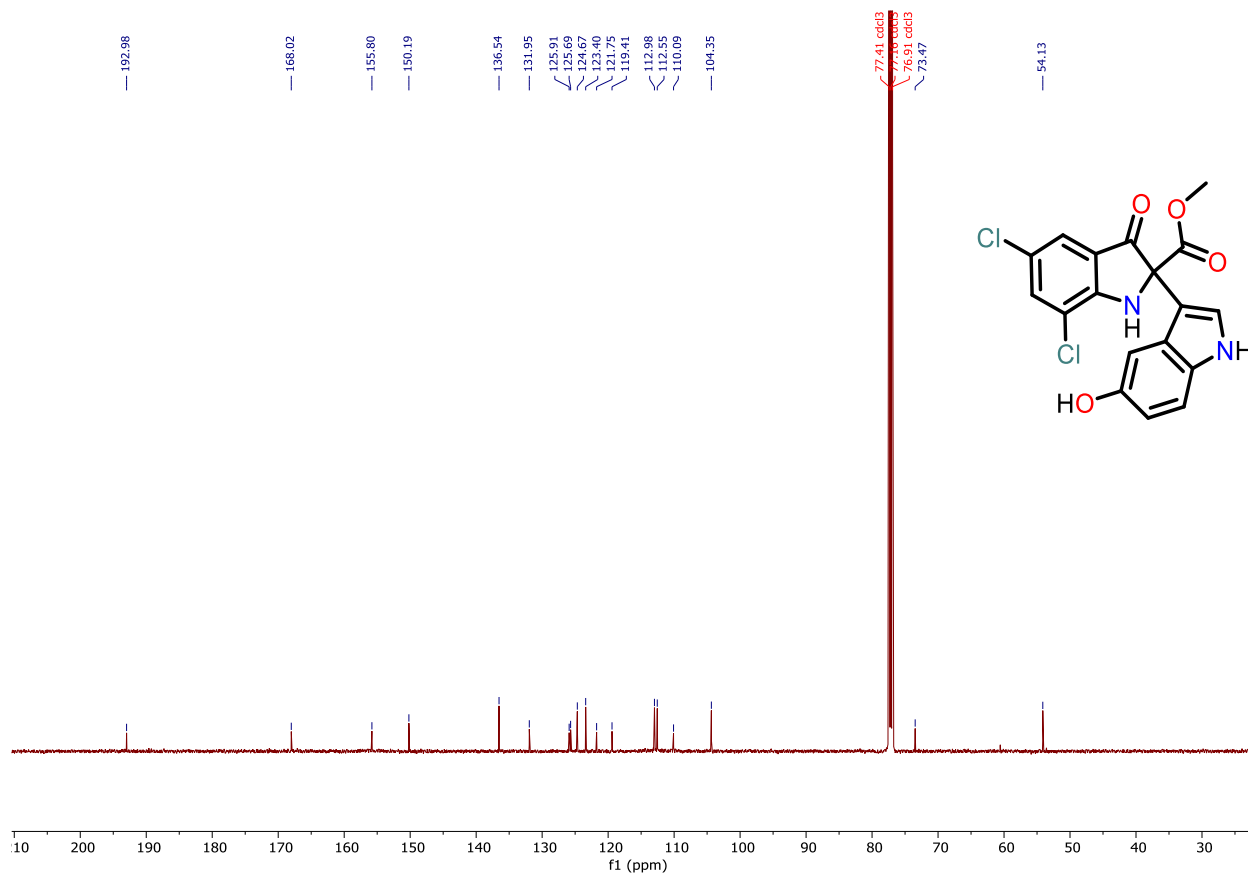


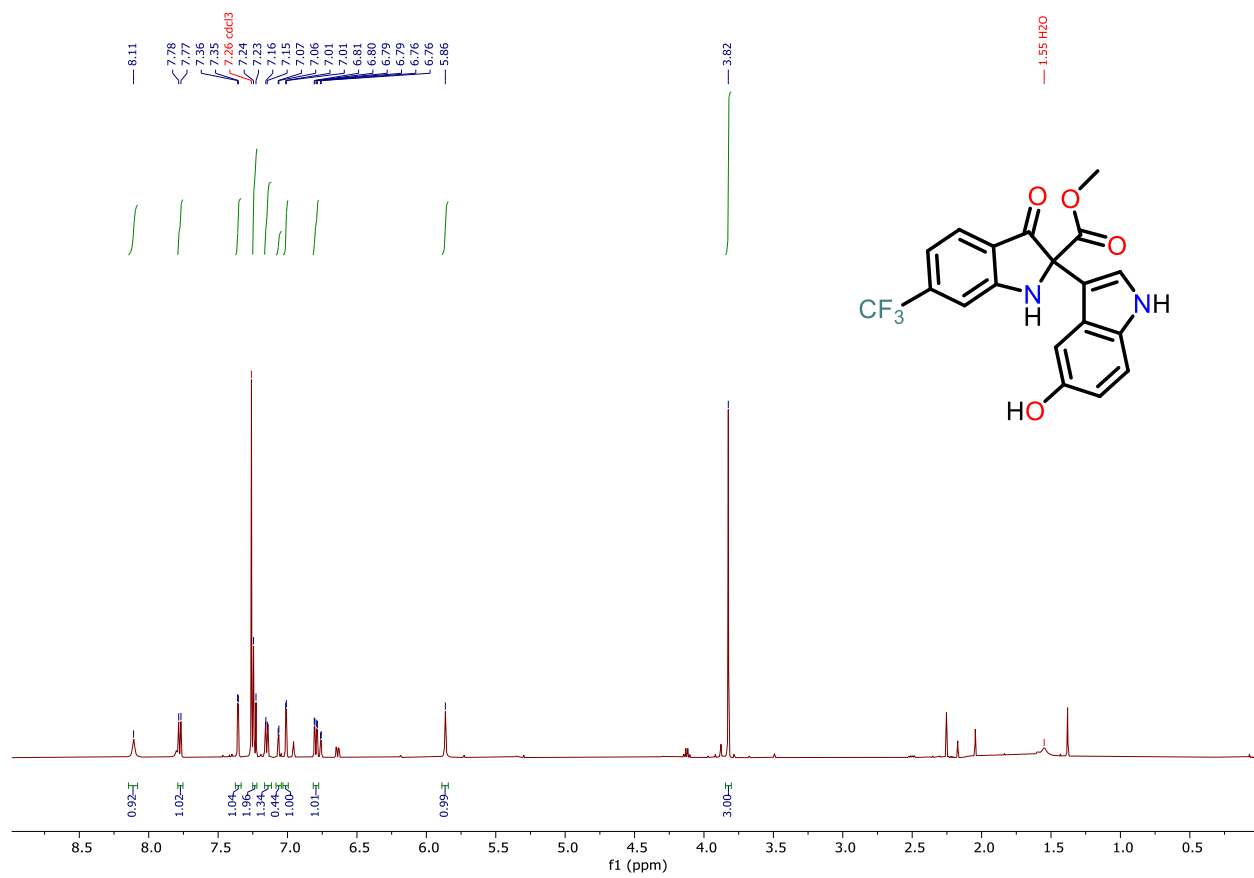


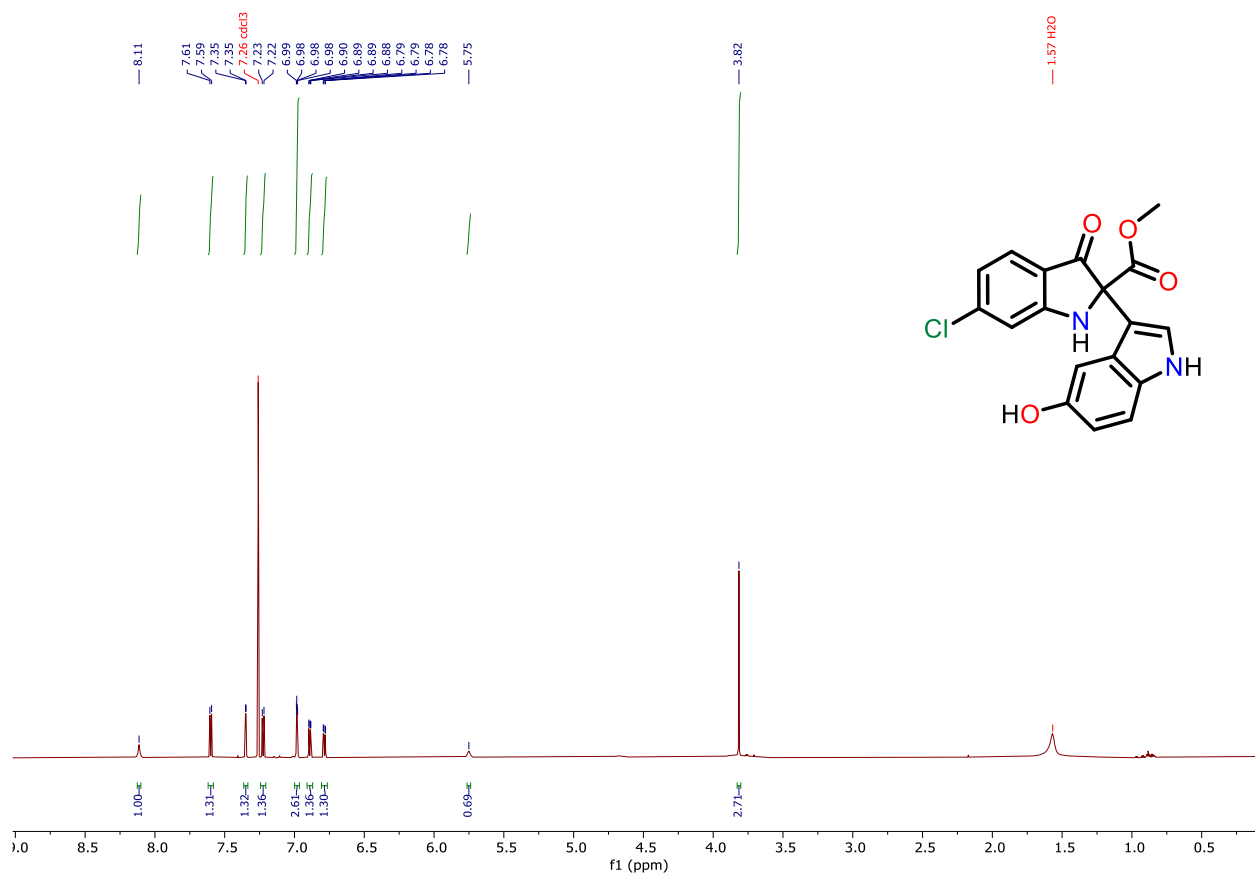


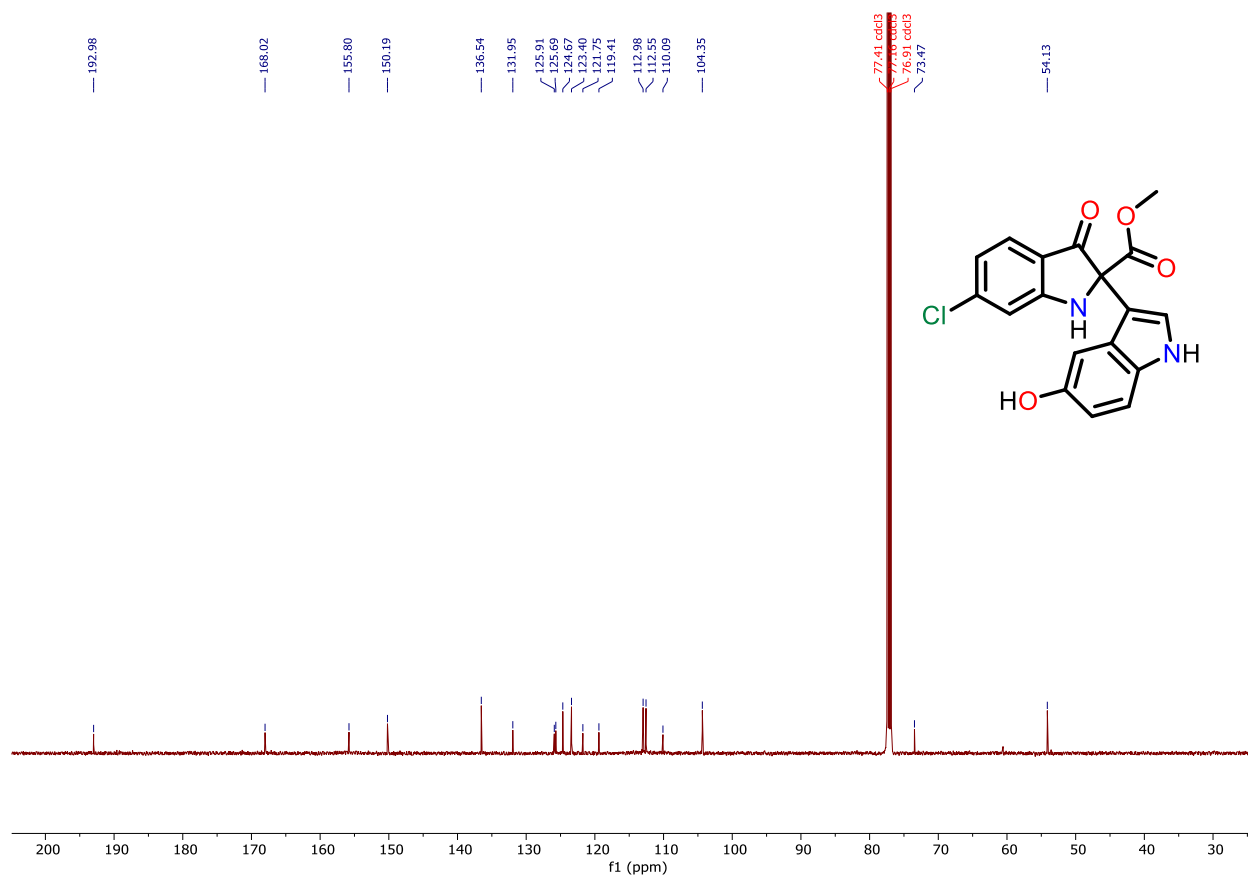


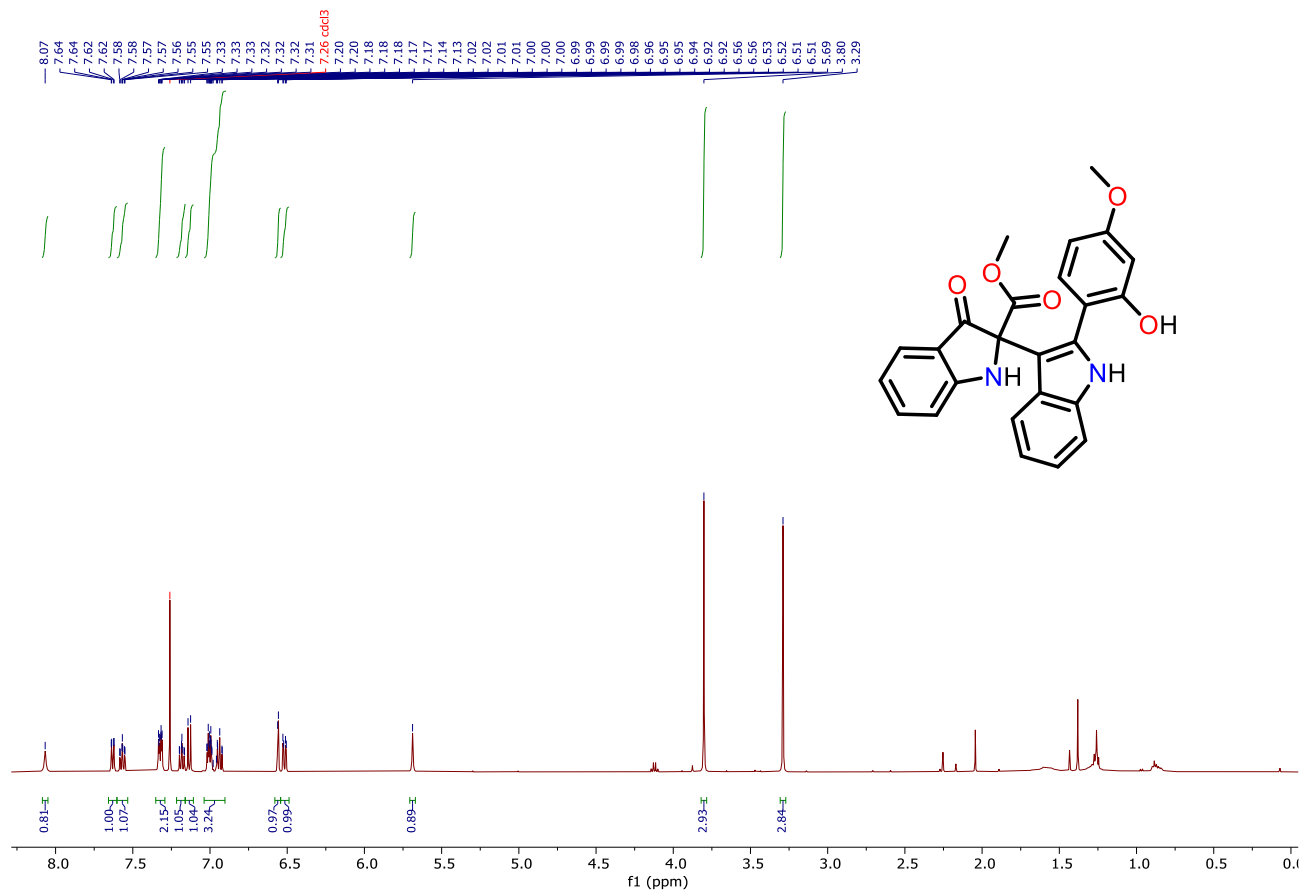


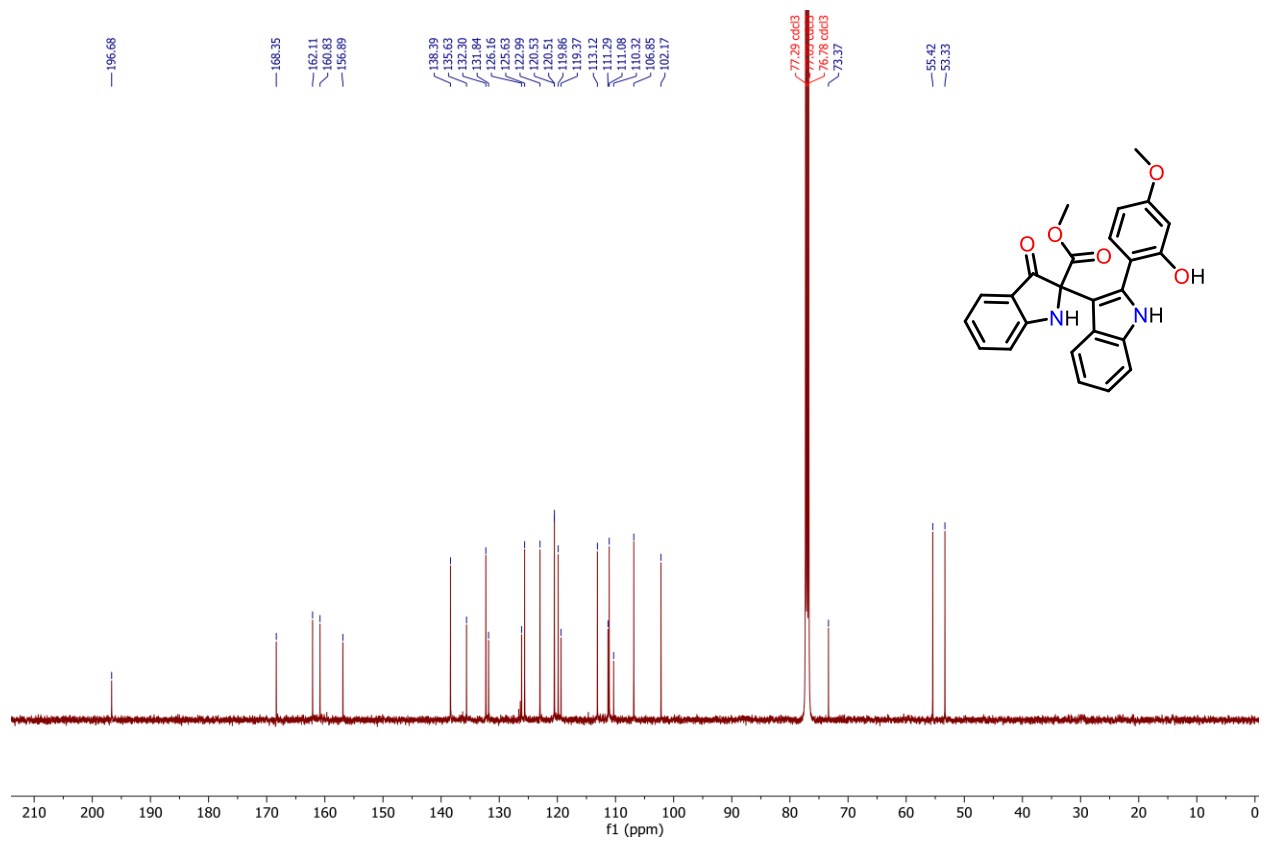


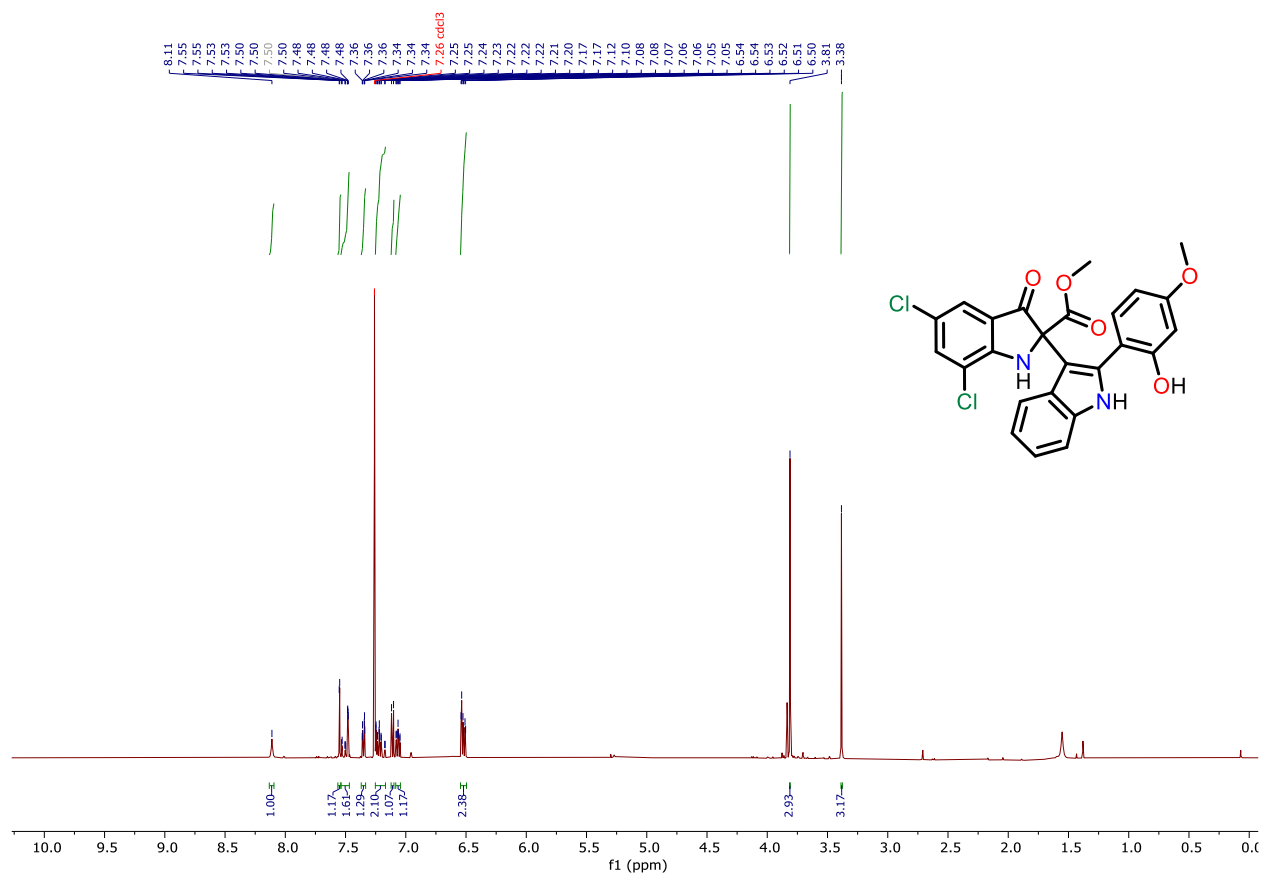


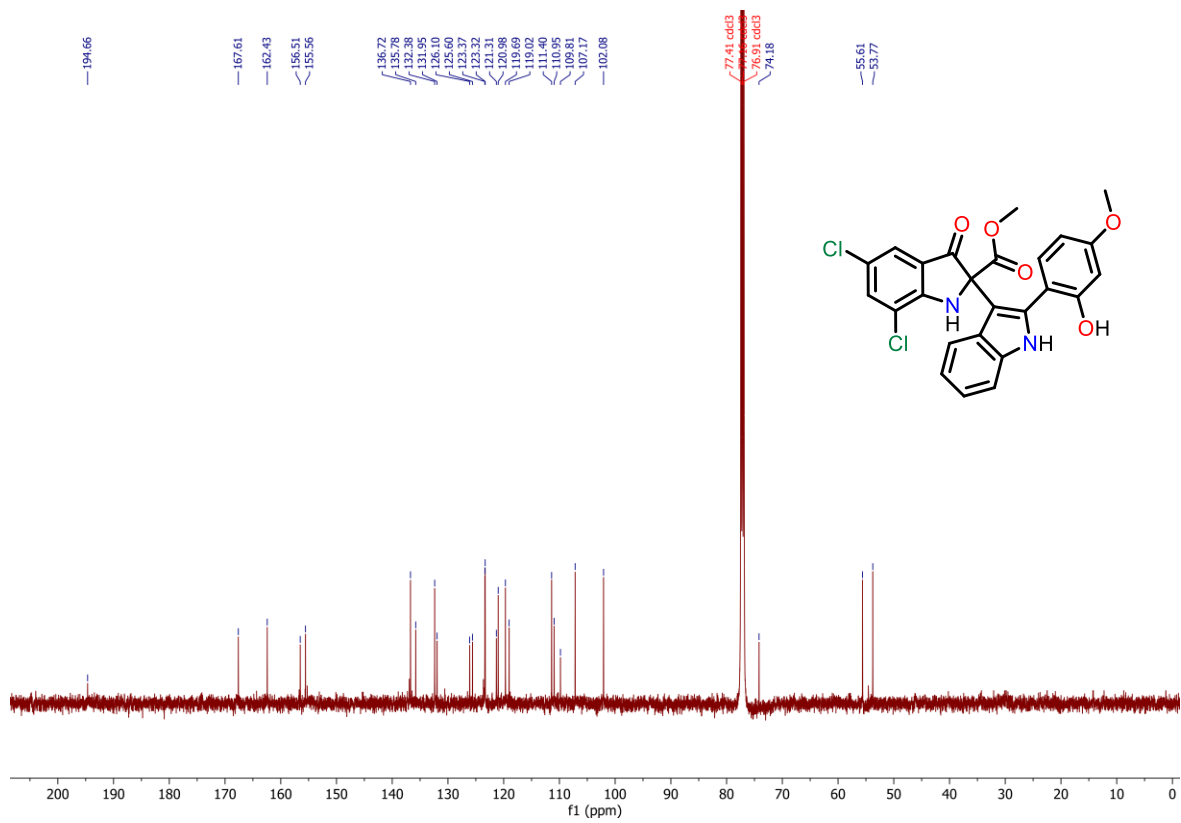


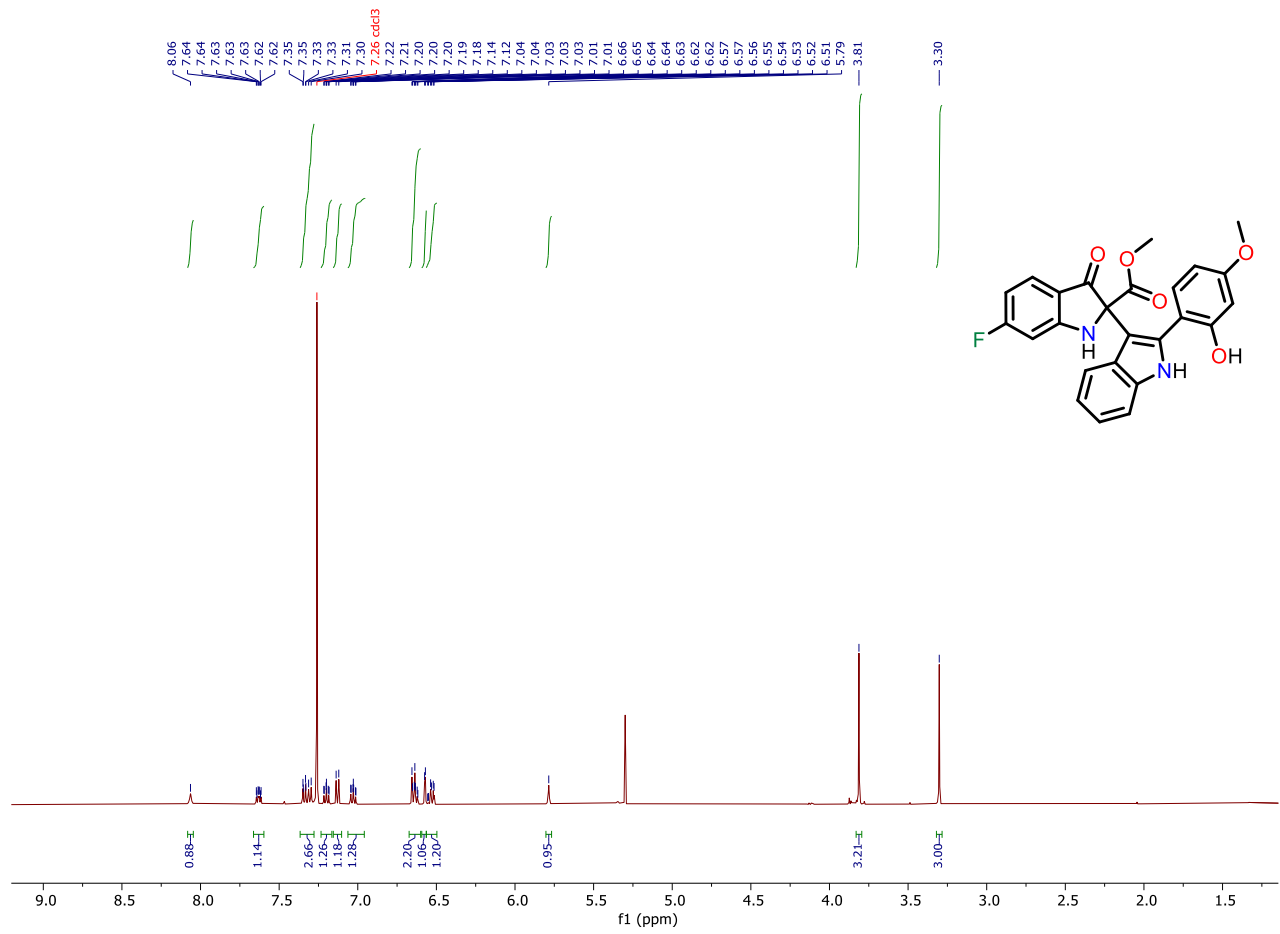


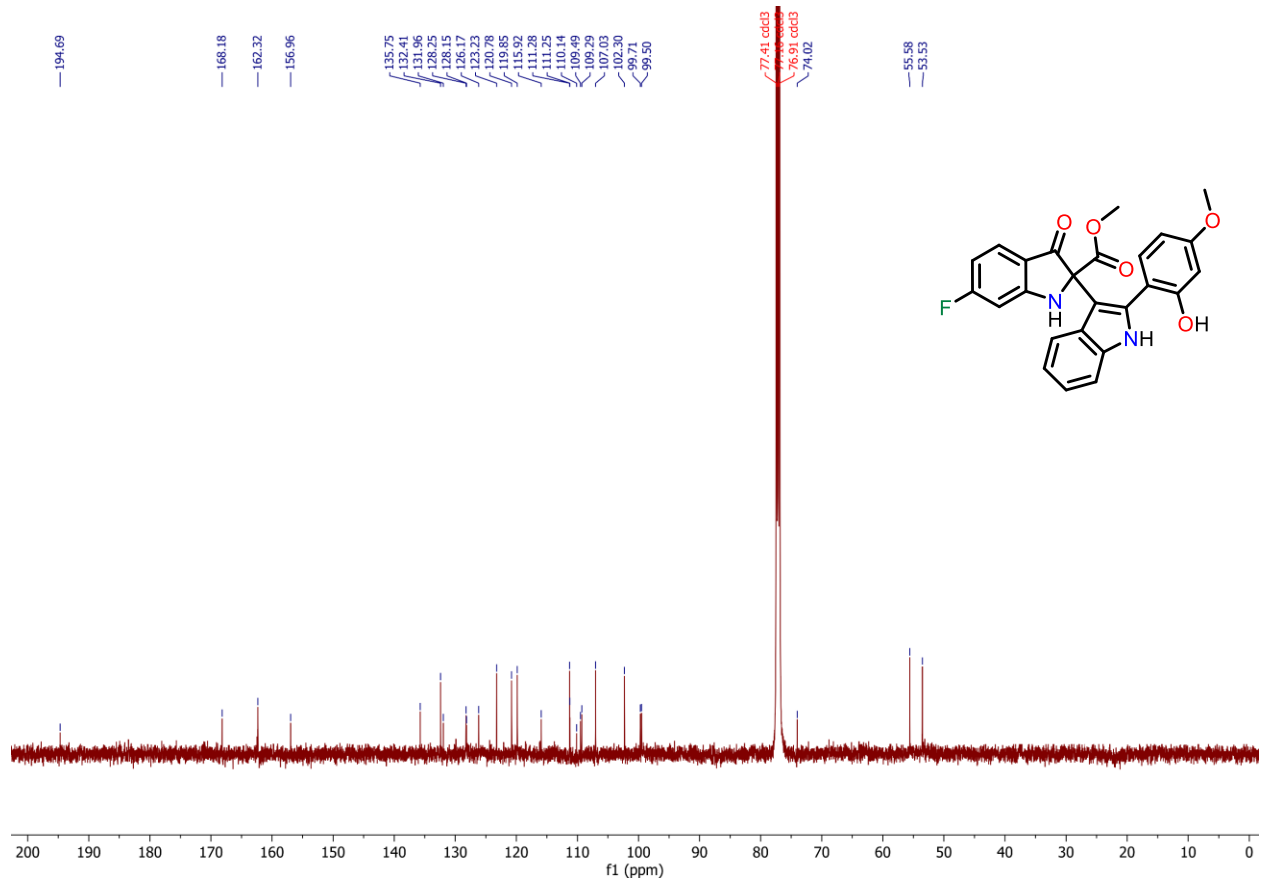


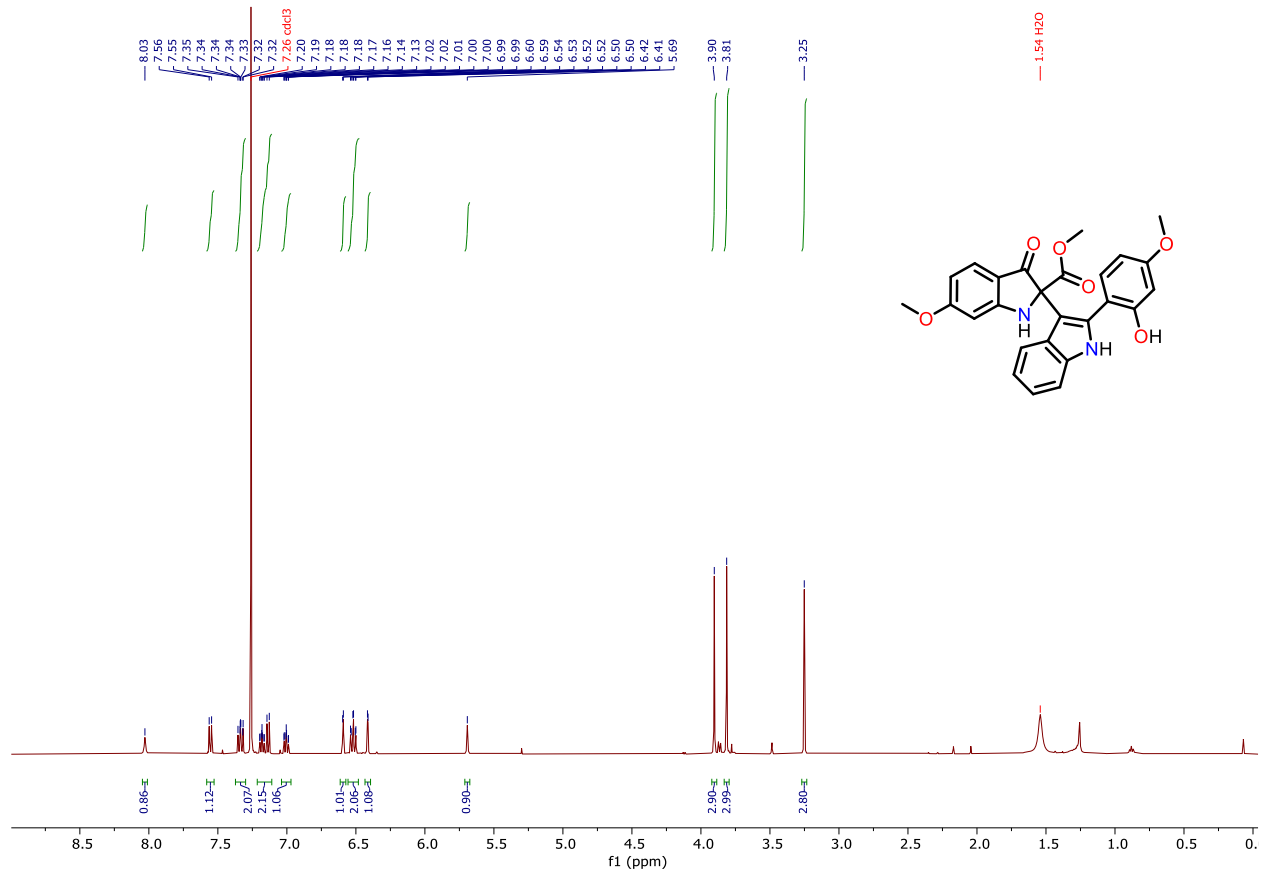


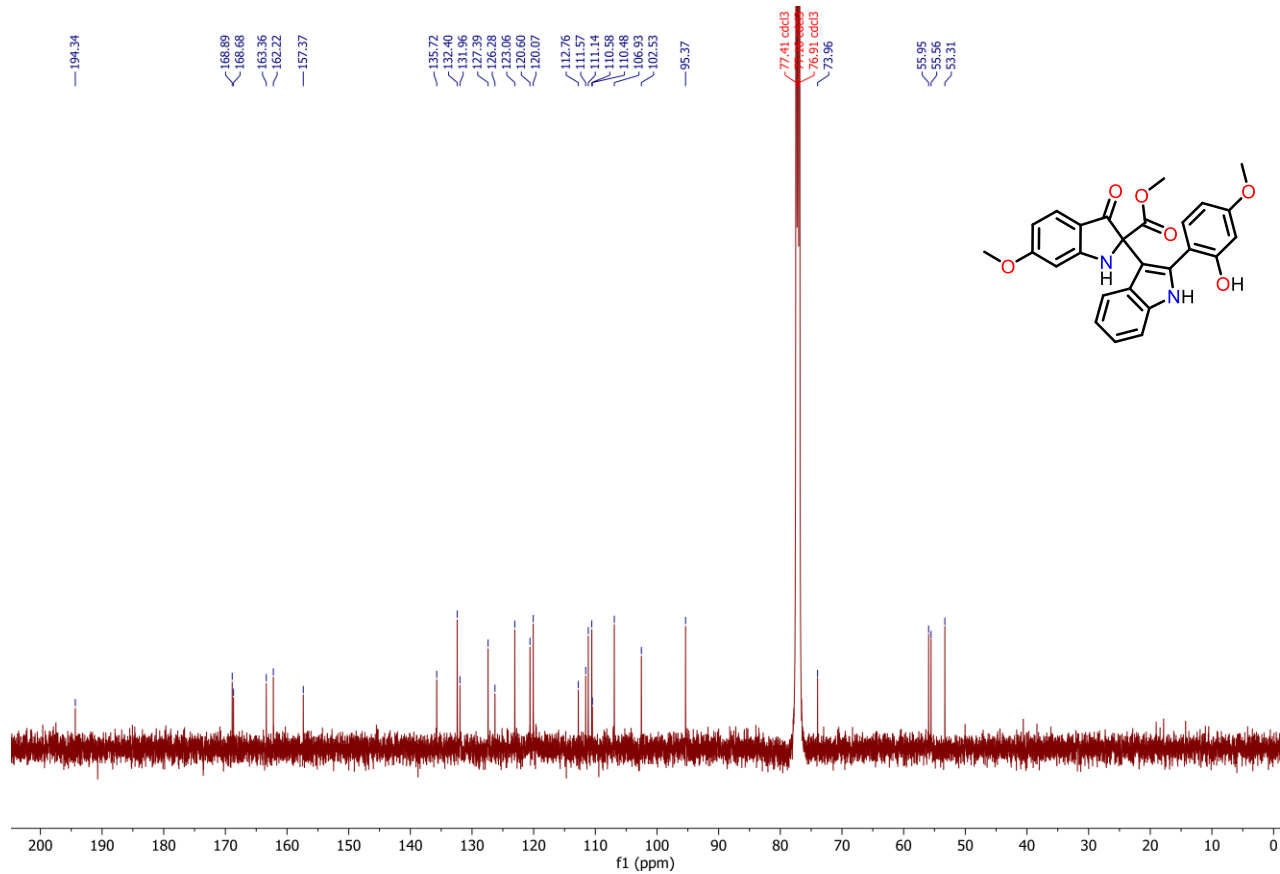


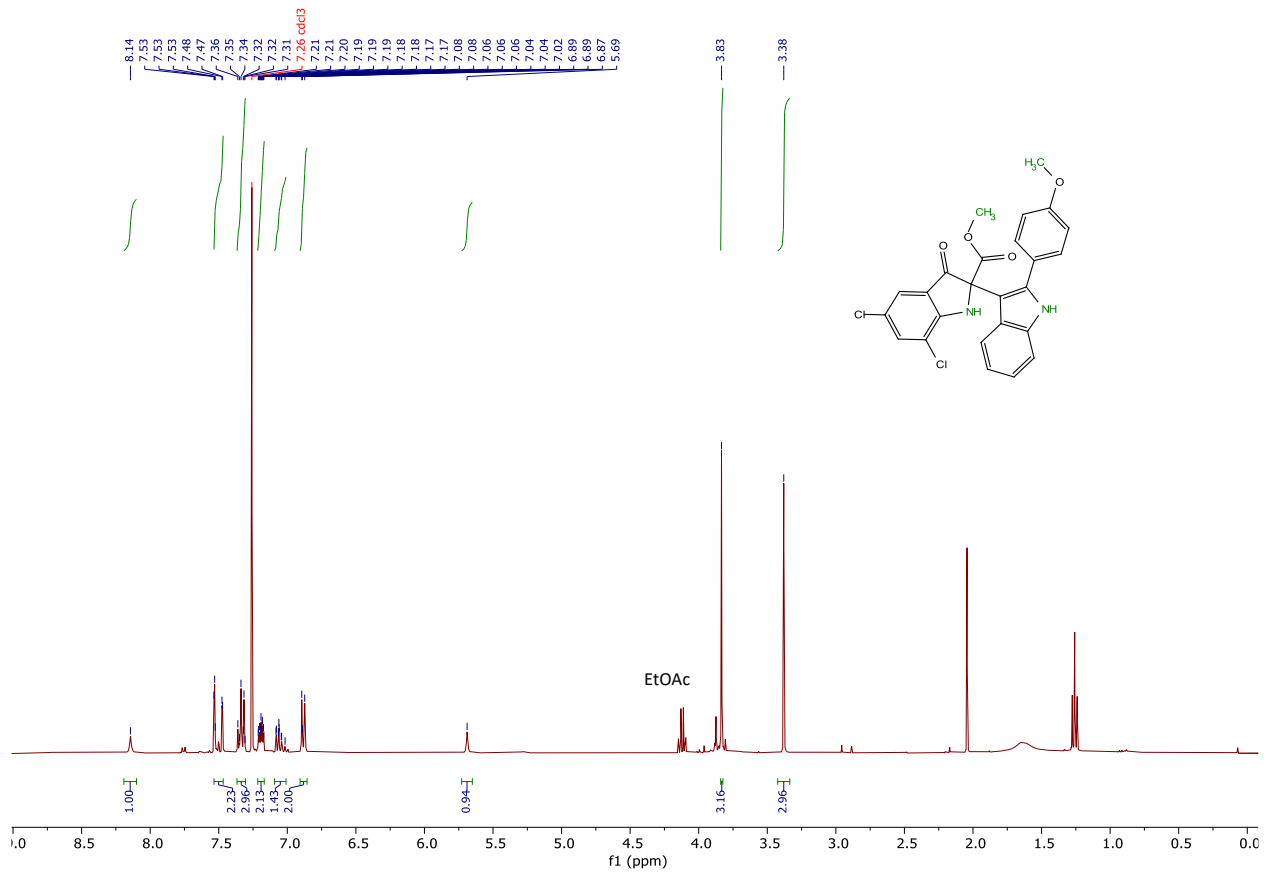




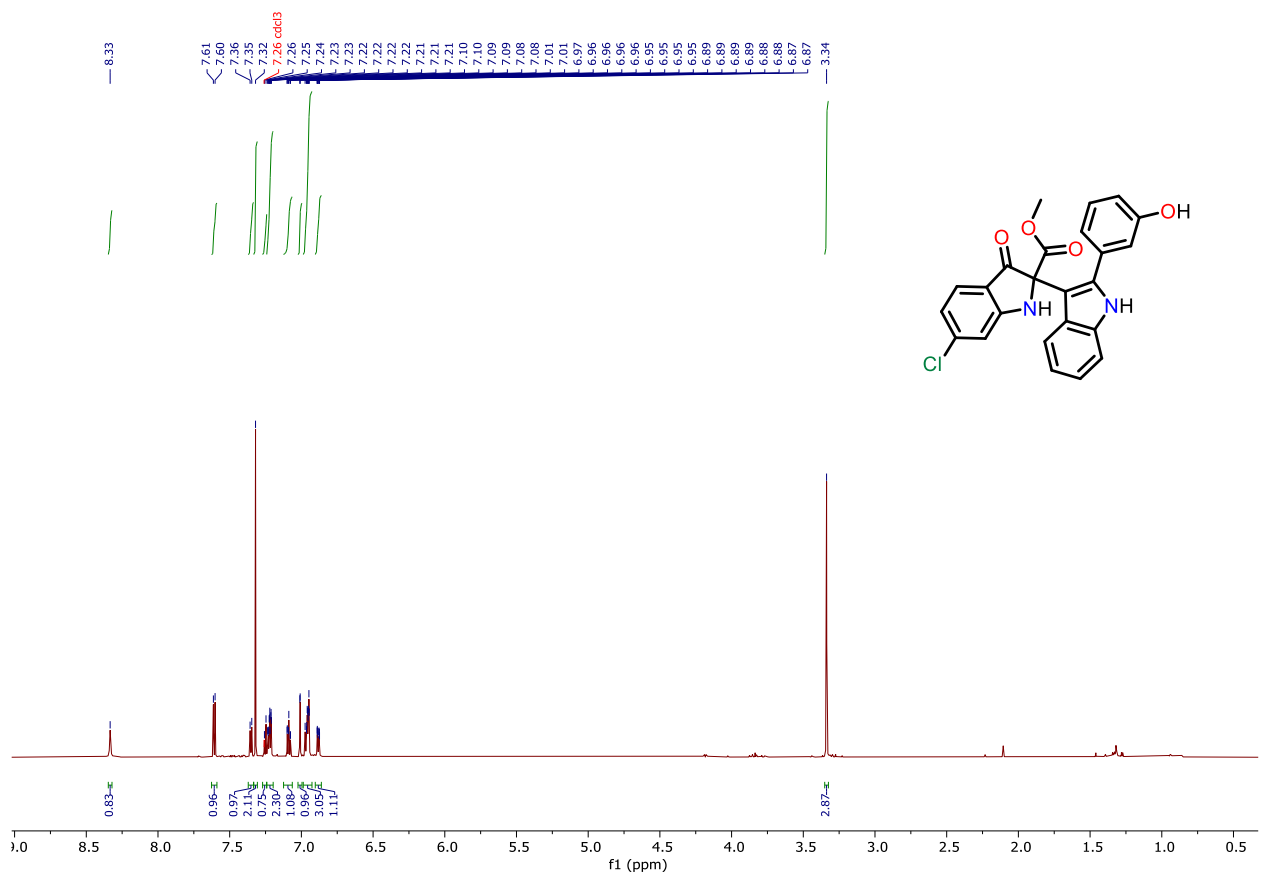


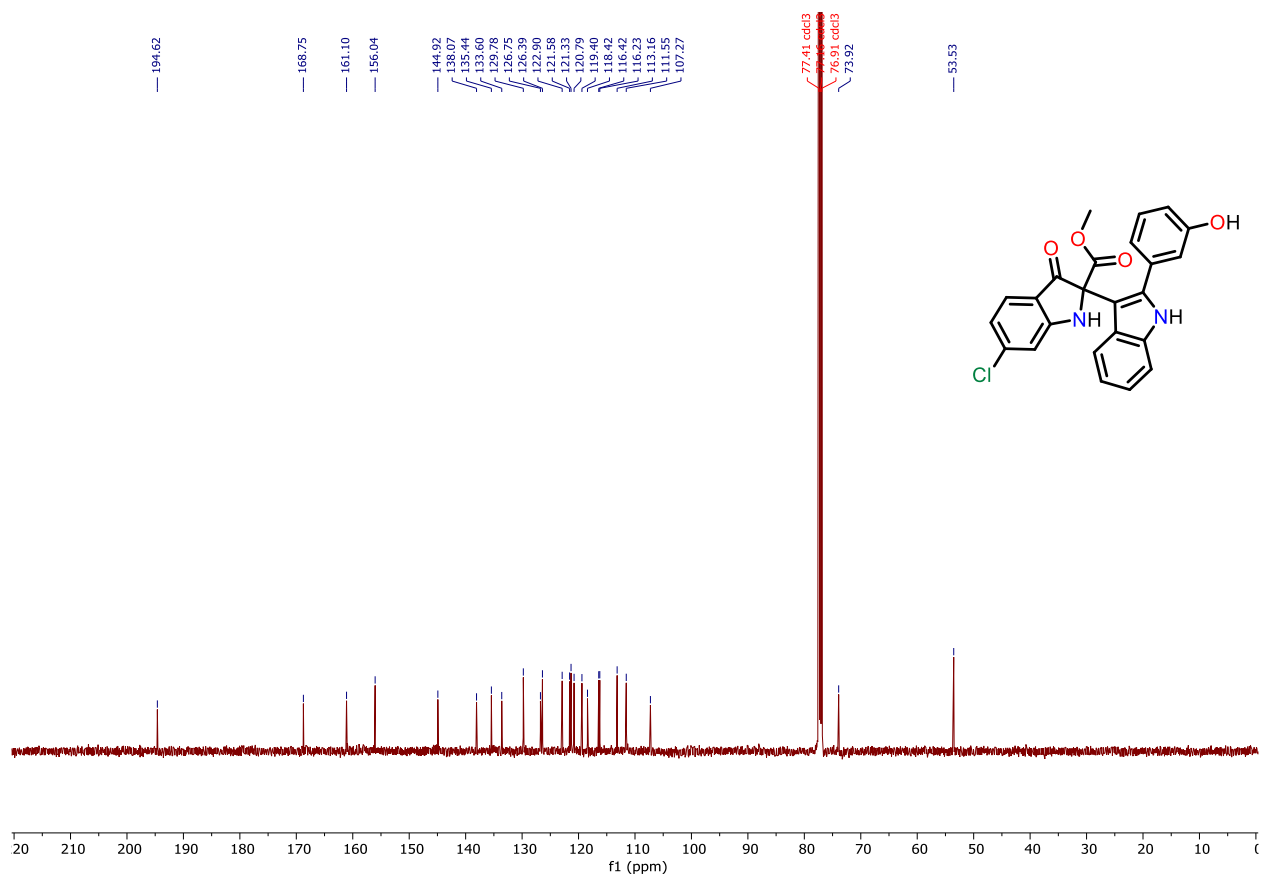


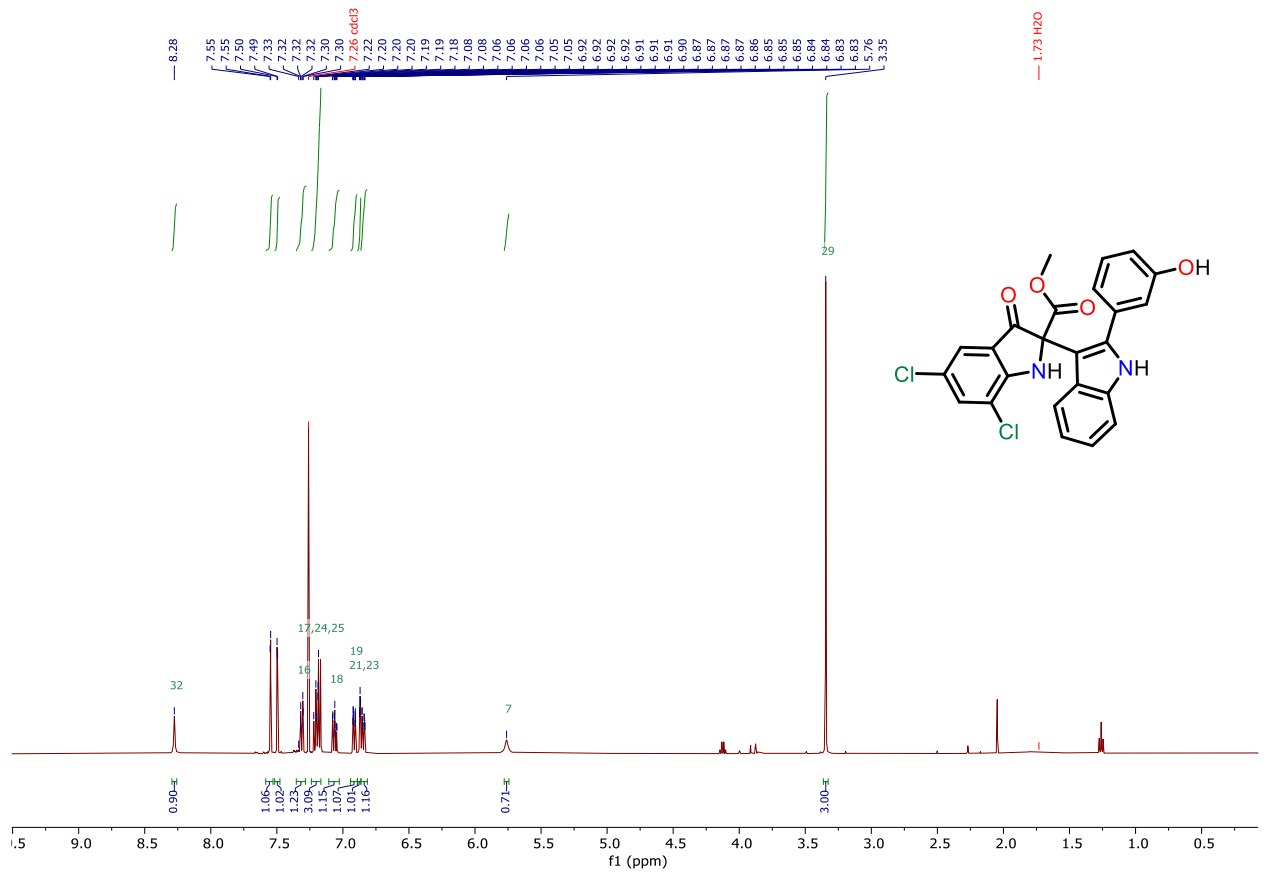


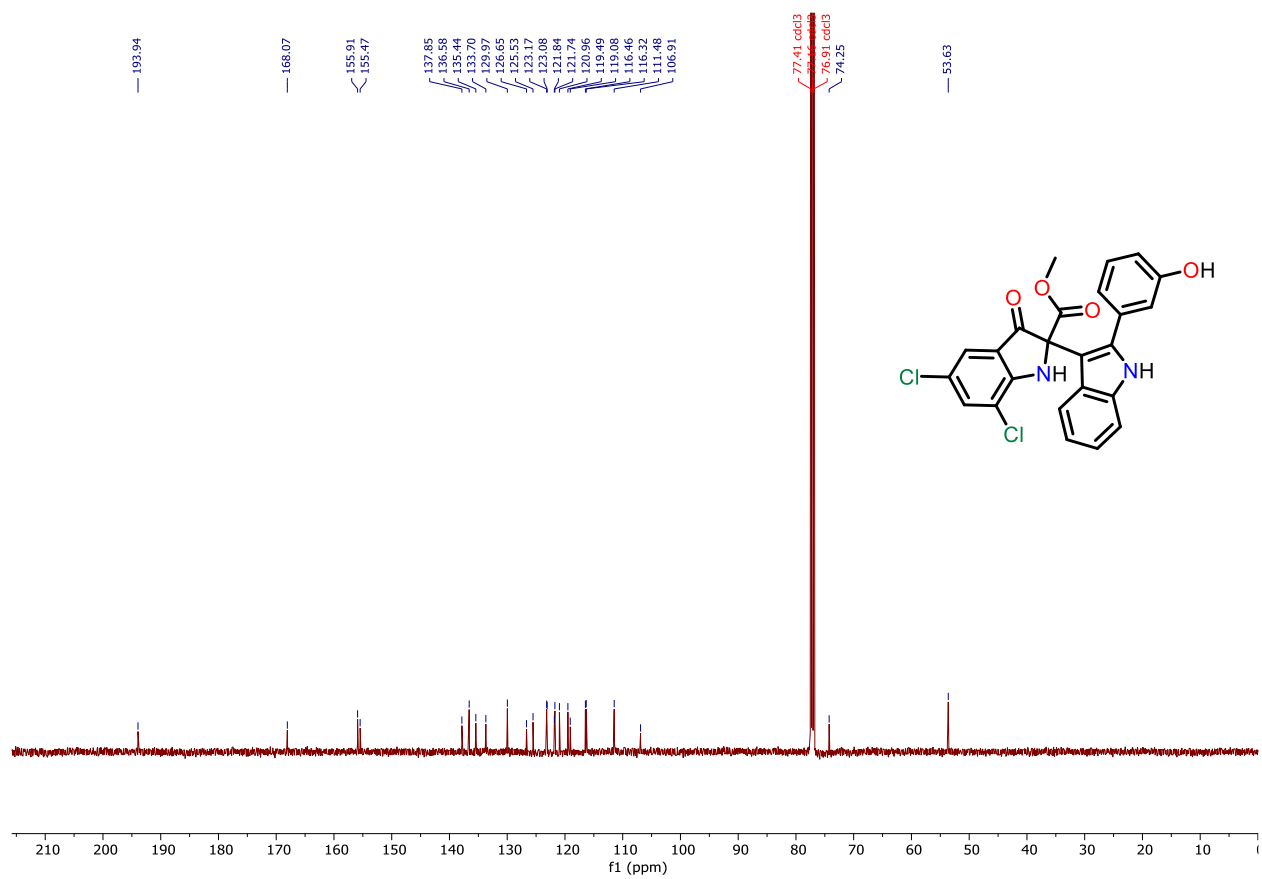


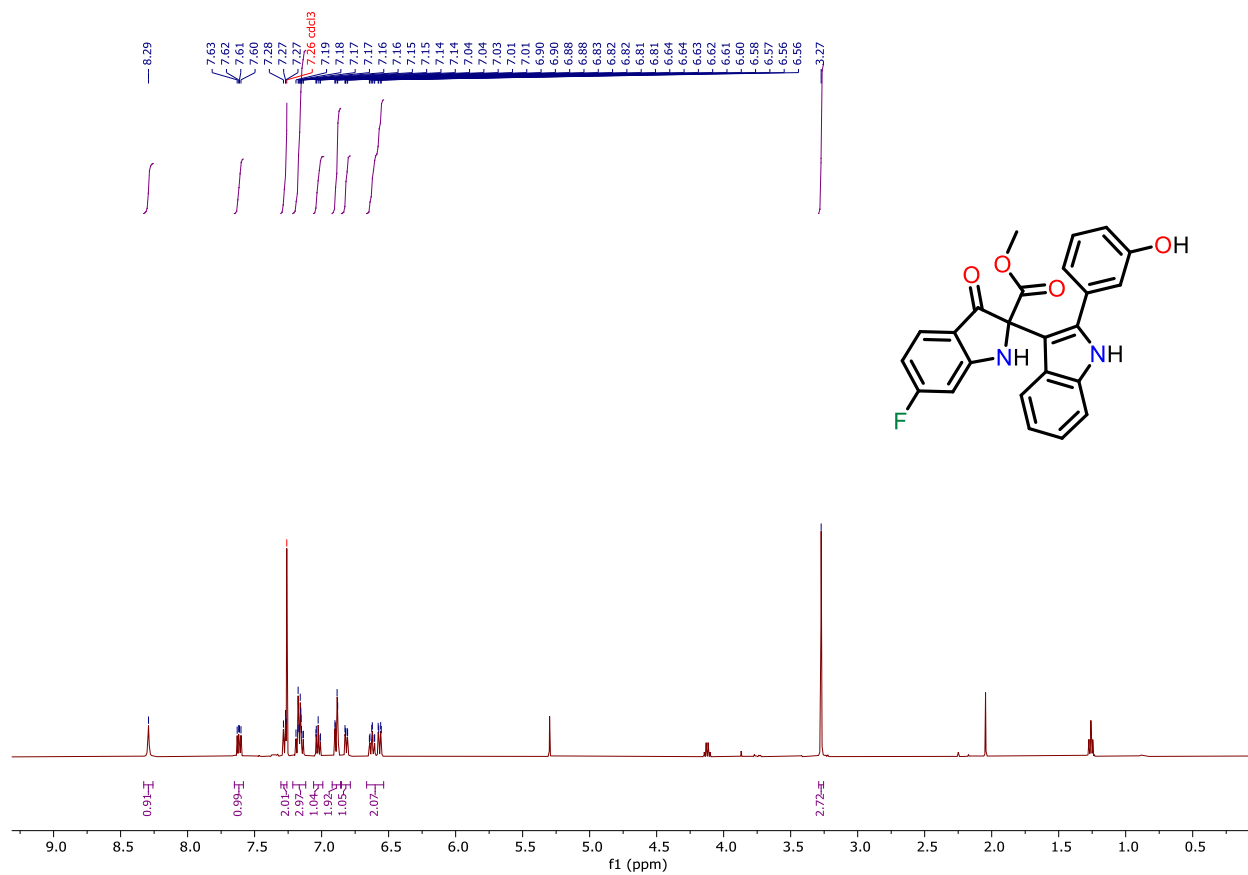
Appendix II
Selected NMR Spectra (Chapter 3)

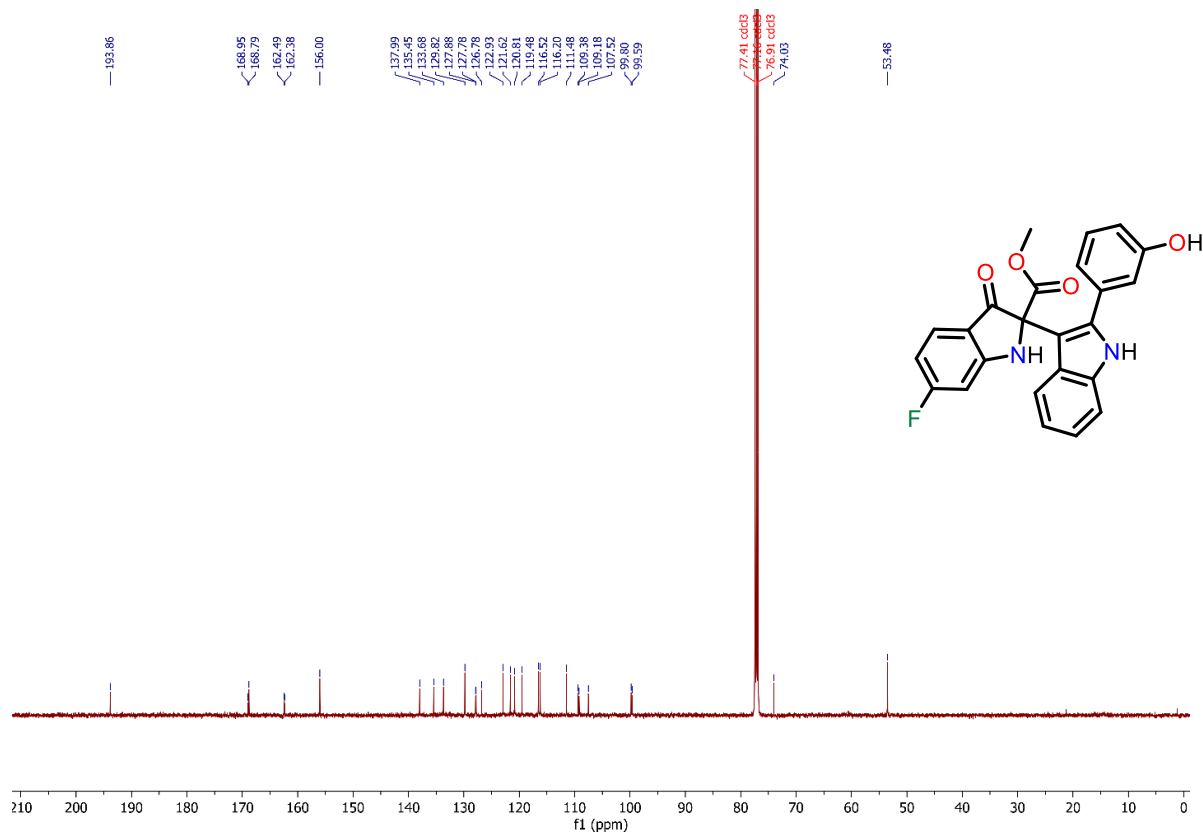


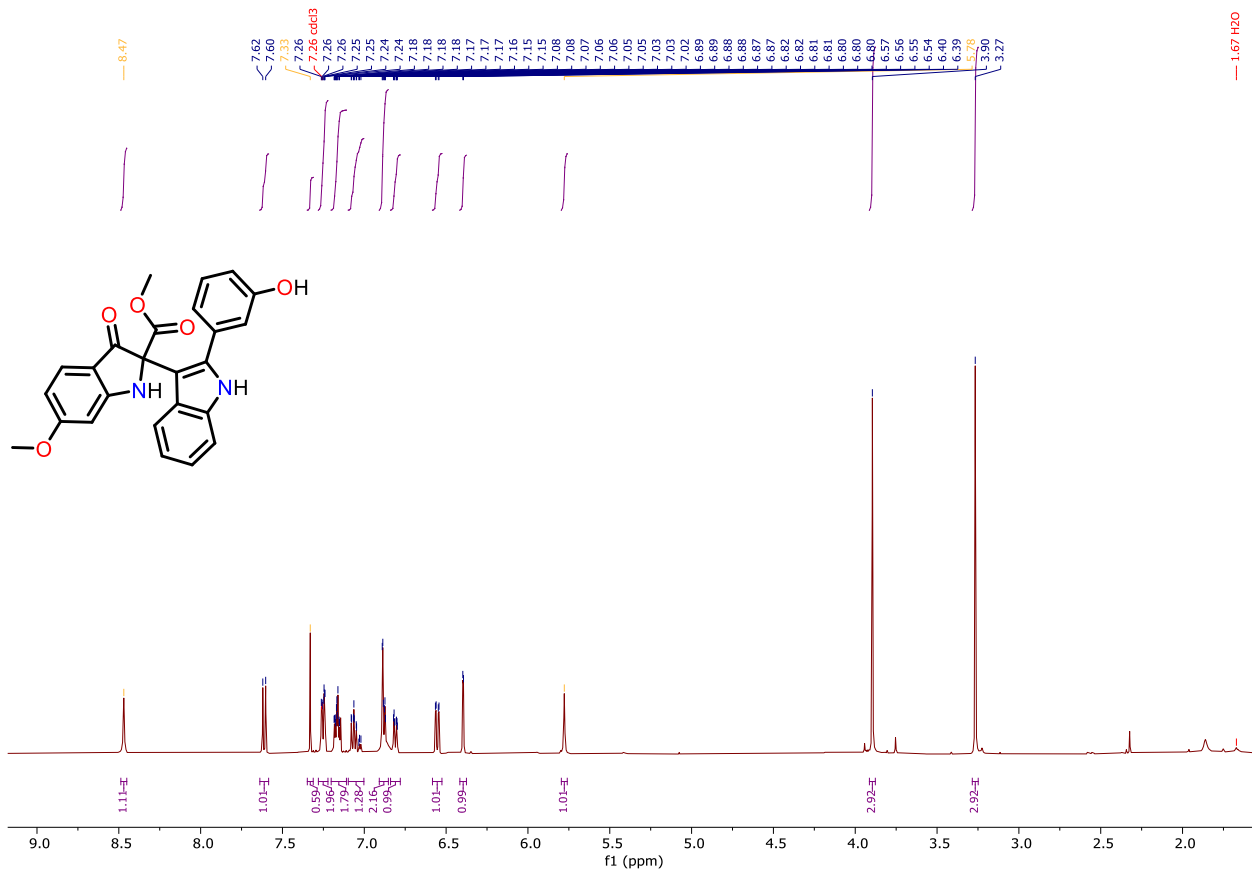


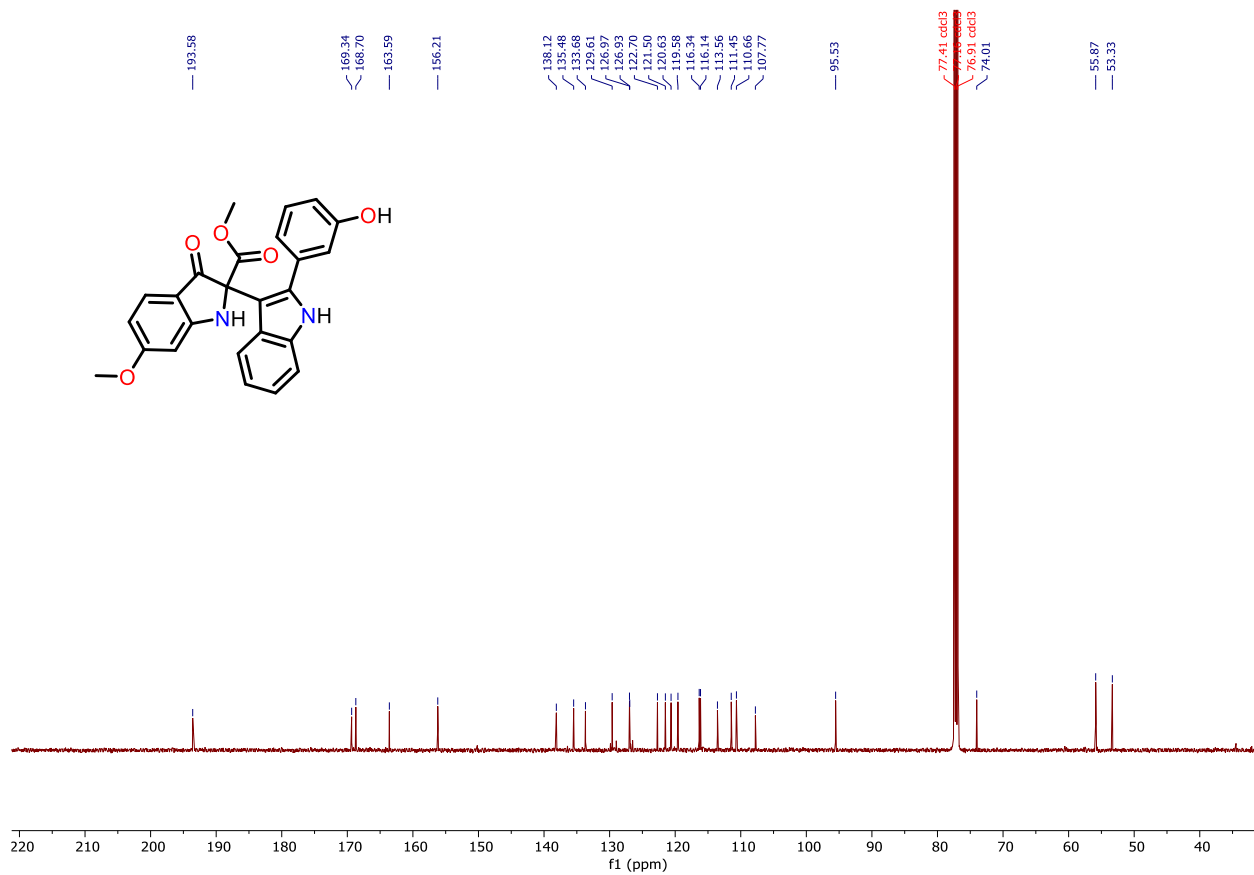


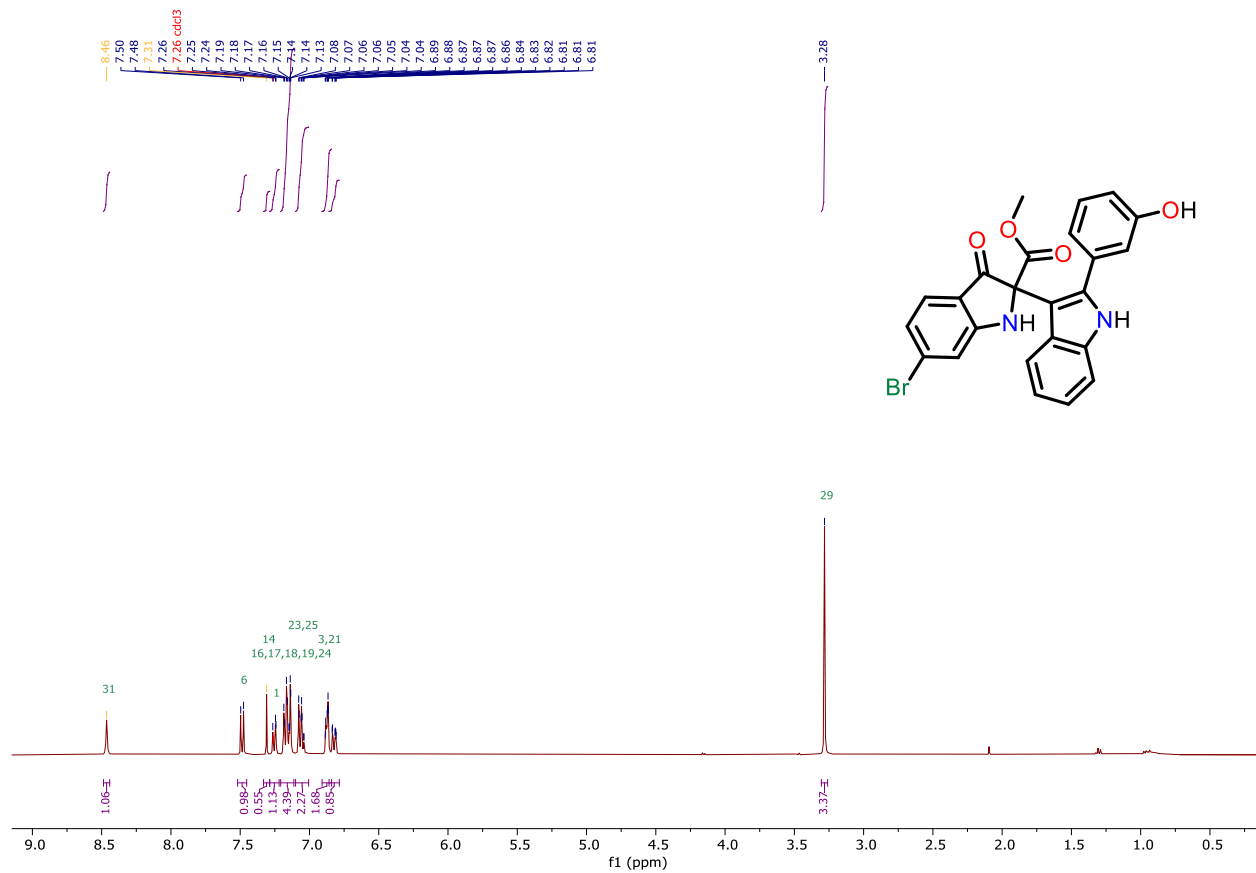


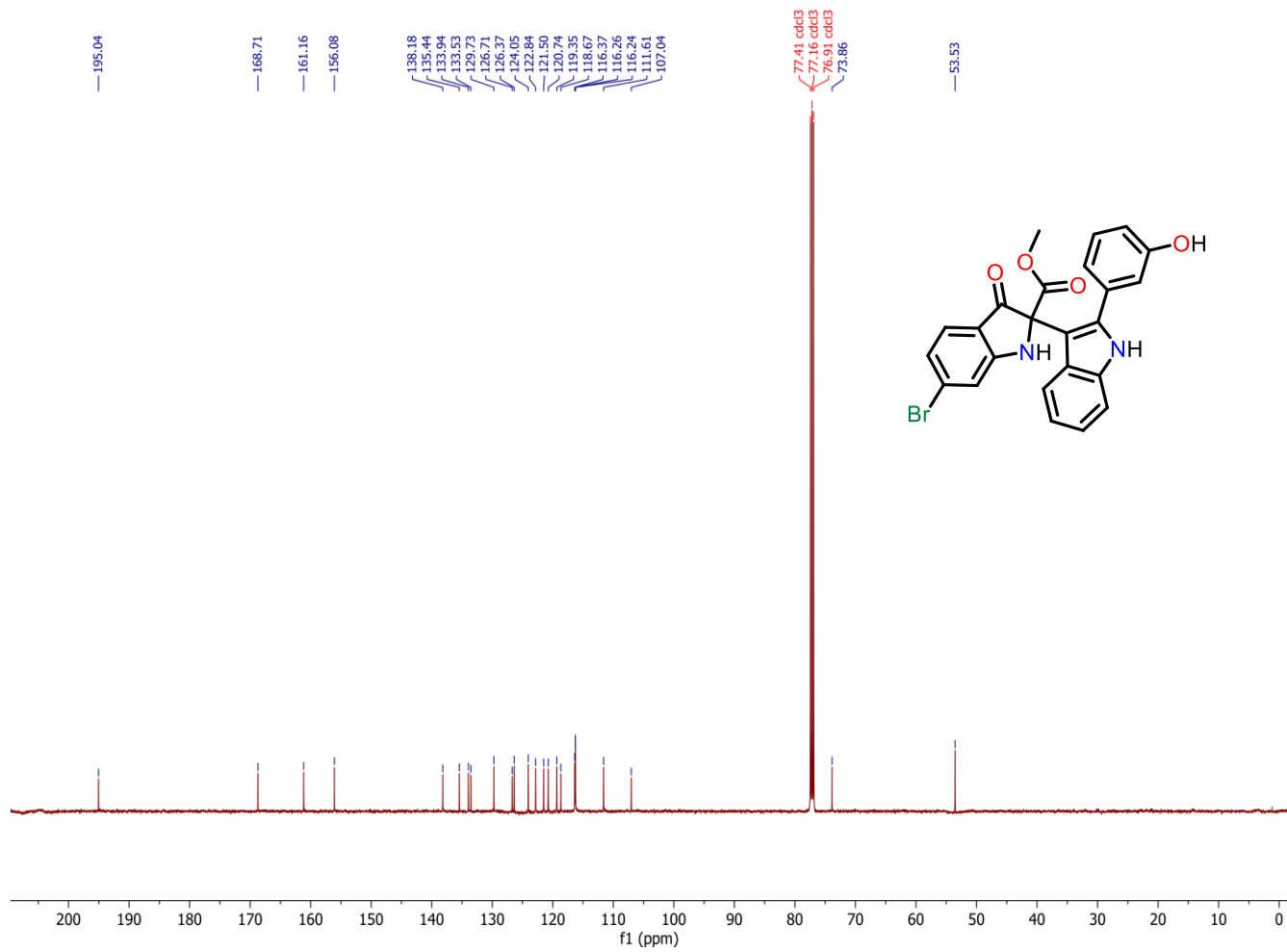


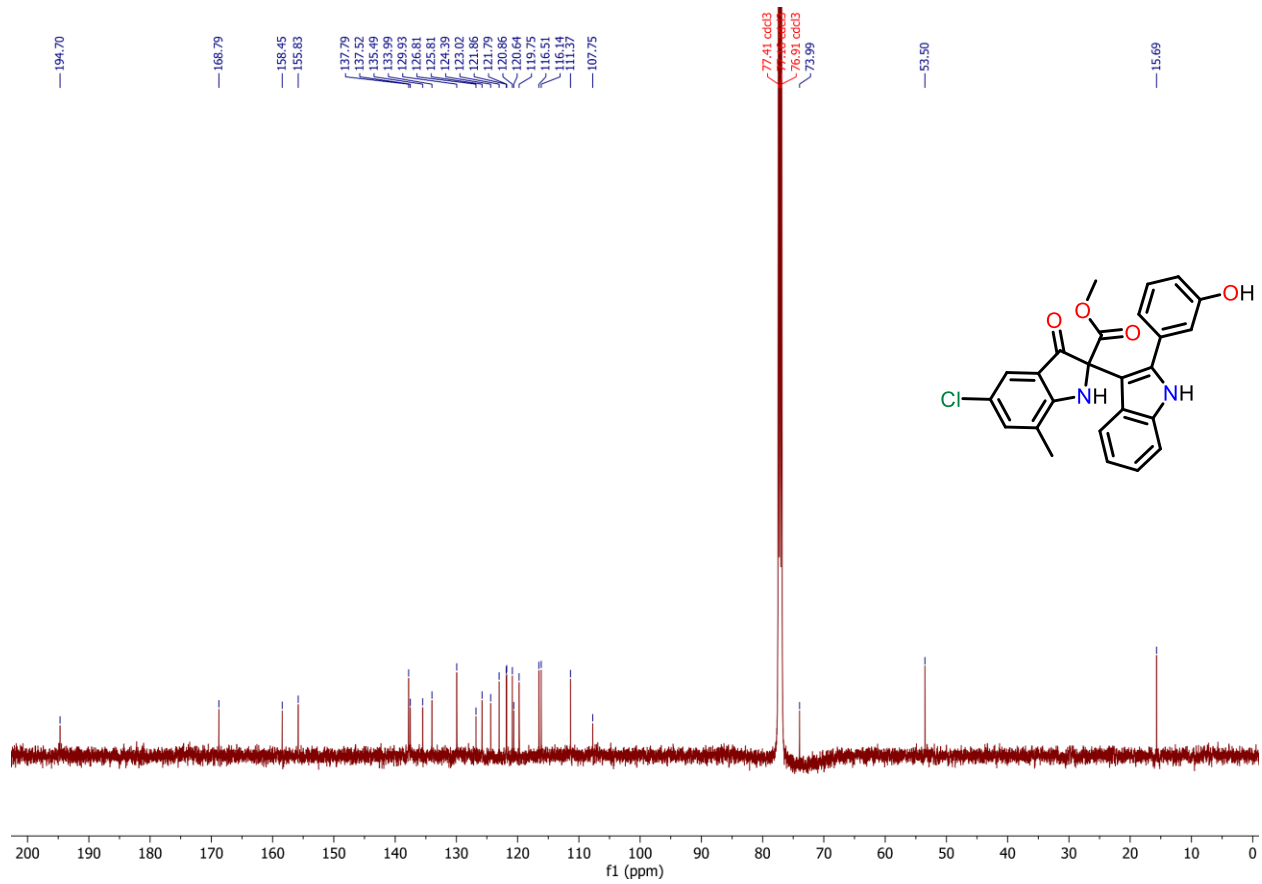




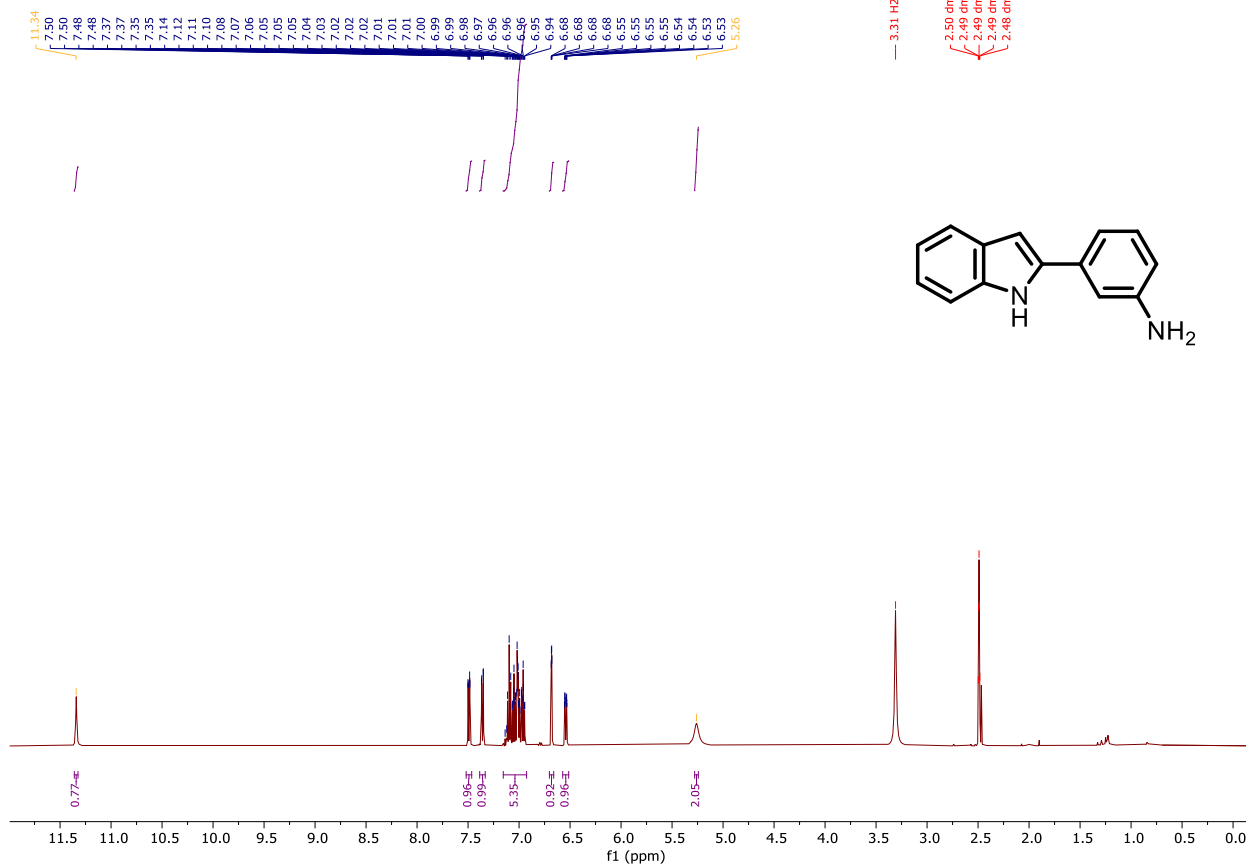


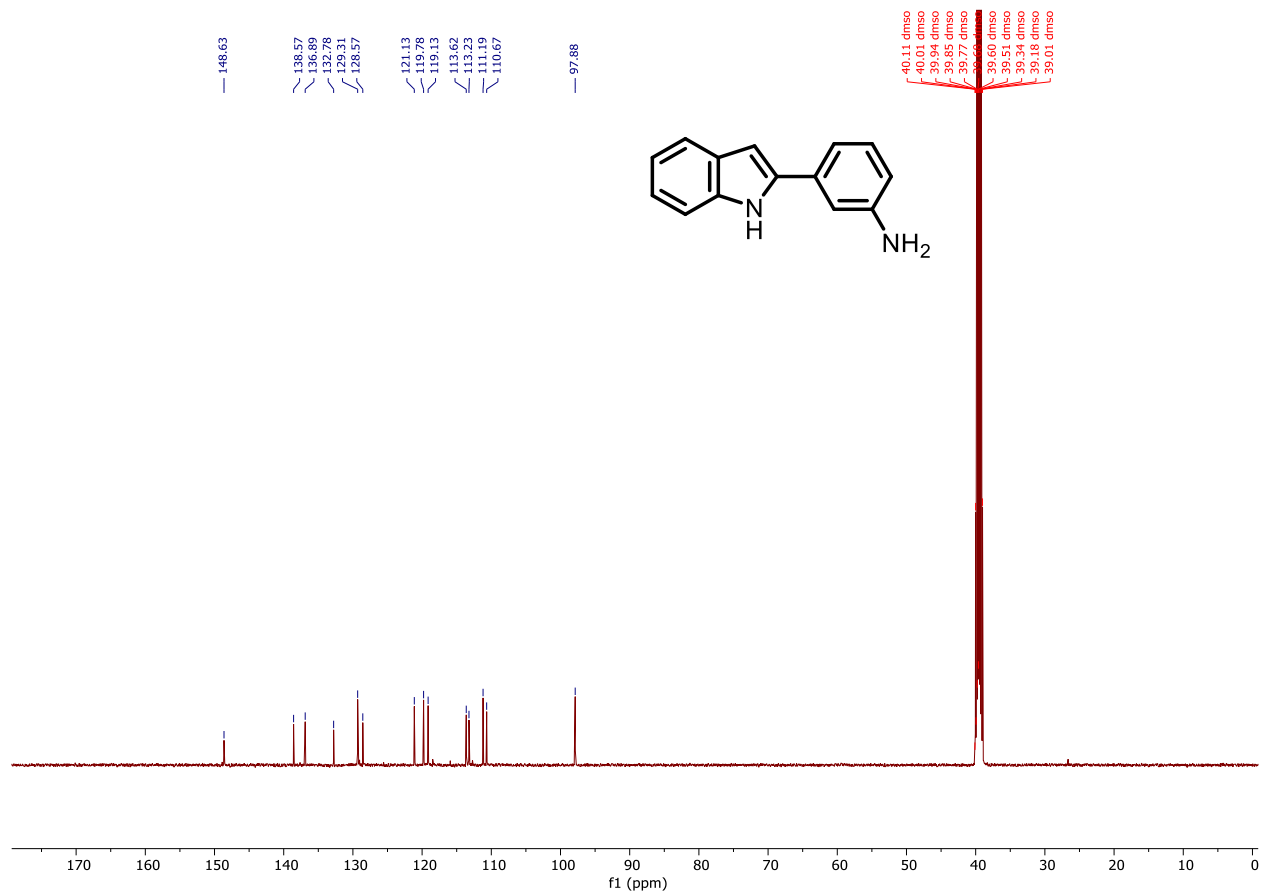


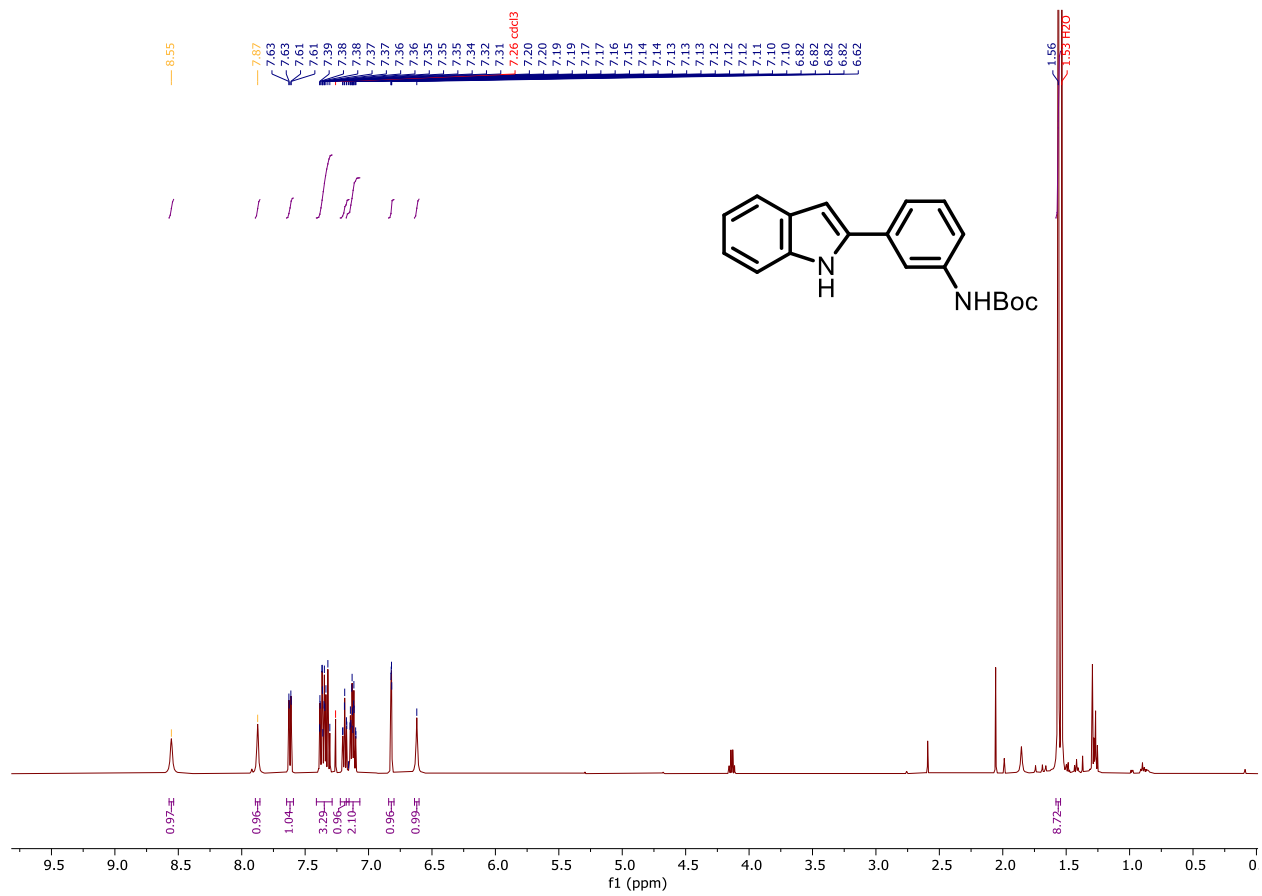


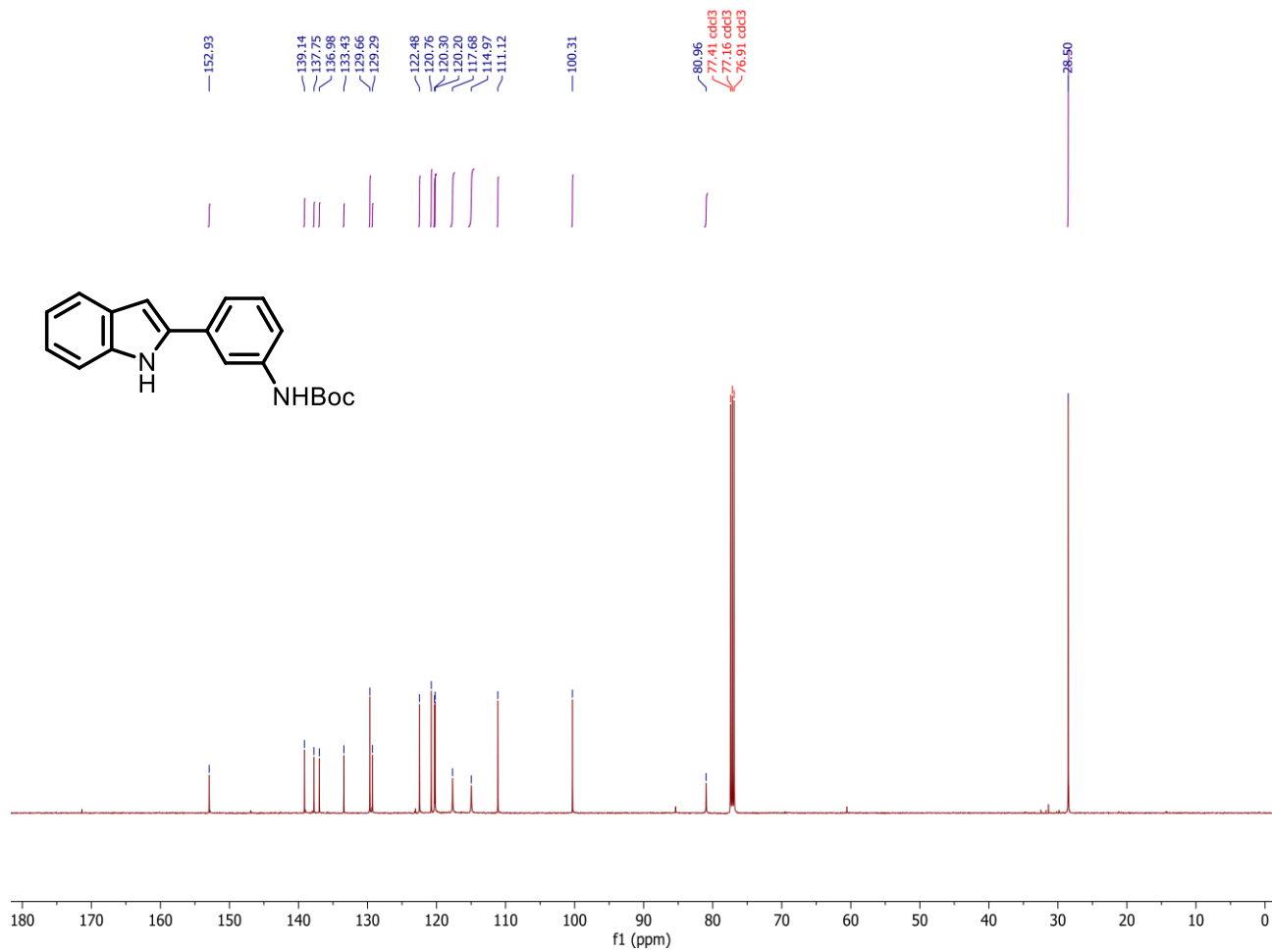


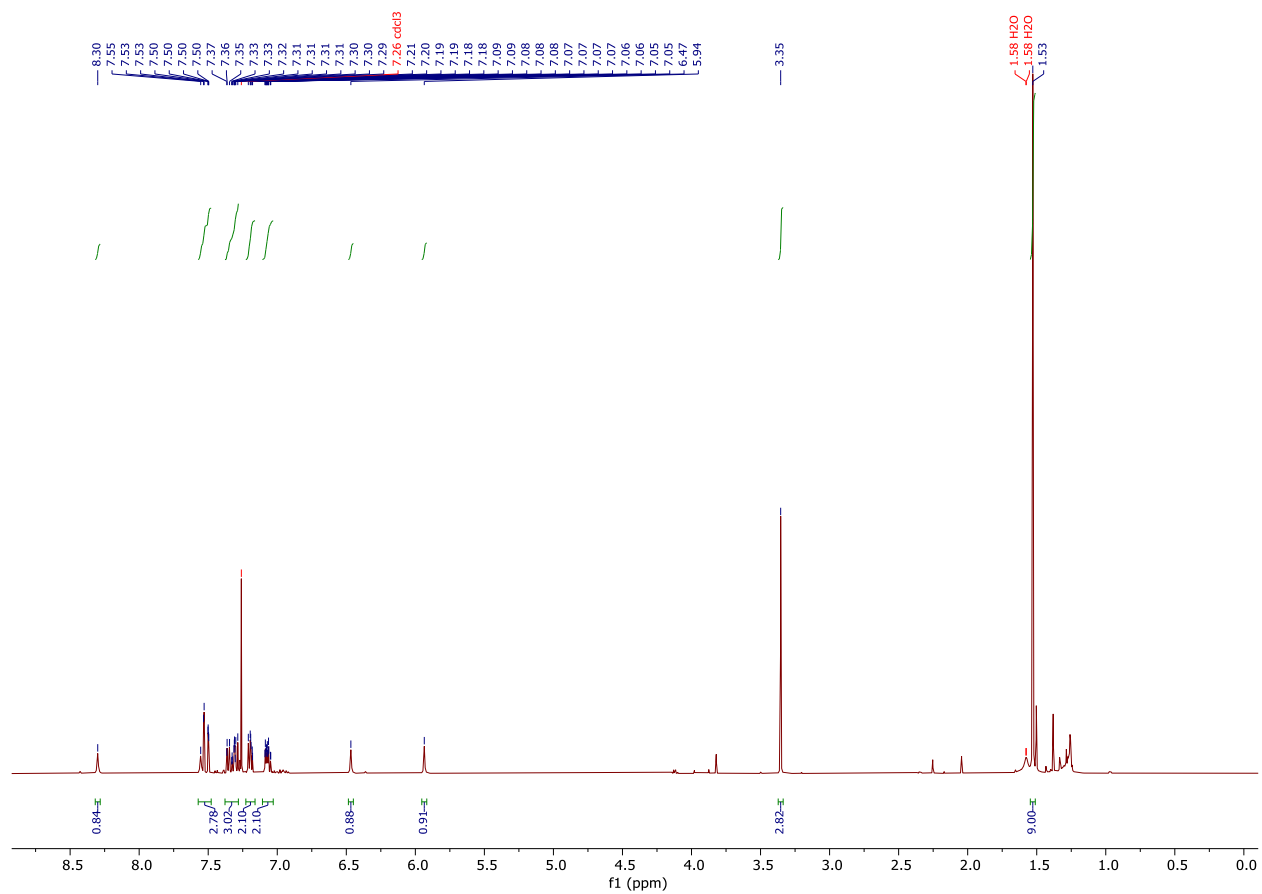
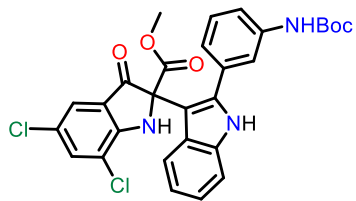
2021.08.19.u5_AO-I-37_loc12_15.56_H1_1D

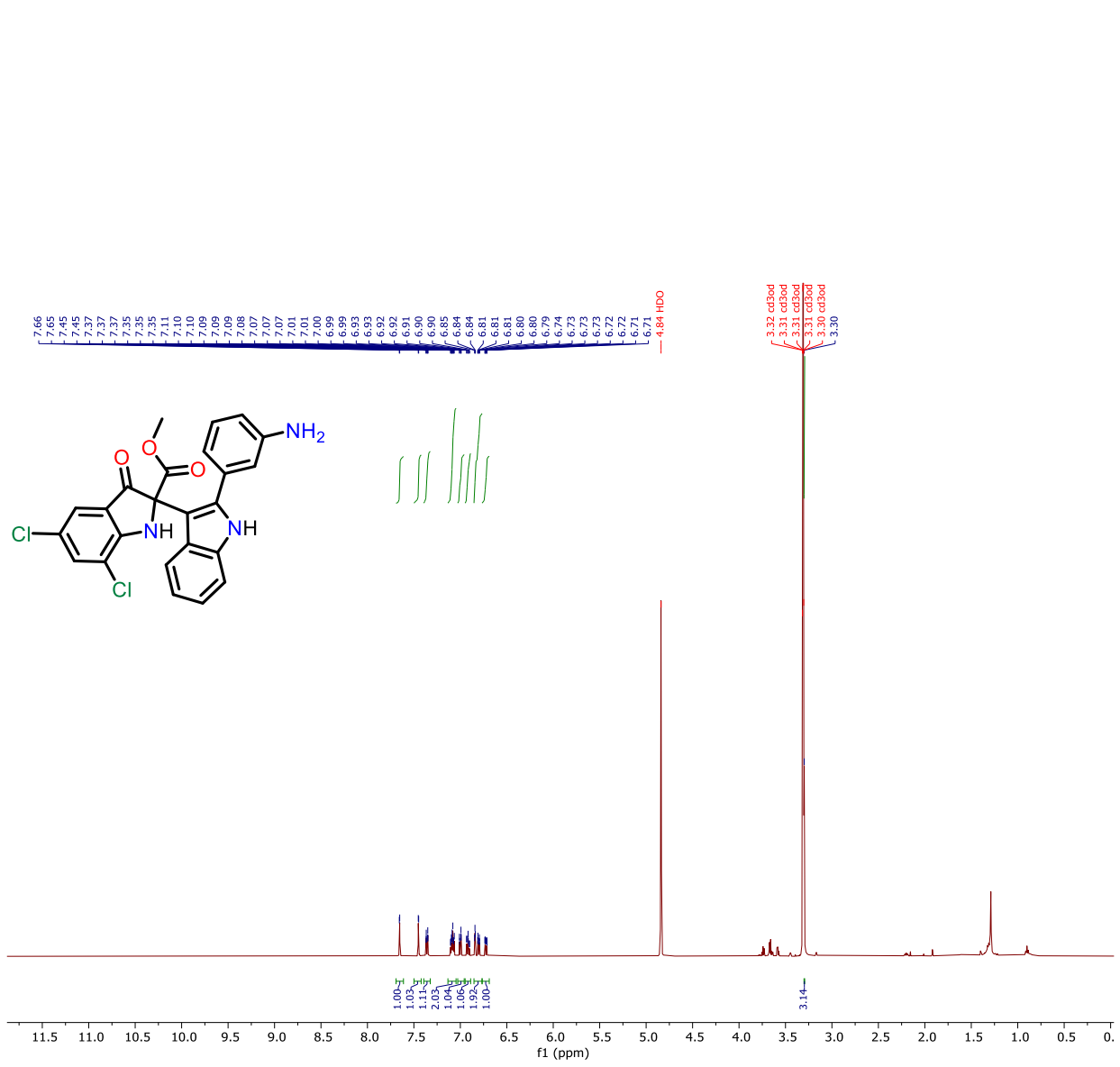


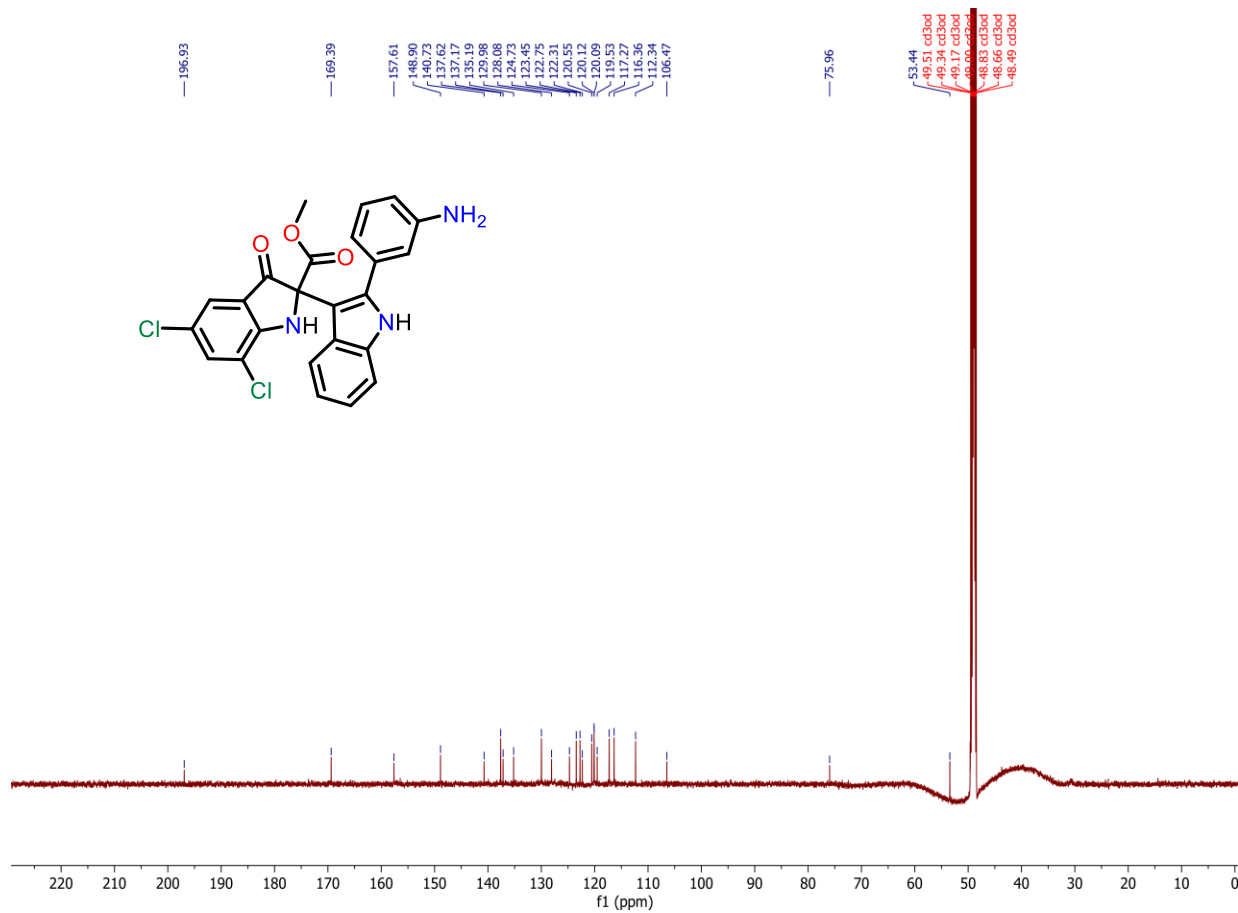


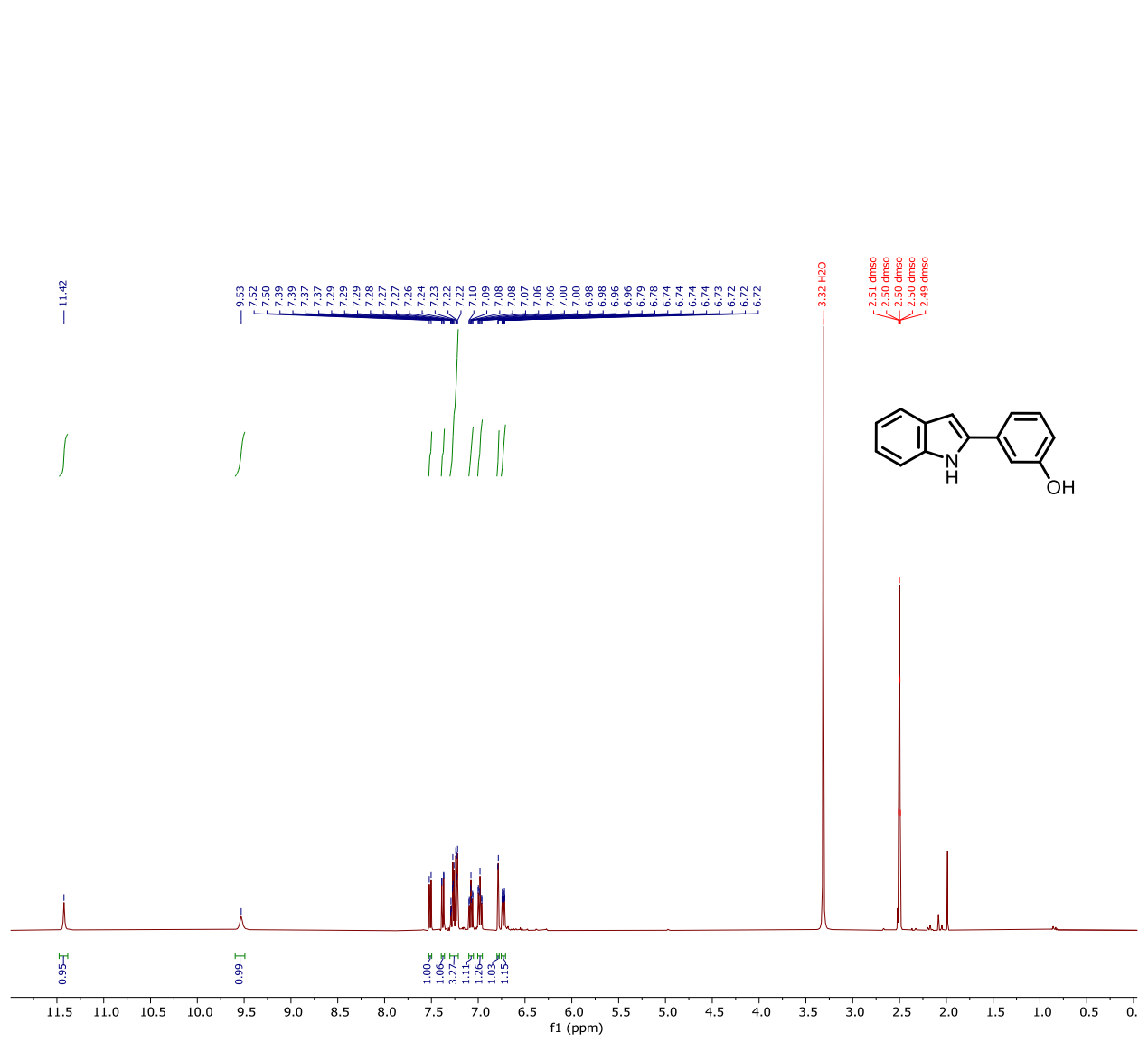


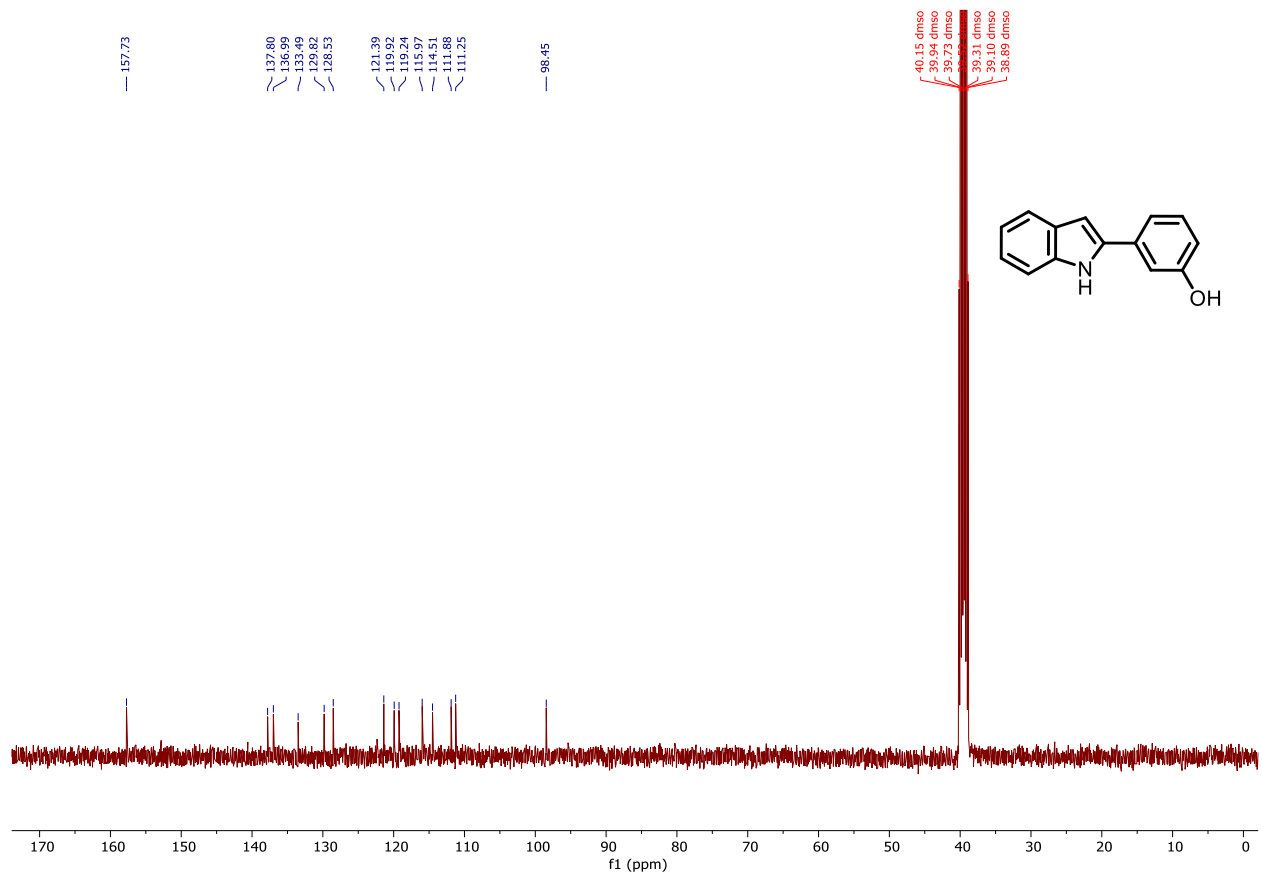


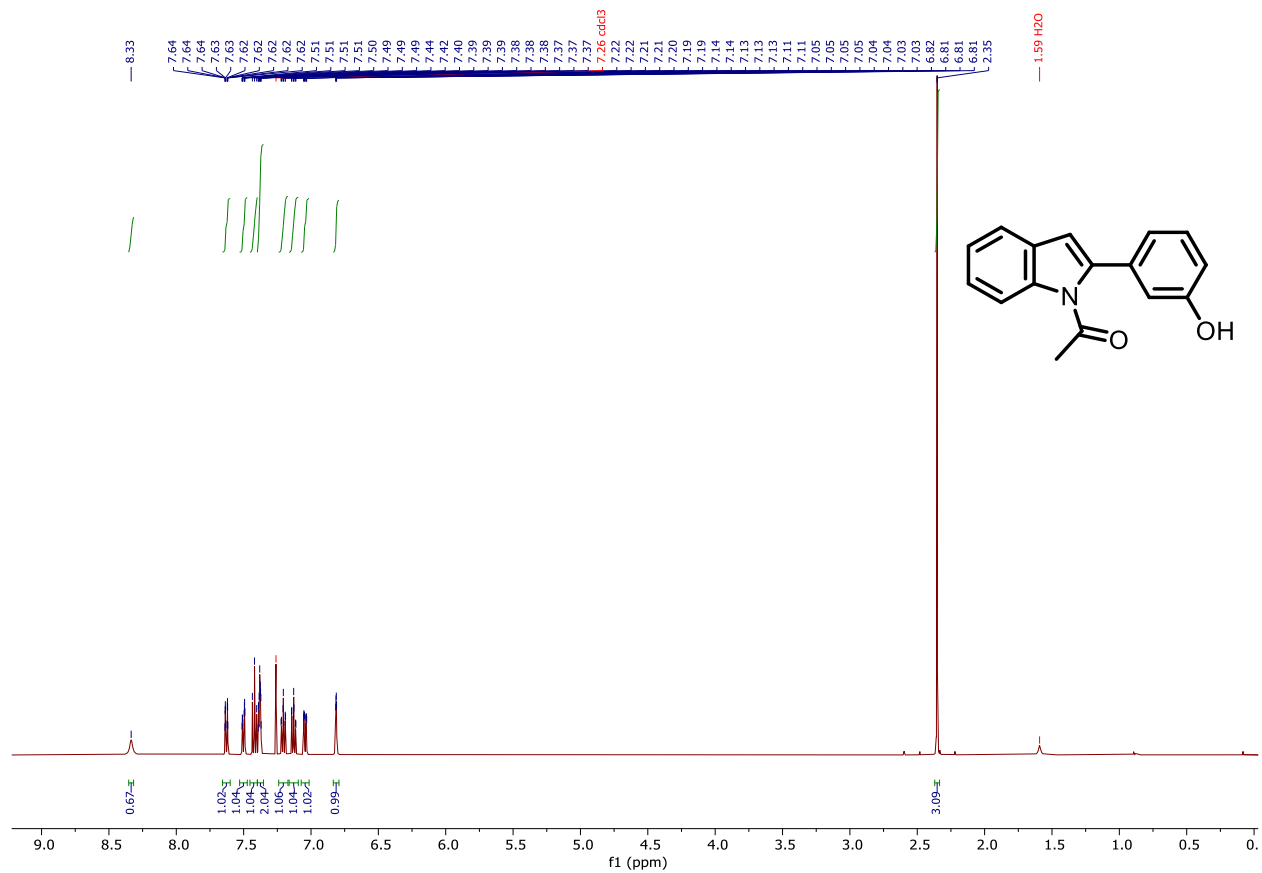


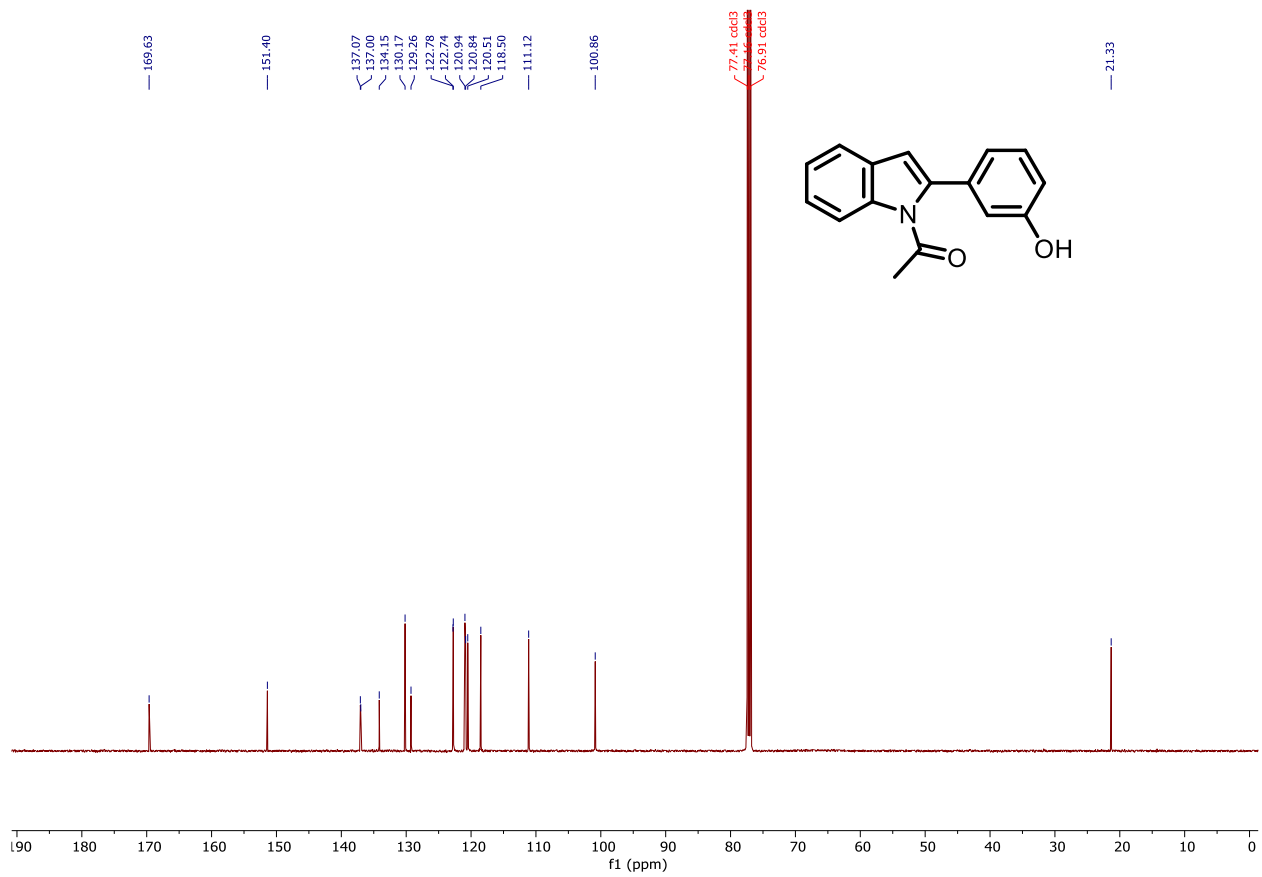


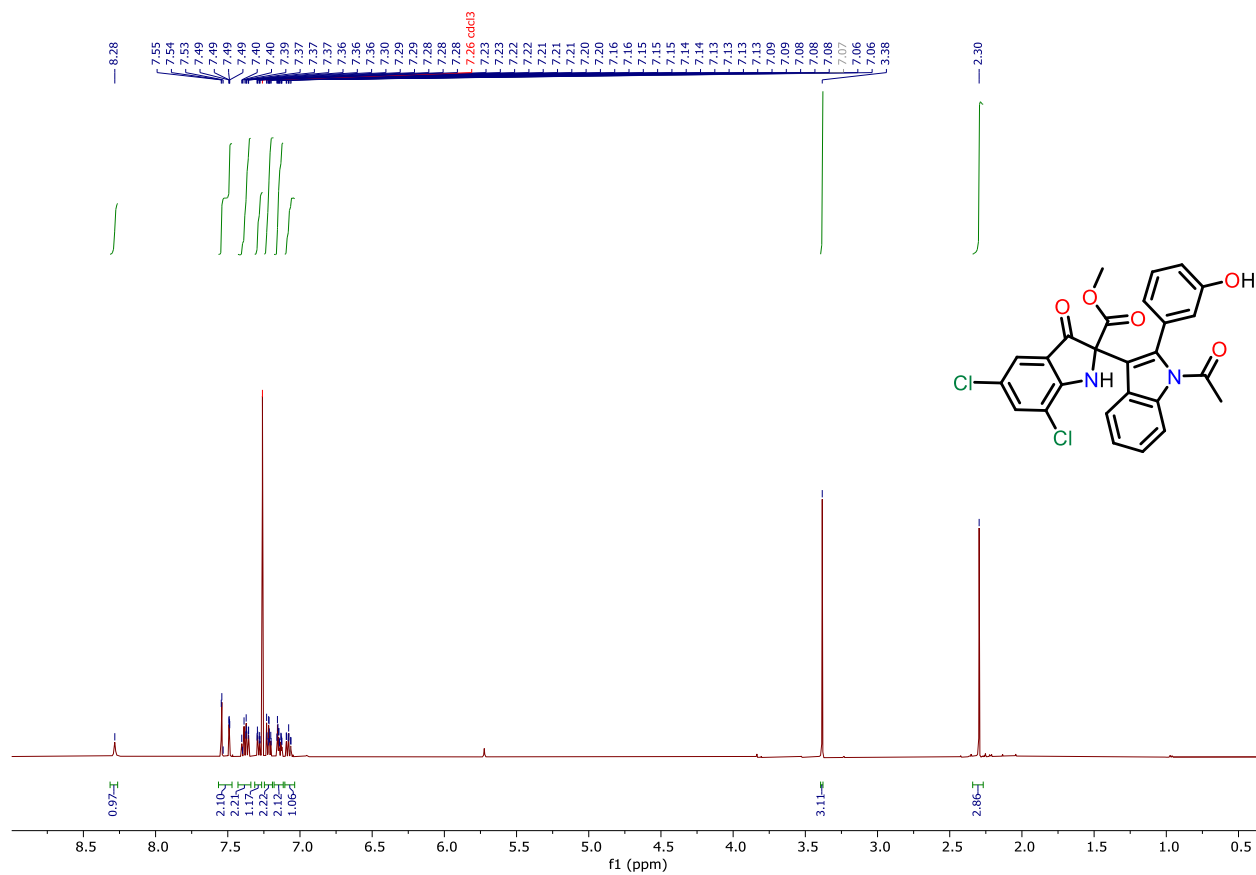


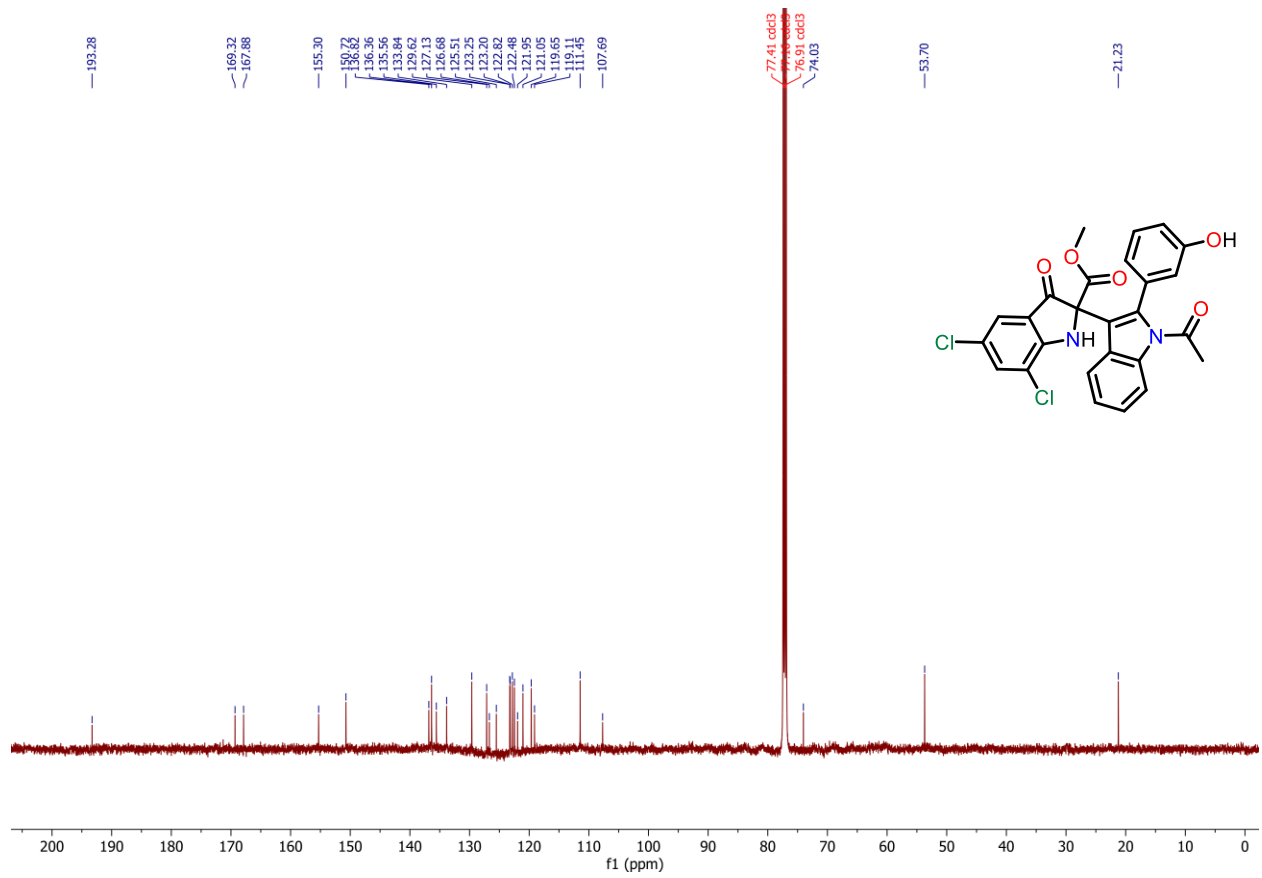




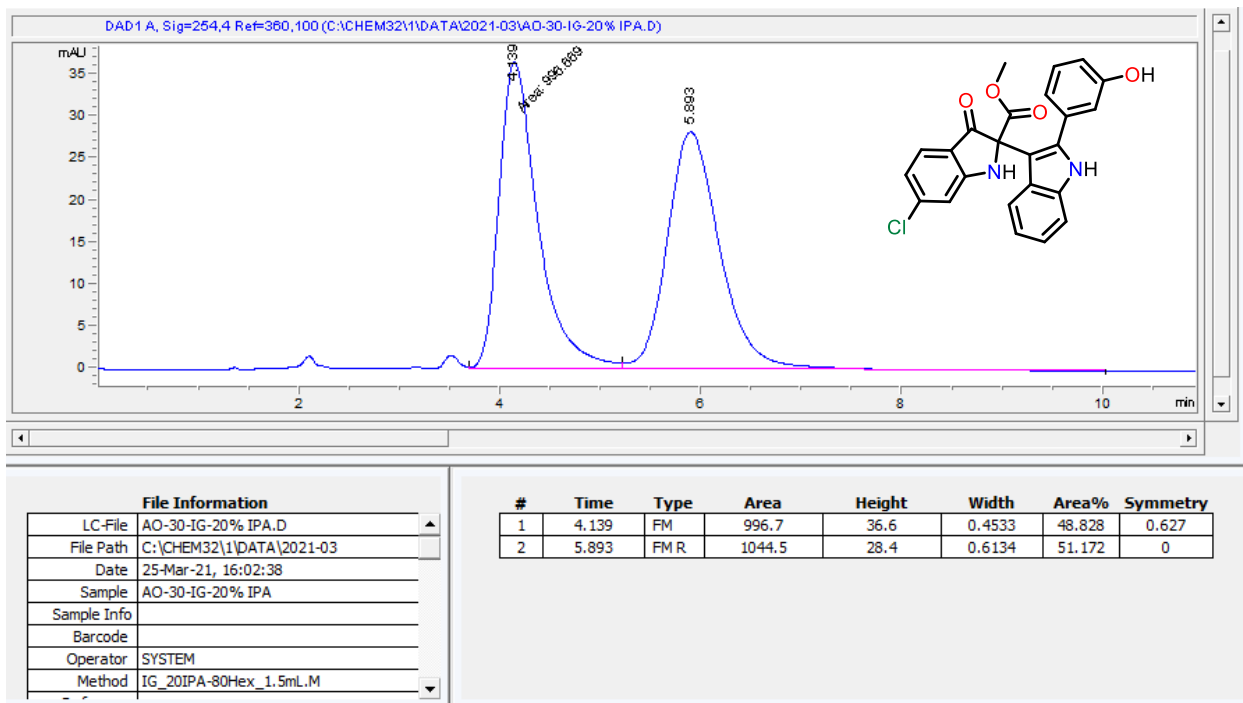




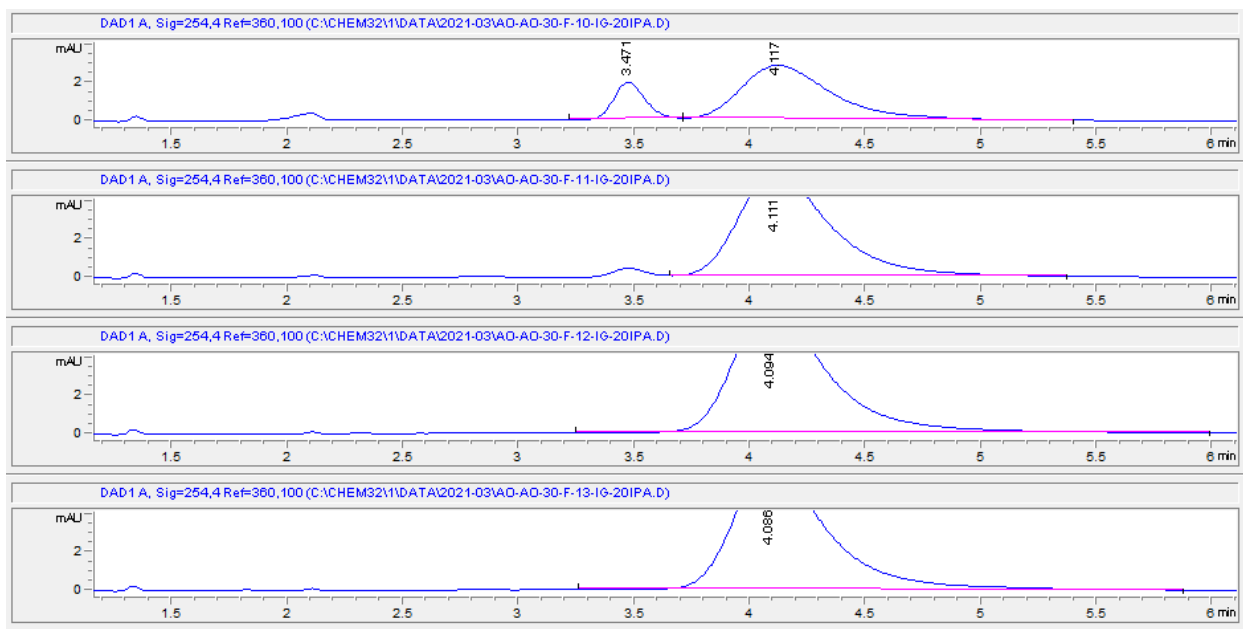




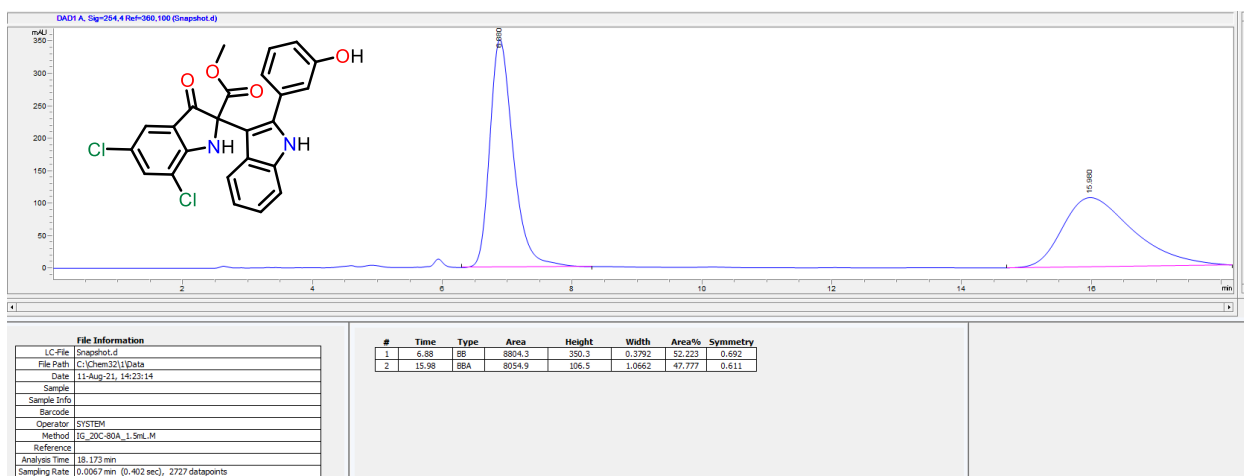
Appendix III
HPLC chromatogram of Compounds 5 & 6 (Chapter 3)



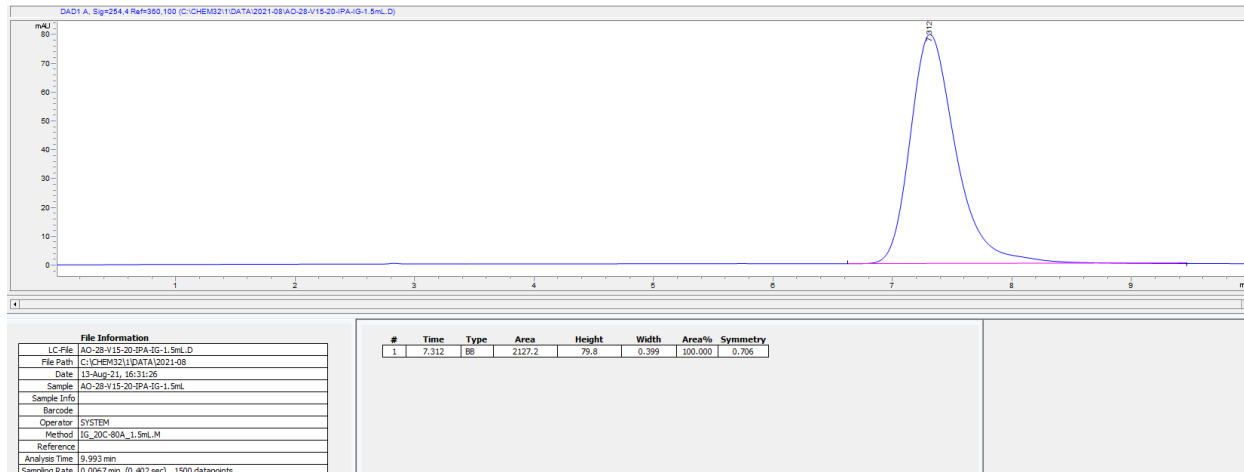
HPLC chromatogram of 5 racemic.



HPLC chromatogram of 5a (*R*), yielded a purity of ~99%.



HPLC chromatogram of **6** racemic.



HPLC chromatogram of **6a** (*R*), yielded a purity of ~99%.